

https://dspace.org/

Trafficking of plasmodium falciparum invasion proteins to the parasite micronemes

Churchyard, Alisje

2017

http://hdl.handle.net/10539/23177

Churchyard, Alisje (2017) Trafficking of plasmodium falciparum invasion proteins to the parasite micronemes, University of the Witwatersrand, Johannesburg, <http://hdl.handle.net/10539/23177>

Downloaded from a DSpace repository. https://dspace.org/

Trafficking of *Plasmodium falciparum* invasion proteins to the parasite micronemes

Alisje Churchyard

A Thesis submitted to the
Faculty of Health Sciences,
University of the Witwatersrand, Johannesburg
in the fulfilment of the requirements for the degree of
Doctor of Philosophy

Johannesburg, 2017

Declaration

I, Alisje Churchyard, declare that this Thesis is my own, unaided work. It is being submitted for the degree of Doctor of Philosophy at the University of the Witwatersrand, Johannesburg. It has not been submitted before for any degree or examination at this or any other University.

_____

Alisje Churchyard

19th day of June 2017

Ethics Clearance

Ethics clearance was obtained for this project.

Ethics number M1702106 (Sub-Study of M130569); The University of the Witwatersrand; Committee for Research on Human Subjects (medical).

The ethics certificate is supplied in Appendix G.

Publications Arising From This Study

Publications:

Title: Trafficking of *Plasmodium falciparum* Proteins: A Novel Anti-malaria Drug Target?

Type of Publication: Abstract

Journal: Blood; volume 128; number 22; page 2443 Impact Factor: 11.847

Authors: Thérèsa L. Coetzer, Alisje Churchyard and Melanie Wepener

Date: 1 December 2016

Manuscripts in Preparation:

Two manuscripts are in preparation and will be submitted for publication in 2017:

Title: **Targeting the micronemes: The molecular trafficking determinants of three *Plasmodium falciparum* invasion proteins** (subject to change)

Journal: Traffic (IF 3.721) or Malaria Journal (IF 3.489)

Authors: Alisje Churchyard, Melanie Wepener and Thérèsa L. Coetzer

Title: **The role of protein escorters in targeting invasion proteins to the apical organelles of *Plasmodium falciparum*** (subject to change)

Journal: Parasites and Vectors (IF 3.234) or PLOS one (IF 4.411)

Authors: Alisje Churchyard and Thérèsa L. Coetzer

Presentations Arising From This Study

International Conferences:

Trafficking of *Plasmodium falciparum* Proteins: A Novel Anti-malaria Drug Target?

Authors: Thérèsa L. Coetzer, Alisje Churchyard and Melanie Wepener

Type of Presentation: Poster presentation Date: December 2016

Conference Name and Venue: The 58th American Society of Hematology Annual Meeting and Exposition, San Diego, California, United States of America

Transgenic *Plasmodium falciparum* parasites expressing chimaeric AMA-1 and SUB2 invasion proteins

Authors: Alisje Steyn and Thérèsa L. Coetzer

Type of Presentation: Oral presentation Date: October 2013

Conference Name and Venue: 6th PAN-African Malaria Conference, Durban, KwaZulu-Natal, South Africa

Synthesis of *Plasmodium falciparum ama-1* and *sub2* mini-genes

Authors: Alisje Steyn and Thérèsa L. Coetzer

Type of Presentation: Poster presentation Date: January 2012

Conference Name and Venue: The South African Society of Biochemistry and Molecular Biology (SASBMB)/ Federation of African Societies of Biochemistry and Molecular Biology (FASBMB) XXIIIrd Conference, Drakensberg, KwaZulu-Natal, South Africa

Local Conferences:

The molecular determinants for trafficking of AMA-1, a malaria invasion protein and vaccine candidate

Authors: Alisje Churchyard and Thérèsa L. Coetzer

Type of Presentation: Oral presentation Date: September 2016

Conference Name and Venue: The Faculty of Health Sciences Research Day, University of the Witwatersrand, Johannesburg, Gauteng, South Africa

The molecular determinants for trafficking of AMA-1, a malaria invasion protein and vaccine candidate

Authors: Alisje Churchyard and Thérèsa L. Coetzer

Type of Presentation: Oral presentation Date: July 2016

Conference Name and Venue: The 2nd South African Malaria Research Conference, University of Pretoria, Gauteng, South Africa

The molecular determinants for trafficking of AMA-1, a malaria invasion protein and vaccine candidate

Authors: Alisje Churchyard and Thérèsa L. Coetzer

Type of Presentation: Oral presentation Date: July 2016

Conference Name and Venue: The South African Society of Biochemistry and Molecular Biology (SASBMB) XXVth Conference, East London International Conference Centre, Eastern Cape, South Africa

Trafficking of *Plasmodium falciparum* invasion proteins, AMA-1 and SUB2

Authors: Alisje Steyn and Thérèsa L. Coetzer

Type of Presentation: Poster presentation Date: September 2014

Conference Name and Venue: The Faculty of Health Sciences Research Day, University of the Witwatersrand, Johannesburg, Gauteng, South Africa

Trafficking of *Plasmodium falciparum* invasion proteins, AMA-1 and SUB2

Authors: Alisje Steyn and Thérèsa L. Coetzer

Type of Presentation: Oral presentation Date: July 2014

Conference Name and Venue: The South African Society of Biochemistry and Molecular Biology (SASBMB) XXIVth Conference, Goudini Spa, Western Cape, South Africa

Synthesis of *Plasmodium falciparum ama-1* and *sub2* mini-genes

Authors: Alisje Steyn and Thérèsa L. Coetzer

Type of Presentation: Poster presentation Date: December 2012

Conference Name and Venue: The Molecular Biosciences Research Thrust Research Day, University of the Witwatersrand, Johannesburg, Gauteng, South Africa

Synthesis of Plasmodium falciparum ama-1 and sub2 mini-genes

Authors: Alisje Steyn and Thérèsa L. Coetzer

Type of Presentation: Poster presentation Date: September 2012

Conference Name and Venue: The Faculty of Health Sciences Research Day, University of the Witwatersrand, Johannesburg, Gauteng, South Africa

Synthesis of *Plasmodium falciparum ama-1* and *sub2* mini-genes

Authors: Alisje Steyn and Thérèsa L. Coetzer

Type of Presentation: Poster presentation Date: September 2011

Conference Name and Venue: The Molecular Biosciences Research Thrust Research Day, University of the Witwatersrand, Johannesburg, Gauteng, South Africa

Abstract

Malaria continues to be a global health problem. Despite a marked reduction in mortality over the last 15 years, these hard-fought gains are threatened by growing resistance of the *Plasmodium falciparum* malaria parasite to artemisinin, the frontline drug used in treatment of the disease. Clinical symptoms of malaria are caused by the intra-erythrocytic phase of the parasite life cycle. Entry into the erythrocyte is accomplished by several specialised invasion proteins, which are stored in unique apical secretory organelles known as micronemes and rhoptries. Very little is known about the trafficking signals and transport mechanisms of invasion proteins to these organelles.

Three micronemal proteins, Apical Membrane Antigen-1 (*Pf*AMA-1), Subtilisin-like protease 2 (*Pf*SUB2) and Erythrocyte Binding Antigen 181 (*Pf*EBA181) were investigated with the aim of identifying domains responsible for targeting the micronemes. Selected domains were amplified and mini-genes were created by overlap extension PCR. A pARL-mCherry plasmid containing a *Pfama-1* stage-specific promoter that is only active during the schizont stage of parasite development when micronemes are formed, was used to create mCherry-tagged constructs. *P. falciparum* parasites were transfected by electroporation of the plasmid constructs. Transgenic parasites were selected by drug pressure and the expression of red fluorescent mCherry-tagged chimaeric proteins was visualised in live parasites. Co-localisation studies were performed with a microneme marker to assess if the transgenic mini-proteins reached their destination. Interestingly, all three proteins required different domains to target the micronemes: *Pf*EBA181 required an extended region of a conserved cysteine-rich domain, *Pf*AMA-1 required the prodomain, and *Pf*SUB2 required the transmembrane domain. Since no common targeting signal was identified, the possibility of a protein escorter was explored. The *Pf*AMA-1 prodomain was expressed as a recombinant histidine-tagged protein and immobilised onto Nickel-coated beads, which were exposed to a *P. falciparum* phage display library for four rounds of biopanning. Two novel binding partners were identified: a putative Chaperone Binding Protein and a putative Formin 2.

The identification of the molecular trafficking determinants of three invasion proteins, as well as a potential protein escorter for microneme targeting, represent novel findings that extend our knowledge of a fundamental biological process in the malaria parasite. This pathway may be exploited for drug development and new malaria treatment strategies.

Acknowledgements

Well-deserved thanks must go to Prof TL Coetzer: a remarkable woman, a phenomenal supervisor and a source of constant optimism. Thank you for believing in me.

Thanks to Dr Jude Przyborski for the provision of the pARL-mCherry plasmid, and for technical assistance with the transfection protocol. Thanks also to Marco Pereira and the team from Olympus for the training and technical assistance with the fluorescence microscopy experiments.

To all my lab colleagues, your companionship, motivation and continuous support have been immensely valued. Thanks to: Kuben - for selflessly showing me the ropes in the lab and always giving great advice; Belinda - for your gentle encouragement; Sonja - for sharing your incredible technical skills; Serena - for your friendship, positivity and kindness; Dewaldt - for always offering a vote of confidence. And a special thanks to those who have become dear friends: Mel, Dale, Warren and Nisha- you guys have made the journey worth it, thank you for being my family away from home.

To my family and friends, word cannot describe how incredibly grateful I am for your support over the many years. Mom and Dad, thank you for teaching me the value of hard work, for always pushing me to do better, but mostly, thank you for cheering me on, every step of the way, and for never letting me give up on my dreams.

To Luke, thank you for your continued love and support. You have not only been there every step of the way, but you have constantly shown me that I am capable of more than even I thought possible. I could not have done this without you.

Funding

A huge thank you to all the funding bodies that contributed to this research project:
Post-Graduate Merit Award – The University of the Witwatersrand
Post-Graduate Scholarship – The University of the Witwatersrand
Medical Faculty Research Endowment Fund – The University of the Witwatersrand
Grant-holder linked bursary – National Research Foundation (NRF)
Masters Fellowship – Belgian Technical Cooperation (BTC)

Table of Contents

Declaration ii

Ethics Clearance ii

Publications iii

Presentations iii

Abstract vi

Acknowledgements vii

Table of Contents viii

List of Figures xv

List of Tables xx

Nomenclature xxi

Units of Measure xxiv

Greek Alphabet xxv

List of Amino Acids xxv

Chapter 1: Introduction 1

1.1 The Malaria Epidemic 1

1.1.1 Challenges in Vector Control 1

1.1.2 Challenges in Parasite Control 2

1.1.3 The Way Forward 3

1.2 The *P. falciparum* Life Cycle 3

1.3 Erythrocyte Invasion 5

1.4 The Apical Organelles 9

1.4.1 The Biogenesis of Apical Organelles 9

1.4.2 Structural Differences Between the Apical Organelles 10

1.4.3 Discharge of Invasion Proteins from the Apical Organelles 10

1.5 Trafficking Pathways 12

1.5.1 Protein Export to the Host Cell 12

1.5.2 Internal Protein Trafficking 13

1.5.3 Protein Sorting 14

1.5.4 Transport by Vesicles 15
1.6 Targeting the Rhoptries 16
1.7 Targeting the Micronemes 17
1.8 The Purpose of this Study 18
1.8.1 Project Aims 18
1.8.2 Project Objectives 18
Chapter 2: Materials and Methods 19
2.1 Malaria Cultures 19
2.1.1 Erythrocyte Preparation 19
2.1.2 Maintaining a *P. falciparum* Culture 19
2.1.3 Synchronising a Culture 20
2.1.4 Freezing and Thawing a Parasite culture 20
2.2 *Plasmodium falciparum* Nucleic Acid Isolation 21
2.2.1 Genomic DNA Isolation 21
2.2.2 Parasite RNA Isolation 22
2.2.3 Assessment of Isolated Nucleic Acids 23
2.2.3.1 Agarose Gel Electrophoresis 23
2.2.3.2 NanoDrop 24
2.3 Polymerase Chain Reaction 24
2.3.1 Primer Design 24
2.3.2 cDNA Synthesis 25
2.3.3 PCR Amplification of *P. falciparum* Mini-genes/ Domains 25
2.3.4 Overlap Extension PCR Amplification 26
2.4 Plasmid Isolation for Cloning 27
2.5 Preparation for Cloning 29
2.5.1 Restriction Enzyme Digests of PCR Products 29
2.5.2 Restriction Enzyme Digests and Alkaline Dephosphorylation of Plasmids 29
2.5.3 Creation of Chemically Competent XL10 and DH5α Cells 30
2.6 Cloning 30
2.6.1 Ligation Reaction 30
2.6.2 Transformation 30
2.6.3 Creating Glycerol Stocks of Transformed Bacterial Cells 31
2.6.4 Verification of Clones 31
2.6.4.1 Plasmid Isolation 31
2.6.4.2 Restriction Enzyme Digest Analysis of Clones 32

2.6.4.3 Sequence Verification of Clones 32
2.7 Creating *P. falciparum* Transgenic Parasites 32
2.7.1 Preparation of pARL-mCherry Plasmids for Transfection 32
2.7.2 Preparation of Erythrocytes for Transfection 33
2.7.3 The Transfection Protocol 34
2.7.4 Maintaining *P. falciparum* Transgenic Parasites 34
2.7.5 Verification of Transfection 34
2.7.5.1 DNA Isolation from *P. falciparum* Transgenic Parasites 34
2.8 Microscopy of Live *P. falciparum* Transgenic Parasites 35
2.9 Co-localisation Studies 36
2.10 Protein Expression and Purification 37
2.10.1 Cloning and Expression Vectors 37
2.10.2 Transformation of Rosetta™ 2(DE3) Bacterial Cells 38
2.10.3 Protein Expression 39
2.10.3.1 Bacterial Cultures for Protein Expression 39
2.10.3.2 Protein Purification of His-tagged Recombinant Proteins 39
2.10.3.3 Protein Purification of GST-tagged Recombinant Proteins 41
2.10.3.4 Assessment of Purified Proteins by SDS-PAGE 42
2.10.3.5 Quantitation of Purified Recombinant Protein 44
2.10.3.6 Assessment of Purified Recombinant Proteins by Western Blot 44
2.11 Biopanning Using Phage Display Libraries 45
2.11.1 Bacterial Cultures for Biopanning 45
2.11.2 Phage Amplification and Plaque Assays 46
2.11.3 Biopanning 46
2.11.4 PCR Amplification and Sequencing of Selected Recombinant Phages 47
2.11.5 BLT5403 and Bacteriophage Glycerol Stocks 48
2.12 *In Vitro* Binding Assays 48
Chapter 3: *P. falciparum* Apical Membrane Antigen-1 50
3.1 Introduction 50
3.1.1 *Pf*AMA-1 as a Vaccine Candidate 50
3.1.2 Expression and Function of *Pf*AMA-1 50
3.1.3 The Sequence and Structure of *Pf*AMA-1 52
3.1.4 *Pf*AMA-1 Polymorphisms 55
3.1.5 Post-translational Modifications & Trafficking of *Pf*AMA-1 56
3.1.6 Research Objectives 57



3.2 Materials and Methods 57

3.3 Results 57

3.3.1 Exchanging promoters in the pARL-mCherry plasmid 57

3.3.1.1 Preparation of the pARL-mCherry plasmid 57

3.3.1.2 Creating Control mCherry Transgenic Parasite Lines 58

3.3.1.3 Comparison of the *crt* and *ama-1* Promoters 59

3.3.2 Creation of *Pfama*-1 Mini-Genes 60

3.3.2.1 Bio-informatic Analysis of *Pf*AMA-1 60

3.3.2.2 Designing *Pfama*-1 Mini-Genes for Parasite Transfections 60

3.3.2.3 Genomic DNA Isolation 61

3.3.2.4 PCR and Overlap Extension PCR 62

3.3.2.5 Generation & Verification of pARL-mCherry Constructs 65

3.3.3 *Pf*AMA-1 Transgenic Parasites 67

3.3.4 Identification of the Domain Targeting *Pf*AMA-1 to the Micronemes 69

3.3.4.1 Live Imaging of *Pf*AMA-1 Transgenic Parasites 69

3.3.4.2 Co-localisation Studies of *Pf*AMA-1 Chimaeric Proteins 71

3.3.5 Creating *Pfama-1* Prodomain Mini-Genes 72

3.3.5.1 Designing *Pfama-1* Prodomain Mini-Genes 73

3.3.5.2 PCR Amplification of the *Pfama-1* Prodomain Mini-Genes 74

3.3.5.3 Cloning the Prodomain Mini-Genes into pARL-mCherry 74

3.3.6 Transgenic Parasites with *Pf*AMA-1 Prodomain Truncations 75

3.3.7 Identification of the Sub-Domain Required for *Pf*AMA-1 Trafficking 76

3.3.7.1 Live Imaging of *Pf*AMA-1 Prodomain Transgenic Parasites 76

3.3.7.2 Co-localisation Studies 77

3.4 Discussion 78

3.4.1 *Pf*AMA-1 Does Not Require a Tyrosine Motif to Target the Micronemes 79

3.4.2 The Cysteine-rich Ectodomain of *Pf*AMA-1 Does Not Contain a Microneme Trafficking Signal 79

3.4.3 The *Pf*AMA-1 Prodomain is Required for Microneme Targeting 81

3.4.4 The Role of Other Prodomains in Trafficking 81

Chapter 4: *P. falciparum* Subtilisin-like Protease 2 83

4.1 Introduction 83

4.1.1 The Importance of Proteases 83

4.1.2 Expression of *Pf*SUB2 84

4.1.3 Function of *Pf*SUB2 85

4.1.4 The Sequence and Structure of *Pf*SUB2 86

4.1.5 Post-translational Modifications of *Pf*SUB2 86
4.1.6 Subcellular Localisation and Trafficking of *Pf*SUB2 87
4.1.7 Research Objectives 87
4.2 Materials and Methods 87
4.3 Results 88
4.3.1 Creation of *Pfsub*2 Mini-Genes 88
4.3.1.1 Bio-informatic Analysis of *Pf*SUB2 88
4.3.1.1 Designing *Pfsub*2 Mini-Genes for Parasite Transfections 88
4.3.1.2 RNA Isolation and cDNA Generation 89
4.3.1.3 PCR and Overlap Extension PCR 90
4.3.1.4 Generation & Verification of pARL-mCherry Constructs 91
4.3.2 *Pf*SUB2 Transgenic Parasites 92
4.3.3 Identification of the Domain Targeting *Pf*SUB2 to the Micronemes 93
4.3.3.1 Live Imaging of *Pf*SUB2 Transgenic Parasites 93
4.3.3.2 Co-localisation Studies of *Pf*SUB2 Chimaeric Proteins 94
4.4 Discussion 95
4.4.1 The *Pf*SUB2 Prodomain Is Not Required for Trafficking 95
4.4.2 The *Pf*SUB2 Transmembrane-Spanning Region is Required for Trafficking to the Micronemes 96
4.4.3 Does *Pf*SUB2 Require a Tyrosine Motif for Microneme Targeting? 97
Chapter 5: *P. falciparum* Erythrocyte Binding Antigen 181 99
5.1 Introduction 99
5.1.1 The Erythrocyte Binding Antigen Proteins 99
5.1.2 The Sequence and Structure of *Pf*EBA181 99
5.1.3 The Role of *Pf*EBA Proteins During Invasion 100
5.1.4 Are the *Pf*EBA Proteins Essential or Redundant? 101
5.1.5 Expression of *Pf*EBA181 102
5.1.6 Trafficking of *Pf*EBA175 103
5.1.7 Trafficking of *Pf*EBA181 104
5.1.8 Research Objectives 104
5.2 Materials and Methods 105
5.3 Results 105
5.3.1 Bio-informatic Analysis of *Pf*EBA181 105
5.3.2 Creation of *Pfeba*181 Mini-Genes 105
5.3.2.1 Designing *Pfeba*181 Mini-Genes for Parasite Transfections 105

5.3.2.2 RNA Isolation and cDNA Generation 106
5.3.2.3 PCR and Overlap Extension PCR 107
5.3.2.4 Generation & Verification of pARL-mCherry Constructs 108
5.3.3 *Pf*EBA181 Transgenic Parasites 109
5.3.4 Identification of the Domain Targeting *Pf*EBA181 to the Micronemes 110
5.3.4.1 Live Imaging of *Pf*EBA181 Transgenic Parasites 110
5.3.4.2 Co-localisation Studies of *Pf*EBA181 Chimaeric Proteins 111
5.4 Discussion 112
5.4.1 A Tyrosine Motif Does Not Target *Pf*EBA181 to the Micronemes 112
5.4.2 Is the *Pf*EBA181 Cysteine-Rich Domain Sufficient to Target the Micronemes? 113
Chapter 6: Identifying Binding Partners 116
6.1 Introduction 116
6.1.1 Protein-Protein Interactions 116
6.1.2 Identifying Protein-Protein Interactions 117
6.1.3 Using Phage Display Libraries to Identify Novel Binding Partners 117
6.1.4 Research Objectives 118
6.2 Materials and Methods 118
6.3 Results 118
6.3.1 Preparation of the pET-15b Constructs 118
6.3.2 Verification of the pET-15b Constructs 120
6.3.3 Recombinant Expression of the Histidine-tagged Proteins 121
6.3.3.1 His-tagged *Pf*EBA181 122
6.3.3.2 His-tagged *Pf*SUB2 124
6.3.3.3 His-tagged *Pf*AMA-1 126
6.3.4 Biopanning *Pf*AMA-1 Against Phage Display Libraries 129
6.3.5 Analysis of *Pf*AMA-1 Binding Partners 131
6.3.6 Verification of *Pf*AMA-1 Binding Partners 132
6.3.7 Preparation of the pGEX-4T-2 Constructs 132
6.3.8 Verification of the pGEX-4T-2 Constructs 134
6.3.9 Recombinant Expression of the GST-tagged Proteins 135
6.3.9.1 GST-tagged *Pf*Formin2 135
6.3.9.2 GST-tagged *Pf*CBP 137
6.3.9.3 *In Vitro* Binding Assays 138
6.4 Discussion 140
6.4.1 Utility of Phage Display Libraries 140

6.4.2 Challenges in Recombinant Expression of *P. falciparum* Proteins.....141
6.4.2.1 Expression of Eukaryotic Proteins in Prokaryotic Hosts..... 141
6.4.2.2 Insoluble Proteins and Low Expression Levels..... 142
6.4.2.3 Abnormal Migration of Recombinant Proteins on Polyacrylamide Gels..... 144
6.4.3 *P. falciparum* Formin2 is Unlikely to be a Microneme Protein Escorter.....144
6.4.4 Could *Pf*CBP be an Invasion Protein Escorter? 146

Chapter 7: Discussion 149

7.1 Stage-Specific Expression of Invasion Proteins 149
7.2 Limitations of the pARL-mCherry Expression System..... 151
7.3 Visualisation of Apically-Located Chimaeric Proteins..... 152
7.4 Visualisation of Microneme Localisation 153
7.5 What Does Disrupted Trafficking Look Like?..... 154
7.6 How Are the Micronemes Targeted?..... 155
7.7 Are Escorters Involved in Targeting Apical Organelles? 156
7.8 A Hypothetical Microneme Targeting Model..... 158
7.9 Future Work..... 159

Appendix A – mCherry cloning 160

Appendix B – Microscopy Controls 163

Appendix C – Enlarged Images.....166

Appendix D – Plasmid Maps 168

Appendix E – Biopanning.....171

Appendix F – List of Suppliers.....177

Appendix G – Ethics Clearance 182

Appendix H – Plagiarism Report 183

References 184

List of Figures

Figure 1.1. Life cycle of the malaria parasite, *P. falciparum*. 4
Figure 1.2. Diagram of a *P. falciparum* merozoite. 6
Figure 1.3. Merozoite reorientation and invasion. 7
Figure 1.4. Schematic depiction of *P. falciparum* invasion ligands and erythrocyte receptors. 8
Figure 1.5. Depictions of two Apicomplexan parasites: *Toxoplasma* and *Plasmodium*. 9
Figure 1.6. The *P. falciparum* moving junction. 12
Figure 1.7. Protein export pathways across the parasite membrane. 13
Figure 1.8. Intracellular protein trafficking in *P. falciparum.* 14
Figure 1.9. Involvement of adaptin complexes and clathrin coats during vesicle formation. 16
Figure 2.1. A schematic depicting the principle of overlap extension PCR. 26
Figure 3.1. Expression levels of *Pfama-1* mRNA in various stages of the life cycle. 51
Figure 3.2. The gene and protein structure of *Pf*AMA-1. 53
Figure 3.3. The structure of the *Pf*AMA-1 ectodomain sub-regions I and II. 53
Figure 3.4. The conserved hydrophobic cleft found in the *Pf*AMA-1 ectodomain. 54
Figure 3.5. A model of the *Tg*AMA-1 and *Tg*RON2 interaction at the moving junction. ..55
Figure 3.6. Polymorphic residues on the surface of *Pf*AMA-1. 56
Figure 3.7. Post-translational modification and trafficking of *Pf*AMA-1. 57
Figure 3.8. mCherry plasmid. 58
Figure 3.9. Fluorescence microscopy of live *P. falciparum* parasites expressing mCherry_*crt* and mCherry_*amap.* 59
Figure 3.10. A schematic representing the domains of *Pf*AMA-1, a *P. falciparum* microneme invasion protein. 60
Figure 3.11. A schematic of the mini-genes designed for invasion protein, *Pf*AMA-1. 61
Figure 3.12. Isolated *P. falciparum* 3D7 DNA. 62
Figure 3.13. Creating *Pfama-1* mini-genes by PCR amplification. 63
Figure 3.14. Creating *Pfama-1*ΔPD by overlap extension PCR. 64
Figure 3.15. Restriction enzyme sites of pARL-mCherry plasmid and constructs. 65
Figure 3.16. Restriction enzyme digestion of control mCherry plasmid for verification of mCherry constructs. 66
Figure 3.17. Verification of *Pfama-1* mCherry constructs. 67

Figure 3.18. PCR verification of the *P. falciparum* transgenic parasite line containing the mCherry plasmid. 68
Figure 3.19. PCR verification of *Pf*AMA-1 transgenic parasite lines. 69
Figure 3.20. Fluorescence images of live schizont stage *P. falciparum* transgenic parasites expressing mCherry-tagged *Pf*AMA-1. 70
Figure 3.21. Co-localisation studies using fixed schizont stage *P. falciparum* parasites expressing mCherry-tagged *Pf*AMA-1. 72
Figure 3.22. A summary of the co-localisation studies using mCherry-tagged *Pf*AMA-1. 73
Figure 3.23. A schematic depicting the *Pfama-1* prodomain mini-genes. 73
Figure 3.24. Creating *Pfama-1* prodomain mini-genes by PCR amplification. 74
Figure 3.25. Verification of *Pfama-1* prodomain mCherry constructs. 75
Figure 3.26. PCR verification of transgenic parasite lines expressing *Pf*AMA-1 with prodomain truncations. 76
Figure 3.27. Fluorescence images of live schizont stage *P. falciparum* transgenic parasites expressing mCherry-tagged *Pf*AMA-1 prodomain truncations. 77
Figure 3.28. Co-localisation studies using fixed schizont stage *P. falciparum* parasites expressing mCherry-tagged *Pf*AMA-1 prodomain truncations. 78
Figure 3.29. A schematic showing the primary structure and *Pf*SUB2 proteolytic cleavage sites of *Pf*AMA-1. 79
Figure 3.30. Sequence alignment of *Pf*AMA-1 ectodomain and *Pf*EBA175 C-terminal cysteine-rich domain. 80
Figure 4.1. Schematic of the predicted structural features of subtilases of the malaria parasite. 83
Figure 4.2. mRNA expression of *Pfsub*2 during the asexual intra-erythrocytic cycle. 84
Figure 4.3. A model depicting proteolytic shedding of merozoite coat proteins. 85
Figure 4.4. The gene and protein structure of *Pf*SUB2. 86
Figure 4.5. A schematic representing the domains of *Pf*SUB2, a *P. falciparum* microneme invasion protein. 88
Figure 4.6. A schematic of the mini-genes designed for *P. falciparum* invasion protein, SUB2. 88
Figure 4.7. Isolated *P. falciparum* 3D7 RNA. 89
Figure 4.8. Creating *Pfsub2* mini-genes by overlap extension PCR. 91
Figure 4.9. Verification of *Pfsub2* mCherry constructs. 92
Figure 4.10. PCR verification of *Pf*SUB2 transgenic parasite lines. 93

Figure 4.11. Fluorescence images of live schizont stage *P. falciparum* transgenic parasites expressing mCherry-tagged PfSUB2. 94
Figure 4.12. Co-localisation studies using fixed schizont stage *P. falciparum* parasites expressing mCherry-tagged *Pf*SUB2. 95
Figure 4.13. Summary of *Pf*SUB2 localisation experiments. 97
Figure 4.14. The amino acid residues in the transmembrane-spanning region of *Pf*SUB2. 98
Figure 5.1. Shared structural features of members of the EBL superfamily. 99
Figure 5.2. The gene and protein structure of *Pf*EBA181. 100
Figure 5.3. The proteins of the human erythrocyte membrane. 100
Figure 5.4. mRNA expression levels of *Pfeba*181 during the asexual intra-erythrocytic cycle. 102
Figure 5.5. Alignment of the cysteine-rich regions of *Plasmodium* EBL proteins..... 103
Figure 5.6. The *Pfeba*181 mini-gene. 104
Figure 5.7. A schematic representing the domains of *Pf*EBA181, a *P. falciparum* microneme invasion protein. 105
Figure 5.8. A schematic depicting the mini-genes designed for *P. falciparum* invasion protein, *Pf*EBA181 106
Figure 5.9. Alignment of the extended cysteine-rich regions of EBA175 and EBA181... 106
Figure 5.10. Creating *Pfeba181* mini-genes by overlap extension PCR. 108
Figure 5.11. Verification of *Pfeba181* mCherry constructs. 109
Figure 5.12. PCR verification of *Pf*EBA181 transgenic parasite lines. 110
Figure 5.13. Fluorescence images of live schizont stage *P. falciparum* transgenic parasites expressing mCherry-tagged *Pf*EBA181 111
Figure 5.14. Co-localisation studies using fixed schizont stage *P. falciparum* parasites expressing the original mCherry-tagged *Pf*EBA181. 111
Figure 5.15. Co-localisation studies using fixed schizont stage *P. falciparum* parasites expressing mCherry-tagged *Pf*EBA181 112
Figure 5.16. Sequence alignment of the transmembrane domains and cytoplasmic tails of *Pf*EBA175 and *Pf*EBA181 113
Figure 5.17. Sequence alignment of the cysteine-rich domains of *Pf*EBA181 and *Pf*EBA175. 114
Figure 6.1. A schematic depicting the inhibition of a protein-protein interaction. 116
Figure 6.2. The primer binding sites for the creation of the pET-15b inserts. 119
Figure 6.3. Visualisation of pET-15b plasmid and PCR amplicons for cloning. 120

Figure 6.4. Restriction enzyme sites of pET-15b plasmid and constructs. 121
Figure 6.5. Verification of the pET-15b constructs. 121
Figure 6.6. Expression and immunoblot detection of *Pf*EBA181 proteins 123
Figure 6.7. Expression and purification of His-tagged *Pf*EBA181_ExtCys 124
Figure 6.8. Expression and immunoblot detection of *Pf*SUB2 proteins. 125
Figure 6.9. Expression and purification of His-tagged *Pf*SUB2_JxTail 126
Figure 6.10. Expression of recombinant *Pf*AMA-1 protein. 127
Figure 6.11. Optimisation of *Pf*AMA-1 purification. 128
Figure 6.12. Expression and purification of His-tagged *Pf*AMA-1 129
Figure 6.13. Immunoblot detection of purified His-tagged *Pf*AMA-1. 129
Figure 6.14. A schematic depicting biopanning of *Pf*AMA-1 against a *P. falciparum* phage display library. 130
Figure 6.15. PCR amplification of phage after four rounds of biopanning against *Pf*AMA-1. 131
Figure 6.16. The primer binding sites for PCR amplification of the *Pf*AMA-1 binding partners 132
Figure 6.17. Visualisation of pGEX-4T-2 plasmid and PCR amplicons for cloning. 133
Figure 6.18. Restriction enzyme sites of pGEX-4T-2 plasmid and constructs 134
Figure 6.19. Verification of the pGEX-4T-2 constructs. 135
Figure 6.20. Expression and purification of GST-tagged *Pf*Formin2 136
Figure 6.21. Expression and purification of GST-tagged *Pf*CBP. 137
Figure 6.22. Immunoblot detection of GST-tagged *Pf*CBP 138
Figure 6.23. SDS-PAGE quantitation of proteins for *in vitro* binding assays. 139
Figure 6.24. Secondary structure predictions of *Pf*AMA-1, putative *Pf*Formin2 and putative *Pf*CBP. 143
Figure 6.25. mRNA expression levels of *Pf*Formin2. 145
Figure 6.26. mRNA expression levels of *Pf*CBP 146
Figure 6.27. mRNA expression levels of *Pf*AMA-1 147
Figure 7.1. Comparison of the transcription levels of *P. falciparum* invasion proteins. 150
Figure 7.2. Visual representation of apical localisation. 153
Figure 7.3. Deletion of the trafficking domain results in a localisation change from the rhoptries to the parasitophorous vacuole (adapted from Richard *et al.,* 2009). 155
Figure 7.4. Domains of three *P. falciparum* invasion proteins: *Pf*AMA-1, *Pf*SUB2 and *Pf*EBA181. 156

Figure 7.5. A hypothetical rhoptry targeting model. 157
Figure 7.6. Hypothetical intracellular trafficking pathway to the micronemes. 158
Figure 9.1. Fluorescence images of control experiment using wild-type *P. falciparum* parasites..... 163
Figure 9.2. Co-localisation controls: EBA antibody with and without a fluorophore. 165
Figure 10.1. Co-localisation studies using fixed schizont stage *P. falciparum* parasites expressing mCherry-tagged *Pf*AMA-1. 166
Figure 10.2. Co-localisation studies using fixed schizont stage *P. falciparum* parasites expressing mCherry-tagged *Pf*AMA-1 prodomain truncations. 167
Figure 11.1. The mCherry plasmid. 168
Figure 11.2. The pET-15b plasmid. 169
Figure 11.3. The pGEX-4T-2 plasmid. 170
Figure 12.1. Identification of putative *P. falciparum* Formin2 as a binding partner of *Pf*AMA-1. 175
Figure 12.2. Identification of putative *P. falciparum* Chaperone Binding Protein as a binding partner of *Pf*AMA-1..... 176

List of Tables

Table 2.1. Components for the synthesis of first-strand cDNA. 25
Table 2.2. Components for casting SDS Poly-acrylamide gels. 43
Table 3.1. Expected PCR product sizes of domains within *Pfama*-1 mini-genes. 63
Table 3.2. Expected PCR product sizes of *Pfama-1* prodomain mini-genes. 74
Table 4.1. Expected PCR product sizes of domains within *Pfsub2* mini-genes. 90
Table 5.1. Erythrocyte receptor and *Plasmodium* ligand interactions 101
Table 5.2. Expected PCR product sizes of domains within *Pfeba181* mini-genes. 107
Table 6.1. Expected PCR product and pET-15b construct sizes. 119
Table 6.2. Binding partners identified for His-*Pf*AMA-1 132
Table 6.3. Expected PCR product and pGEX-4T-2 construct sizes. 133
Table 6.4. Quantities of GST- and His-tagged proteins for *in vitro* binding assays. 139
Table 6.5. Summary of Recombinant Proteins. 142
Table 8.1. Primer information for generating *Pfama-1* mini-genes for mCherry constructs. 160
Table 8.2. Primer information for generating *Pfsub2* mini-genes for mCherry constructs. 161
Table 8.3. Primer information for generating *Pfeba181* mini-genes for mCherry constructs. 161
Table 8.4. Primer information for verification of mCherry-expressing transgenic parasites. 162
Table 12.1. Primer information for generating amplicons for pET-15b constructs 172
Table 12.2. Primer information for sequencing of T7 bacteriophage. 173
Table 12.3. Primer information for generating amplicons for pGEX-4T-2 constructs. 174

Nomenclature

A. gambiae	*Anopheles gambiae*
A230	Absorbance at 230 nm
A260	Absorbance at 260 nm
A280	Absorbance at 280 nm
aa	amino acid
ACD	Acid citrate dextrose
AMA	Apical membrane antigen
AP	Adaptor protein, Adaptin
bp	basepair
BSA	Bovine serum albumin
C-terminal	Carboxy terminal
Cat	Catalytic domain
CBP	Chaperone binding protein
cDNA	Complementary DNA
COP	Coat protein complex
Cys	Cysteine rich domain
DBL	Duffy binding-like
DMSO	Dimethyl sulfoxide
DNA	Deoxyribonucleic acid
DNase	Deoxyribonuclease
dNTP	Deoxynucleotide
DPAP1	Dipeptide aminopeptidase 1
DTT	Dithiothreitol
E. coli	*Escherichia coli*
EBA	Erythrocyte binding antigen
EBL	Erythrocyte binding ligand
ED	Ectodomain
EDTA	Ethylenediaminetetraacetic acid
EMBL-EBI	European Molecular Biology Laboratory - European Bioinformatics Institute
ER	Endoplasmic reticulum
ExtCys	Extended region of the cysteine rich rdomain

FH	Formin homology
FV	Food vacuole
GFP	Green fluorescent protein
GP	Glycophorin
GPI	Glycosylphosphatidylinositol
GST	Glutathione S-transferase
HA	Haemagglutinin tag
hDHFR	Human dihydrofolate reductase gene
HRP2	Histidine rich protein 2
HSP	Heat shock protein
IDT	Integrated DNA Technologies
IEM	Immunoelectron microscopy
IRS	Indoor residual spraying
ITN	Insectide treated bed net
JESEBL	EBA181
Jx	Juxtamembrane domain
KIX	Kinase-inducible domain interacting
LB	Luria Broth
MBP	Maltose binding protein
MIC	Microneme protein
mRNA	Messenger RNA
MSP	Merozoite surface protein
NPXY	Tyrosine motif with asparagine and proline residues
N-terminal	Amino terminal
OD	Optical density
OD600nm	Optical density at 600 nm
P. falciparum (or *Pf*)	*Plasmodium falciparum*

PAGE	Polyacrylamide gel electrophoresis
PAN	Plasminogen-apple-nematode
PBS	Phosphate-buffered saline
PC	Pearson's coefficient
PCR	Polymerase chain reaction
PD	Prodomain
PEXEL/HT	Plasmodium export element/host targeting
pfu	Plaque forming unit
PIPES	Piperazinediethanesulphonic acid
PTEX	*Plasmodium* translocon of exported proteins
PV	Parasitophorous vacuole
PVM	Parasitophorous vacuole membrane
RAMA	Rhoptry associated membrane antigen
RAP	Rhoptry-associated protein
RDT	Rapid diagnostic test
RE	Restriction enzyme
RH	Reticulocyte binding-like homologous protein
Rhop	Rhoptry protein (*P. falciparum*)
RNA	Ribonucleic acid
RNase	Ribonuclease
RON	Rhoptry neck protein
ROP	Rhoptry protein (*T. gondii*)
rpm	Revolutions per minute
RT	Reverse Transcriptase
SDS	Sodium dodecyl sulphate
SORTLR	Sortilin-like receptor
SP	Signal peptide
SUB	Subtilisin-like protease
T. gondii (or *Tg*)	*Toxoplasma gondii*
TAE	Tris buffer, acetic acid and EDTA
Tail	Cytoplasmic tail
TB	Terrific Broth
TBS	Tris-buffered saline

TE	Tris buffer and EDTA
tER	Transitional ER
TM	Transmembrane domain
TRAP	Thrombospondin-related anonymous protein
TruncCys	Truncated region of the cysteine rich domain
UD	Unknown domain
UV	Ultraviolet
V	Voltage
WHO	World Health Organisation
Y2H	Yeast two-hybrid
YXXΦ	Tyrosine motif with a bulky hydrophobic amino acid

Units of Measure

˚C	Degree Celsius
cm3	Cubic centimetre
µF	microfarad
µg	microgram
µl	microliter
µm	micrometer
µM	micromolar
mg	milligram
ml	milliliter
mM	millimolar
M	molar
ng	nanogram
nm	nanometer
nM	nanomolar
Da	Dalton
kDa	kiloDalton

Greek Alphabet

α	Alpha	ν	Nu
β	Beta	ξ	Xi
γ	Gamma	ο	Omicron
δ	Delta	π	Pi
ε	Epsilon	ρ	Rho
ζ	Zeta	σ	Sigma
η	Eta	τ	Tau
θ	Theta	υ	Upsilon
ι	Iota	φ	Phi
κ	Kappa	χ	Chi
λ	Lambda	ψ	Psi
μ	Mu	ω	Omega

List of Amino Acids

Single Letter	Three Letter	Full Name
A	Ala	Alanine
R	Arg	Arginine
N	Asn	Asparagine
D	Asp	Aspartic acid
C	Cys	Cysteine
Q	Gln	Glutamine
E	Glu	Glutamic acid
G	Gly	Glycine
H	His	Histidine
I	Ile	Isoleucine
L	Leu	Leucine
K	Lys	Lysine
M	Met	Methionine
F	Phe	Phenylalanine
P	Pro	Proline
S	Ser	Serine
T	Thr	Threonine
W	Trp	Tryptophan
Y	Tyr	Tyrosine
V	Val	Valine

Chapter 1: Introduction

1.1 The Malaria Epidemic

Malaria is an infectious disease, which is transmitted by the female *Anopheles* mosquito and is prevalent along the equatorial belt where the tropical and sub-tropical climates suit the mosquito host. Malaria was responsible for almost half a million deaths in 2015, mostly African children under the age of 5 years (WHO, 2016). There are five species of *Plasmodium* parasites that cause malaria in humans, of which *P. falciparum* is responsible for the most severe form. The devastating effects of malaria are especially noticeable in rural Africa, where communities have limited access to proper healthcare.

Over the last decade there has been a steady decline in malaria related deaths due to increased efforts within various sectors to curb the disease. The latest World Health Organisation (WHO) Malaria Report boasts that malaria mortality has been reduced by nearly 50%: from 864000 deaths in 2000 to 429000 in 2015 (WHO, 2016). These recent advances, however, do not come without their problems.

1.1.1 Challenges in Vector Control

P. falciparum and other *Plasmodium* species (*P. knowlesi, P. malariae, P. ovale and P. vivax*) are transmitted through the bite of an infected female *Anopheles* mosquito. Over the last 15 years, there has been a renewed focus on targeting the mosquito.

Current measures to facilitate vector control include the use of indoor residual spraying (IRS) and insecticide treated bed nets (ITNs). IRS intervention is the application of insecticides inside houses so that when the mosquito rests after her meal, she would come in direct contact with the poisonous substance.

The number of households in malaria endemic regions that have access to ITNs has increased from less than 2% of the population in 2000 to 79% in 2015 (WHO, 2016). Unfortunately, if only households with enough nets to protect every family member are counted, this figure decreases to a mere 42% (WHO, 2016). Access to these ITNs, however, does not necessarily provide protection from infection. There is evidence of misuse of the nets, despite the topic being controversial due to a reliance on self-reported data (Eisele *et al.,* 2011). Reports

indicate that in fishing villages, ITNs are often used for fishing and other household tasks related to obtaining and securing food (McLean *et al.,* 2014; Minakawa *et al*, 2008). Furthermore, there is a concern that ITNs are uncomfortable to use when the temperatures are high (Pulford *et al.,* 2011).

There are four insecticide classes currently used in IRS and ITNs, however, resistance to all of these have been noted (WHO, 2016). Of the 73 malaria-endemic countries monitored by the World Health Organisation, 60 have reported resistance to at least one insecticide and 50 have reported resistance to two or more insecticide classes (WHO, 2016). Since pyrethroids are the only insecticides that are considered safe for human contact, they are used in ITNs. Unfortunately, over 75% of the monitored countries reported resistance in 2015.

Typically, feeding happens at night, with mosquitoes being most active after dusk until a blood meal is consumed (Tirados *et al.,* 2006). To exacerbate the already complicated malaria epidemic, entomologists have noticed a change in the behavioural patterns of the *Anopheles* mosquito. Incidents of infected *A. gambiae* mosquitoes feeding on more than one human per night are almost double that of uninfected mosquitoes (Koella *et al.,* 1998). A review discussing mosquito behaviour and particularly behavioural resistance and adaptation, confirms that certain *Anopheles* species (including *A. gambiae* and *A. funestus*) have started feeding earlier in the day, which would enable them to find a blood meal before people are in the safety of their homes where preventative measures have been put in place (Sokhna *et al.,* 2013).

It is widely believed that the increased prevalence of insecticides in areas where mosquitoes typically feed, through the use of ITNs and IRS, has been the direct cause of the change in feeding behaviour (Sokhna *et al.,* 2013; Tirados *et al.,* 2006).

1.1.2 Challenges in Parasite Control

Despite an ongoing search for a suitable malaria vaccine, there is still no promise of a roll-out in the near future. Vaccine development for *P. falciparum* is complicated due to the ability of the parasite to constantly vary the proteins presented to the host, making it difficult for the immune system to detect the infection (Scherf *et al.,* 2008). In addition, the parasite is able to rapidly invade and replicate within erythrocytes, which are terminally differentiated cells that lack antigen presentation pathways (Hafalla *et al,* 2011).

RTS,S/AS01 is the only vaccine to have completed Phase 3 testing, but further studies are required to obtain meaningful feedback on safety, impact and feasibility (WHO, 2016).

With the growing coverage of the malaria programs, the parasite is able to evolve in response to the selective pressure, which compromises the effectiveness of the diagnostic tools and treatments. The most common rapid diagnostic tests (RDTs) use the histidine-rich protein 2 (HRP2) antigen for the quick diagnosis of malaria-positive patients. Since 2010, some parasites in certain South American countries have been found to lack the HRP2 protein, which causes further problems in identifying and treating patients (WHO, 2016).

Artemesinin is the current gold standard anti-malaria drug and is used in combination therapies to treat patients. Unfortunately, a steady wave of artemisinin resistance has been spreading throughout South East Asia since 2008 (WHO, 2016) and is suspected, but not yet confirmed, in India (Mishra *et al.,* 2015). Despite the growing artemisinin resistance, combination therapies using artemisinin derivatives (artemether-lumefantrine and artesunate-amodiaquine) continue to be effective in killing the parasite and treating patients in Africa (WHO, 2016).

1.1.3 The Way Forward

There are many successes in the global fight against malaria, but there are clear challenges that make it a difficult task. It is thus imperative that malaria eradication strategies are reviewed so that the WHO vision of a 90% reduction in malaria cases and deaths by the year 2030, and the ultimate goal of a "world free of malaria" can be achieved.

This goal is not attainable without introducing a number of novel eradication strategies: we need suitable vector control methods, improved RDTs, new drugs with which to treat patients, as well as drugs to target gametocytes so that transmission to new hosts can be prevented.

1.2 The *P. falciparum* Life Cycle

The *P. falciparum* life cycle (reviewed by Hafalla *et al.,* 2011) is complex and involves both a human and a mosquito host (Figure 1.1). A malaria infection occurs when an infected female *Anopheles* mosquito bites a human host and injects up to 100 sporozoites into the

dermis. These sporozoites will traverse the skin cells and migrate to the liver. Sporozoites move by gliding, which is powered by an actin-myosin motor (Menard, 2001). After traversing several hepatocytes, the sporozoite will infect a final liver cell and replicate by multiple rounds of nuclear divisions and cytokinesis. This process is called schizogony and results in the eventual release of many merozoites into the blood stream, ready to initiate the pathogenic erythrocyte cycle. Each merozoite can rapidly invade a red blood cell through sialic acid-dependent and -independent pathways. Once inside the red cell, each merozoite will develop into a ring, trophozoite and schizont stage over a period of 40 to 48 hours, after which the erythrocyte will rupture releasing as many as 32 new daughter merozoites back into the blood stream. Due to the ongoing lysis of red blood cells and the host's response to the release of parasite toxins, in addition to cytoadherence of the parasites to the endothelium, this is the phase of the life cycle that is directly responsible for the symptomatic presentation of the disease (Miller *et al.,* 2002).

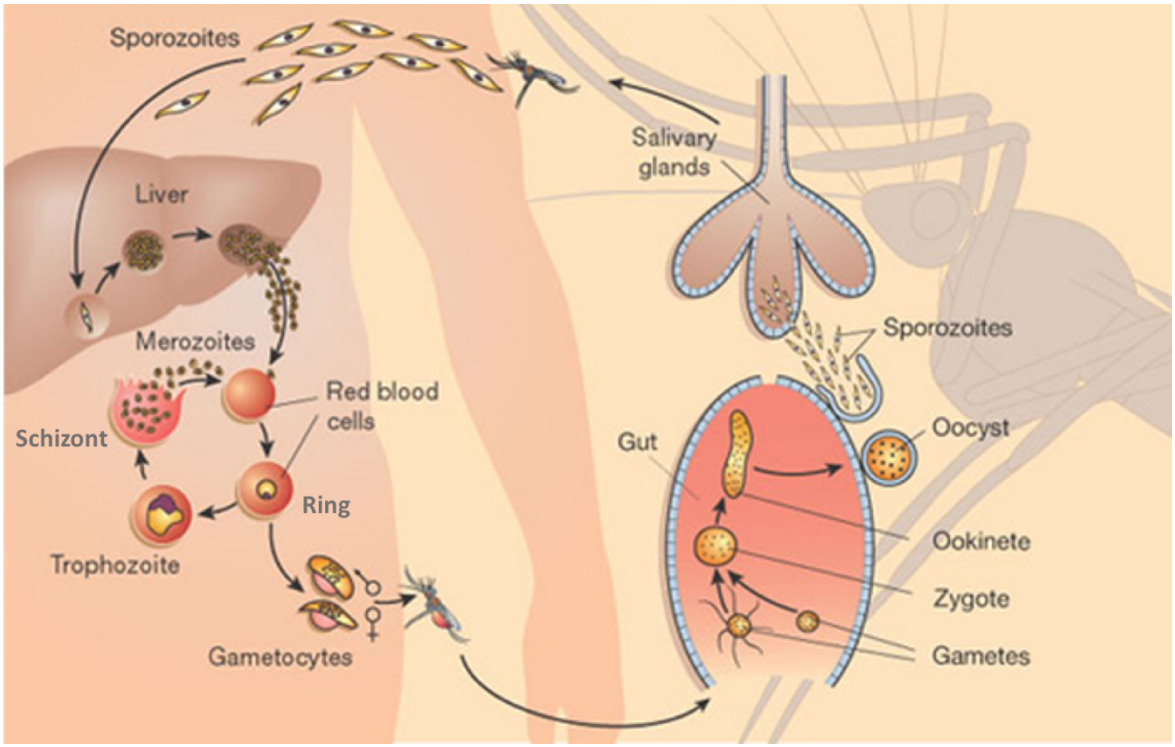


Figure 1.1. Life cycle of the malaria parasite, *P. falciparum*.
A depiction of the life cycle of *P. falciparum* as it occurs in the two hosts: the female *Anopheles* mosquito, and a human host. (taken from Ménard, 2005; with slight modifications).

A number of the trophozoites will not complete the asexual cycle, instead they will continue to form sexual gametocytes (Josling & Llinas, 2015). After twelve to fourteen days, the gametocytes have differentiated into mature male and female gametocytes and are ready to

be taken up by the female *Anopheles* mosquito when she feeds on an infected person. Inside the mosquito gut, the gametocytes will experience a sudden drop in temperature, a change in pH, as well as exposure to new compounds such as xanthurenic acid, which will lead to the gametocytes transforming into gametes. Male gametes produce flagellae, which enable them to move through the blood meal to find and fertilise female gametes. The resultant diploid zygote will form an ookinete, which is able to traverse the mosquito gut wall and form oocysts underneath the basal lamina. New rounds of replication will result in the release of sporozoites, which are stored in the mosquito salivary glands, thus completing the cycle (Miller *et al.,* 2002).

The host immune system's ability to detect infection is severely reduced because the parasite mainly resides in hepatocytes and anucleate red blood cells, and it constantly varies the proteins presented to the host (Scherf *et al.,* 2008). Since red blood cells circulate through the spleen, there is a chance that the parasites can be detected. To overcome this problem, *P. falciparum*-infected red cells are modified during infection (Elsworth *et al.,* 2014a). Adhesive proteins on the surface of these infected erythrocytes cause them to adhere to the walls of blood vessels, allowing them to avoid detection by the spleen (Hafalla *et al.,* 2011).

1.3 Erythrocyte Invasion

The malaria parasite and other protozoans, such as *Toxoplasma,* belong to the phylum Apicomplexa, defined by the presence of a group of specialised secretory organelles called the apical complex (Cowman *et al.,* 2012). These organelles (Figure 1.2) consist of the rhoptries, micronemes and dense granules, and secrete crucial invasion proteins, which utilise sialic acid-dependent and –independent pathways during red blood cell invasion (Cowman & Crabb*.,* 2006).

Erythrocyte invasion by the *P. falciparum* merozoite is complex (reviewed by Cowman *et al.,* 2012), and unfortunately, our understanding of the interactions and events that take place during invasion is largely based on *in vitro* studies (Weiss *et al.,* 2015; Boyle *et al.,* 2013).

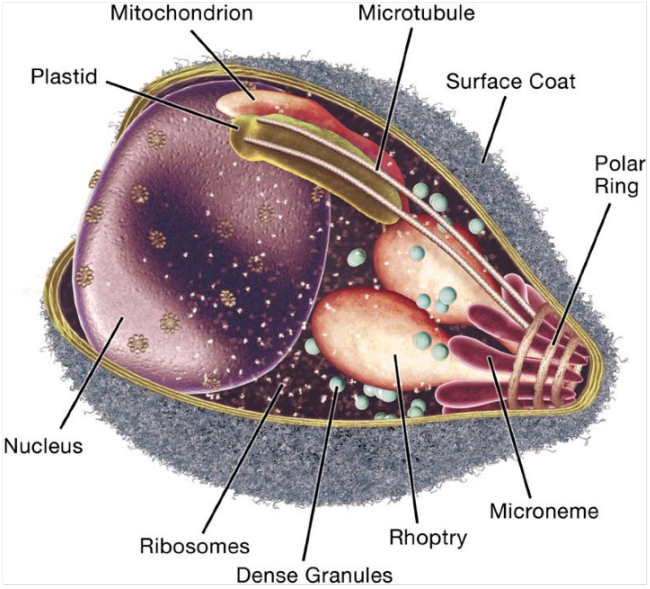


Figure 1.2. Diagram of a *P. falciparum* merozoite.
Merozoites are asexual malaria parasites, which invade host erythrocytes. The secretory organelles – rhoptries, micronemes and dense granules – are visible at the apical end of the parasite. The nucleus is visible at the posterior end. (taken from Cowman & Crabb, 2006).

When the merozoite first comes into contact with the host erythrocyte, a cascade of events takes place (Weiss *et al.,* 2015). Any part of the surface of the parasite is able to form a reversible initial attachment with the red blood cell (Bannister & Dluzewski, 1990), a process which is facilitated by a glycosyl-phosphatidyl inositol (GPI)-anchored protein complex (Li *et al.,* 2004). Merozoite surface proteins (*Pf*MSPs) and other partner proteins make up the GPI-anchored protein complex, which is distributed on the merozoite surface. *Pf*MSP-1 is a major vaccine candidate (O' Donnell *et al.,* 2000; Beeson *et al.,* 2016).

Subsequently, several other invasion proteins, which are stored within the apical organelles, will be released (Gaur *et al.,* 2004; Figure 1.3 A). Apical membrane antigen 1 (*Pf*AMA-1), for example, is secreted from the micronemes to assist in reorientation of the merozoite, since antibodies to inhibit *Pf*AMA-1 blocked the reorientation process (Mitchell *et al.,* 2004).

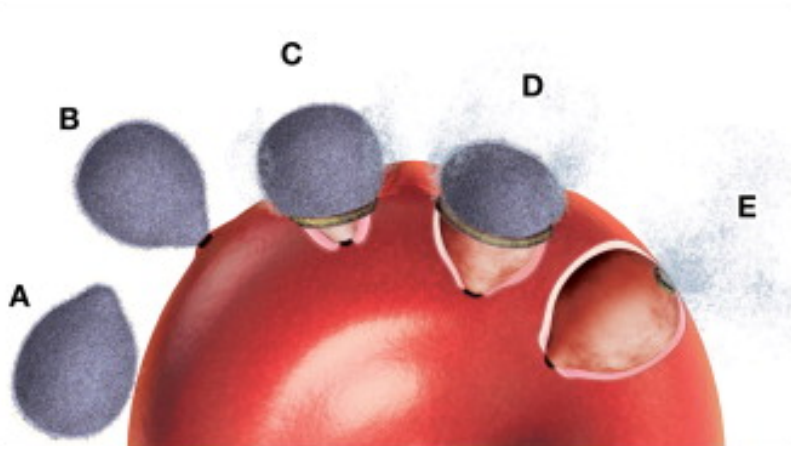


Figure 1.3. Merozoite reorientation and invasion.
A – Initial contact and recognition of surface proteins, followed by reorientation of the merozoite. **B –** Attachment of the apical end of the merozoite to the erythrocyte surface, signified by tight junction formation. **C –** Movement of the tight junction (now called the moving junction) from the apical to the posterior end of the merozoite. **D –** Shedding of the surface coat as the moving junction approaches the posterior end. **E –** The red cell membrane is resealed and the parasitophorous vacuole is formed. (taken from Cowman & Crabb, 2006).

Once the parasite orientation is such that the apical pole points directly to the erythrocyte membrane, invasion can take place. A second interaction between the merozoite and host cell results in permanent attachment and the formation of a tight junction (Figure 1.3 B; Bannister & Dluzewski, 1990). The apical organelles will then release proteins required for invasion.

The parasite has access to alternative invasion pathways, and as such there are several parasite ligands that interact with and bind to various erythrocyte receptors (Figure 1.4; Paul *et al.,* 2015). Most of these proteins have been shown to be dispensable (Paul *et al.,* 2015), which confirms that the parasite can facilitate invasion through any of these ligand-receptor interactions (Beeson *et al.,* 2016).

The Duffy binding-like (DBL) proteins belong to a family of adhesins involved in interacting with and binding to erythrocyte receptors during invasion. The proteins in this family of Erythrocyte Binding Ligands (EBL), contain two N-terminal domains that bind to an erythrocyte membrane receptor (Figure 1.4; Rodriguez *et al.,* 2000). The most well-known of the DBL proteins is Erythrocyte Binding Antigen 175 (*Pf*EBA175), which utilises sialic acid-dependent and -independent pathways to mediate invasion (Duraisingh *et al.,* 2003). An alternative group of ligands is the *Pf*RH (reticulocyte binding-like homologous) family,

consisting of at least 5 proteins, that recognise and bind to receptors on the erythrocyte during invasion (Figure 1.4; Beeson *et al.,* 2016).

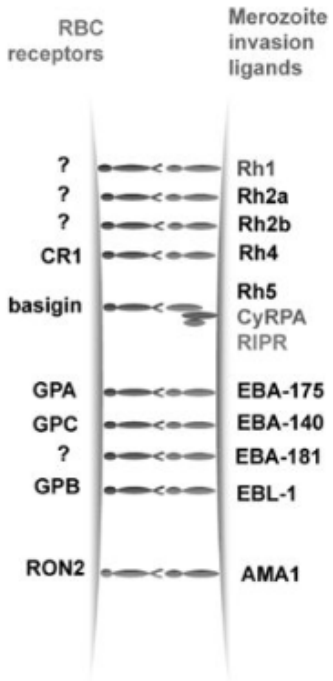


Figure 1.4. Schematic depiction of *P. falciparum* invasion ligands and erythrocyte receptors. This schematic emphasises the large number of ligand-receptor interactions that take place during erythrocyte invasion by a *P. falciparum* merozoite. *Pf*RH5 has been shown to interact with basigin by forming a functional complex with GPI-conjugated protein (CyRPA). *Pf*EBL proteins recognise and bind to glycophorins (GP). *Pf*AMA-1 and several *Pf*RON proteins form a complex, which forms part of the moving junction. (Adapted from Paul *et al.,* 2015).

The parasite's actin-myosin motor drives the merozoite into the host cell through movement of the tight junction from the apical to the posterior end (Figure 1.3 C; Keeley & Soldati, 2004). One of the crucial steps of merozoite entry by this moving junction, is the removal or "shedding" of the parasite ligands from the merozoite surface by proteases such as the Subtilisin-like Protease 2 (*Pf*SUB2; Figure 1.3 D; Harris *et al.,* 2005b; Howell *et al.,* 2003). During invasion, the erythrocyte membrane is reorganised to allow the parasite to be enveloped within a parasitophorous vacuole (PV; Cowman & Crabb, 2006). Once the parasite is within the host cell, the tight junction will be at the posterior end of the merozoite, sealing the parasite within the PV and thus creating a compartment ideal for the development of the parasite, away from the host cell cytoplasm (Figure 1.3 E; Cowman & Crabb, 2006; Beeson *et al.,* 2016). After the parasite has successfully penetrated the host cell, the moving junction will disappear (Aikawa *et al.,* 1978). Replication and division takes place and

results in the release of 16 to 32 new daughter merozoites into the blood stream, ready to invade new erythrocytes.

1.4 The Apical Organelles

Since humans don't have apical organelles, and because they are vital for erythrocyte invasion, these specialised secretory organelles are of significant interest for vaccine and drug development. Because of the similarity in parasite biology, *T. gondii* is often used as a model for researching *P. falciparum* molecular functions (Figure 1.5).

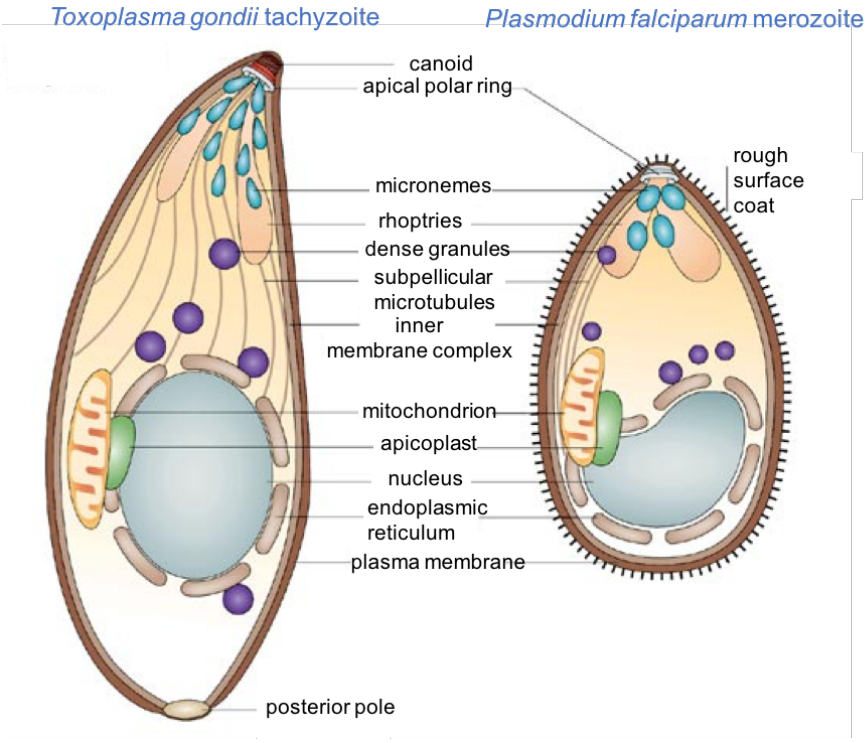


Figure 1.5. Depictions of two Apicomplexan parasites: *Toxoplasma* and *Plasmodium*.
T. gondii tachyzoites (left) and *P. falciparum* merozoites (right) have a similar morphology. The apical organelles, namely the micronemes and rhoptries, are the defining feature of all Apicomplexan parasites. These images are not drawn to scale, the actual length of a tachyzoite is ±10µm while a merozoite is ±1.5µm in length. (adapted from Baum *et al.,* 2006).

1.4.1 The Biogenesis of Apical Organelles

Development of the apical organelles was studied by Margos *et al.,* (2004) using immunofluorescence and electron microscopy. It was determined that apical organelles developed in the final 10 to 12 hours of asexual development of the intra-erythrocytic parasite stage. Formation of the rhoptries occurred first, during nuclear development,

whereas micronemes and dense granules were only fully segmented at the conclusion of nuclear development.

Unlike the mitochondrion or apicoplast (a conserved plastid-like organelle that is found within many Apicomplexans), which divide by binary fission, apical organelles are synthesised *de novo* (Kats *et al.,* 2008). The molecular mechanism of apical organelle formation is not fully understood, but it is believed that the proteins which are destined for these organelles may be involved in their formation (Kats *et al.,* 2008). An example supporting this hypothesis is *P. falciparum* Rhoptry protein 148 (*Pf*Rhop148), which is targeted to the rhoptries prior to invasion, but can be detected before the rhoptries appear (Lobo *et al.,* 2003).

1.4.2 Structural Differences Between the Apical Organelles

Rhoptries are easily identified as two pear-shaped organelles with defined neck and bulb regions (Figure 1.2 and Figure 1.5). They are fully formed and can be visualised by electron microscopy during the mature schizont stage of the asexual parasite (Bannister *et al.,* 2000). Each of the rhoptries is approximately 650 nm long and 300 nm in diameter at the base of the bulb.

Micronemes are smaller structures that occur in clusters around the rhoptry neck (Figure 1.2 and Figure 1.5; Blackman & Bannister, 2001). Each microneme is a thin elongated organelle measuring approximately 165 nm in length and 65 nm in diameter (Bannister *et al.,* 2003).

Dense granules are rounded structures with sizes similar to the micronemes (Bannister *et al.,* 2003). Unlike the micronemes however, dense granules are not concentrated at the apical end of the merozoite (Figure 1.2 and Figure 1.5).

1.4.3 Discharge of Invasion Proteins from the Apical Organelles

Micronemes and rhoptries store proteins required prior to and during invasion. Dense granules, on the other hand, discharge their contents through the sides of the merozoite after invasion of the host red blood cell (Bannister *et al.,* 2003).

After parasite egress from the ruptured erythrocyte, the merozoite is briefly exposed to the host immune system and the exposed surface antigens are vulnerable to detection by antibodies. To avoid detection, the parasite employs a "just-in-time" invasion mechanism (Kats *et al.,* 2008), which means that invasion proteins are discharged, at precise points in time, through the apex of the parasite (Kats *et al.,* 2006; Bannister *et al.,* 2003; Cowman & Crabb, 2006).

This was first noted in studies performed by Carruthers & Sibley (1997) in *T. gondii*, which demonstrated that proteins were discharged from the apically located secretory organelles in an organized fashion: micronemes first, then rhoptries and the dense granules last. Based on these observations, it was hypothesised that these organelles not only discharge proteins in stages, but that proteins are stored according to function (Carruthers, 1999).

Upon contact between the merozoite and host erythrocyte, the *T. gondii* parasite triggers calcium ion release and the discharge of the microneme proteins (Carruthers *et al.,* 1999). Micronemes store adhesins required for initial attachment (Kats *et al.,* 2006) and proteins such as *Pf*AMA-1, which is required for reorientation (Mitchell *et al.,* 2004). Once the apical tip is adjacent to the erythrocyte membrane, the parasite must activate invasion, a process which is triggered by the proximity of the apical end of the merozoite and the host cell (Kats *et al.,* 2008). This process is likely to involve ligands, which are present on the apical tip, such as the DBL family proteins (Duraisingh *et al.,* 2003) and the reticulocyte binding protein homologue (*Pf*Rh; Triglia *et al.,* 2005).

Immediately after this attachment, microneme protein *Pf*EBA175 as well as certain rhoptry neck proteins such as *Pf*RON2 are released (Figure 1.6; Kats *et al.,* 2008). These proteins, together with *Pf*AMA-1, form the tight junction, which facilitates invasion. Rhoptries store a large number of proteins, such as lipids and other proteins required for the creation of the moving junction and the construction of the PV. The neck and bulb of the rhoptry store different proteins (Kats *et al.,* 2006): the neck proteins will be secreted first (perhaps those that are required for junction formation), followed by the bulb proteins (which may be required for PV formation and erythrocyte invasion). There is however evidence that microneme and rhoptry proteins overlap in function (Stubbs *et al.,* 2005).

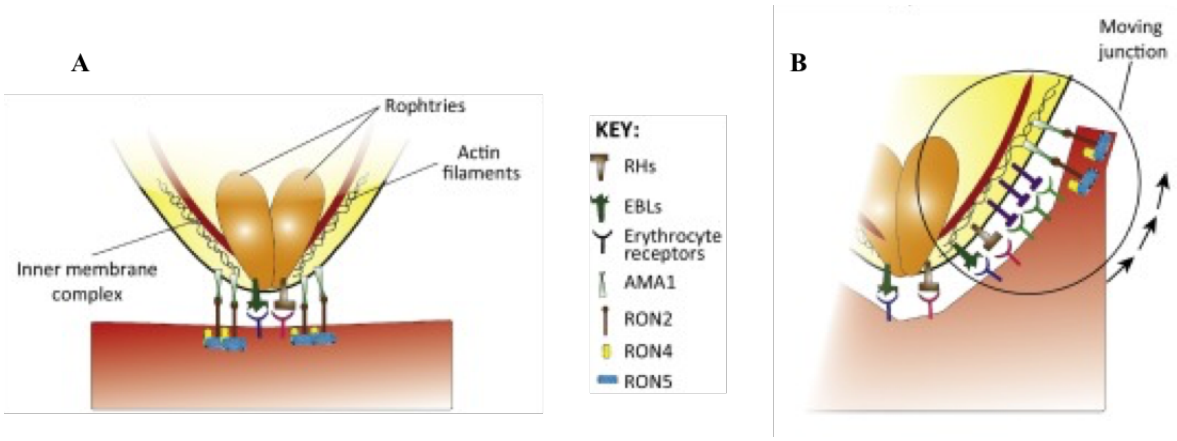


Figure 1.6. The *P. falciparum* moving junction.
A – A schematic depicting the apical tip of a *P. falciparum* merozoite during the initial stages of invasion. The invasion protein complex includes *Pf*AMA-1, *Pf*EBL, *Pf*RH proteins and various proteins from the Rhoptry Neck (RON) family, which bind to erythrocyte receptors. **B –**The Moving Junction facilitates invasion of the parasite into the host erythrocyte. (adapted from Ahouidi *et al.,* 2016).

In *Plasmodium* species, only four dense granule proteins have been identified (Kats *et al.,* 2008). These proteins form part of the channels in the PV, which allow for traffic between the parasite and host erythrocyte (Kats *et al.,* 2006).

1.5 Trafficking Pathways

Transport of malaria proteins can be grouped into two main types: the export of proteins from the parasite into the host erythrocyte, and protein transport within the parasite.

As is true for other eukaryotic cells, *P. falciparum* merozoites require complex molecular machinery to transport proteins in and out of organelles and vesicles before they reach their target destination. Since the publication of the parasite genome (Gardner *et al.,* 2002), it is clear that there are many homologues of the core eukaryotic secretory proteins (for example coat proteins, ribosylation factors, etc), but the specific roles of these components have not been proven experimentally (Tonkin *et al.,* 2006).

1.5.1 Protein Export to the Host Cell

There have been many recent advances in understanding the protein export pathways (Figure 1.7; Tonkin *et al.,* 2006), such as identifying PEXEL/HT (*Plasmodium* export element/host targeting) motif, the signal motif, which is utilised for targeting proteins across the PV membrane (PVM) into the erythrocyte cytoplasm (Marti *et al.,* 2004; Hiller *et al.,* 2004).

The protein export complex, *Plasmodium* translocon of exported proteins (PTEX; De Koning-Ward *et al.,* 2009; Elsworth *et al.,* 2014), recognises the N-terminal sequence motif in these proteins and facilitates transport across the PVM, by recruiting heat shock protein 101 (HSP101; Beck *et al.,* 2014) to unfold proteins prior to entry into a pore in the PVM (Bullen *et al.,* 2012). Proteins are then refolded upon entry into the host cell cytoplasm.

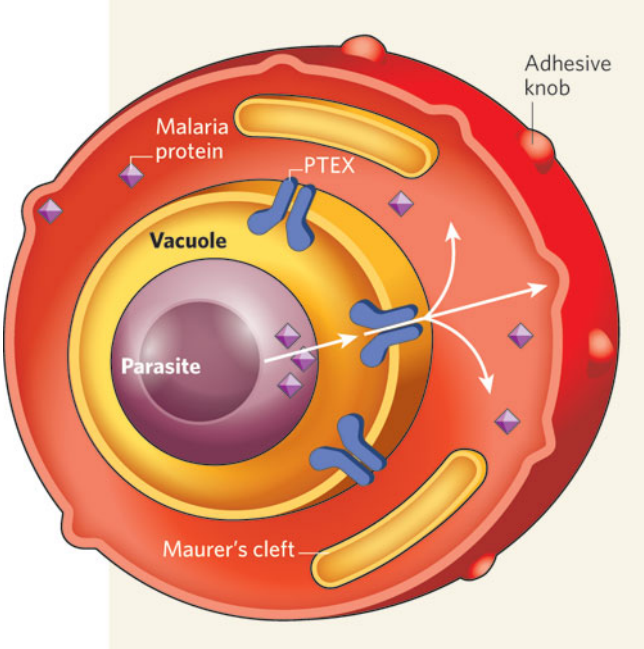


Figure 1.7. Protein export pathways across the parasite membrane.
The *P. falciparum* parasite utilises a protein complex, the *Plasmodium* translocon of exported proteins (PTEX), which allows it to export proteins from the parasite cytoplasm, across the PVM into the erythrocyte cytoplasm. (taken from Reiff and Striepen, 2009).

1.5.2 Internal Protein Trafficking

Targeting signals and trafficking pathways to the apicoplasts (apicomplexan plastids) have been identified (Tonkin *et al.,* 2006). As in other organisms, which have multimembrane-bound plastids, proteins are targeted from the Endoplasmic Reticulum (ER) to the apicoplasts via transit peptides (Waller *et al.,* 2000) to traverse the various membranes of the apicoplasts (Deponte *et al.,* 2012; Figure 1.8).

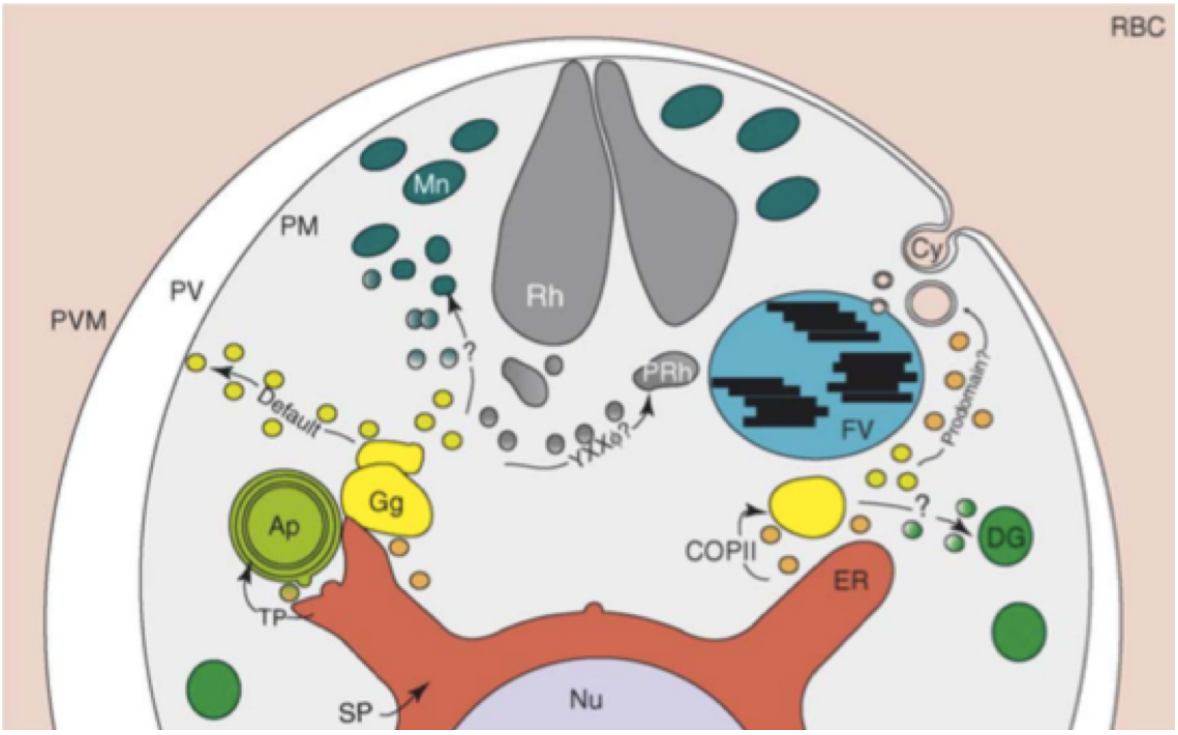


Figure 1.8. Intracellular protein trafficking in *P. falciparum*.
The *P. falciparum* parasite (light grey) is contained within the PV (white) and is separated from the erythrocyte cytoplasm (Cy; peach) by the PV membrane (PVM). The ER (red) is depicted as a perinuclear structure, and the nucleus (Nu; purple) can be found opposite the apical complex. Trafficking to organelles within the early secretory pathways include the food vacuole (blue), apicoplast (Ap; light green) and Golgi (yellow). From the Golgi, tyrosine motifs (YXXΦ) are required for rhoptry (Rh; grey) targeting through pre-rhoptry compartments (PRh) and unknown mechanisms are utilised for microneme (Mn; dark teal) and dense granule targeting (DG; green). (PM- parasite membrane; SP- signal peptide; TP- transit peptide; COPII- coat protein). (taken from Tonkin *et al.,* 2006).

In contrast, targeting proteins to the apical organelles, remains poorly characterised (Deponte *et al.,* 2012; Tonkin *et al.,* 2006). It is estimated that more than 50 proteins are involved in merozoite invasion of the red blood cells: some of which are expressed on the parasite surface, but the majority are stored in the apical organelles (Kats *et al.,* 2008). Since many of these proteins are of major interest for vaccine and drug research, understanding the trafficking mechanisms and pathways to the apical organelles would be invaluable.

1.5.3 Protein Sorting

There are two classical pathways that can be utilised for protein targeting to membrane-bound organelles (Kats *et al.,* 2008). In the first pathway, proteins are synthesised and post-translationally modified before being inserted into the target organelle with the assistance of a chaperone by translocation across the membranes.

The alternative is a classic eukaryotic secretory pathway, which initially directs proteins to an early secretory compartment such as the ER (summarised in Figure 1.8). Most *P. falciparum* invasion proteins utilise this pathway. A conserved short hydrophobic signal sequence is located at the N-terminus of these invasion proteins, and is required to target the proteins to the ER after synthesis (reviewed in Deponte *et al.,* 2012). Following post-translational processing in the ER, proteins targeting the apical organelles have to be sorted from those targeting other organelles such as the apicoplasts and the food vacuole (a lysosomal-like compartment for digesting haemoglobin).

Brefeldin A is a fungal metabolite, which arrests proteins in the ER, thus preventing transport to the Golgi (Klausner *et al.,* 1992). Studies using Brefeldin A treatment have shown that proteins destined for the apical organelles are often directed via the Golgi to their final destination (Kats *et al.,* 2008). However, trafficking mechanisms and pathways beyond the Golgi apparatus remain unclear (Figure 1.8) and there have been no conserved targeting motifs identified for trafficking to the apical organelles.

1.5.4 Transport by Vesicles

Vesicular trafficking is well studied in higher eukaryotes, especially targeting of transmembrane proteins to lysosomes (Dell'Angelica *et al.,* 2000).

An early secretory pathway to the Golgi includes the use of transport vesicles, which are formed by coat protein complex II (COPII; Deponte *et al.,* 2012). Assembly and budding of COPII vesicles occur in the transitional ER (tER), a ribosome-free domain of the ER. Transport of the cargo occurs along microtubules to the cis-Golgi membrane (Figure 1.8).

Another example occurs at the exit face of the Golgi and involves adaptor protein (AP or adaptin) complexes (Robinson, 2004). Adaptins interact with membrane-bound cargo receptors and mediate vesicle formation using clathrin (Pearse, 1976). Signal sequences located within the cytoplasmic tails of cargo proteins are recognised by certain subunits of the AP complexes, which are associated with a particular trafficking pathway (Robinson, 2004). Coat proteins, for example clathrin, are then recruited to interact with the cargo protein and form the structures for vesicle budding (Figure 1.9; Hirst & Robinson, 1998).

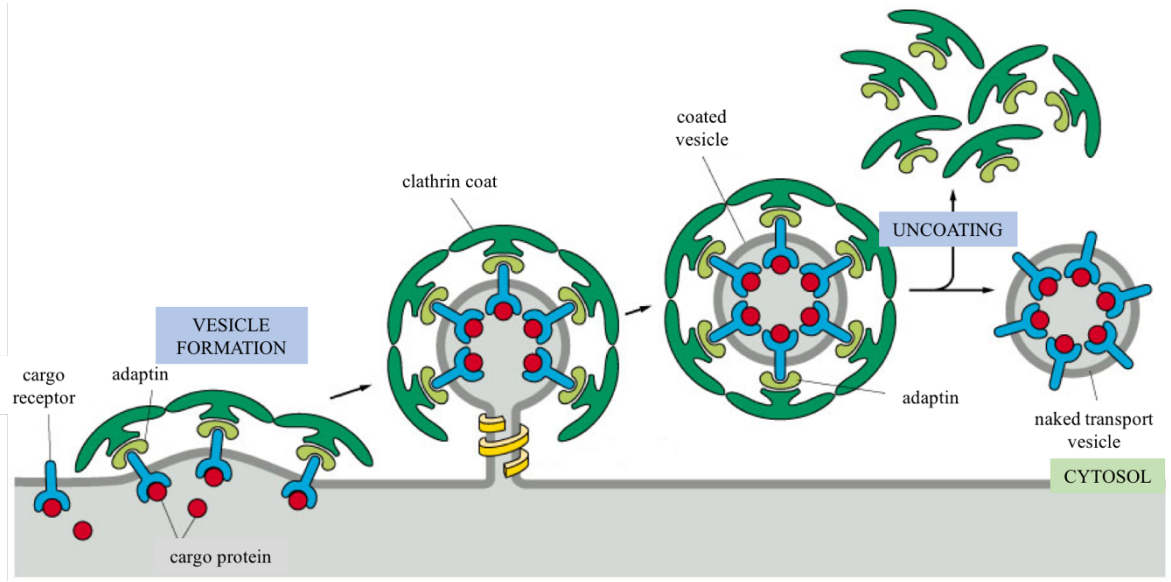


Figure 1.9. Involvement of adaptin complexes and clathrin coats during vesicle formation. Cargo proteins are incorporated into clathrin coated vesicles for transport within the secretory pathways of eukaryotes. Specific adaptor complexes (or adaptins) are recruited, which will direct the cargo-complex to a specific location. (adapted from Sebastian *et al.,* 2006)

1.6 Targeting the Rhoptries

Rhoptry targeting is sensitive to Brefeldin A treatment, which indicates that proteins destined for the rhoptries are trafficked through the ER and Golgi (Howard & Schmidt, 1995).

There are no known requirements for rhoptry targeting in *P. falciparum,* although several proteins possess C-terminal tyrosine motifs. There is evidence in Apicomplexan parasites, *Toxoplasma* (Ngô *et al.,* 2003) and *Plasmodium* (Bhanot *et al.,* 2003), of AP complexes recognising these tyrosine motifs in the cytoplasmic tails of transmembrane proteins and facilitating protein trafficking (Figure 1.8).

There are five known adaptor proteins (reviewed in Huang, 2011), each made up of 4 sub-units that recognise specific sorting motifs: the μ1 subunit of AP-1 recognises YXXΦ, where X is any amino acid and Φ is a bulky hydrophobic amino acid; and β1 recognizes NPXY (Robinson & Bonifacino, 2001). As depicted in Figure 1.9, AP-1 escorters promote clathrin assembly for vesicular budding and transport to the target site (Robinson & Bonifacino, 2001). In *T. gondii*, AP-1 has been implicated in transporting invasion protein, *Tg*RON2 to the rhoptries (Hoppe *et al.,* 2000).

Soluble rhoptry proteins, however, do not contain tyrosine motifs and are targeted to the rhoptries by interactions with other membrane-bound proteins. An example is rhoptry-associated protein 2 (*Pf*RAP2), which relies on an interaction with *Pf*RAP1 to target the rhoptries. In turn, *Pf*RAP1 binds to rhoptry associated membrane antigen (RAMA; (Topolska *et al.,* 2004), which is a GPI-anchored protein in the rhoptries. When the binding site in *Pf*RAP1 is deleted, the *Pf*RAP protein complex is mis-targeted (Baldi *et al.,* 2000).

Another post-Golgi escorter protein, a sortilin-like receptor (SORTLR), has been identified in *T. gondii* and has been implicated in the biogenesis of the micronemes and rhoptries, as well as in the transport of transmembrane proteins, *Tg*ROP (rhoptry protein) and *Tg*MIC (microneme protein) to the apical organelles (Sloves *et al.,* 2012). The *Tg*SORTLR cytoplasmic tail interacts with other proteins involved in trafficking, such as adaptor complexes and clathrin to facilitate vesicle sorting. A putative *P. falciparum* SORTLR homologue (PF3D7_1451800) has been identified recently (Krai *et al.,* 2014), but its function as an escorter protein has not been investigated. *Pf*SORTLR is expressed in the Golgi in late trophozoite and schizont stages, which may suggest a role in targeting proteins to the apical organelles.

1.7 Targeting the Micronemes

As with Apicomplexan rhoptry proteins and mammalian transmembrane proteins, several microneme proteins contain a C-terminal tyrosine sorting motif. In *T. gondii,* MIC2 and MIC6 are targeted to the micronemes using tyrosine motifs in the acidic cytoplasmic tails (Di Cristina *et al.,* 2000). A mutation of the tyrosine motif of *P. falciparum* thrombospondin-related anonymous protein (*Pf*TRAP) causes the microneme protein to be erroneously transported to the parasite surface (Bhanot *et al.,* 2003).

This method of targeting the micronemes is however not utilised for many other microneme proteins. Microneme protein *Pf*EBA175 requires the cytoplasmic tail to function as an invasion protein, but it is not needed for correct delivery to the micronemes (Treeck *et al.,* 2006). Instead, proteins belonging to this family of erythrocyte binding ligands possess a conserved C-terminal cysteine-rich domain, which has been shown to target *Pf*EBA175 to the micronemes (Treeck *et al.,* 2006).

In *T. gondii,* there is evidence of escorter proteins interacting with soluble microneme proteins and facilitating trafficking (Reiss *et al.,* 2001). However, no such trafficking mechanism has been described for *P. falciparum* microneme proteins (Tonkin *et al.,* 2006).

1.8 The Purpose of this Study

Protein trafficking pathways to the rhoptries are starting to be unraveled (Deponte *et al.,* 2012), however, very little is known about how invasion proteins are transported to the micronemes. As discussed previously, the micronemes contain important proteins which are utilised for the initial attachment to the erythrocyte and reorientation of the *P. falciparum* parasite. These fundamental biological processes are critical in preparing the parasite for invasion into the red cell. Studying the microneme-targeting pathway will provide important insights into the biology of *P. falciparum* and may reveal unique features that could be exploited in novel treatment strategies.

1.8.1 Project Aims

- To identify the molecular targeting determinants of three *P. falciparum* micronemal invasion proteins, *Pf*AMA-1, *Pf*SUB2 and *Pf*EBA181.
- To investigate the role of putative escorter proteins in trafficking of invasion proteins.

1.8.2 Project Objectives

1. Assess the molecular determinants for microneme targeting by:
   a. Creating fluorescently-tagged chimaeric proteins containing certain domains of three invasion proteins, *Pf*AMA-1, *Pf*SUB2 and *Pf*EBA181.
   b. Creating transgenic parasite lines, which express these fluorescently-tagged chimaeric proteins.
   c. Performing microscopy studies to determine the localisation of each chimaeric protein within the *P. falciparum* parasite.

2. Investigate novel binding partners/ escorter proteins for the microneme targeting domain of *Pf*AMA-1 by:
   a. Performing biopanning using *P. falciparum* phage display libraries.
   b. Verifying the binding partners using in-solution binding assays.

Chapter 2: Materials and Methods

Suppliers of chemicals and equipment are listed in Appendix F. All reagents were prepared using purified water from the MilliQ® Integral Water Purification System and stored at room temperature unless otherwise stated. Sterilisation of reagents was performed either by autoclaving at 121˚C for 20 minutes or by filtration using 0.8/0.2µm Acrodisc® PF Syringe Filters. *P. falciparum* culturing procedures were conducted in a sterile flow hood.

2.1 Malaria Cultures

2.1.1 Erythrocyte Preparation

Human erythrocytes were utilised for the maintenance of *P. falciparum* cultures. Blood was kindly donated by volunteers in 6ml acid citrate dextrose (ACD) tubes.

Erythrocytes were separated from whole blood by centrifugation at 4400rpm in an Eppendorf 5702R centrifuge for 10 minutes at 4˚C. Plasma and buffy layers which collected above the erythrocytes were aspirated using a sterile Pasteur pipette and pump. The erythrocytes were washed twice with Phospate Buffered Saline (PBS; 10mM Na_2HPO_4, 1.5mM KH_2PO_4, 137mM NaCl, 2.7mM KCl; pH 7.4). The washed erythrocytes were re-suspended in an equal volume of RPMI-1640 incomplete culturing medium (with 50mg Hypoxanthine and 50mg Gentamicin per 1 litre of medium), stored at 4°C and used for no longer than 10 to 14 days.

2.1.2 Maintaining a *P. falciparum* Culture

Plasmodium falciparum 3D7 parasites were kindly donated by the Department of Pharmacy and Pharmacology (University of the Witwatersrand). Parasites were maintained according to the continuous culturing technique first described by Trager & Jensen (1976), with slight modifications. Parasites were cultured in fresh human erythrocytes at a 5% haematocrit, and sealed culture flasks were kept in a humidified incubator at 37˚C. Complete culturing medium (incomplete medium supplemented with 0.5% Albumax and 0.2% $NaHCO_3$) was replenished on a daily basis. The culture flasks were filled with a 2% Oxygen-containing gas mixture (2% oxygen, 5% carbon dioxide, 93% nitrogen). To assess the viability and percentage parasitaemia of the parasite cultures, a blood smear was stained with Rapi-diff haematology stain and viewed using a light microscope at 1000x magnification.

Parasitaemia was determined by calculating the percentage infected erythrocytes out of the total number of erythrocytes.

2.1.3 Synchronising a Culture

To maintain parasites in the same stage of the life cycle, cultures were synchronised by a sorbitol treatment method according to Lambros & Vanderberg (1979). Sorbitol permeabilises the erythrocyte membrane of late stage parasites resulting in lysis, thereby killing the parasite. Because early stage infected erythrocytes are left intact, sorbitol treatment was applied to cultures containing mostly ring stage parasites.

Erythrocytes were harvested by centrifugation of the whole culture at 2500rpm in an Eppendorf 5702R centrifuge for 5 minutes at room temperature. The supernatant was aspirated and 5% D-Sorbitol was added to the parasitised red blood cells in a 10:1 ratio. The cells were carefully suspended in the sorbitol solution and incubated for 5 minutes at room temperature. The intact ring stage-containing erythrocytes were collected by centrifugation as before and placed back into culture as described in 2.1.2.

2.1.4 Freezing and Thawing a Parasite culture

For long term storage of *P. falciparum* parasites, infected erythrocytes were frozen in liquid nitrogen according to standard protocols (Normark, 2008).

Ten millilitres of a 3D7 *P. falciparum* culture at approximately 5% ring stage parasitaemia was subjected to centrifugation at 2500rpm in an Eppendorf 5702R centrifuge for 5 minutes at room temperature to collect the infected erythrocytes. The cells were suspended in an equal volume (0.5ml) of a glycerol freezing solution (28% glycerol in freezing PBS: 123mM NaCl, 83mM Na_2HPO_4, 32mM KH_2PO_4; pH7.4). The mixture was transferred to a 2ml Cryotube, incubated at room temperature for 5 minutes, then stored in liquid nitrogen.

Frozen parasites can be thawed again for use in culture according to standard protocols (Blomqvist, 2008). The cryotube was collected from the liquid nitrogen stores and kept at 37˚C to allow the glycerol-parasite mixture to thaw. The thawed suspension was transferred into a calibrated 15ml tube before adding 100µl 12% NaCl in a dropwise manner. After a 5-minute incubation at room temperature, 10ml 1.6% NaCl was added. The erythrocytes were

collected by centrifugation at 2500rpm in an Eppendorf 5702R centrifuge for 5 minutes at room temperature and re-suspended in 0.9% NaCl and 0.2% glucose. The tube was centrifuged as before, the supernatant aspirated and the collected erythrocytes were transferred into a 25cm^3 culture flask containing prepared erythrocytes up to a final volume of 500µl (10% final haematocrit) and 4.5ml double Albumax complete culturing medium (incomplete medium supplemented with 1% Albumax and 0.2% $NaHCO_3$). The culture flask was gassed as before and kept at 37˚C.

2.2 *Plasmodium falciparum* Nucleic Acid Isolation

2.2.1 Genomic DNA Isolation

Genomic DNA was isolated from 3D7 *P. falciparum* cultures containing mainly late trophozoite and schizont stages using the Hypotonic Lysis method (Cowman *et al.,* 2008).

Five millilitres of a 3D7 *P. falciparum* culture, at approximately 5% late stage parasitaemia, was transferred to a 15ml Nunc tube. The erythrocytes were collected by centrifugation at 2500rpm in an Eppendorf 5702R centrifuge for 5 minutes at room temperature. The supernatant (culturing medium) was aspirated and the erythrocyte pellet (± 250µl) was washed by resuspending the pellet gently in 14ml PBS and centrifuging as before. Four volumes (± 1000µl) of Hypotonic Solution (5mM KH_2PO_4, pH 7.4 using K_2HPO_4) were added to the pellet of erythrocytes to enable lysis. The mixture was carefully resuspended before adding 250µl 18% sodium dodecyl sulphate (SDS), which would denature the parasite proteins.

After 2-3 minutes of incubation at room temperature, 2ml of a 1:1 phenol:chloroform mixture was added. The tube was inverted several times and centrifuged in an Eppendorf 5702 centrifuge at 4400rpm for 10 minutes at 4˚C to separate the genomic DNA from the proteins and other debris. The uppermost layer (aqueous phase) contained the genomic DNA, which was collected and transferred to a new 15ml Nunc tube. To facilitate DNA precipitation, one tenth of a volume of 3M sodium acetate (CH_3COONa; pH 5.0) followed by two and a half volumes ice cold 100% ethanol were added to the aqeous phase. The tube was inverted several times and the contents transferred in 1ml aliquots to 1.5ml Eppendorf tubes, after which they were subjected to at least one hour of incubation at -70˚C, followed

by centrifugation at 13200rpm in an Eppendorf 5415R centrifuge for 30 minutes at 4˚C to collect the DNA.

The supernatant was removed and DNA pellet was resuspended in 600µl Tris-EDTA buffer (TE buffer; 10mM Tris-HCl, 1mM EDTA; pH 8.0). To remove contaminating single-stranded RNA from the sample, 6µl RNAse A was added to the tube, which was incubated in a water bath at 37˚C for 30 minutes. An equal volume (600 µl) of 1:1 phenol:chloroform mixture was added to the tube, which was inverted and centrifuged in an Eppendorf 5415R centrifuge at 10000rpm for 5 minutes at 4˚C. The aqueous phase was carefully transferred into a sterile 1.5ml Eppendorf tube and subjected to a second extraction step using phenol:chloroform as before.

After centrifugation, the aqueous layer (± 600µl) was collected in a new Eppendorf tube. To ensure proper removal of all phenol, the DNA was extracted with 600µl chloroform. After centrifugation as before, the aqueous layer (± 500µl) was collected in a new Eppendorf tube in which the DNA was precipitated as previously described by using 3M sodium acetate and 100% ethanol. The DNA pellet was washed once by adding 1000µl 70% ethanol to the tube and centrifuging at 10000rpm in an Eppendorf 5415R centrifuge for 10 minutes at 4˚C. The ethanol supernatant was discarded, the pellet allowed to air dry and dissolved in 50µl TE buffer. The isolated DNA was stored at 4˚C, or at -20˚C for long term storage.

2.2.2 Parasite RNA Isolation

RNA was isolated from 3D7 *P. falciparum* cultures containing mid to late schizont stages using TRI Reagent® according to the manufacturer's protocol, under sterile conditions and using RNase-free plasticware and solutions.

A 5ml 3D7 *P. falciparum* culture, of approximately 5% synchronised schizont-stage parasitaemia, was transferred to a sterile 15ml Nunc tube. The erythrocytes were collected by centrifugation at 2500rpm in an Eppendorf 5702R centrifuge for 5 minutes at room temperature. The supernatant (culturing medium) was aspirated and the erythrocyte pellet (± 250µl) was re-suspended in 2ml sterile PBS. To lyse the erythrocytes, 20µl of a 5% saponin solution (haemolytic agent) was added to the erythrocyte-PBS mixture. The tube was inverted several times to mix the contents and then incubated at room temperature for 5 minutes. The extracted parasites were collected by centrifugation at 4400rpm (Eppendorf

5702R) for 10 minutes at 4˚C. The supernatant was aspirated and the saponin lysis step repeated if lysis was not sufficient. The parasite pellet was washed twice with 5ml sterile PBS and the supernatant discarded.

To isolate the parasite RNA, 1ml TRI Reagent® was added to the tube according to the manufacturer's instructions. The pellet was disrupted by repeated pipetting, after which the mixture was transferred to a sterile 1.5ml Eppendorf tube and allowed to incubate at room temperature. After 5 minutes, 200µl chloroform was added to the tube and the solution was vortexed. After another 15-minute incubation period at room temperature, the RNA was isolated by centrifugation at 12000rpm in an Eppendorf 5415R centrifuge for 15 minutes at 4˚C.

The RNA-containing aqueous phase (± 500µl) was extracted from the tube using a pipette, taking care to not disturb the lower layers containing DNA and other contaminants. An equal volume of 2-propanol was added to the RNA suspension in a new sterile tube. The RNA was precipitated by incubation for 10 minutes at room temperature followed by centrifugation at 9000rpm in an Eppendorf 5415R centrifuge for 5 minutes at 4˚C. The supernatant was aspirated and the RNA pellet washed with 1ml 75% ethanol. The tube was vortexed briefly, centrifuged as before and the supernatant removed. The pellet was allowed to air dry for 5 to 10 minutes and re-suspended in 20µl nuclease-free water by incubation in a water bath at 60˚C for 15 minutes. Isolated RNA was stored at -70˚C.

2.2.3 Assessment of Isolated Nucleic Acids

2.2.3.1 Agarose Gel Electrophoresis

The quantity and quality of isolated nucleic acids were determined by agarose gel electrophoresis.

A 1% agarose gel was cast by melting 0.5g agarose in 50ml 1x TAE buffer (40mM Tris, 2mM Acetic Acid, 1mM EDTA; pH 8.0), adding 5µl of 10µg/ml ethidium bromide and allowing the mixture to set in a gel casting chamber. Samples of 1-5µl (containing a loading dye) and a DNA base pair standard (size range of 80 to 10 000bp) were loaded on the gel and electrophoresed, in 1x TAE buffer, at 100V for approximately one hour.

The gel was visualised using ultra violet (UV) light in a SynGene GelDoc system and GeneSnap GeneGenius version 6.05 image acquisition software.

2.2.3.2 NanoDrop

The quantity and purity of isolated nucleic acids were determined using a NanoDrop ® ND-1000 Spectrophotometer and ND-1000 software version 3.8.1. Absorbance of the samples was determined at wavelengths of 260, 280 and 230 nm to determine the amounts of DNA, protein and phenol contaminants.

2.3 Polymerase Chain Reaction

Polymerase chain reaction (PCR) was utilised to amplify various inserts required for cloning.

2.3.1 Primer Design

Appropriate primers were designed with the help of the online Integrated DNA Technologies (IDT) OligoAnalyzer Tool version 3.1 to verify that the existence of hairpins, dimers and 3' overlaps would not interfere with the downstream amplification steps. All primer sequences for mCherry clones can be found in Appendix A, and those for pET-15b and pGEX-4T-2 are in Appendix E.

To facilitate directional cloning, primers were designed to include appropriate restriction endonuclease cleavage sites as well as random bases on both sides of the recognition sites to allow for efficient cleavage by the restriction endonucleases (www.neb.com). For pARL-mCherry constructs, a start codon was included in the forward primer and for pET-15b and pGEX-4T-2 constructs, a stop codon was included in the reverse primer.

For overlap extension PCR, primers were designed with overlapping 3' sequence overhangs to allow resultant amplicons to be joined together. The principle of overlap extension PCR is described in section 2.3.4.

Primers were synthesised by Inqaba Biotec, South Africa, and supplied in a lyophilised form. Primers were reconstituted in nuclease free water to a stock concentration of 100µM, from which 10µM working stock dilutions were made. All primer stocks were stored at -20˚C.

2.3.2 cDNA Synthesis

First-strand cDNA was synthesised from the isolated total RNA (see 2.2.2) using the SuperScript® III First-Strand Synthesis System for Reverse Transcriptase (RT) PCR according to the manufacturer's protocol.

Approximately 2µg total RNA (determined by NanoDrop® ND-1000) was combined with an appropriate gene-specific reverse primer, a deoxynucleotide (dNTP) solution mix and nuclease-free water in a sterile 0.6ml PCR tube, according to Table 2.1. The tube was incubated at 65˚C for 5 minutes to linearise the RNA; followed by 1 minute incubation on ice to cool the tube before the addition of the RT enzyme.

To complete the reaction, First-Strand Buffer, DTT, an RNase inhibitor and SuperScript® III RT enzyme were added to the tube containing the RNA solution. The contents were mixed thoroughly by pipetting and subjected to incubation at 55˚C for one hour followed by inactivation of the enzyme for 15 minutes at 70˚C. The synthesised cDNA was stored at -20˚C.

Table 2.1. Components for the synthesis of first-strand cDNA.

Step	Component	Amount per reaction	Final concentration per reaction
1	Total RNA	X µl	1-5µg
	10µM Reverse primer	2µl	1µM
	10mM dNTP mix	1µl	0.5mM
	Nuclease-free H_2O	X µl	
	Total volume = 13µl		
2	5X First-Strand Buffer	4µl	1X
	0.1 M DTT	1µl	5mM
	40U/µl RiboLock RNase Inhibitor	1µl	40U
	200U/µl SuperScript® III RT enzyme	1µl	200U
	Final volume = 20µl		

2.3.3 PCR Amplification of *P. falciparum* Mini-genes/ Domains

High fidelity PCR reactions were carried out using Phusion® Flash High Fidelity PCR Master Mix, which is a unique blend of *Taq* DNA Polymerase and a thermostable DNA polymerase with proofreading activity, enhancing the accuracy during amplification. PCR reactions of 20-50µl were made up by combining PCR master mix (half of the reaction volume), 100 to 200ng DNA or 1µl cDNA template, 0.5µM of each forward and reverse

primer and nuclease free water in a sterile nuclease free 0.6ml PCR tube, and were carried out according to the manufacturer's specifications in a thermocycler.

The PCR parameters for all reactions can be found in Appendix A and Appendix E. Amplification of the inserts required for cloning was performed in a two-step process: 5 cycles allowing for the binding of the *P. falciparum* specific region of the primers, followed by 30 cycles allowing for the amplification of the full region of interest. PCR products were visualised by agarose gel electrophoresis as described in 2.2.3.1 and stored at -20˚C.

2.3.4 Overlap Extension PCR Amplification

To eliminate an internal region or join two amplified domains together to form mini-genes, an overlap extension PCR (Ho *et al.,* 1989) was used (Figure 2.1).

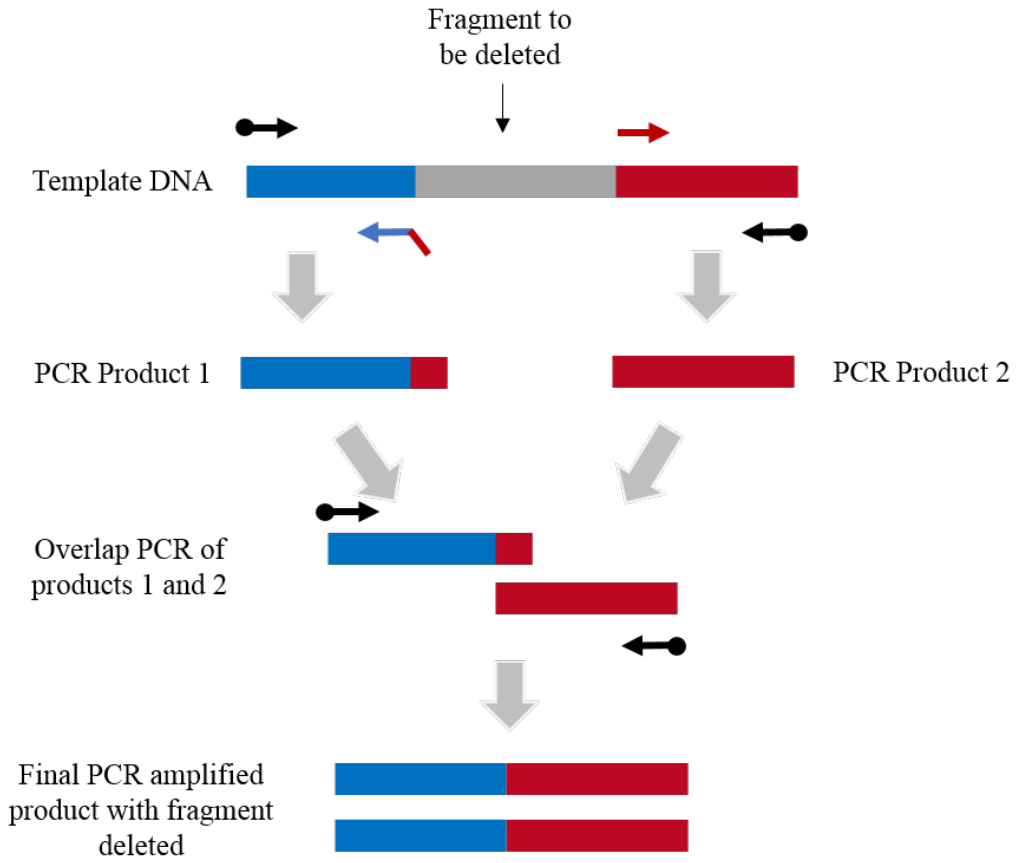


Figure 2.1. A schematic depicting the principle of overlap extension PCR.
Black arrows (➞) indicate primers with restriction endonuclease cleavage sites (●), which are used to fuse Product 1 and Product 2 together in the overlap PCR step. The internal reverse primer is depicted in blue (←) and has an 3' overhang (depicted in red; ←), which is complementary to part of Product 2.

High fidelity PCR amplification was carried out as described in 2.3.3, utilising oligonucleotide primers to generate fragments with overlapping ends. The resultant fragments were then fused by an annealing step of the overlapping ends, whereby the 3' overlap served as a primer for the 3' extension of the complementary strand. Amplification of the final product was performed by PCR.

2.4 Plasmid Isolation for Cloning

An alkaline extraction procedure (Birnboim & Doly, 1979) was followed to isolate the following plasmids required for cloning experiments: pARL-mCherry-*amap* (original plasmid was kindly donated by J. Przyborski & modified to include the *ama-1* promoter by Wepener, 2014), pET-15b and pGEX-4T-2. Plasmid maps can be found in Appendix D.

A culture of 5ml sterile Luria Broth (LB; 1% (w/v) Tryptone, 1% (w/v) NaCl, 0.5% (w/v) yeast extract, 10mM Tris-HCl; pH 8.0) in a 50ml sterile Erlenmeyer flask was supplemented with 100µg/ml ampicillin and inoculated with a scraping from a 60% glycerol stock of *E. coli* XL10 cells, containing the appropriate plasmid. The inoculated broth was incubated at 37˚C for 16 to 18 hours in a shaking incubator (250rpm).

To assess the cell growth, the optical density (OD) of a sample of the culture was determined at 600nm (OD_{600nm}) using a spectrophotometer. Exponential phase was identified when the culture OD_{600nm} reached approximately 1.0. While a final OD_{600nm} ranging from 3.0 to 6.0 was preferred to indicate stationary phase, an $OD_{600nm} > 2.0$ was accepted for bacterial cells containing pARL-mCherry plasmid, which typically exhibited poor growth.

To harvest the cells, the culture was transferred to a 15ml Nunc tube and centrifuged for 10 minutes at 4400rpm in an Eppendorf 5702R centrifuge at 4˚C. The supernatant was discarded, the pellet completely re-suspended in 500µl ice cold Resuspension solution (50mM glucose, 10mM EDTA, 25mM Tris-HCl; pH 8.0) and allowed to incubate for 5 minutes at room temperature. To lyse *E. coli*, 1000µl of a freshly prepared Lysis solution (0.2M NaOH, 1% SDS) was added to the suspension and gently mixed by inversion of the tube. After a 5-minute incubation on ice, 750µl ice cold Neutralisation solution (1.6M potassium acetate and 3.2M acetic acid, pH 4.8) was added; the tube was inverted to facilitate

thorough mixing and neutralisation of the lysis action and the mixture was incubated on ice for 5 minutes.

To separate the extracted plasmid from the *E. coli* DNA and cell debris, the tube was centrifuged at 4400rpm for 10 minutes at 4˚C until the flocculate was pelleted and the supernatant was clear. The plasmid-containing supernatant was transferred to four 2ml Eppendorf tubes.

An equal volume (500µl) of a 1:1 phenol:chloroform mixture was added to the suspension in each tube; the tube was inverted several times and centrifuged in an Eppendorf 5415R centrifuge at 13200rpm for 5 minutes at 4˚C. The plasmid-containing aqueous phase (± 450µl) in each tube was transferred to two new sterile 1.5ml Eppendorf tubes, to which 2.5 volumes (± 1125µl) ice cold 100% ethanol was added to precipitate the plasmid DNA. Following a 5-minute incubation period at room temperature, the plasmid DNA was pelleted by centrifugation at 13200rpm for 10 minutes at 4˚C. The supernatant was discarded and the DNA pellets allowed to air dry for approximately 10 minutes. The plasmid pellets were combined by resuspension in a total volume of 400µl TE buffer.

To remove contaminating RNA, 4µl RNase A was added to the tube, which was incubated for 1 hour at 37˚C. A volume of 40µl ice cold Neutralisation solution followed by 500µl of a 1:1 phenol:chloroform mixture were added to the tube. The tubes were inverted to ensure the contents were properly mixed before centrifugation at 13200rpm for 5 minutes at 4˚C. The DNA containing aqueous phase (± 400µl) was carefully transferred to a new Eppendorf tube, to which 500µl chloroform was added. The tube was inverted and centrifuged as before, the aqueous phase was transferred to a new 2ml Eppendorf tube and the DNA precipitated using sodium acetate and 100% ethanol as described in 2.2.1.

The DNA pellet was air dried for 15 minutes at room temperature and re-suspended in 30 to 50µl TE buffer. DNA quality and quantity were determined according to 2.2.3. Plasmid DNA was stored at 4˚C or -20˚C for long term storage.

2.5 Preparation for Cloning

2.5.1 Restriction Enzyme Digests of PCR Products

To prepare the inserts (2.3.3) for cloning, PCR products were purified using the Macherey-Nagel NucleoSpin® PCR Clean-up Kit according to the manufacturer's instructions and eluted in 15-50µl nuclease-free water.

If non-specific DNA fragments of larger than 80bp were present in the sample, PCR products were purified by a gel extraction procedure using the Macherey-Nagel NucleoSpin® Gel Extraction Kit according to the manufacturer's instructions. Samples (approximately 50µl) were separated by agarose gel electrophoresis according to 2.2.3.1. Using a sterile scalpel, the DNA fragment of the correct size was visualised under UV light, excised from the gel and purified according to the manufacturer's instructions.

The purified product was digested with appropriate FastDigest® restriction endonucleases (Appendix A and E) according to the manufacturer's specifications. A second purification with the Macherey-Nagel NucleoSpin® PCR Clean-up Kit ensured that the enzymes and salts were removed prior to cloning. Digested products were eluted in 15µl nuclease free water, quantitated according to 2.2.3 and stored at -20˚C.

2.5.2 Restriction Enzyme Digests and Alkaline Dephosphorylation of Plasmids

To prepare the isolated plasmids (2.4) for cloning, digestion with appropriate FastDigest® restriction endonucleases (Appendix A and E) was performed according to the manufacturer's specifications. To prevent the linearised plasmid from re-ligating, dephosphorylation using FastAP™ Thermosensitive Alkaline Phosphatase was performed according to the manufacturer's instructions.

Subsequently, purification was performed using the Macherey-Nagel NucleoSpin® Gel and PCR Clean-up Kit according to the manufacturer's instructions. Linearised and dephosphorylated plasmid was eluted in 15-50µl nuclease free water, quantitated according to 2.2.3 and stored at -20˚C.

2.5.3 Creation of Chemically Competent XL10 and DH5α Cells

Chemically competent bacterial cells were created according to Seidman *et al.,* (1997), with slight modifications. To prepare the bacterial culture, a two-step growth technique was utilised. XL10 or DH5α *E. coli* cells were used to inoculate a 10ml starter culture according to 2.4. The culture was incubated at 37˚C in a shaking incubator (250rpm) for 16-18 hours. Once stationary phase (OD_{600nm} >2.0) was reached, the 10ml culture was used to inoculate a 100ml LB grow in a 1000ml Erlenmeyer flask (supplemented with 100µg/ml ampicillin). The culture was incubated at 37˚C shaking at 250rpm for 90 minutes until an OD_{600nm} reading of 0.3-0.6 was achieved. The cells were immediately stored on ice.

The cells were harvested by centrifugation in a Beckman Coulter Avanti® J-E centrifuge at 6000rpm for 10 minutes at 4˚C in a 250ml centrifuge tube. The supernatant was discarded and the bacterial pellet was re-suspended in 10ml ice cold sterile PIPES Buffer (15% glycerol (v/v), 100mM $CaCl_2$, 10mM 1.4-piperazinediethanesulphonic acid; pH 7.0 with NaOH). The suspension was incubated on ice for 20 minutes and centrifuged as before. The bacterial cells were re-suspended in 2ml cold PIPES Buffer and stored as 100µl aliquots in 1.5ml Eppendorf tubes at -70˚C.

2.6 Cloning

2.6.1 Ligation Reaction

Digested and purified vector and insert DNA were quantified according to 2.2.3.1 on a 1% agarose gel against a mixed range of base pair standards.

A total of 200ng vector and insert DNA were combined in a 600µl PCR tube according to a 5:1 insert to vector ratio as determined by the online In-Fusion® Molar Ratio Calculator. A 20µl ligation reaction was performed using the Rapid DNA Ligation Kit according to the manufacturer's protocol, with a 30-minute incubation at 16˚C. A control reaction of vector DNA and water instead of insert DNA was included.

2.6.2 Transformation

Once ligation was completed, competent *E. coli* XL10 or DH5α cells (2.5.3) were transformed with 100ng of the vector construct. For the large pARL-mCherry plasmid

constructs, XL10 cells were preferred and for smaller pET-15b and pGEX-4T-2 plasmid constructs, DH5α bacterial cells were used.

A 100µl aliquot of the chemically competent cells per vector construct was thawed on ice. Half of the ligation reaction (10µl) was added, the cells mixed gently by tapping and incubated on ice for 30 minutes. Heat shock was conducted in a water bath at 42˚C for 90 seconds followed by a 5-minute incubation on ice. The cells were gently spread on 1.5% agar plates containing 100µg/ml ampicillin. To ensure an even spread of colonies, two plates were prepared: a "low" plate containing 20% of the cell mixture and a "high" plate" containing the rest of the cells. The plates were allowed to dry for 10 minutes at room temperature, inverted and incubated at 37˚C for 18-20 hours.

2.6.3 Creating Glycerol Stocks of Transformed Bacterial Cells

After 18-20 hours of incubation at 37°C, transformed bacterial colonies were picked from agar plates using a sterile pipette tip and transferred to a BD Falcon™ Round-bottom Snap Cap tube containing 2ml LB medium supplemented with 100µg/ml ampicillin (and 50µg/ml chloramphenicol for Rosetta™ 2(DE3) cells). The inoculated broth was incubated at 37˚C for 16 to 18 hours in a shaking incubator (250rpm).

To store the cells for future use, 500µl of the culture was transferred to a 2ml Eppendorf tube containing 500µl of a sterile 60% glycerol solution (made with milliQ water and filter sterilised). The tube was inverted several times to ensure proper mixing of the glycerol and the bacterial culture; and the samples were stored at -70°C.

2.6.4 Verification of Clones

2.6.4.1 Plasmid Isolation

To verify that prepared DNA fragments were correctly inserted into plasmid vectors, a Macherey-Nagel NucleoSpin® Plasmid kit was used to extract plasmid constructs. The principle of the kit is similar to that of the alkaline extraction procedure discussed in 2.4, but includes the use of a silica membrane to concentrate and purify extracted plasmid. This method is ideal for the isolation of plasmid from small culture volumes (1-5ml).

To prepare the bacterial culture, 2ml sterile LB was transferred to a 14ml BD Falcon™ Round-bottom Snap Cap tube and was supplemented with 2µl 100mg/ml ampicillin. The broth was inoculated either with a scraping from a 60% glycerol stock of *E. coli* XL10 cells, containing the appropriate plasmid or directly from a single bacterial colony growing on an agar plate. The inoculated broth was incubated at 37˚C for 16 to 18 hours in a shaking incubator (250rpm).

To harvest the cells, the culture was transferred to a 2ml Eppendorf tube and centrifuged in an Eppendorf 5415R centrifuge for 5 minutes at 13200rpm at 4˚C. Plasmid extraction was performed according to the kit specifications. The quality and quantity of the isolated plasmid was determined by gel electrophoresis or NanoDrop® according to 2.2.3 and samples were stored at 4˚C or -20˚C for long term storage.

2.6.4.2 Restriction Enzyme Digest Analysis of Clones

Restriction enzyme digests were performed on extracted plasmids after transformation to verify that inserts of the correct size were ligated into the plasmid backbone. Reactions were set up using appropriate FastDigest® restriction endonucleases (described in the results chapters) according to the manufacturer's instructions. Empty plasmid vectors were used as controls. Digested DNA fragments were analysed by gel electrophoresis according to 2.2.3.1.

2.6.4.3 Sequence Verification of Clones

Plasmid constructs containing inserts of the correct sizes were sent to Inqaba Biotec™ (South Africa) for sequencing to verify that inserts were error free and in-frame.

2.7 Creating *P. falciparum* Transgenic Parasites

2.7.1 Preparation of pARL-mCherry Plasmids for Transfection

To isolate large amounts of plasmid (>100µg) for the transfection of *P. falciparum* parasites, a NucleoBond® Xtra Maxi Plus (Macherey-Nagel) kit was used. Bacterial cells were lysed using a NaOH/ SDS lysis method similar to 2.4 and plasmid isolation and purification was performed using a unique silica-based anion-exchange resin.

To prepare the bacterial culture, a two-step growth technique was utilised. A 5ml starter culture was prepared according to 2.4 and incubated at 37˚C in a shaking incubator (250rpm) for approximately 8 hours. Once exponential phase (OD_{600nm} ~ 1.0) was reached, 1ml samples were used to inoculate two 250ml LB cultures in 1000ml Erlenmeyer flasks (supplemented with ampicillin to a final concentration of 100µg/ml). These cultures were incubated at 37˚C shaking at 250rpm for 16 to 18 hours.

Cultures were assessed by spectrophotometry as described in 2.4.1. If bacterial cell growth was satisfactory (OD_{600nm} > 2.0), the cells were harvested by centrifugation in a Beckman Coulter Avanti® J-E centrifuge at 6250rpm for 15 minutes at 4˚C in two 500ml centrifuge tubes.

The plasmid extraction was performed according to the manufacturer's low-copy plasmid purification protocol. To desalinate and concentrate the plasmid eluate, NucleoBond® Finalizers were used according to the kit instructions. The quality and quantity of the isolated plasmid were determined by gel electrophoresis (2.2.3.1). Samples were stored at -20˚C.

On the day prior to transfection, approximately 150µg (at least 100µg) of isolated plasmid was extracted using a phenol:chloroform procedure, followed by a standard sodium acetate precipitation step in a 2ml Eppendorf tube (see 2.4). The tube was incubated at -70˚C overnight to allow the DNA to precipitate.

On the day of the transfection, the DNA was pelleted in an Eppendorf 5415R centrifuge at 13200rpm for 30 minutes at 4˚C. The pellet was washed once with 1ml 70% ethanol, air dried for approximately 15 minutes in a laminar flow cabinet and re-suspended in 30µl sterile TE buffer.

2.7.2 Preparation of Erythrocytes for Transfection

Fresh whole blood was collected from a human volunteer in a 6ml ACD tube. The erythrocytes were collected by centrifugation in an Eppendorf 5702R centrifuge for 10 minutes at 4˚C. The plasma and buffy coat were aspirated and the erythrocytes were used immediately for the transfection.

2.7.3 The Transfection Protocol

Transfection was carried out in a laminar flow cabinet under sterile conditions. A volume of 370µl pre-warmed Cytomix (37˚C; 120mM KCl, 0.15mM $CaCl_2$, 8.7mM K_2HPO_4, 1.3mM KH_2PO_4, 25mM Hepes, 2mM EGTA, 5mM $MgCl_2$; pH 7.6), followed by 200µl human erythrocytes (see 2.7.2), was added to the 2ml Eppendorf tube containing the 30µl plasmid DNA (see 2.7.1). The suspension was mixed carefully by pipetting, transferred to a 2mm BioRad GenePulser® cuvette and electroporated in a Bio-Rad GenePulse Xcell™ electroporator, at 310 V, with a resistance of 950 µF for no more than 15 milliseconds.

The electroporated erythrocytes were transferred to a $25cm^3$ culture flask, containing 5ml complete culturing medium and ring-stage parasites at a final concentration of 1%. The culture flask was gassed and incubated as described in 2.1.2.

2.7.4 Maintaining *P. falciparum* Transgenic Parasites

The *P. falciparum* transgenic parasites were cultured daily as described in 2.1.2. During the next ring cycle, 48 hours after transfection, 2nM of WR99210 (10mM WR99210 stock in DMSO was used to prepare a 10µM working stock in incomplete culturing medium; used 1µl working stock in a 5ml culture) was administered to the cultures on a daily basis. Parasites which had taken up the pARL-mCherry plasmid expressed the human Dihydrofolate Reductase gene (hDHFR), which confers resistance against WR99210. Parasites lacking the plasmid died from compound exposure within approximately 7 days.

Parasites were maintained under selective pressure using WR99210, however, the culturing technique was adapted to only culturing on alternate days until parasites were visible again (20-60 days), after which daily culturing was resumed. As soon as a ~3% ring-stage parasitaemia was established, glycerol stocks of the transgenic parasites were prepared according to 2.1.4.

2.7.5 Verification of Transfection

2.7.5.1 DNA Isolation from *P. falciparum* Transgenic Parasites

To verify that the transgenic *P. falciparum* parasites had taken up the plasmid construct, parasite DNA was isolated (Tirasophon *et al.,* 1991, Vu *et al.,* 1995) and PCR analysis was performed.

One millilitre of a trophozoite stage culture (>3% parasitaemia) was transferred to a 2ml Eppendorf tube, to which 1ml Lysis Buffer (34mM NaCl, 1% Triton-X-100, 1.2mM EDTA) was added. The tube was vortexed briefly then centrifuged in an Eppendorf 5415R centrifuge at 13200rpm for 10 minutes at 4˚C. The supernatant was discarded, 100µl Tris Buffer (10mM Tris-HCl, 50mM KCl; pH 8.3) added to the pellet and the tube vortexed. The parasites were collected by centrifugation at 13200rpm in an Eppendorf 5415R centrifuge for 5 minutes at 4˚C and the supernatant discarded. The pellet was suspended in 100µl PCR Buffer (10mM Tris-HCl, 50mM KCl, 3mM $MgCl_2$; pH 8.8) and subsequently boiled for 10 minutes to extract the DNA. For long term storage of the DNA, optional phenol:chloroform/ chloroform clean-up steps followed by ethanol precipitation according to 2.2.1, were included. The aqueous phase was collected and stored at 4°C in a 1.5ml Eppendorf tube.

PCR analysis was performed according to 2.3.3 (Waters *et al.,* 1997), using 1µl of the DNA sample and pARL-mCherry vector specific primers (Appendix A). *P. falciparum* 3D7 DNA was included as a negative control and original plasmid DNA (2.7.1) served as a positive control. GoTaq or DreamTaq polymerase was used for these PCR reactions because high fidelity amplification was not necessary. For long term storage, an optional ethanol precipitation could be performed on the DNA samples.

2.8 Microscopy of Live *P. falciparum* Transgenic Parasites

To verify that transgenic parasites were expressing the mCherry-tagged proteins and to localise these proteins, fluorescence microscopy was performed. To prepare the fluorescently labelled transgenic parasites for visualisation, 300µl of a schizont-stage culture at a parasitaemia of approximately 3-5% was diluted in 700µl incomplete culturing medium in a 1.5ml Eppendorf tube. The parasite nucleus was stained by adding 4µl of a freshly made 5mg/ml DAPI stock (at a final concentration of 0.2µg/ml) or 1mg/ml Hoechst 33258 pentahydrate (at a final concentration of 6µg/ml), and incubation in the dark at room temperature for 5 minutes or 2 hours, respectively.

The tube was centrifuged in an Eppendorf 5415R centrifuge at 3300 rpm for 3 minutes at 4˚C and the supernatant was discarded. The erythrocytes were washed twice with 1ml incomplete culturing medium and centrifugation as above. The erythrocytes were gently re-

suspended in 200µl incomplete medium and stored in an Eppendorf tube wrapped in tin foil to prevent the light sensitive nuclear stains from fading.

A volume of 5µl of the prepared sample was placed on a clean microscope slide and carefully mounted with a coverslip. The fluorescent parasites were viewed at 1000x magnification on an Olympus BX-41 fluorescence microscope, fitted with a U-25ND25 Olympus neutral density filter and multi-channel mirror cubes for colour visualisation: U-MWU2 for DAPI visualisation (excitation between 330 and 385nm; emission above 410mn), U-MWB2 for GFP visualisation (excitation between 460 and 490nm; emission above 510nm), 49306 Filter for mCherry visualisation (excitation between 467 and 596nm; emission above 609nm). Images were captured with an Olympus DP72 camera and processed using CellSense Dimensions 1.7 software. Microscopy control experiments were performed to confirm that no auto-fluorescence or colour-bleeding occurred (results shown in Appendix B).

2.9 Co-localisation Studies

To assess more precisely the localisation of the fluorescently tagged chimaeric proteins, *P. falciparum* transgenic cultures were fixed (Tonkin *et al.,* 2004) and co-localisation studies performed using microneme marker Erythrocyte Binding Antigen 175 (EBA175).

A 5ml culture of mixed, mostly late stages at a high parasitaemia (>3%) was pelleted by centrifugation in a 15ml Nunc tube for 5 minutes at 2500rpm in an Eppendorf 5702R centrifuge at room temperature. The supernatant was aspirated, the erythrocyte pellet re-suspended in 1ml PBS and transferred to a 1.5ml Eppendorf tube. The washed erythrocytes were collected by centrifugation in an Eppendorf 5415R centrifuge at 3300rpm for 3 minutes at room temperature and the supernatant was discarded. The red cells were fixed in 1ml of a freshly made fixing solution (4% paraformaldehyde and 0.0075% glutaraldehyde in PBS) for 30 minutes in the dark at room temperature. The erythrocytes were collected by centrifugation as before, washed once in 1ml PBS and permeabilised in 1ml permeabilisation solution (0.1% Triton X-100 in PBS) for 10 minutes in the dark. The erythrocytes were collected by centrifugation at 16000rpm in an Eppendorf 5415R centrifuge for 3 minutes and the supernatant discarded.

The cells were washed with 1ml PBS and treated with 1ml freshly made 0.1mg/ml sodium borohydride (0.005g $NaBH_4$ in 50ml PBS) for 10 minutes in the dark to remove any free aldehyde groups. After collecting the cells by centrifugation at 16000rpm in an Eppendorf 5415R centrifuge, 1ml of a blocking solution was added (3% BSA in PBS) and the tube incubated at room temperature for 1 hour.

The erythrocytes were collected by centrifugation as before and the supernatant discarded. A volume of 1ml 3% BSA-PBS containing 1:1000 EBA175 mouse primary antibody was added to the erythrocytes, and incubated in the dark for 1 hour. The cells were washed twice with 1ml PBS and then exposed to 1ml 3% BSA-PBS containing 5µg/ml (2mg/ml stock) Alexa Fluor® 488 goat anti-mouse secondary antibody and 4µl of a 50µg/ml DAPI working stock for 1 hour in the dark. The erythrocytes were washed twice in PBS as before and re-suspended in 100µl PBS.

Prepared cells may be stored at 4˚C in tubes wrapped in tin foil. Aliquots of 5µl were loaded onto glass microscope slides, mounted with coverslips and assessed by fluorescence microscopy as in 2.8. Co-localisation was assessed by determining Pearson's Coefficients (PC) using CellSense Dimensions 1.7 software. Co-localisation control experiments were performed to ensure that no auto-fluorescence or colour-bleeding occurred as a result of the co-localisation protocol (results shown in Appendix B).

2.10 Protein Expression and Purification

To identify novel binding partners for micronemal invasion proteins, appropriate *P. falciparum* AMA-1, SUB2 and EBA181 domains were expressed in pET-15b vectors as recombinant proteins with Histidine tags for use in biopanning experiments. The binding partners were subsequently expressed in pGEX-4T-2 vectors as recombinant proteins with GST tags and used in binding assays to verify their interactions with the invasion proteins.

2.10.1 Cloning and Expression Vectors

Cloning for the purpose of protein expression was performed using the techniques described before. The domains responsible for targeting AMA-1, SUB2 and EBA181 to the parasite micronemes were amplified by PCR (2.3), prepared for cloning by restriction enzyme digestion (2.5.1) using restriction endonucleases *Bam*HI and *Nde*I, and ligated into prepared

pET-15b plasmids (2.6.1). Chemically competent XL10 bacterial cells were transformed (2.6.2) with the plasmid constructs and clones were verified by restriction enzyme digest analysis (2.6.4.2) and sequencing (2.6.4.3).

2.10.2 Transformation of Rosetta™ 2(DE3) Bacterial Cells

Expression of eukaryotic proteins require codons that are rarely used by *E. coli* cells. Rosetta™ 2(DE3) host strains have been designed to supply seven rare tRNAs for the codons AUA, AGG, AGA, CUA, CCC, GGA and CGG, which allow for unlimited translation of proteins (Novagen, 2011). Once pET-15b and pGEX-4T-2 plasmid constructs were verified by sequencing, chemically competent Rosetta™ 2(DE3) cells were transformed with the prepared constructs according to the manufacter's protocol (Novagen, 2011).

A volume of 3µl of purified plasmid was added to a thawed 20µl aliquot of competent cells. The suspension was mixed carefully by swirling or tapping the tube and incubated on ice for 5 minutes. The cell-plasmid mixture was heat-shocked at 42°C for 30 seconds and immediately transferred to ice for a further 2-minute incubation period. The volume was made up to a 100µl with room temperature LB, supplemented with 100µg/ml ampicillin and 50µg/ml chloramphenicol. The cells were gently spread on two 1.5% agar plates (low and high plates as in 2.6.2) containing 100µg/ml ampicillin and 50µg/ml chloramphenicol. The plates were allowed to dry for 10 minutes at room temperature, inverted and incubated at 37˚C for 18-20 hours.

Transformed bacterial colonies were picked from the plates using a sterile pipette tip and transferred to a BD Falcon™ Round-bottom Snap Cap tube containing 2ml LB medium with 100µg/ml ampicillin and 50µg/ml chloramphenicol. The inoculated broth was incubated at 37˚C for 16 to 18 hours in a shaking incubator (250rpm).

Glycerol stocks were prepared as described earlier (2.6.3) and plasmid was isolated and digested according to 2.6.4.1 and 2.6.4.2 to verify that the transformed cells carried the desired constructs.

2.10.3 Protein Expression

2.10.3.1 Bacterial Cultures for Protein Expression

Recombinant protein expression was achieved by a three-step bacterial growth technique. A volume of 5ml LB in a 50ml Erlenmeyer flask, supplemented with 100µg/ml ampicillin and 50µg/ml chloramphenicol, was inoculated with a scraping from a Rosetta™ 2(DE3) glycerol stock (from 2.10.2) containing the appropriate plasmid. The inoculated broth was incubated in a shaking incubator at 250rpm at 37°C for approximately 8 hours. Once the OD_{600nm} (determined according to 2.4) reached approximately 0.5 to 1.0, a new 5ml LB flask was inoculated with 1ml of the 8-hour culture. The inoculated broth was incubated in a shaking incubator at 250rpm at 37°C overnight.

The final step for recombinant protein expression was to seed a desired volume of Overnight Express™ medium (60g Overnight Express™ Instant TB Medium powder, 10ml 100% glycerol, made up to 1000ml and autoclaved) in an appropriate Erlenmeyer flask with a 5% inoculant, using the overnight culture. The culture was incubated in a bench-top shaker at 250rpm for 20-24 hours. To limit the accumulation of inclusion bodies and increase the yield of soluble protein (Novagen, 2011), the Overnight Express™ culture was incubated at room temperature (±20°C). The cultures were analysed using a spectrophotometer and used for protein purification once the OD_{600nm} reached 3.0 or higher.

2.10.3.2 Protein Purification of His-tagged Recombinant Proteins

To extract and purify His-tagged recombinant proteins (Promega, 2009), Overnight Express™ cultures were transferred as 50ml aliquots to Nunc tubes and the bacterial cells were collected by centrifugation at 4400rpm in an Eppendorf 5702R centrifuge for 10 minutes at 4°C. The supernatant (spent growth medium) was discarded and the pellets frozen at -70°C for at least 10 minutes. Freeze-thawing and sonication were performed to lyse the *E. coli* and release the DNA.

The frozen tubes were incubated at 37°C in a water bath for approximately 5 minutes to thaw the bacterial pellets. A volume of 1.5ml of His-Binding Buffer (50mM Na_2HPO_4/NaH_2PO_4 buffer, 150mM NaCl; pH 8), containing 1.5µl Protease Inhibitor Cocktail set III (100mM 4-(2-Aminoethyl) benzenesulphonyl fluoride hydrochloride, 80µM Aprotinin, 5mM Bestatin; 1.5mM E-64; 2mM Leupeptin, 1mM Pepstatin A) and 1.5µl DNaseI (stock concentration of

1U/µl), was used to resuspend each bacterial pellet. The tubes were stored at -70°C for at least 10 minutes to freeze the mixture, after which they were transferred back to the water bath for 5 minutes at 37°C to thaw the mixture.

The thawed suspension was transferred to a 15ml Nunc tube. For optimal sonication conditions, each tube contained no more than 2ml of the bacterial pellet-buffer mixture, which was obtained from no more than 50ml of bacterial culture. For cultures with high optical densities (OD_{600nm} > 5.0), 30-40ml culture aliquots were pelleted for the freeze-thaw cycles and sonication. Each bacterial pellet was sonicated for 5 cycles, with the tubes submerged in ice water. Each sonication cycle was performed at 70% amplitude for 30 seconds, with pulses lasting for 1 second with half second intervals. A 30-second break was allowed between each sonication cycle.

To represent the total protein sample, 75µl of the sonicated bacterial cells was transferred to a 2ml Eppendorf, containing an equal volume of His-Binding Buffer. The remainder of the sonicated cells was transferred to a 2ml Eppendorf tube and pelleted by centrifugation at 16000rpm in an Eppendorf 5415R centrifuge for 20 minutes at 4°C. The supernatant, which consisted of the soluble protein fraction, was isolated and the insoluble fraction (the pellet) was resuspended in 1.5ml His-Binding Buffer. Aliquots of 75µl of each of the soluble and insoluble fractions were transferred to separate 2ml Eppendorf tubes, each containing equal volumes of His-Binding Buffer, for further processing (2.10.3.4).

To purify the desired His-tagged recombinant proteins, a Magne-His™ purification system with Nickel-coated magnetic particles and a magnetic separator was utilised according to the kit specifications (Promega, 2009). To prepare the magnetic particles, 10µl of the thoroughly mixed particle slurry was transferred to a 2ml Eppendorf tube. To wash the particles, 100µl His-Binding Buffer was added to the particles, followed by repeated pipetting to mix the particle slurry. The tube was attached to the magnetic separator and the buffer removed using a pipette. This wash step was performed three times and the washed particles were resuspended in a final volume of 100µl His-Binding Buffer.

Imidazole, to a final concentration of 1mM, was added to the soluble protein fraction containing the His-tagged protein of interest. The 100µl particle slurry was transferred to the

soluble fraction and the tube was incubated at 4°C overnight, rotating at 25rpm in an Intelli-Mixer. After binding overnight, the unbound fraction was collected using the magnetic separator and 75µl was again set aside in a 2ml Eppendorf tube containing an equal volume of His-Binding Buffer for further assessment described in 2.10.3.4.

The particles, which should now have the His-tagged recombinant protein bound to them, were washed three times using 500µl to 1ml imidazole Wash Buffer (20-100mM imidazole in His-Binding Buffer; pH 8) to remove non-specific bound proteins. The wash steps were performed by attaching the tubes to an Intelli-Mixer and vigorously rocking the samples at 90rpm for 5 minutes at room temperature. The concentration of imidazole in the Wash Buffer varied between the different proteins, but 20mM or 35mM was usually sufficient to remove any non-specific proteins. To increase stringency, the Imidazole concentration in the Wash Buffer was elevated up to 100mM or the number of washes was increased to five. After each wash step, 75µl of the wash fraction was retained for further assessment described in 2.10.3.4.

Depending on the downstream applications, the His-tagged recombinant protein was either retained on the Magne-His™ particles, or eluted. To elute the bound protein, the particles were resuspended in 50-100µl imidazole Elution Buffer (500mM imidazole in His-Binding Buffer; pH 7.5) and incubated using the Intelli-Mixer to rock the samples at 90rpm for 15 minutes at room temperature. The eluate was collected and a 10µl aliquot transferred to a 2ml Eppendorf tube for further assessment described in 2.10.3.4. A second elution step was performed as above, or the imidazole concentration was increased to 1M in the Elution Buffer should there be any remaining protein on the particles. After all the elution steps, the remaining particles were resuspended in a final volume of 100µl of His-Binding Buffer and 10µl was set aside in a 2ml Eppendorf tube as the final particle fraction for further assessment described in 2.10.3.4.

2.10.3.3 Protein Purification of GST-tagged Recombinant Proteins

The procedure for the extraction and purification of GST-tagged recombinant protein was similar to that of His-tagged proteins as described in 2.10.3.2, with a few modifications (Promega, 2014).

The thawed bacterial pellets were resuspended in 1.5ml GST Buffer (4.2mM Na_2HPO_4, 2mM KH_2PO_4, 140mM NaCl, 10mM KCl; pH 7.2 using NaH_2PO_4), containing 1.5µl Protease Inhibitor Cocktail set III and 1.5µl DNaseI. No imidazole was utilised for the extraction and purification of GST-tagged proteins. The purification of GST-tagged proteins was performed using Magne-GST™ purification system with 10µl glutathione-coated magnetic particles and a magnetic separator according to the kit specifications (Promega, 2014). The salt concentration used in the GST Buffer could be increased (up to 500mM NaCl) to enhance the purification quality and reduce the binding of non-specific proteins to the particles (Promega, 2014).

Incubation of the soluble fraction and particle slurry was performed at 4°C, using an Intelli-Mixer to mix the samples at 25rpm. The binding was either performed overnight as with the His-Purification system, or by following a shorter two-step binding process. The soluble fraction and particle slurry were incubated for 1 hour and then the unbound fraction and magnetic particles were separated using the magnetic separator. The particles were washed twice with 750µl of the GST-Buffer, using an Intelli-Mixer to rock the samples at 90rpm for 5 minutes. The unbound fraction was re-applied to the washed particles and incubated at 4°C for a further 1 hour. This two-step binding process was introduced for the GST-tagged proteins to enhance the binding of specific proteins and increase the yield.

Following binding, the unbound fraction was collected and three wash steps were performed as before: first using 1.5ml GST-Buffer, then two washes using only 750µl. As with the His-Purification system, proteins were either left on the particles or eluted twice using 50-100µl of a GST-Elution Buffer (500mM L-Glutathione, 500mM NaCl, 50mM Tris-HCl; pH 8.1). Samples of each fraction were kept aside as described in 2.10.3.2 for further assessment by SDS-PAGE (2.10.3.4).

2.10.3.4 Assessment of Purified Proteins by SDS-PAGE

The protein fractions from 2.10.3.2 and 2.10.3.3 were prepared for electrophoresis by combining 3 volumes of each sample with 1 volume Boiling Solution (freshly made by mixing 40µl 5x Suspension Solution (50mM Tris-HCl, 5mM EDTA, 5% SDS, 25% sucrose; pH 8.0), 5µl loading dye (2.5% sucrose, 0.5% bromophenol blue) and 5µl β-mercaptoethanol) in 2ml Eppendorf tubes, which were boiled for 6 minutes and allowed to

cool to room temperature. The samples were resolved according to size using a Laemmli sodium dodecyl sulfate poly-acrylamide gel electrophoresis (SDS-PAGE) system according to standard protocols (Gallagher, 2006; Laemmli, 1970).

The gel according to Table 2.2 by first pouring a 12 or 15% SDS poly-acrylamide resolving gel of approximately 6cm and allowing it to polymerize at room temperature for at least 30 minutes. Once set, a 2cm 4% stacking gel was poured on top of the resolving gel with a 10- or 15-well comb inserted. The gel was allowed to polymerize for a further 20-30 minutes until the stacking gel was set.

The boiled protein fractions were loaded into the wells and separated alongside a Spectra™ protein ladder. The gel was electrophoresed in Laemmli Buffer (25mM Tris, 192mM Glycine, 0.1% SDS) at a constant current of 20mA and maximum Voltage of 250V for approximately 2 hours. The gel chamber was connected to a Labcon CPE 50 circulator to ensure that the gel and Laemmli Buffer were maintained at 4°C for good resolution of the protein fractions.

Table 2.2. Components for casting SDS Poly-acrylamide gels.

Component	Resolving Gel	Resolving Gel	Stacking Gel
	12%	15%	4%
Milli-Q Water	2300 µl	1025 µl	1630 µl
10% (w/v) SDS	53 µl	53 µl	6,7 µl
4x Resolving Buffer (0.5 M Tris-HCl; pH 8.8)	2500 µl	2500 µl	
4x Stacking Buffer (0.5 M Tris-HCl; pH 6.8)			833 µl
30% (w/v) Acrylamide	4000 µl	5000 µl	433 µl
1% (w/v) Bis-acrylamide	1100 µl	1375 µl	333 µl
10% (w/v) freshly made ammonium persulfate	67 µl	67 µl	67 µl
TEMED	5 µl	5 µl	2,5 µl
Final Volume	10 000 µl	10 000 µl	3 300 µl

After electrophoresis, the SDS Poly-acrylamide gel was removed from the gel chamber and stained overnight using Coomassie Blue (0.05% Coomassie Brilliant Blue R-250 (w/v), 25% Isopropanol (v/v), 10% acetic acid (v/v)) according to standard procedures (Sasse & Gallagher, 2003). The gel was destained for 2 hours in 10% methanol/ 10% acetic acid, followed by an overnight incubation in 10% acetic acid. The SynGene GelDoc system and

GeneSnap GeneGenius version 6.05 image acquisition software were used to photograph the gel.

2.10.3.5 Quantitation of Purified Recombinant Protein

To determine how much recombinant protein was eluted after purification using the Magne-His™ system (2.10.3.2) or the Magne-GST™ system (2.10.3.3), a bovine serum albumin (BSA) standard was used. A range of concentrations of solubilised BSA standard was loaded onto the gel for comparison with the eluted protein fraction. The SynGene GelDoc system and GeneSnap GeneGenius version 6.05 image acquisition software were used to generate a standard curve based on the BSA standards, and then to determine the relative amount of protein in the eluted sample.

2.10.3.6 Assessment of Purified Recombinant Proteins by Western Blot

For immunodetection of the separated protein samples (2.10.3.4), a tank transfer system was utilised according to standard procedures (Gallagher *et al.,* 2004) to electrophoretically transfer the proteins from the poly-acrylamide gel onto a nitrocellulose membrane. A nitrocellulose membrane was placed on top of the gel, sandwiched between blotting paper and thin sheets of sponge. The transfer was conducted at 35V at 4°C overnight, with the sandwich cassette in a vertical position, fully submerged in pre-cooled transblot buffer (25mM Tris, 192mM Glycine, 0.1% (w/v) SDS, 20% (v/v) methanol).

To confirm that the proteins had been successfully transferred from the poly-acrylamide gel to the nitrocellulose membrane, the gel and membrane were both stained to detect proteins. The gel, which should be clear of any protein, was stained using Coomassie Blue as in 2.10.3.4 and the membrane was stained for 5 minutes using a non-permanent method which utilises Ponceau S (1% Ponceau S, 7% glacial acetic acid). After confirming that all the protein material had been transferred to the nitrocellulose membrane, water was used to rinse off the stain.

The membrane was washed in Tris-buffered saline (TBS; 50mM Tris-HCl, 150mM NaCl; pH 7.5) for 10 minutes while gently rotating at 50rpm on a bench-top shaker. To prevent any nonspecific binding of the antibodies to the nitrocellulose membrane, a 1-hour incubation of the membrane was performed using either QIAgen Anti-His HRP conjugate blocking

solution or 3% BSA in TBS blocking solution (0.45g BSA in 15ml TBS) for His-tagged and GST-tagged proteins respectively. A 1:2 000 dilution of anti-His horse radish peroxidase (HRP) conjugate primary antibody in 1% BSA-TBS or a 1:100 000 dilution of anti-GST HRP-conjugated primary antibody in 1% BSA-TBS was applied to the membrane, while shaking gently, for 1 hour at room temperature to detect the His-tagged and GST-tagged proteins respectively. To remove unbound antibodies, the membrane was subjected to three washes using 0.25% Tween-TBS, followed by one wash using only TBS, for 10 minutes while shaking. SuperSignal® West Pico Chemiluminescent Substrate of approximately 3ml was applied to the membrane and allowed to incubate for 5 minutes. The substrate was removed and the proteins were visualised using a SynGene GelDoc system.

After visualisation and image capturing using the GeneSnap GeneGenius image acquisition software, the membrane was stained using amido black (0.1% amido black, 10% acetic acid, 25% isopropanol) for 5 minutes. The membrane was destained for 30 minutes in 10% methanol/ 10% acetic acid followed by 30 minutes incubation in 10% acetic acid. The stained membrane was photographed as before.

2.11 Biopanning Using Phage Display Libraries

To identify binding partners for the *P. falciparum* micronemal invasion proteins, biopanning was performed against phage display libraries according to the Novagen T7Select® System manual (Novagen, 2011). Several mixed asexual stage *P. falciparum* cDNA phage display libraries have been created by members of the PMRU, Dr SB Lauterbach and Mr D Liebenberg (Lauterbach *et al.,* 2003), and were used for the biopanning experiments described below.

2.11.1 Bacterial Cultures for Biopanning

A BLT5403 *E. coli* culture was started from a glycerol stock in a 50ml Erlenmeyer flask containing 5ml M9LB medium (18.7mM NH_4Cl, 22mM KH_2PO_4, 22mM Na_2HPO_4, 0.4% (w/v) glucose, 1mM $MgSO_4$, in LB) supplemented with 50µg/ml ampicillin. The culture was incubated in a shaking incubator at 250rpm at 37°C overnight until an OD_{600nm}>3.0 was reached. The BLT5403 culture was used to set up new cultures for phage amplification (2.11.2), plaque assays (2.11.2) or creating glycerol stocks (2.11.5).

2.11.2 Phage Amplification and Plaque Assays

For phage amplification, 100µl of the overnight BLT5403 culture was used to seed 50ml of M9LB, supplemented with 50µg/ml ampicillin, in a 250ml Erlenmeyer flask to start a new culture. The culture was incubated for approximately 2 to 3 hours in a shaking incubator at 250rpm at 37°C until the OD_{600nm} reached log phase, indicated by an OD_{600nm} of 0.5 to 0.6. The log phase culture was inoculated with glycerol stock scrapings of the various *P. falciparum* phage display libraries (2.11) and incubated overnight in a shaking incubator at 250rpm and 37ºC for the amplification of the phage.

The phage lysate was collected by adding sodium chloride (at a final concentration of 0.5M) to the BLT5403/phage culture to further facilitate the lysis of the *E. coli*, followed by centrifugation at 10000rpm in a Beckman Coulter Avanti® J-E centrifuge for 10 minutes at 4ºC. The supernatant contained the phage, which was transferred to a sterile tube and stored at 4ºC until the plaque assay was performed.

A plaque assay was performed to determine the viral load or the "titre" of the phage lysates. A series of phage dilutions ranging from 10^{-2} to 10^{-9} were prepared, by adding an appropriate volume of the phage lysates to TBS in a final volume of 1ml. A 100µl aliquot of each of these dilutions was combined with 250µl BLT5403 culture with an OD_{600nm} of 1.0. Each of these mixtures were combined with 3ml molten top agarose (1% (w/v) tryptone, 0.5% (w/v) yeast extract, 85.6mM NaCl, 0.6% (w/v) agarose) and poured onto pre-warmed agar plates, containing 50µg/ml ampicillin. Once the top agarose mixture had set, the plates were inverted and incubated for 4 hours at 37ºC.

The plaques on each plate were counted to calculate the viral titre i.e. the number of plaque forming units (pfu) per milliliter of phage lysate, according to the formula:

Viral Titre (pfu/ml) = #plaques x dilution x 10

where 10 accounts for the 0.1ml of initial phage plated

2.11.3 Biopanning

Once the viral titre of the original phage display library had been determined (2.11.2), a $1x10^7$ pfu/ml phage dilution was made using TBS in a total volume of 500µl. A volume of

10µl washed MagneHis™ particles was incubated with the phage for 1 hour at room temperature with rotation using an Intelli-Mixer. This step helped limit non-specific interactions by removing any phage that bound to the MagneHis™ particles. A magnetic separator was used to collect the unbound phage fraction, which was then applied to ≥8µg recombinant *Pf*AMA-1 protein bound to MagneHis™ particles. The phage-protein-particle slurry was incubated for 1 hour as before.

The MagneHis™ particles were collected as before and washed five times with 2ml 0.05% Tween-TBS by inversion on an Intelli-Mixer for 10 minutes at room temperature. The washed particles were transferred to a 50ml log phase BLT5403 culture, prepared as described in 2.11.2 and incubated overnight at 37ºC to allow the phage to amplify.

The phage lysate was collected as before (2.11.2) and used in a plaque assay to determine the viral titre (2.11.2) for the next round of biopanning. Glycerol stocks were prepared for long term storage of the phage library as described in 2.11.5.

Four rounds of biopanning were performed to enrich for specific protein interactions with the *Pf*AMA-1 recombinant protein. After the final round of biopanning, the plaque assay was performed according to 2.11.2. The resultant plaques represented T7 bacteriophage with DNA inserts of various *P. falciparum* proteins. The plaques were analysed by PCR amplification and sequencing as described in 2.11.4.

2.11.4 PCR Amplification and Sequencing of Selected Recombinant Phages

After four rounds of biopanning had been completed, individual plaques were selected and used for PCR analysis and preparation for long term storage (2.11.5).

For PCR analysis of the T7 bacteriophage, well isolated plaques were extracted from the top agarose layer of the agar plates using a sterile loop and transferred to a 500µl PCR tube containing 50µl 10mM EDTA (pH 8.0). The tube was vortexed briefly and incubated at 65ºC for 10 minutes. After the tube had cooled, a PCR reaction was set up using 1µl of the phage, GoTaq or DreamTaq polymerase and T7 backbone primers. Primer sequences and PCR conditions are listed in Appendix E.

The PCR products were resolved on a 1% agarose gel against a mixed base pair standard as described in 2.2.3.1. The empty T7 cassette product is 216bp, thus products of 300bp or larger were considered for further analysis. Selected phage were sent to Inqaba Biotec™ (South Africa) for sequencing. The sequencing reactions were performed on the amplified PCR products using the T7SelectUp primer (see Appendix E for the primer sequence).

2.11.5 BLT5403 and Bacteriophage Glycerol Stocks

Once a BLT5403 *E. coli* culture reached stationary phase (determined by an $OD6_{00nm}$>3.0), glycerol stocks were prepared by combining 1.5ml of the culture with 150µl of 80% sterile glycerol (prepared using MilliQ water and filter sterilised) in an Eppendorf tube. The tube was inverted to mix the contents and stored at -70ºC.

Glycerol stocks of the phage lysates were prepared as described above, including the initial phage before biopanning, as well as of the phage lysates after each round of biopanning. For long term storage of individual plaques, a sterile loop ring was used to isolate the plaque from the top agarose layer of the agar plates, which was transferred to an Eppendorf tube containing 1ml phage extraction buffer (20mM Tris-HCl, 100mM NaCl, 6mM MgSO4; pH 8.0). A volume of 100µl 80% glycerol was added and the stock was stored at -70ºC.

2.12 *In Vitro* Binding Assays

Due to the possibility of false-positive results obtained when biopanning against a phage display library (2.11), *in vitro* binding assays were conducted to verify the protein interactions.

Recombinant GST- and His-tagged proteins were expressed and purified as described in 2.10. The eluted proteins were dialysed using a Slide-A-Lyzer MINI dialysis unit (with a molecular weight cut-off of 10kDa) with either TBS for the GST-tagged proteins (pH 7.5) or His-Buffer for the His-tagged proteins (pH 8.0), according to the manufacturer's specifications. Samples of 100µl were carefully loaded onto the membrane of the dialysis tube and the cap was attached. The tubes were attached to a Styrofoam floater, which was placed into 200ml TBS or His-Buffer, such that the membrane made contact with the buffer, but care was taken to ensure that the sample was level with, or slightly above the buffer. The

samples were incubated for 30 minutes at room temperature and the buffer was replaced every 10 minutes.

After dialysis, the protein samples were recovered using a pipette and quantified by SDS-PAGE analysis (2.10.3.4) against a BSA standard (2.10.3.5). An amount of 0.5µg of His-tagged *Pf*AMA-1 was re-attached to 5µl MagneHis™ particles for 1 hour at 4ºC. Increasing amounts of each of the GST-tagged binding partners was applied to the *Pf*AMA-1/particle samples in a total volume of 150µl His-Buffer for 1 hour at 4ºC using an Intelli-Mixer (setting 90º; 50rpm) to rock the tubes. A magnetic separator was used to collect the particles, which were rinsed twice with 1ml His-Buffer for 5 minutes using an Intelli-Mixer before resuspension in 15µl His-Buffer.

To account for non-specific binding, purified GST protein as well as heat-denatured GST-tagged binding partners were applied to His-tagged *Pf*AMA-1. The samples were analysed by SDS-PAGE as described in 2.10.3.4.

Chapter 3: *P. falciparum* Apical Membrane Antigen-1

3.1 Introduction

P. falciparum apical membrane antigen 1 (*Pf*AMA-1), was first described in 1989 (Peterson *et al.,* 1989) and plays a major role in invasion of the merozoite into the host erythrocyte. While invasion proteins have orthologues throughout the *Plasmodium* species, most are not generally conserved within the phylum (Cowman & Crabb, 2006). *Pf*AMA-1, however, is highly conserved throughout the Apicomplexan parasites (Cowman & Crabb, 2006).

3.1.1 *Pf*AMA-1 as a Vaccine Candidate

During invasion of the host erythrocyte, the merozoite surface antigens are briefly exposed to the host immune system. The parasite employs what has been referred to as a 'just-in-time' method of invasion (Kats *et al.,* 2008), whereby the proteins are secreted from the apical organelles at precisely the point that they are needed, i.e. during, or shortly prior to, initial attachment. This allows the parasite to minimise recognition by protecting essential ligands from antibody detection.

Despite this brief exposure during invasion, certain surface antigens are still likely targets for vaccine and drug development (Beeson *et al.,* 2016). *Pf*AMA-1 has been one of the major vaccine candidates (Tyler *et al.,* 2011; Beeson *et al.,* 2016) mainly because: (1) antibodies designed to recognise the ectodomain of *P. knowlesi* AMA-1 are able to prevent invasion of erythrocytes and (2) using various forms of *Pk*AMA-1 for immunisation, such as *Pk*AMA-1 peptides, recombinant proteins and antigen purified from parasites, has proven successful in protecting erythrocytic-stage infection in animal studies. *Pf*AMA-1 has been tested in 23 human trials on its own, and in 9 additional trials in combination with other antigens (Beeson *et al.,* 2016). These trials have elicited an antibody response, but have not been successful in protecting patients against malaria. This is presumably due to polymorphisms on the exposed surface of *Pf*AMA-1 (Bai *et al*., 2005), which presents a major hurdle for vaccine development (Remarque *et al*., 2008).

3.1.2 Expression and Function of *Pf*AMA-1

*Pf*AMA-1 is synthesised in the schizont stage, during the last few hours of maturation of the asexual intra-erythrocytic parasite (Howell *et al.,* 2001). mRNA levels peak during the

schizont stage (Figure 3.1 A; Otto *et al.,* 2010) and some expression was detected in the late trophozoite stages (Figure 3.1 B; Lopez-Barragan *et al.,* 2011)

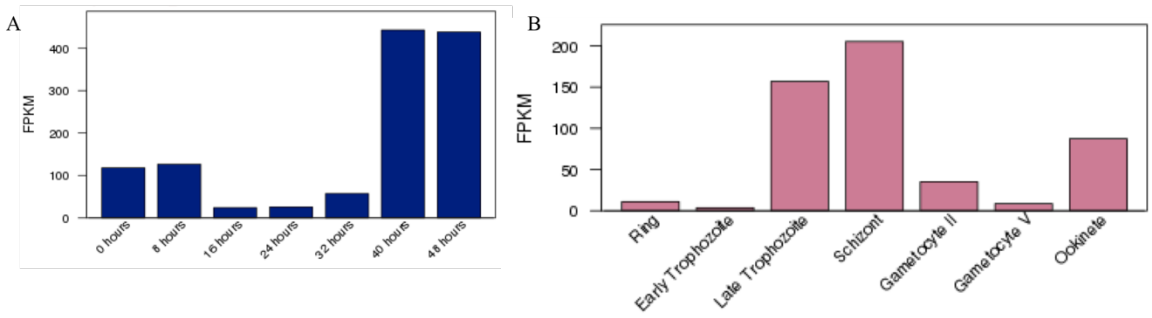


Figure 3.1. Expression levels of *Pfama-1* mRNA in various stages of the life cycle.
RNA was extracted from synchronised 3D7 *P. falciparum* parasites at several time points post-infection (indicated on the x-axis) and the transcriptome was sequenced. Fragments per kilo-base of exon model per million mapped reads (FPKM) on the y-axis indicates the transcript levels at: (A) the selected time points during the intra-erythrocytic stages, and (B) during the different life stages in the human and mosquito host. *Pfama-1* expression levels peak 40 to 48 hours post-infection, during the schizont stage. (Adapted from Aurrecoechea *et al*., 2008; PlasmoDB)

After post-translational processing of the protein, it accumulates within the micronemes (Healer *et al.,* 2002) and is secreted through the rhoptry neck (Howell *et al.,* 2001), where it is involved in invasion. *Pf*AMA-1 is required for invasion, but its precise role in the process is less clear. Evidence exists for the involvement of *Pf*AMA-1 in merozoite reorientation, rhoptry secretion, formation of the moving junction, as well as replication of the asexual intra-erythrocytic stages.

Antibodies against *Pf*AMA-1 inhibit invasion by blocking reorientation of the merozoite, although they do not prevent initial attachment (Mitchell *et al.,* 2004). In studies where *P. knowlesi* cultures were treated with antibodies against *Pk*AMA-1 (Mitchell *et al.,* 2004), the merozoites could make contact with the host erythrocyte in a random loose attachment. However, the parasite was unable to orientate itself so that the apical pole could attach and the moving junction did not form (Mitchell *et al.,* 2004).

Various attempts to knock-out AMA-1 in *P. falciparum* (Triglia *et al.,* 2000) and *T. gondii* (Mital *et al.,* 2005) have been unsuccessful, which strongly suggests that the protein has vital functions. A conditional knock-out experiment using a transgenic *T. gondii* parasite line (Mital *et al.,* 2005), showed that in the absence of *Tg*AMA-1, tachyzoites could form an initial attachment, but could not invade host cells. Furthermore, it was found that rhoptry

secretion in *Tg*AMA-1 knock-out parasites was impaired, while micronemes functioned normally (Mital *et al.,* 2005). These findings suggest that *Tg*AMA-1 is involved in establishing the permanent attachment of the apical pole to the host cell, as well as regulation of rhoptry secretion (Mital *et al.,* 2005).

The formation of the tight junction is one of the key aspects of merozoite invasion. The merozoite is anchored to the erythrocyte membrane by proteins such as *Pf*RH5, which binds to the basigin protein receptor (Crosnier *et al.,* 2011; Beeson *et al.,* 2016). As the merozoite moves into the host cell, the moving junction exists as a ring-like structure that allows the host plasma membrane and the PVM to flow over each other until the parasite has been enveloped (Tyler *et al.,* 2011). The details of the junction formation are poorly understood (Tyler *et al.,* 2011; Beeson *et al.,* 2016). *Tg*AMA-1 is expressed on the tachyzoite membrane during invasion, while rhoptry proteins *Tg*RON4/5/8 are bound to receptors on the host cell membrane. The membrane-spanning *Tg*RON2, has been proposed to act as the linker between *Tg*AMA-1 and the *Tg*RON4/5/8 proteins (Besterio *et al.,* 2009; Tyler *et al.,* 2011), and together these proteins form the junction complex. The RON2 and AMA-1 interaction has been confirmed in *T. gondii* (Tyler & Boothroyd, 2011) and *P. falciparum* (Lamarque *et al.,* 2011). Tight junction formation is speculated to be triggered when *Pf*AMA-1 binds to *Pf*RON2, which in turn appears to be enabled through the binding of *Pf*RH5 and the basigin receptor (Beeson *et al.,* 2016).

Aside from the intra-erythrocytic stages, *Pf*AMA-1 is also expressed in the pre-erythrocytic sporozoites and is required for the invasion of hepatocytes (Silvie *et al.,* 2004).

3.1.3 The Sequence and Structure of *Pf*AMA-1

*Pf*AMA-1 is a classical type 1 integral membrane protein and comprises of several domains (Figure 3.2), of which the most important for invasion are the ectodomains and the cytoplasmic tail (Remarque *et al.,* 2008; Tyler *et al.,* 2011). The bulk of *Pf*AMA-1 is the ectodomain, which is made up of three sub-domains (Figure 3.2; Howell *et al.,* 2001). The ectodomain contains 16 conserved cysteines, which contribute to disulphide bonding (Hodder *et al.,* 1996).

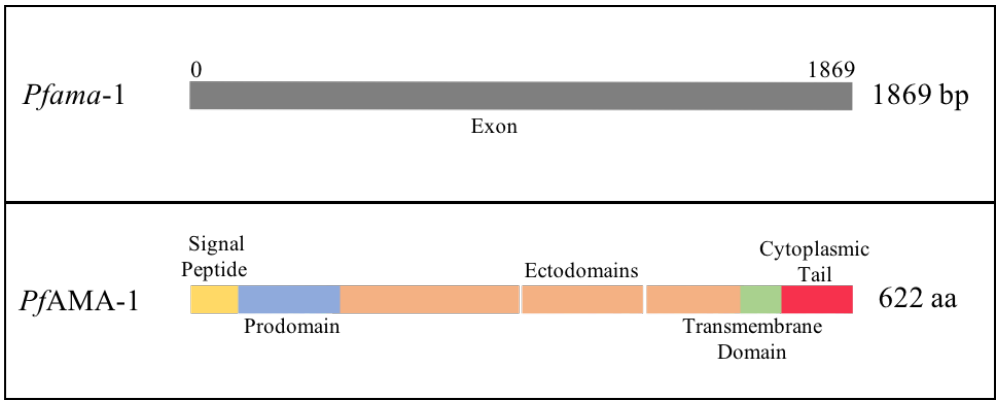


Figure 3.2. The gene and protein structure of *Pf*AMA-1.
*Pf*AMA-1 is encoded by a gene of 1869 base pairs (bp) consisting of a single exon. *Pf*AMA-1 is synthesized as a protein of 622 amino acids (aa), which consists of several domains, including an N-terminal signal peptide (yellow), a prodomain (blue), three ectodomains (orange), a transmembrane-spanning region (green) and a cytoplasmic tail (red).

Crystallisation of the ectodomains of *P. vivax* AMA-1 revealed that the first two sub-domains possess a PAN (plasminogen-apple-nematode) domain fold (Pizarro *et al.,* 2005), which is significant because these folds are implicated in facilitating protein-protein or protein-carbohydrate interactions, especially with adhesion proteins (Tyler *et al.,* 2011). X-ray crystallography of the highly conserved ectodomain sub-regions I and II (Figure 3.3), identified an important feature of the *Pf*AMA-1 ectodomain: a conserved hydrophobic cleft, which is protected by unstructured loops from sub-domains I and II (Figure 3.4; Bai *et al.,* 2005). This structural feature of *Pf*AMA-1 is crucial for invasion of host erythrocytes.



Figure 3.3. The structure of the *Pf*AMA-1 ectodomain sub-regions I and II.
A stereo view of the *Pf*AMA-1 ectodomain, showing the interconnected domains: the signal peptide (blue), ectodomain sub-region I (yellow), sub-region II (red) and disordered loops (violet). (Adapted from Bai *et al.,* 2005).

The hydrophobic cleft is not only conserved throughout the Apicomplexan organisms, but is exposed on the surface, which makes it a good target for vaccine intervention. A monoclonal antibody, designated 4G2, designed to recognise and bind to the ectodomain cleft, prevented invasion of the host erythrocyte (Collins *et al.,* 2009).

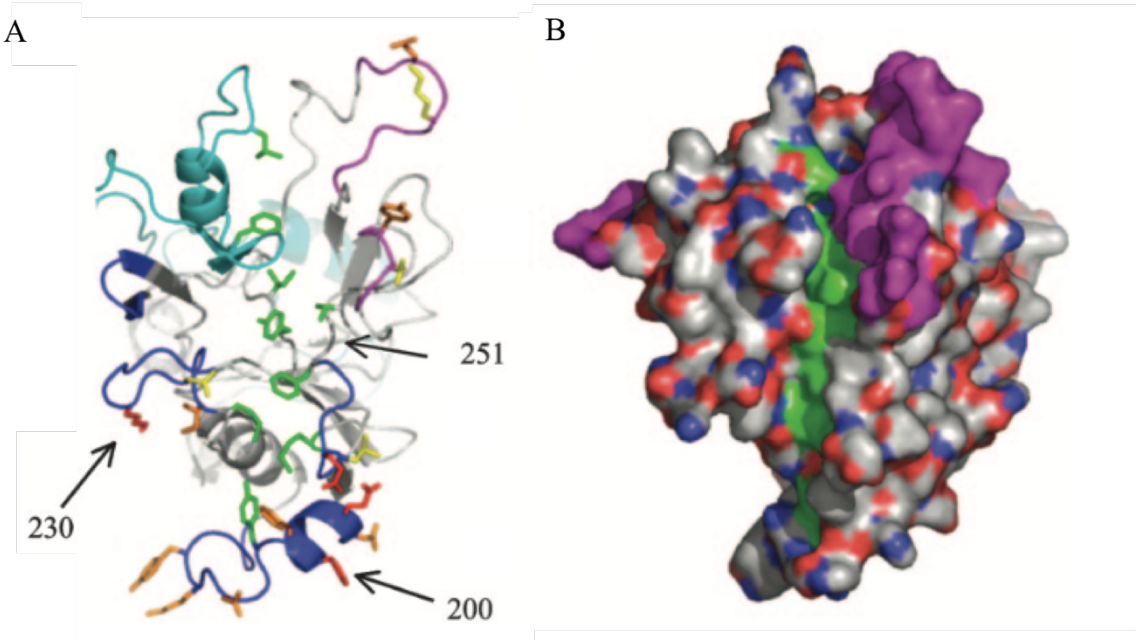


Figure 3.4. The conserved hydrophobic cleft found in the *Pf*AMA-1 ectodomain.
The *Plasmodium*-conserved ectodomain sub-regions I and II of *Pf*AMA-1 were crystallised, which identified a hydrophobic cleft (light green in A and B) surrounded by the unstructured loops of sub-regions I and II. **A –** A stereo view of the structure showing the surface-exposed hydrophobic residues of the conserved cleft (light green). The tyrosine residue at position 251 (marked with an arrow), is identical in all Apicomplexan sequences. There are five highly polymorphic residues (in red) in *P. falciparum* sequences, four of which surround the bottom end of the hydrophobic cleft: K230 and H200 are marked with arrows. Dimorphic sites (yellow and orange), ordered loops from sub-region I (dark blue) and sub-region II (turquoise), as well as disordered loops (violet) are shown. **B –** A surface view of the hydrophobic cleft showing carbon and sulphur atoms that are part of the hydrophobic cleft (light green). Other carbon and sulphur atoms (white), oxygen atoms (red), nitrogen atoms (blue), as well as the disordered regions (violet) are also shown. (Adapted from Bai *et al.,* 2005).

A peptide, designated R1, which was designed to bind within or adjacent to the hydrophobic cleft, blocked the interaction between *Pf*AMA-1 and *Pf*RON2, and thus prevented invasion (Harris *et al.,* 2005a). The R1 peptide shares sequence similarity with *Pf*RON2 (Tyler & Boothroyd, 2011), which makes it likely that it is able to mimic the *Pf*AMA-1 binding domain of *Pf*RON2 (Figure 3.5; Lamarque et al., 2011; Tyler *et al.,* 2011).

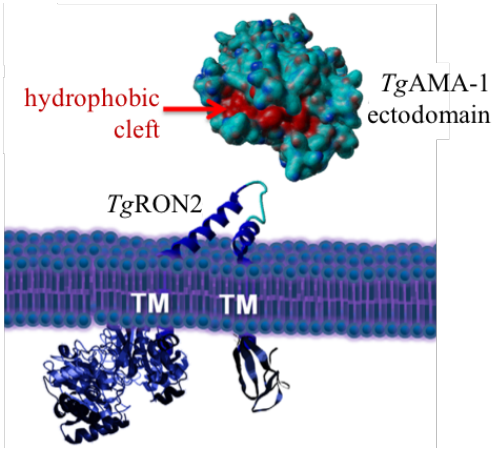


Figure 3.5. A model of the *Tg*AMA-1 and *Tg*RON2 interaction at the moving junction.
The *Tg*AMA1 ectodomain was created by molecular surface rendering, with the amino acids from the hydrophobic cleft coloured in red. With no structure available for *Tg*RON2, the protein was schematised based on secondary structure predictions, with the transmembrane (TM) domains spanning the parasite membrane. (Adapted from Lamarque *et al.,* 2011).

The cytoplasmic tail of *Pf*AMA-1 was erroneously thought to be implicated in correct targeting to the parasite micronemes based on evidence that other micronemal proteins, such as *Tg*MIC2, require conserved amino acids in the cytoplasmic tail for trafficking (di Cristina *et al.,* 2004). A study performed in 2009, however, showed that this was not the case for *Pf*AMA-1. In this study, several transgenic parasite lines with cytoplasmic tail mutations were created, which showed that the cytoplasmic tail was not required for trafficking, but that it was essential for invasion of the host cell (Treeck *et al.,* 2009).

The cytoplasmic tail sequence of *Pf*AMA-1 shares little homology with other Apicomplexan parasites, with only three of the 55 amino acids being conserved: A tryptophan at position 603; a threonine at position 613 and a serine at position 610 (Tyler *et al.,* 2011). The serine residue undergoes phosphorylation, which appears to be of importance to the function of *Pf*AMA-1 since a mutation of this residue inhibited erythrocyte invasion (Treeck *et al.,* 2009; Leykauf *et al.,* 2010).

3.1.4 *Pf*AMA-1 Polymorphisms

One of the major hurdles for vaccine and drug development for *Pf*AMA-1 is the existence of polymorphisms on the exposed surface (Remarque *et al.,* 2008). There are five highly polymorphic residues within the *Pf*AMA-1 sequence at positions 187, 197, 200, 230 and 243 surrounding the hydrophobic cleft (visible in Figure 3.4 and Figure 3.6; Bai *et al.,* 2005). Most of the polymorphisms in *Pf*AMA-1 are dimorphic, with only two residues found in the

population of sequences. Figure 3.6 shows the polymorphisms of *Pf*AMA-1. The contrast in the presence of polymorphisms on the two sides, or "faces", is clear, one appears to be polymorphic (Figure 3.6 B) and the other is relatively non-polymorphic (Figure 3.6 A). This discovery has led to the hypothesis that a single polymorphic face of *Pf*AMA-1 is exposed on the surface of the parasite (Bai *et al.,* 2005).

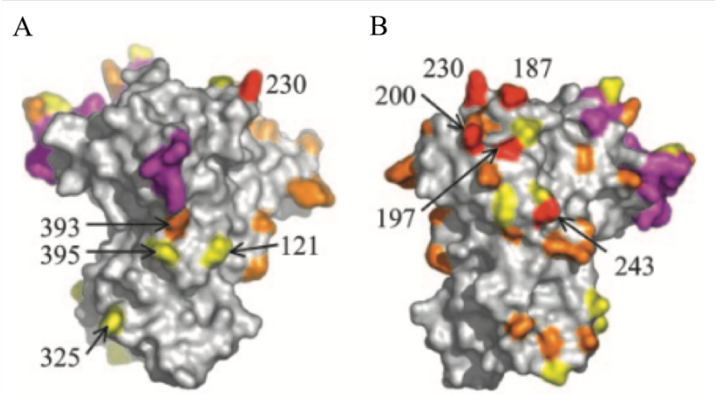


Figure 3.6. Polymorphic residues on the surface of *Pf*AMA-1.
Residues 197, 200, 230 and 243 are four of the five highly polymorphic residues found in the *Pf*AMA-1 sequences. They occur as a cluster (red), while the dimorphic residues (orange and yellow) are scattered. Disordered areas are also indicated (violet). **A –** Surface view of the non-polymorphic face of *Pf*AMA-1, with dimorphic residues 121, 325, 393 and 395. **B –** Surface view of the polymorphic face of *Pf*AMA-1, with the five polymorphic residues indicated. (Adapted from Bai *et al.,* 2005).

3.1.5 Post-translational Modifications & Trafficking of *Pf*AMA-1

Post-translational trafficking of *Pf*AMA-1 (summarised in Figure 3.7) leads the protein through the ER where the 24 amino acid signal peptide is cleaved (Healer *et al.,* 2002). The remainder of the protein is transported to the micronemes by an unknown mechanism and then undergoes a further processing event which removes the N-terminal prodomain (Healer *et al.,* 2002). This event is thought to be responsible for the translocation of the resultant 66kDa protein to the surface of the merozoite (Howell *et al*., 2001; Woehlbier *et al*., 2010). It has been proposed that *Pf*AMA-1 exits the micronemes by mediating an interaction with an escorter protein (Healer *et al.,* 2002), such as has been described for *Pf*RAP1 and *Pf*RAP2 (Baldi *et al.,* 2000) and *Tg*MIC proteins (Reiss *et al.,* 2001). *Pf*AMA-1_{66} is further cleaved at the N-terminus by *Pf*SUB2, resulting in either *Pf*AMA-1_{44} or *Pf*AMA-1_{48} (Woehlbier *et al*., 2010), allowing only the residual membrane bound region to enter the red blood cell.

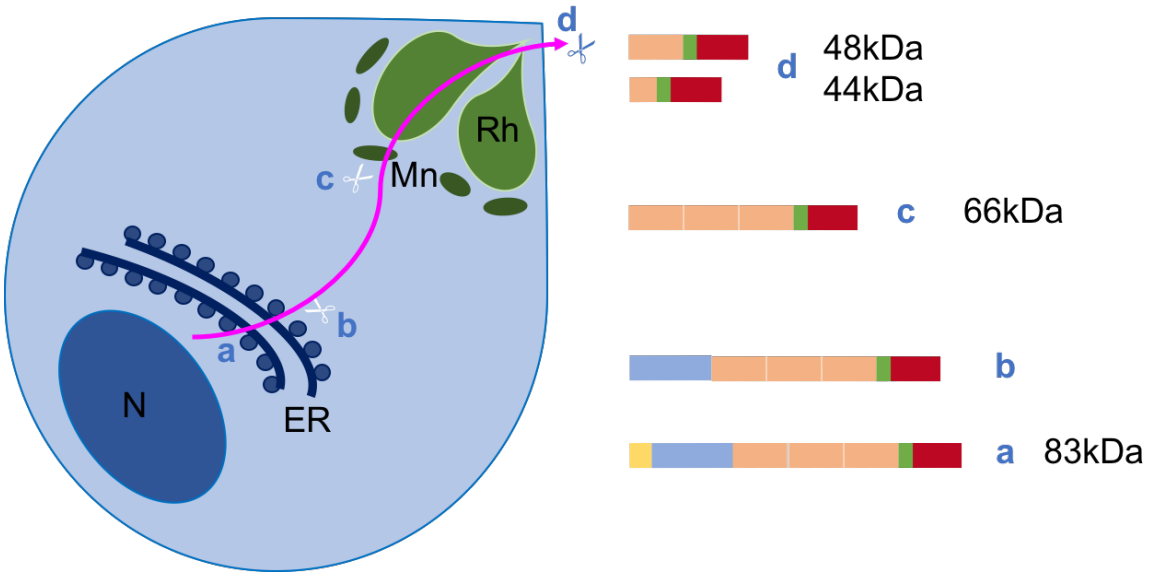


Figure 3.7. Post-translational modification and trafficking of *Pf*AMA-1.
*Pf*AMA-1 is synthesised as an 83kDa protein with a signal peptide for transport through the ER (a). After removal of the signal peptide in the ER (b), *Pf*AMA-1 traffics to the micronemes (Mn) where the N-terminal pro-sequence is cleaved (c). The 66kDa polypeptide is transported through the neck of the rhoptry (Rh), and onto the merozoite surface (d). *Pf*AMA-1_{66} then undergoes proteolytic cleavage at one of two sites by *Pf*SUB2, resulting in products of 44 or 48kDa, before invasion occurs.

3.1.6 Research Objectives

The aim of the research conducted in this chapter was to identify the molecular determinants for the trafficking of *Pf*AMA-1.

This was achieved by creating several transgenic parasite lines expressing fluorescently-tagged chimaeric *Pf*AMA-1 peptides, and conducting co-localisation studies to determine which of the protein domains were required for the correct targeting of *Pf*AMA-1 to the micronemes.

3.2 Materials and Methods

The materials and methods used to investigate *Pf*AMA-1 are described in Chapter 2.

3.3 Results

3.3.1 Exchanging promoters in the pARL-mCherry plasmid

3.3.1.1 Preparation of the pARL-mCherry plasmid

The pARL-mCherry plasmid was kindly provided by Dr. J. Przyborski (University of Marburg, Germany) and prepared by a colleague in the *Plasmodium* Molecular Research

Unit (Wepener, 2014). The *crt* promoter, responsible for continuous expression of proteins, was excised and replaced with a more appropriate *Pfama-1* promoter (*amap*), which would ensure stage-specific expression of the transgenic invasion proteins. Sequencing performed by Inqaba Biotec™ confirmed that the promoters had been successfully exchanged.

The pARL-mCherry_*amap* plasmid, from here on referred to as mCherry, was isolated from LB cultures (OD_{600nm} = 2.6) and prepared for cloning by alkaline phosphatase treatment and restriction enzyme digestion using Fast Digest® *Xho*I and Fast Digest® *Avr*II. The linearised plasmid DNA migrated at the expected size of 7339bp as shown in Figure 3.8.

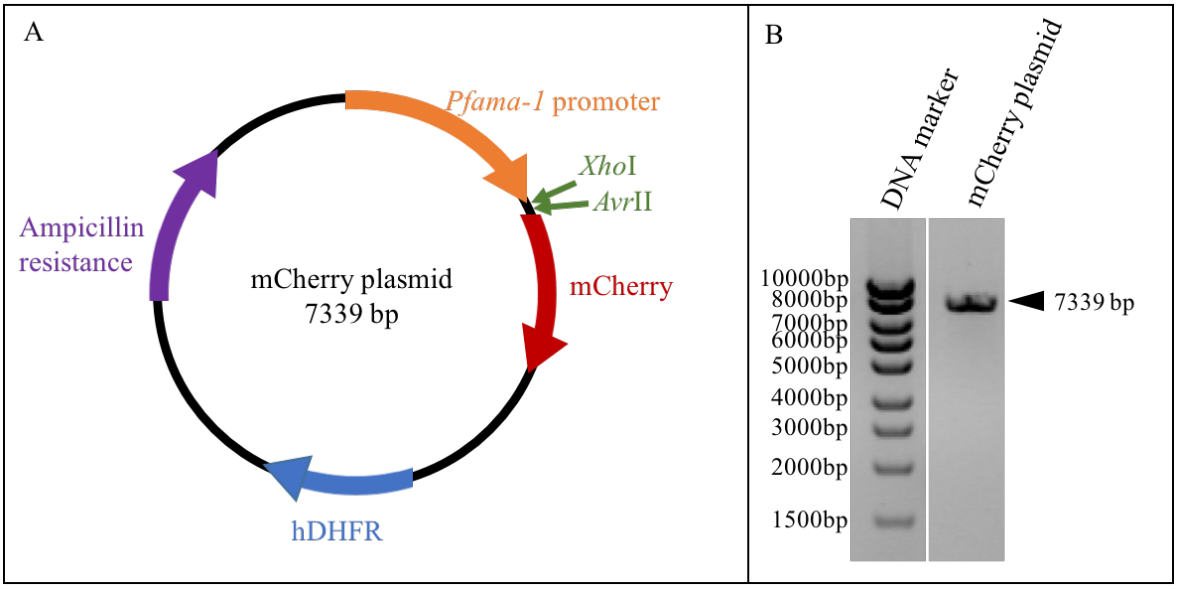


Figure 3.8. mCherry plasmid.
A – A schematic depicting the pARL-mCherry plasmid, modified from the pARL2-GFP vector (Przyborski *et al.,* 2005). The *Pfama-1* promoter ensures that expression of the chimaeric proteins occurs only during the late stages of the parasite life cycle (Wepener, 2014). The plasmid encodes an ampicillin resistance gene for positive selection after bacterial transformation and a human dihydrofolate reductase (hDHFR) gene which confers resistance against WR99210 compound as a positive selection strategy after parasite transfection (Fidock & Wellems, 1997). *Xho*I and *Avr*II restriction endonuclease sites were used for directional insertion of the mini-genes into the mCherry backbone. **B –** Size validation of mCherry plasmid after restriction endonuclease digestion and alkaline phosphatase treatment as performed by gel electrophoresis against a base pair (bp) standard.

3.3.1.2 Creating Control mCherry Transgenic Parasite Lines

3D7 *P. falciparum* parasites were electroporated with the original mCherry_*crt* or the modified mCherry_*amap* plasmid. WR99210 compound was administered to the cultures to ensure that only parasites with the plasmid survived. Live parasites were visible in the mCherry_*crt* and mCherry_*amap* transgenic cultures 25 and 42 days after transfection,

respectively. At a parasitaemia of at least 3%, DNA was isolated and microscopy experiments were performed.

3.3.1.3 Comparison of the *crt* and *ama-1* Promoters

Fluorescence microscopy was performed using live *P. falciparum* transgenic parasites, containing either the original mCherry_*crt* or the modified mCherry_*amap* plasmid. Hoechst staining was used to identify the nucleus. Under control of the *crt* promoter, red mCherry fluorescence was visible in the parasite cytoplasm, throughout the ring, trophozoite and schizont stages (Figure 3.9). In the presence of the *ama-1* promoter, however, red mCherry fluorescence was limited to the late schizont stage only, with no red fluorescence observed in the ring or trophozoite stages (Figure 3.9). This confirmed that the two promoters had been successfully exchanged and all transgenic proteins would be expressed in the late intra-erythrocytic stages only, mimicking normal invasion protein expression patterns. No auto-fluorescence or colour bleeding was seen during fluorescence imaging studies

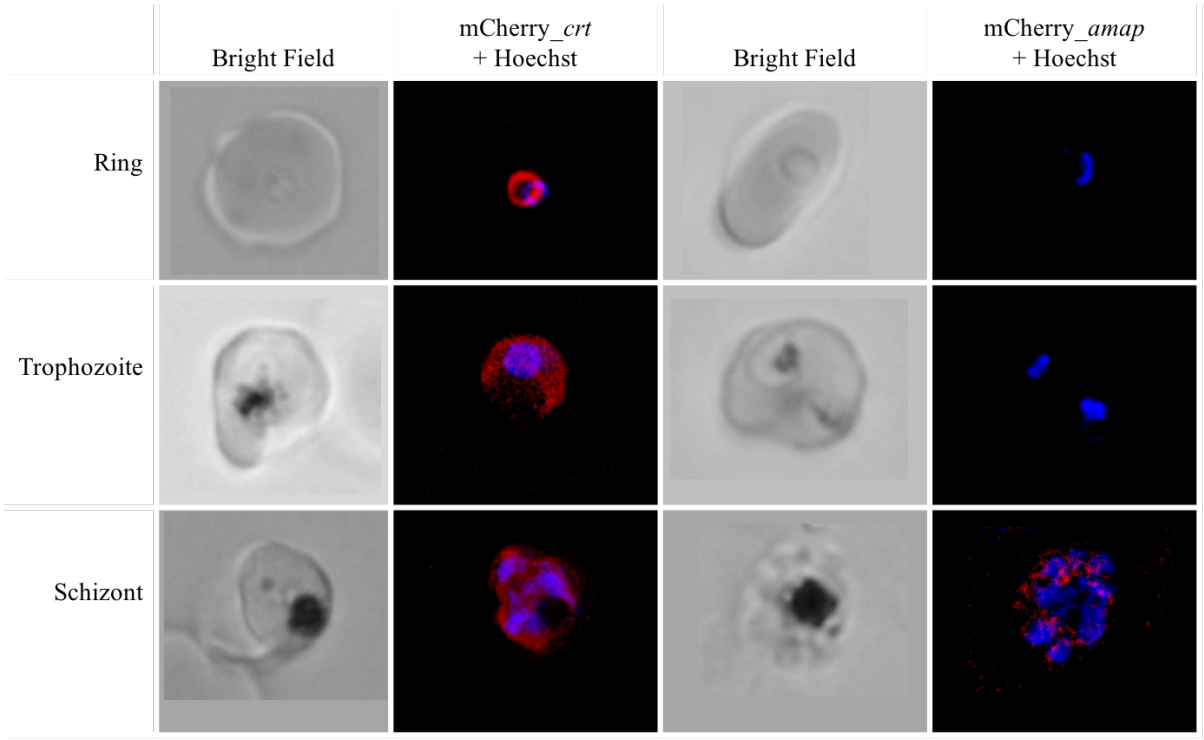


Figure 3.9. Fluorescence microscopy of live *P. falciparum* parasites expressing mCherry_*crt* and mCherry_*amap*.
Parasites were viewed at 1000x magnification. Under control of the *Pfcrt* promoter, mCherry (red) expressed throughout intra-erythrocytic asexual life stages, whereas with the *Pfamap* promoter in place, expression was limited to the late, schizont stage only. The nuclei were stained blue with Hoechst dye.

3.3.2 Creation of *Pfama*-1 Mini-Genes

3.3.2.1 Bio-informatic Analysis of *Pf*AMA-1

The sequence of *Pfama*-1 was obtained from the online *Plasmodium* database (PlasmoDB version 30; www.plasmodb.org; Aurrecoechea *et al*., 2008). *Pf*AMA-1 is encoded by the single exon PF3D7_1133400 gene, which is located on chromosome 11. *Pf*AMA-1 is a type 1 integral membrane protein, of 622 amino acids (aa) with a molecular weight of 83kDa (Aurrecoechea *et al.,* 2008; Peterson *et al.,* 1989). Figure 3.10 shows the domains of this invasion protein.

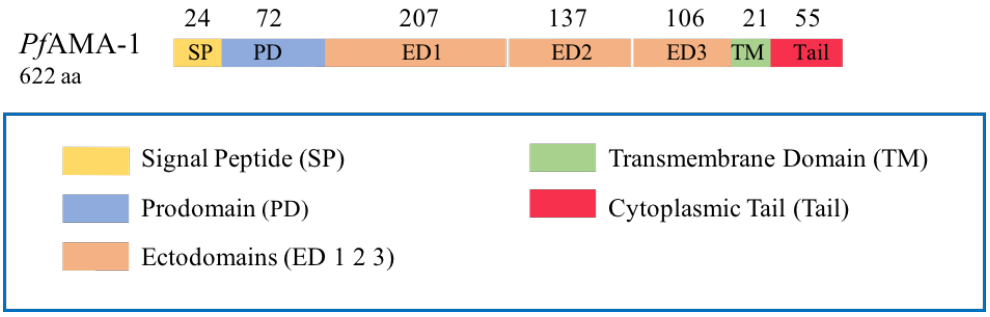


Figure 3.10. A schematic representing the domains of *Pf*AMA-1, a *P. falciparum* microneme invasion protein.
The number of amino acids (aa) in each domain is indicated.

3.3.2.2 Designing *Pfama*-1 Mini-Genes for Parasite Transfections

To assess which of the various domains (Figure 3.10) are involved in targeting *Pf*AMA-1 to the *P. falciparum* micronemes, several mini-genes were designed (Figure 3.11).

As mentioned in Chapter 1, invasion proteins contain an N-terminal signal sequence which is responsible for targeting the protein to the parasite ER. The Signal Peptide (SP) was therefore included in all of the generated chimaeric proteins to ensure correct targeting via the ER. The remaining domains were sequentially removed for each mini-gene, which allowed the examination of each domain as a trafficking determinant for *Pf*AMA-1 to the micronemes.

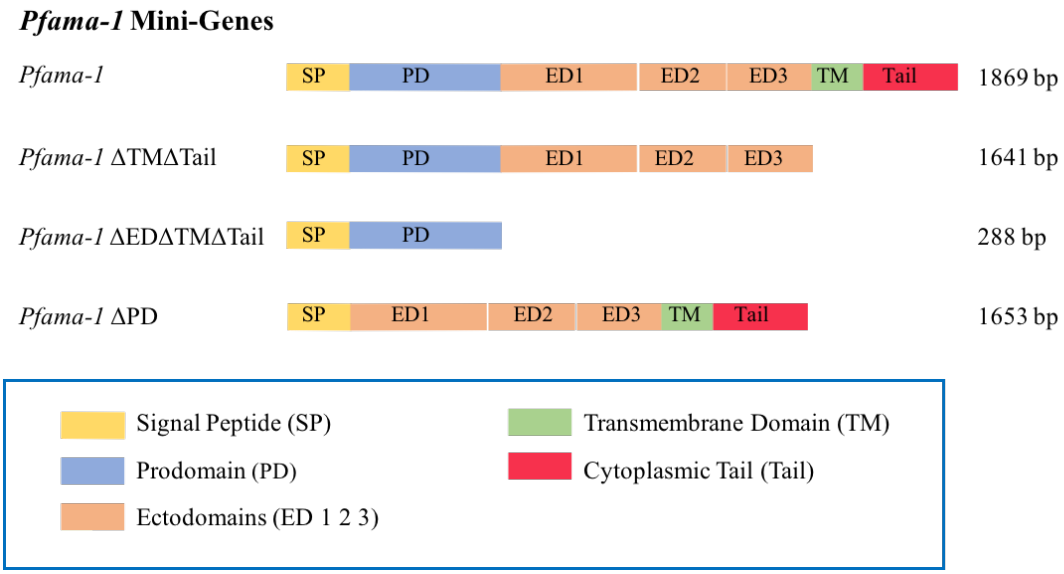


Figure 3.11. A schematic of the mini-genes designed for invasion protein, *Pf*AMA-1. Base pair (bp) sizes of mini-genes are indicated on the right.

3.3.2.3 Genomic DNA Isolation

Since *Pfama-1* contains no introns, genomic DNA was used for the creation of the mini-genes. Genomic DNA was isolated from wild-type *P. falciparum* 3D7 parasites and the quantity and purity were determined by agarose gel electrophoresis and NanoDrop® spectrophotometry. The A_{260}/A_{280} values ranged from 1.88 to <3.0, where the higher values were indicative of samples containing contaminating RNA (NanoDrop® Technologies, 2007). The A_{260}/A_{230} values were generally in the acceptable range of 1.8 to 2.5, but sometimes were as low as 1.5, indicative of residual phenol contamination (Wilfinger *et al.,* 1997). Agarose gel electrophoresis of the DNA sample (Figure 3.12.) used to create the mini-genes, indicated that it was not degraded and contained no visible RNA contaminants.

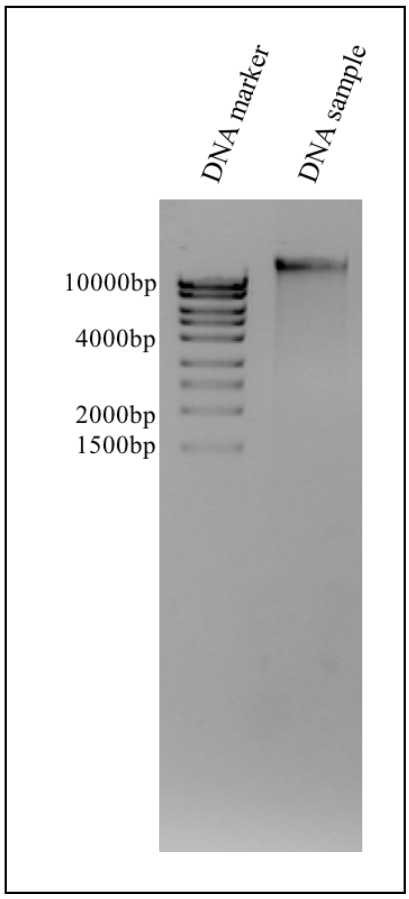


Figure 3.12. Isolated *P. falciparum* 3D7 DNA.
Assessment of isolated genomic DNA by electrophoresis using an 1% agarose gel against a high range base pair standard.

3.3.2.4 PCR and Overlap Extension PCR

Pfama-1 mini-genes were generated by PCR and overlap extension PCR using appropriate primers. In some instances, to avoid long stretches of adenine or thymine nucleotides commonly found in *P. falciparum* or to exclude the stop codon at the end of the gene, the location of the primer binding site was selected upstream or downstream of the desired site. This resulted in the amplified regions varying from the actual domain size (Figure 3.11 and Table 3.1).

All PCR products migrated according to their expected sizes (Table 3.1) as assessed by agarose gel electrophoresis. PCR products were slightly larger than the domain sizes due to additions to the primers, as described in Appendix A. PCR parameters are also listed in Appendix A.

Table 3.1. Expected PCR product sizes of domains within *Pfama*-1 mini-genes.

Gene	Mini-genes	Domains	Region to be amplified (bp)	PCR Product size (bp)
Pfama-1	Full length	SP-PD-ED-TM-Tail	1866	1886
	ΔTMΔTail	SP-PD-ED	1641	1661
	ΔEDΔTMΔTail	SP-PD	324	344
	ΔPD Product 1	SP	72	103
	ΔPD Product 2	ED-TM-Tail	1578	1588
	ΔPD Final Product	SP + ED-TM-Tail	1650	1670

Three of the four *Pfama-1* mini-genes were created by PCR amplification (Figure 3.13), utilising forward and reverse primers flanking the regions of interest.

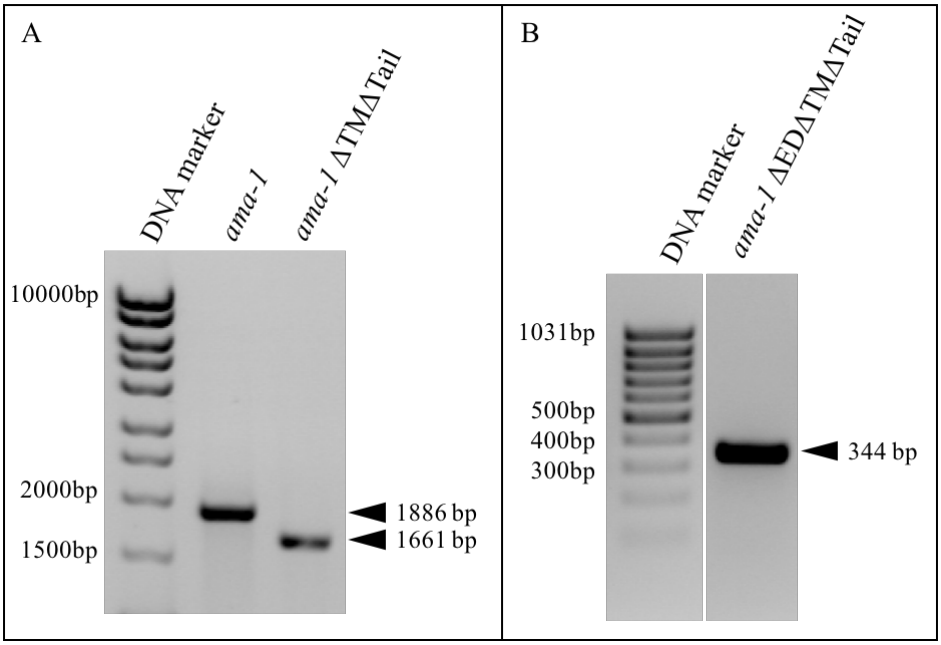


Figure 3.13. Creating *Pfama-1* mini-genes by PCR amplification.
Size validation of mini-genes by gel electrophoresis against a base pair standard. **A** – *Pfama-1* and *Pfama-1*ΔTmΔTail mini-genes. **B** – *Pfama-1*ΔEDΔTMΔTail mini-gene.

To delete the prodomain, *Pfama-1*ΔPD was created by overlap extension PCR (Figure 3.14). First the signal peptide was amplified to generate a PCR product of 103bp (Product 1; Figure 3.14 A), containing a 21bp 3' overhang. Next, the ectodomain to cytoplasmic tail region of the gene was amplified, resulting in an amplicon of 1588bp (Product 2; Figure 3.14 B). Subsequently, these two products were fused together by an overlap extension PCR protocol, resulting in a 1670bp mini-gene which excluded the *Pfama-1* prodomain (Figure 3.14 C). During the overlap extension PCR, the overhang of product 1 attaches to product 2, which results in a loss of 21bp from the final product.

Due to the small size of Product 1, it was necessary to verify that the signal peptide had indeed been fused to Product 2. The difference between a fragment of 1588bp and 1670bp was not easily identified by gel electrophoresis, thus a restriction endonuclease digest was performed on the final product after overlap extension PCR. Digestion using FastDigest® *Eco*RI resulted in two fragments of 1399 and 271bp (Figure 3.14 D) as expected, instead of 1399 and 189bp, verifying that the overlap extension PCR was successful in the creation of *Pfama-1*ΔPD.

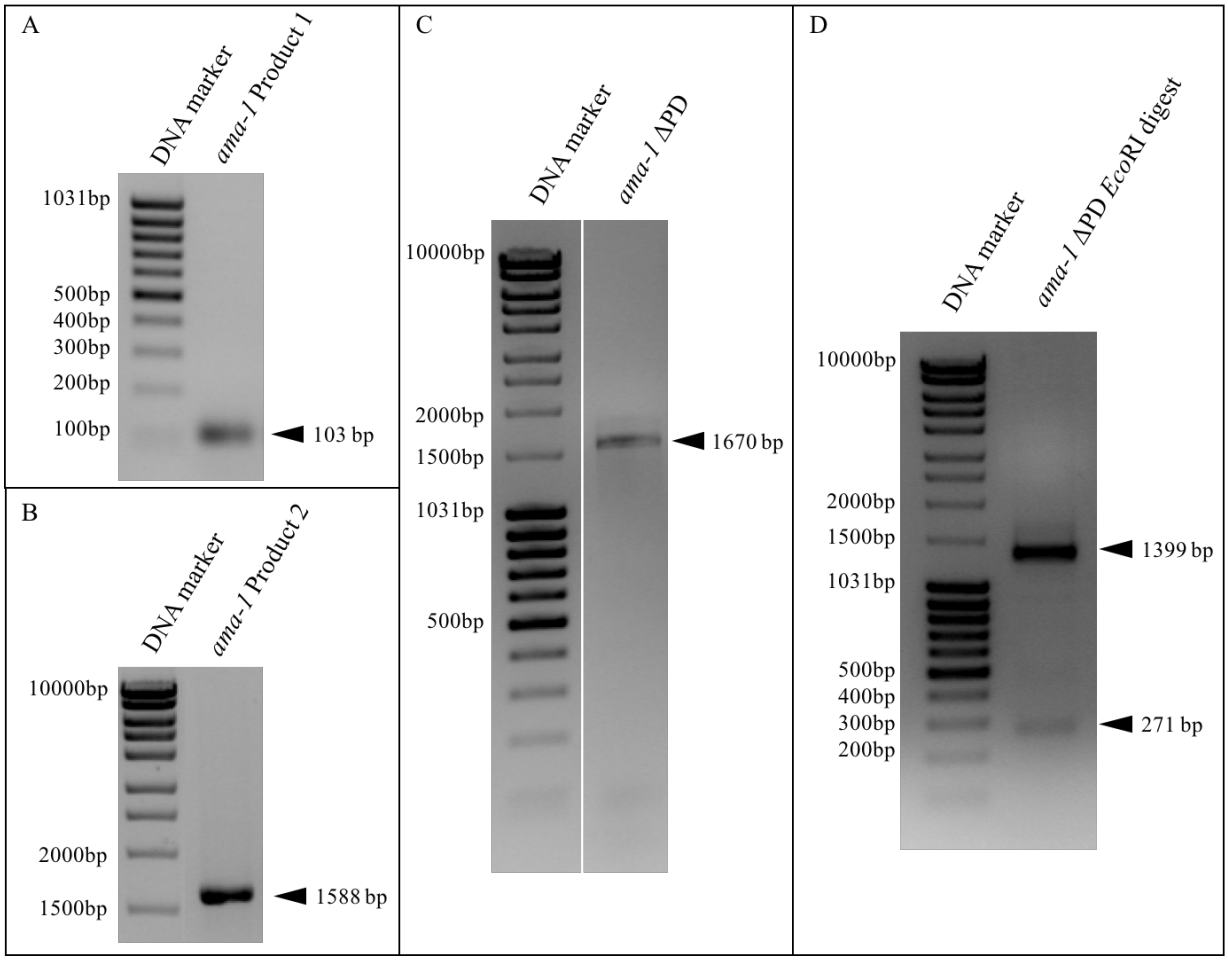


Figure 3.14. Creating *Pfama-1*ΔPD by overlap extension PCR.
Size validation of domains by gel electrophoresis against a base pair standard. **A** – *Pfama-1* Product 1: signal peptide. **B** – *Pfama-1* Product 2: ED-TM-Tail. **C** – *Pfama-1*ΔPD generated by overlap extension PCR using Product 1 and Product 2. **D** – Verification of overlap extension PCR by *Eco*RI restriction endonuclease digestion of *Pfama-1*ΔPD. The correct amplicon resulted in two fragments of 1399 and 271bp, instead of 1399 and 189bp.

3.3.2.5 Generation & Verification of pARL-mCherry Constructs

After restriction endonuclease digestion with *Xho*I and *Avr*II, *P. falciparum* amplicons and mCherry plasmid were quantified by gel electrophoresis and ligated in a 5:1 ratio. Competent *E. coli* XL10 cells were transformed with 100ng of the ligated constructs and 10 to 500 colonies grew on the ampicillin-treated agar plates.

Colonies were picked, amplified and the plasmid isolated for verification. Restriction endonuclease digestion of the mCherry control plasmid (Figure 3.16) and the *Pfama-1* mCherry constructs (Figure 3.17) confirmed that amplicons of the correct sizes had been inserted into the mCherry plasmid. To minimise costs, various combinations of restriction endonucleases were used, instead of *Xho*I and *Avr*II that had been used for cloning. Positive clones were sequenced by Inqaba Biotec™, which confirmed that inserts were error-free and in-frame.

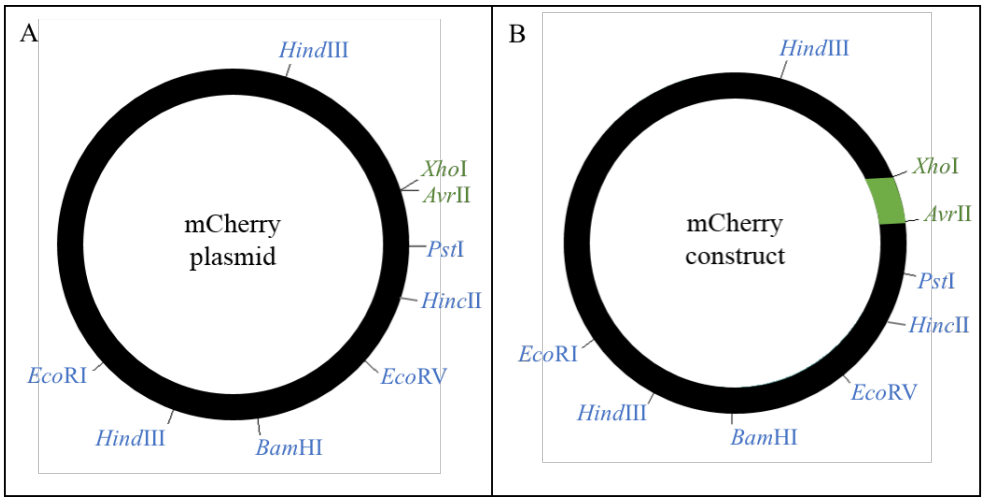


Figure 3.15. Restriction enzyme sites of pARL-mCherry plasmid and constructs.
A – Empty mCherry plasmid. **B –** mCherry construct created by directional insertion of mini-gene shown in green. Verification of clones was performed by restriction endonuclease digestion using selected FastDigest® enzymes.

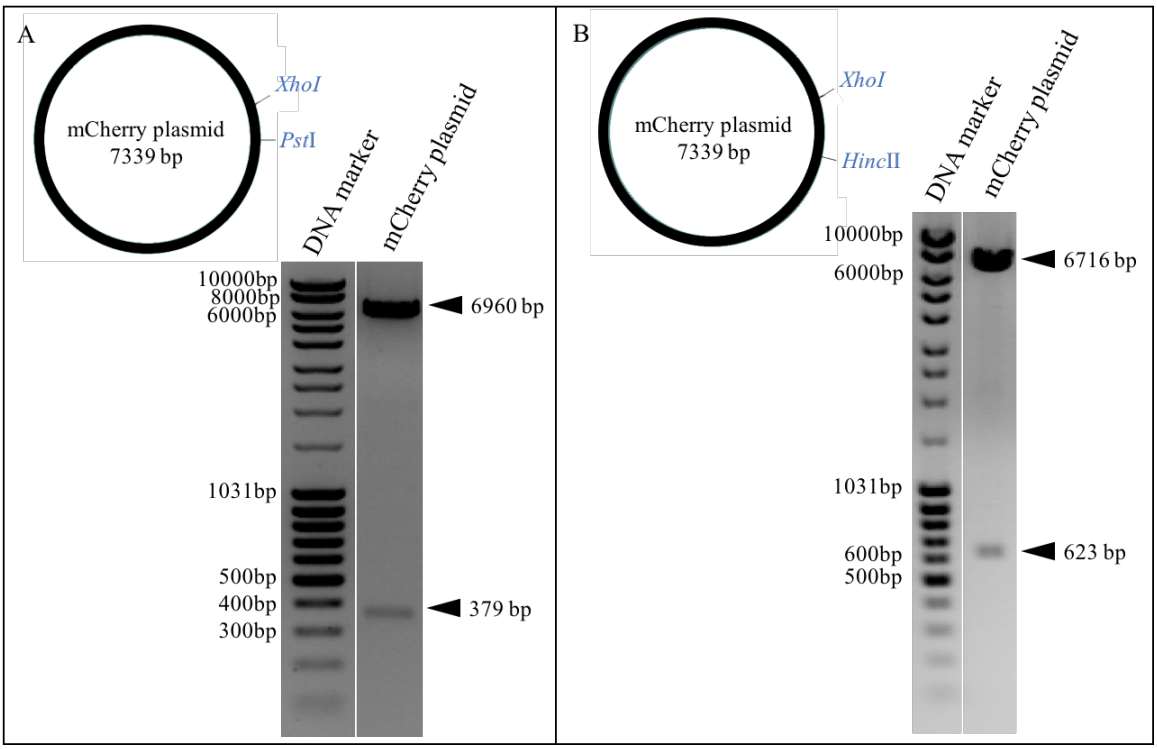


Figure 3.16. Restriction enzyme digestion of control mCherry plasmid for verification of mCherry constructs.

Size validation of mCherry plasmid after restriction endonuclease digestion by gel electrophoresis against a base pair standard. **A –** Digestion of the control mCherry plasmid with *Xho*I and *Pst*I resulted in two fragments of 6960 and 379 base pairs. **B –** Digestion of the control mCherry plasmid with *Xho*I and *Hinc*II resulted in two fragments of 6716 and 623 base pairs.

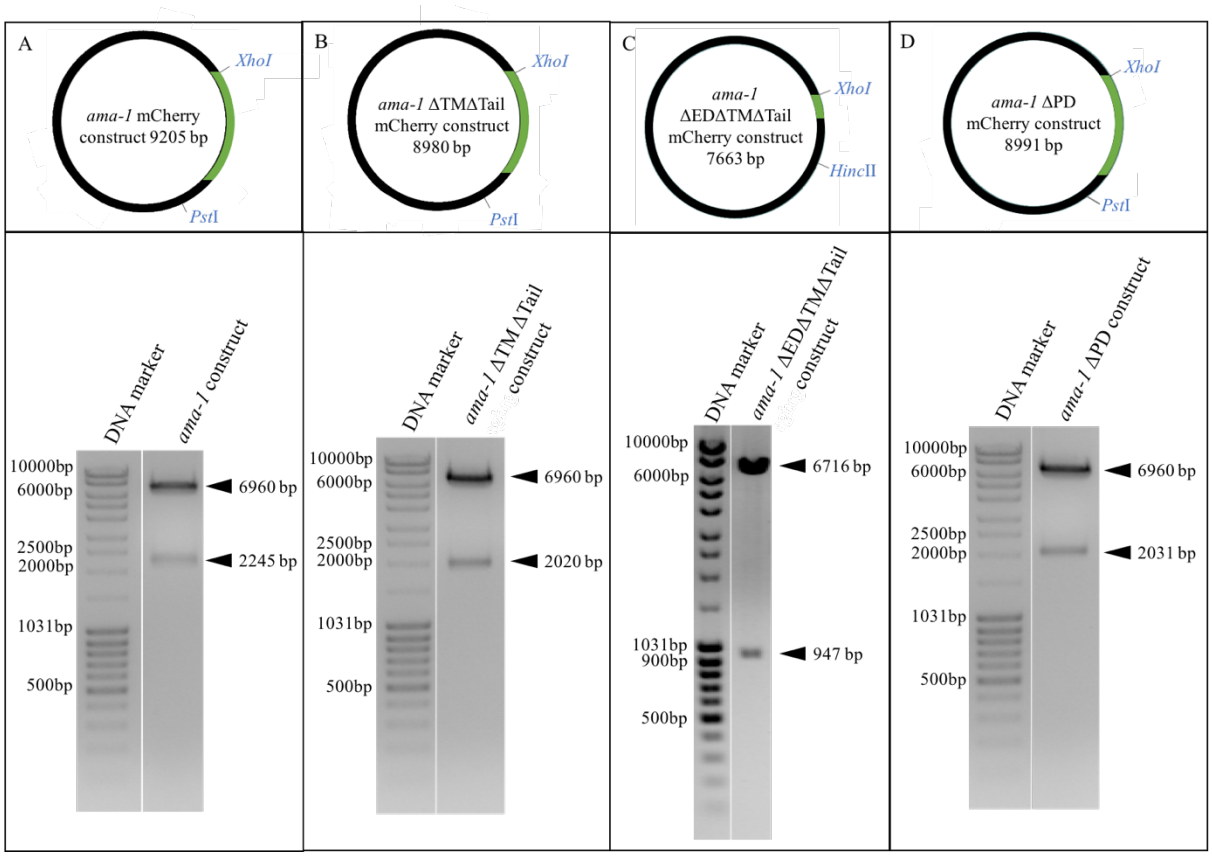


Figure 3.17. Verification of *Pfama-1* mCherry constructs.
Size validation of four *Pfama-1* mCherry constructs was done by restriction endonuclease digestion and visualization by gel electrophoresis against a base pair standard. Successful insertion of the *Pfama-1* mini-genes resulted in two fragments. **A –** Full length *Pfama-1* digested with with *Xho*I and *Pst*I yielded 6860bp and 2245bp. **B –** ΔTMΔTail digested with *Xho*I and *Pst*I yielded 6860bp and 2020bp. **C –** ΔEDΔTMΔTail digested with *Xho*I and *Hinc*II yielded 6716bp and 947bp. **D –** ΔPD digested with *Xho*I and *Pst*I yielded 6860bp and 2031bp.

3.3.3 *Pf*AMA-1 Transgenic Parasites

3D7 *P. falciparum* parasites were electroporated with the prepared plasmid constructs. WR99210 compound was administered to the cultures to ensure that only parasites with the plasmid survived. From 25 to 42 days after transfection, live parasites were visible in the transgenic cultures.

To confirm that the transgenic parasites contained the desired constructs, PCR verification was performed using mCherry backbone primers flanking the mini-gene insert site. A PCR product of 534bp was obtained when the mCherry transgenic line, expressing only mCherry, was used (Figure 3.18). PCR parameters and primer information can be found in Appendix A.

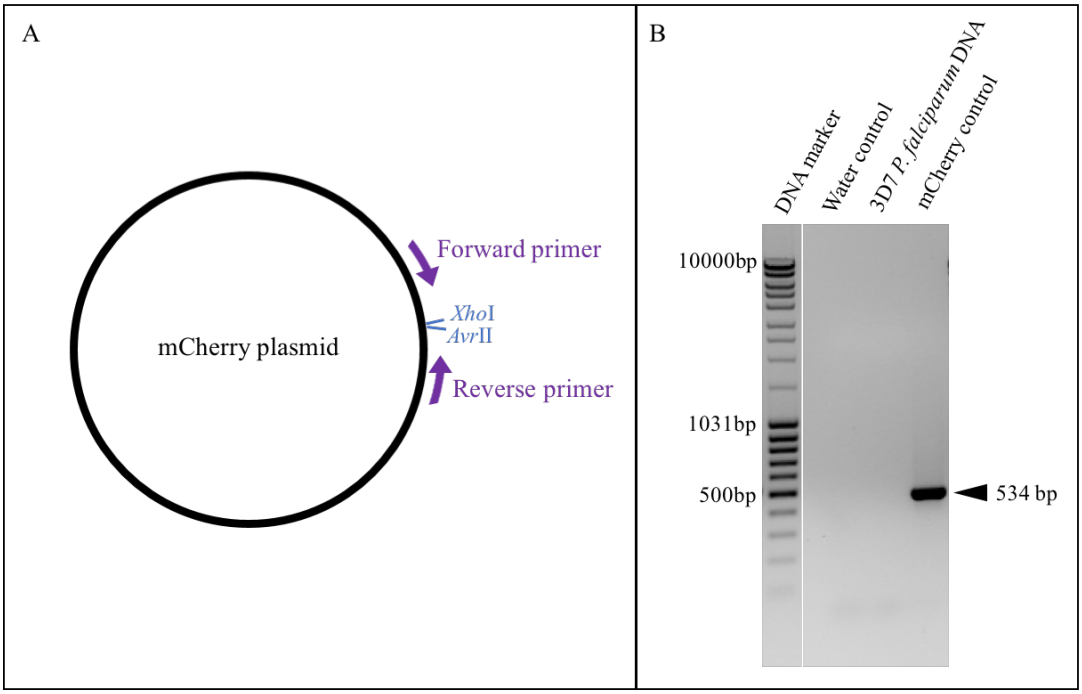


Figure 3.18. PCR verification of the *P. falciparum* transgenic parasite line containing the mCherry plasmid.
A – mCherry primers flanking the mini-gene insert were used to confirm that DNA extracted from transgenic parasites contained the gene of interest. The forward primer binding site was chosen within the *ama-1* promoter region and the reverse primer binding site was within the mCherry coding region. **B** – PCR verification of mCherry transgenic parasite lines by agarose gel electrophoresis. A reaction without DNA template was included as a negative "water" control. As expected, no PCR product was obtained in the reaction with wild-type 3D7 *P. falciparum* DNA as template. A product of 534bp was amplified when using the control mCherry transgenic line, which did not have a mini-gene insert.

The PCR products migrated according to the expected sizes as determined by agarose gel electrophoresis (Figure 3.19). Due to the binding sites of the primers, all amplified products were 534bp larger (Figure 3.18) than the mini-gene insert sizes: 2400bp, 2175bp, 858bp and 2184bp for the full length; ΔTMΔTail; ΔEDΔTMΔTail and ΔPD AMA-1 mCherry transgenic lines, respectively. These results confirmed that all four *Pf*AMA-1 transgenic cultures carried the appropriate constructs.

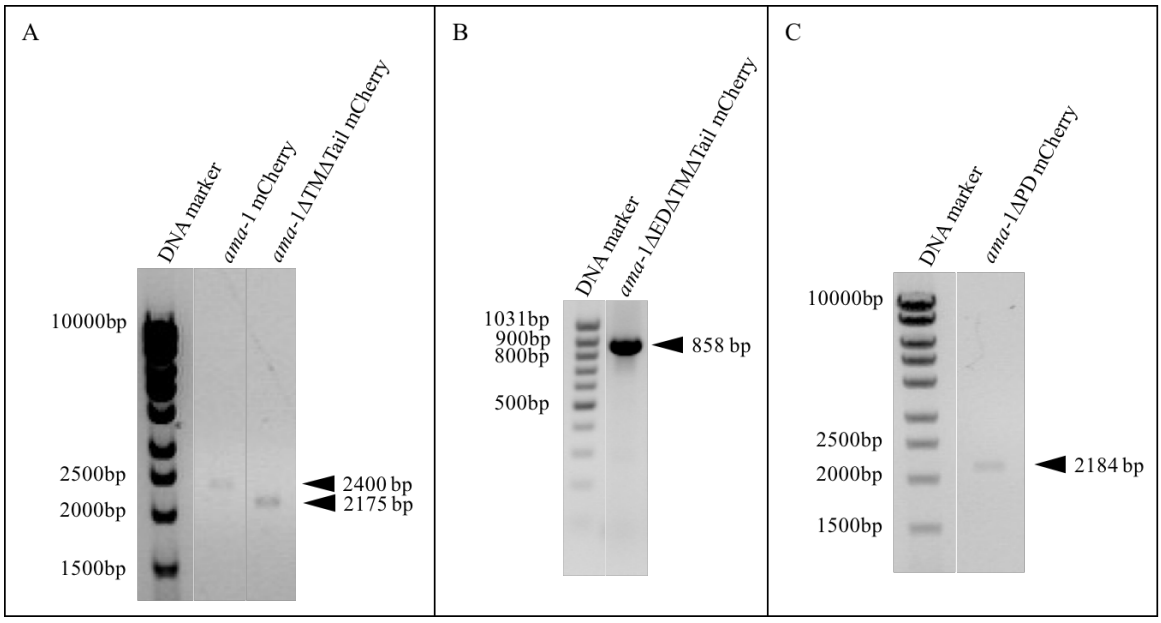


Figure 3.19. PCR verification of *Pf*AMA-1 transgenic parasite lines.
Transgenic parasite DNA was amplified using mCherry backbone primers to confirm successful uptake of plasmid constructs. Size validation was performed by gel electrophoresis against a base pair standard and all the PCR products were confirmed to be the correct sizes: **A** –*Pfama*-1 mCherry 2400bp; *Pfama*-1ΔTMΔTail mCherry 2175bp. **B** –*Pfama*-1ΔEDΔTMΔTail mCherry 858bp. **C** – *Pfama*-1ΔPD mCherry 2184bp.

Unfortunately, the yield of PCR products was poor for the clones with large mini-genes (>2000bp; Figure 3.19 A & C) compared to the smaller mini-gene (<1000bp; Figure 3.19 B). Attempts to enhance the yield of these products included using different polymerases, as well as adjusting the PCR protocol by lengthening the extension times, varying the denaturation times and increasing the number of cycles.

3.3.4 Identification of the Domain Targeting *Pf*AMA-1 to the Micronemes

3.3.4.1 Live Imaging of *Pf*AMA-1 Transgenic Parasites

Transgenic *P. falciparum* cultures were prepared for microscopy by DAPI treatment to stain the parasite nuclei. No auto-fluorescence or colour-bleeding was observed during microscopy (Appendix B). Rapid photo-bleaching of the mCherry signal was observed when fluorescence images were captured, often leading to very faint fluorescent signals. To improve the stability of the signals, light exposure on the samples was reduced by the use of a ND-25 neutral density filter. This filter is placed between the light source and the sample and only allows 25% of the light onto the sample, which is sufficient to visualise the fluorescence and capture an image before the signal fades.

*Pf*AMA-1 is expressed in the schizont stages after the micronemes have developed, thus schizont stage cultures were used for microscopy experiments. The parasite depicted in the top panel of Figure 3.20 expressed the full length mCherry-tagged *Pf*AMA-1. The red fluorescence appeared as small puncta that did not co-localise with the blue parasite nucleus, implying apical localisation.

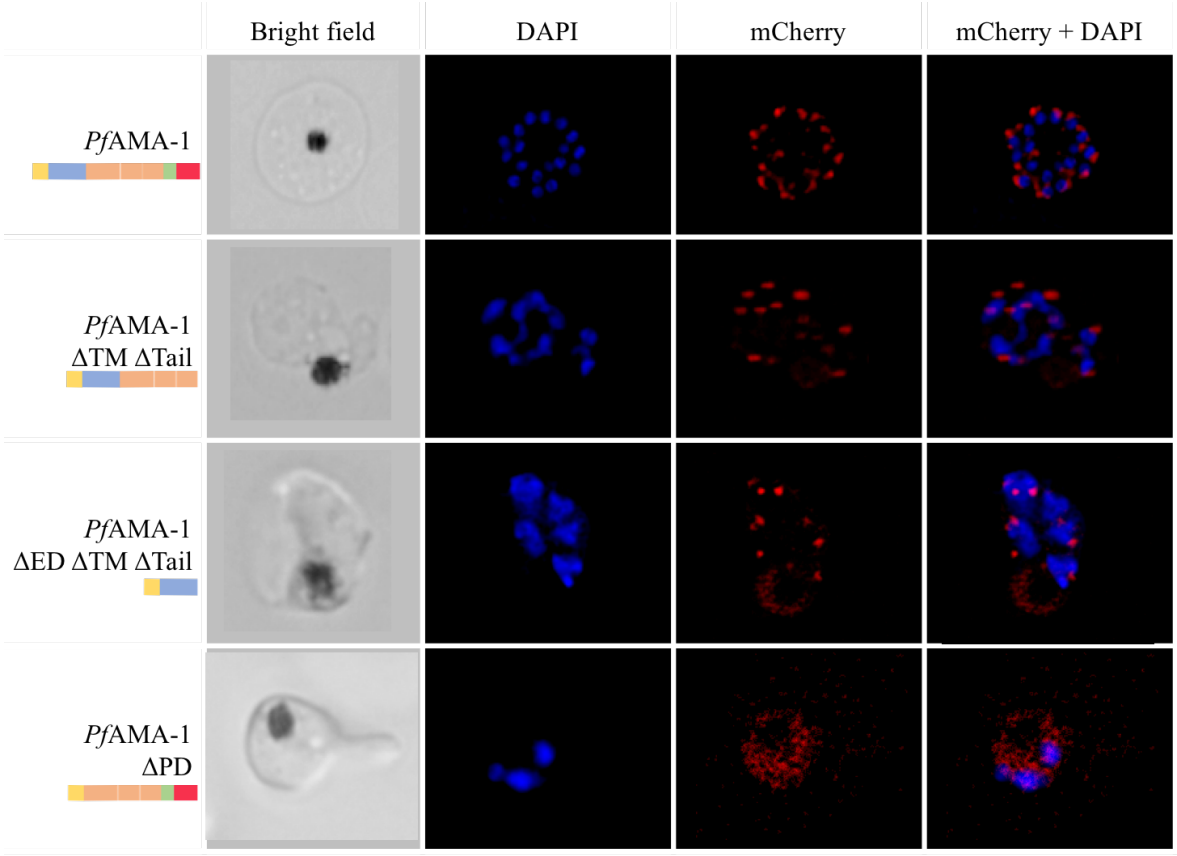


Figure 3.20. Fluorescence images of live schizont stage *P. falciparum* transgenic parasites expressing mCherry-tagged *Pf*AMA-1.
Parasites were viewed at 1000x magnification. mCherry causes red fluorescence of chimaeric *Pf*AMA-1 proteins. DAPI is a blue nuclear stain. **Top Panel**: Full length *Pf*AMA-1 localised to points, which did not co-localise with the nucleus (blue), and appeared to be in the apical region. **Middle Panels**: Removal of the transmembrane domain and cytoplasmic tail (ΔTM and ΔTail respectively) and ectodomains (ΔED) did not change expression patterns. **Bottom Panel**: The deletion of the prodomain (ΔPD) resulted in a noticeable change in the mCherry fluorescence. The protein appeared dispersed throughout the parasite cytoplasm.

When the transmembrane domain, cytoplasmic tail and three ectodomains were removed (*Pf*AMA-1ΔTMΔTail and *Pf*AMA-1ΔEDΔTMΔTail; middle panels of Figure 3.20), the red fluorescence of the mCherry tag remained punctate. However, when the prodomain was absent (*Pf*AMA-1ΔPD; bottom panel of Figure 3.20), the protein appeared dispersed in the

parasite cytoplasm and was no longer confined to the apical region. These findings suggest that the prodomain of *Pf*AMA-1 is required for targeting the micronemes.

3.3.4.2 Co-localisation Studies of *Pf*AMA-1 Chimaeric Proteins

To determine which organelle the mCherry tagged chimaeric proteins localised to, imaging experiments were performed using a known microneme marker, PfEBA175. Transgenic parasite cultures were fixed, permeabilised and incubated with DAPI to stain the nucleus, as well as an anti-EBA175 antibody with a green fluorochrome, which would identify the micronemes. Co-localisation control experiments were performed (Appendix B), which confirmed that no auto-fluorescence or colour-bleeding occurred as a result of the co-localisation protocol.

*Pf*EBA175 appeared as puncta (Figure 3.21), which is consistent with the localisation pattern of micronemes in schizont stage *P. falciparum* parasites (Treeck *et al.,* 2006). The full length *Pf*AMA-1 protein appeared apically distinct and co-localised with the microneme marker, giving a yellow signal (Figure 3.21 top panel). Despite some distinct red and green puncta on the overlay, the expression patterns of the mCherry-tagged protein and GFP-tagged microneme marker were very similar and a Pearson's coefficient of 0.70 indicated that co-localisation was achieved. Upon removal of the transmembrane domain, cytoplasmic tail and ectodomains (Figure 3.21 middle panels), the mCherry signal remained punctate and co-localised with the microneme marker, confirming that these domains are not required to target *Pf*AMA-1 to the micronemes. These observations were supported by Pearson's coefficients of 0.69 and 0.80 respectively.

When the *Pf*AMA-1 prodomain alone was deleted (Figure 3.21 bottom panel), the mCherry fluorescence appeared dispersed and no longer co-localised with the microneme marker. This was supported by a Pearson's coefficient of 0.24, which confirmed that the prodomain of *Pf*AMA-1 is required to target the protein to the micronemes.

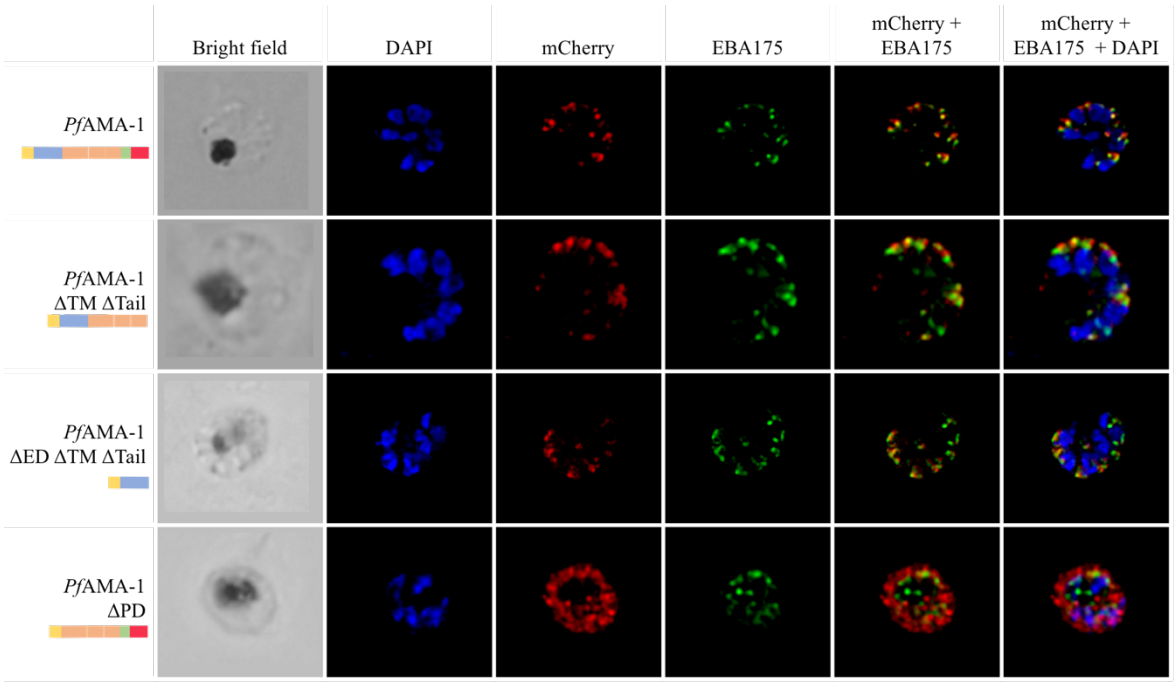


Figure 3.21. Co-localisation studies using fixed schizont stage *P. falciparum* parasites expressing mCherry-tagged *Pf*AMA-1.
Parasites were viewed at 1000x magnification. mCherry causes red fluorescence of chimaeric *Pf*AMA-1 proteins. DAPI is a blue nuclear stain. A microneme marker, *Pf*EBA175, with a green fluorochrome was used to determine the localisation of mCherry tagged proteins within the transgenic parasites. Should the red mCherry-tagged proteins co-localise with the green micronemes, a yellow signal will be obtained when an overlay between the red and green colour channels is performed. Pearson's coefficients (PC) are a numerical indicator of co-localisation, with values close to 1 indicating strong co-localisation. **Top Panel**: Full length *Pf*AMA-1 showed a punctate pattern that co-localised with the green *Pf*EBA175 microneme signal, indicated by the yellow fluorescence observed in the overlay (PC 0.70). **Middle Panels**: Removal of the transmembrane domain and cytoplasmic tail (ΔTM and ΔTail; PC 0.69) and ectodomains (ΔED; PC 0.80) gave a similar pattern. **Bottom Panel**: In the absence of only the prodomain (ΔPD), the mCherry fluorescence was dispersed and no longer co-localised with the green microneme marker (PC 0.24). (An enlarged version of this image can be seen in in Appendix C; Figure 10.1).

3.3.5 Creating *Pfama-1* Prodomain Mini-Genes

The first set of mini-genes (Figure 3.11) was designed to determine which of the *Pf*AMA-1 domains are required to target the parasite micronemes. Fluorescence microscopy (Figure 3.20) and co-localisation studies (Figure 3.21) using transgenic lines expressing these chimaeric proteins showed that the prodomain alone was responsible for correct localisation (Figure 3.22).

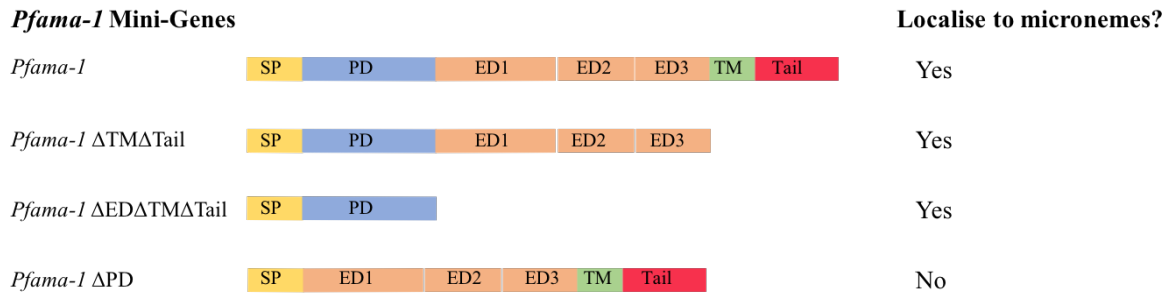


Figure 3.22. A summary of the co-localisation studies using mCherry-tagged *Pf*AMA-1.
The results of the co-localisation studies performed on four mCherry-tagged chimaeric *Pf*AMA-1 proteins showed that the prodomain (PD; in blue) was required for correct trafficking to the parasite micronemes.

To further assess which specific region of the *Pf*AMA-1 prodomain is required to target the micronemes, three more mini-genes were designed.

3.3.5.1 Designing *Pfama-1* Prodomain Mini-Genes

In each of these mini-genes, 54bp were systematically deleted from the C-terminal end of the prodomain (Figure 3.23). The signal peptide, which is required for trafficking through the ER, was included in the mini-genes.

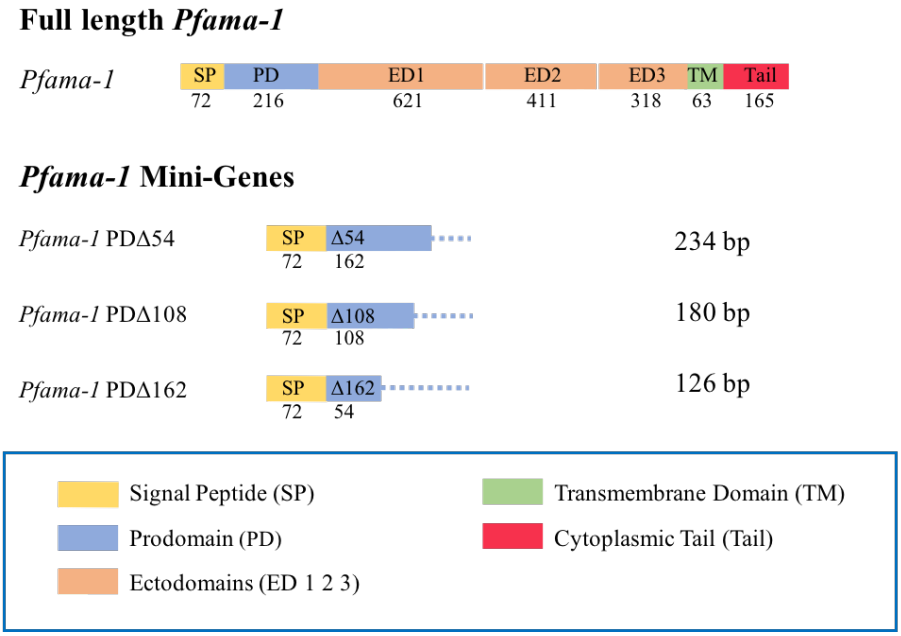


Figure 3.23. A schematic depicting the *Pfama-1* prodomain mini-genes.
Three mini-genes were designed with successive deletions of 54bp from the C-terminal end of the prodomain. The sizes of each domain and of the mini-genes are shown in base pairs (bp).

3.3.5.2 PCR Amplification of the *Pfama-1* Prodomain Mini-Genes

The three *Pfama-1* prodomain mini-genes were generated by PCR amplification using genomic DNA (Figure 3.12) and appropriate primers flanking the region of interest. The primer sequences and PCR parameters can be found in Appendix A.

Table 3.2. Expected PCR product sizes of *Pfama-1* prodomain mini-genes.

Gene	Mini-genes	Domains	Domain size (bp)	PCR product size (bp)
Pfama-1	PDΔ54	SP-PDΔ54	234	254
	PDΔ108	SP-PDΔ108	180	200
	PDΔ162	SP-PDΔ162	126	146

All PCR products migrated according to their expected sizes (Table 3.2) as assessed by agarose gel electrophoresis (Figure 3.24). PCR products were slightly larger than the domain sizes due to additions to the primers as described in Appendix A.

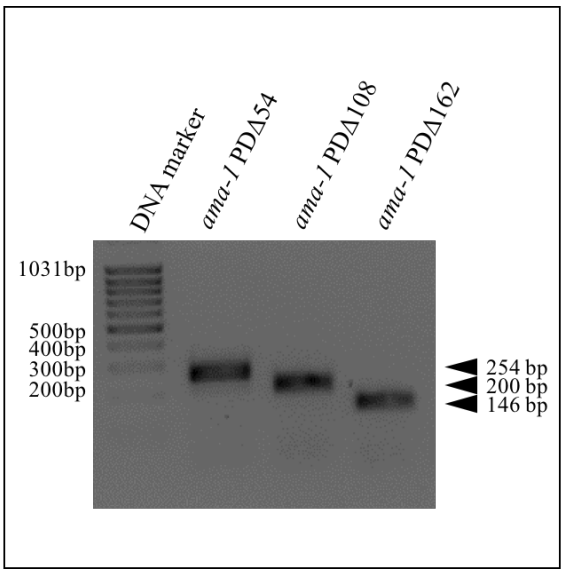


Figure 3.24. Creating *Pfama-1* prodomain mini-genes by PCR amplification.
Size validation of mini-genes by gel electrophoresis against a base pair standard.

3.3.5.3 Cloning the Prodomain Mini-Genes into pARL-mCherry

After restriction endonuclease digestion, *P. falciparum* amplicons and mCherry plasmid were quantified by gel electrophoresis and ligated in a 5:1 ratio. Competent *E. coli* XL10 cells were transformed with 100ng of the ligated constructs and 10 to 500 colonies grew on the ampicillin-treated agar plates.

Colonies were picked, amplified and the plasmid isolated for verification. Restriction endonuclease digestion of the mCherry control plasmid and the *Pfama-1* prodomain mCherry constructs (Figure 3.25) using FastDigest® enzymes *Xho*I and *Pst*I, confirmed that amplicons of the correct sizes were inserted into the mCherry plasmid. Positive clones were sequenced by Inqaba Biotec™, which confirmed that inserts were error free and in-frame.

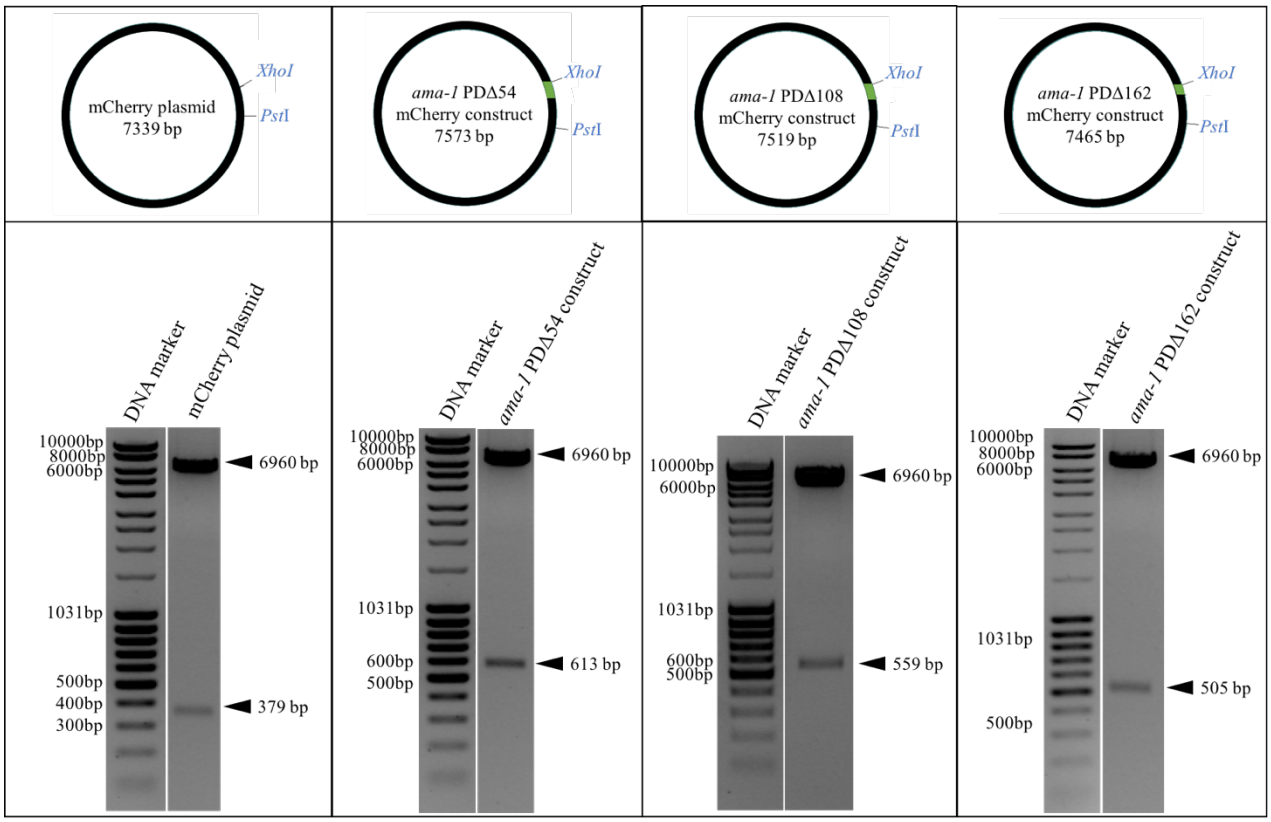


Figure 3.25. Verification of *Pfama-1* prodomain mCherry constructs.
Size validation of constructs after *Xho*I and *Pst*I restriction endonuclease digestion by gel electrophoresis against a base pair standard. **A –** Digestion of the control mCherry plasmid, resulted in two fragments of 6960 and 379bp each. **B to D – S**uccessful ligation resulted in the 379bp fragment increasing in size according to the size of the mini-gene insert.

3.3.6 Transgenic Parasites with *Pf*AMA-1 Prodomain Truncations

3D7 *P. falciparum* parasites were electroporated with the three prepared plasmid constructs. WR99210 compound was administered to the cultures so that only parasites with the plasmid survived. From 28 to 31 days after transfection, live parasites were visible in the transgenic cultures. To confirm that the transgenic parasites contained the desired constructs, PCR verification was performed using mCherry backbone primers flanking the mini-gene insert site (Figure 3.18). PCR parameters and primer information can be found in Appendix A.

The resultant products migrated according to the expected sizes as determined by agarose gel electrophoresis (Figure 3.26). Due to the binding sites of the primers, all amplified products were 534bp larger (Figure 3.18) than the mini-gene insert sizes: 768bp, 714bp and 660bp for the PDΔ54; PDΔ108; PDΔ162 *Pf*AMA-1 mCherry transgenic lines respectively. These results confirmed that all three of *Pf*AMA-1 transgenic cultures carried the appropriate constructs.

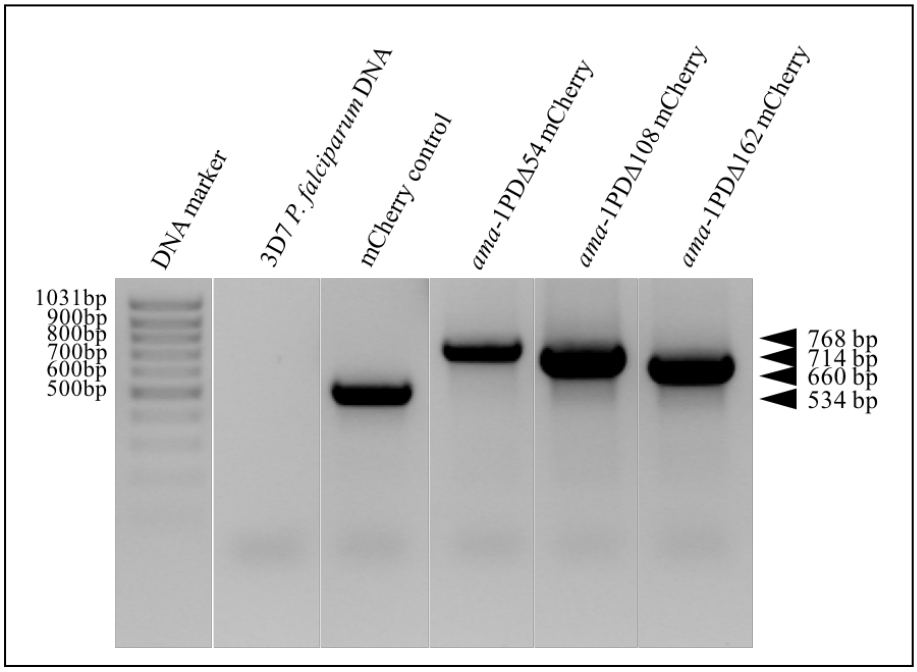


Figure 3.26. PCR verification of transgenic parasite lines expressing *Pf*AMA-1 with prodomain truncations.
PCR analysis of transgenic parasite DNA using mCherry backbone primers to confirm the presence of the plasmid constructs. Size validation was performed by gel electrophoresis against a base pair standard.

3.3.7 Identification of the Sub-Domain Required for *Pf*AMA-1 Trafficking

3.3.7.1 Live Imaging of *Pf*AMA-1 Prodomain Transgenic Parasites

Transgenic *P. falciparum* cultures were prepared for microscopy by DAPI treatment to stain the parasite nuclei. When half of the prodomain (i.e. the C-terminal 108bp) was deleted, the pattern of mCherry fluorescence was different compared to *Pf*AMA-1ΔEDΔTMΔTail, when the full prodomain was present (Figure 3.27; bottom panel). In addition to distinct puncta appearing at the apex of the merozoites, red fluorescence was also visible in other regions of the schizont. These results suggest that the deleted 108bp are required for microneme localisation.

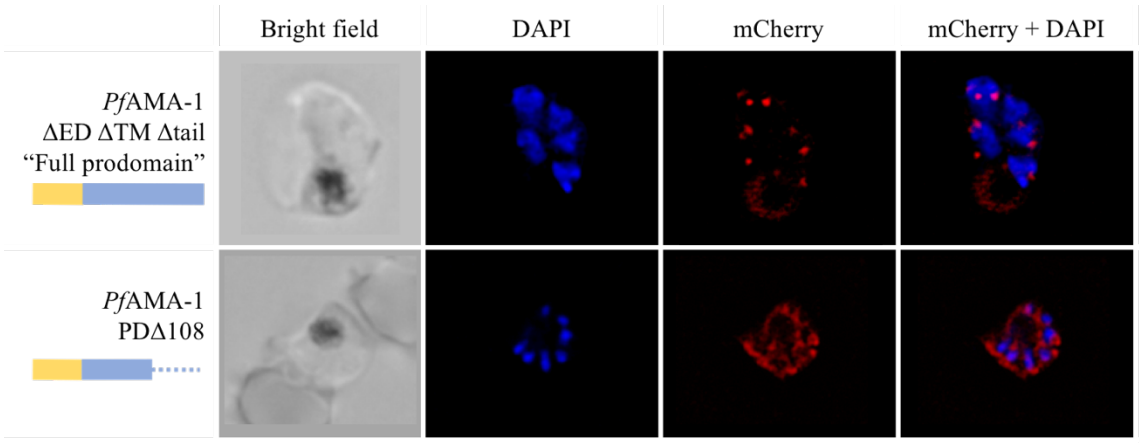


Figure 3.27. Fluorescence images of live schizont stage *P. falciparum* transgenic parasites expressing mCherry-tagged *Pf*AMA-1 prodomain truncations.
mCherry causes red fluorescence of chimaeric *Pf*AMA-1 prodomain truncated proteins. DAPI is a blue nuclear stain.
Top Panel: When the full prodomain was present, mCherry localisation was punctate and apically distinct, as is expected for microneme localisation. **Bottom Panel:** When the C-terminal half of the prodomain was deleted (PDΔ108), the localisation pattern changed and red fluorescence was no longer limited to the apex.

3.3.7.2 Co-localisation Studies

Transgenic parasite cultures were fixed, permeabilised and incubated with DAPI to stain the nucleus, as well as an anti-EBA175 antibody with a green fluorochrome, which would allow the identification of the micronemes.

As a point of reference, images from the *Pf*AMA-1ΔEDΔTMΔTail co-localisation were included in Figure 3.28 (top panel): the apically distinct mCherry fluorescence co-localised with the green microneme marker, giving a yellow signal and a Pearson's coefficient of 0.80. When 18 or 36aa were deleted from the C-terminal of the prodomain (*Pf*AMA-1 PDΔ54 and PDΔ108), the mCherry fluorescence pattern was altered (Figure 3.28; second and third panels). Despite distinct red puncta that appeared to localise to the apex, microneme localisation was very limited and the signal was more dispersed, with Pearson's coefficients of 0.56 and 0.46 supporting this finding. The dispersed pattern was more pronounced in *Pf*AMA-1 PDΔ162, where the red signal occurred throughout the parasite (Pearson's coefficient of 0.26), indicating mis-targeting of the protein (Figure 3.28; bottom panel).

These findings suggest that the C-terminal 54aa (108bp) of the prodomain are essential for the trafficking of *Pf*AMA-1 to the micronemes.

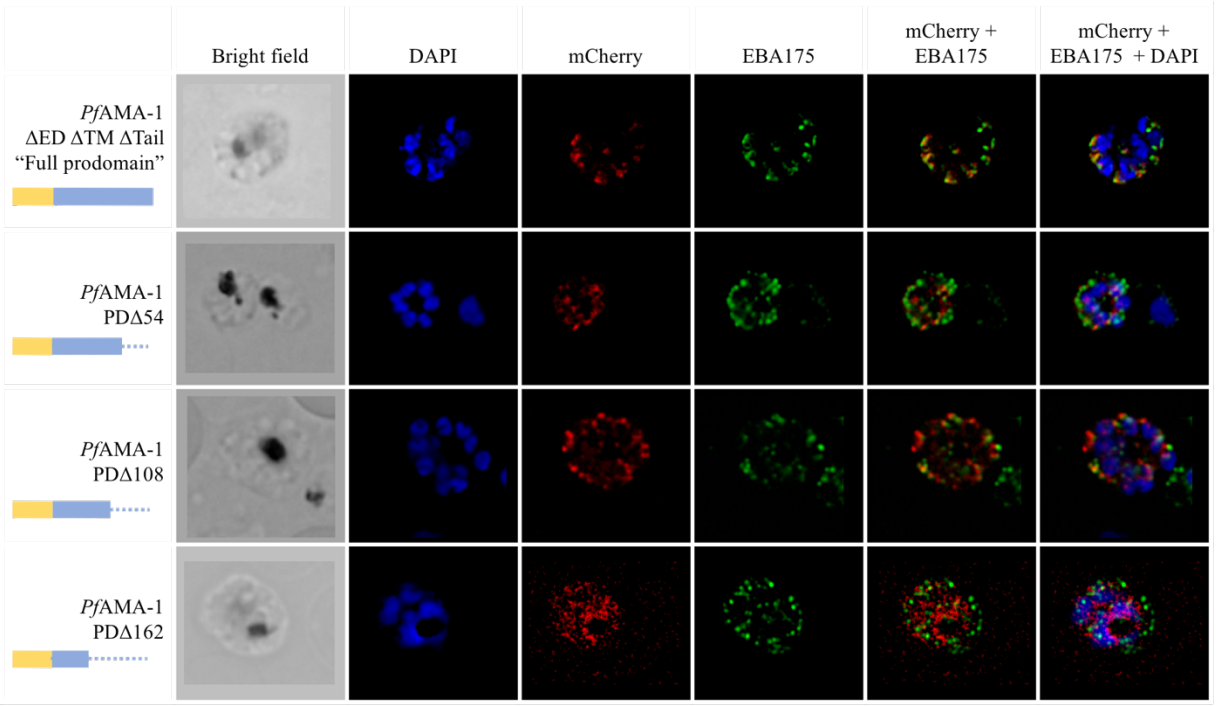


Figure 3.28. Co-localisation studies using fixed schizont stage *P. falciparum* parasites expressing mCherry-tagged *Pf*AMA-1 prodomain truncations.
Parasites were viewed at 1000x magnification. mCherry causes red fluorescence of the chimaeric *Pf*AMA-1 prodomain truncated proteins. DAPI is a blue nuclear stain. A microneme marker, *Pf*EBA175, with a green fluorochrome was used to determine the localisation of mCherry tagged proteins within the transgenic parasites. Pearson's coefficients (PC) are a numerical indicator of co-localisation, with values close to 1 indicating strong co-localisation. **Top Panel**: *Pf*AMA-1ΔEDΔTMΔTail, which consisted only of the signal peptide and the prodomain, were present in the apex and co-localised with the microneme marker (PC 0.80). **Second and Third Panels:** *Pf*AMA-1 PDΔ54 and PDΔ108 yielded partial apical localisation, with minimal overlap with the microneme marker (PC 0.56 and 0.46 respectively). **Bottom Panel**: *Pf*AMA-1 PDΔ162 was dispersed throughout the parasite (PC 0.26). (An enlarged version of this image can be seen in in Appendix C; Figure 10.2).

3.4 Discussion

To date, there is no information on the trafficking mechanism of *Pf*AMA-1 to the micronemes. Through the use of transgenic parasite lines, which express fluorescently-tagged chimaeric peptides, the *Pf*AMA-1 prodomain has been identified as essential for microneme targeting. This is both a novel and unexpected finding. Novel, because no domain has yet been implicated in targeting *Pf*AMA-1 to the micronemes. Unexpected, because another micronemal invasion protein, *Pf*EBA175, a member of the EBL family, possesses a conserved cysteine-rich domain that is required for targeting the micronemes. Furthermore, not all invasion proteins have prodomains.

3.4.1 *Pf*AMA-1 Does Not Require a Tyrosine Motif to Target the Micronemes

The C-terminus of *Pf*AMA-1 is made up of a hydrophobic transmembrane domain and a hydrophilic cytoplasmic tail. Despite the presence of a tyrosine-based sorting motif, YXXϕ, in the cytoplasmic tail, previous studies have already shown this region of *Pf*AMA-1 is not required for trafficking to the micronemes (Treeck *et al.,* 2009). Co-localisation experiments in this study using a truncated *Pf*AMA-1, with the transmembrane domain and cytoplasmic tail deleted, not only confirmed this, but further showed that the transmembrane domain is not required for correct targeting to the micronemes (Figure 3.21).

3.4.2 The Cysteine-rich Ectodomain of *Pf*AMA-1 Does Not Contain a Microneme Trafficking Signal

The bulk of *Pf*AMA-1 is made up of the three sub-regions of the ectodomain. The presence of a hydrophobic cleft (discussed in the literature review) in the folds of the ectodomain regions, makes the ectodomains essential for *Pf*AMA-1 as a ligand.

*Pf*EBA175 trafficking to the micronemes is dependent on a C-terminal conserved cysteine-rich domain (Treeck *et al.,* 2006). Other members of the *Pf*EBL family share these 8 conserved cysteines, and it is proposed that all members of this protein family target the micronemes using this domain (Treeck *et al.,* 2006). The *Pf*AMA-1 ectodomain contains 16 conserved cysteine residues (Howell *et al.,* 2003; Figure 3.29), which are required for the formation of intramolecular disulphide bonds and thus the folding of the protein, and may be implicated in microneme targeting.

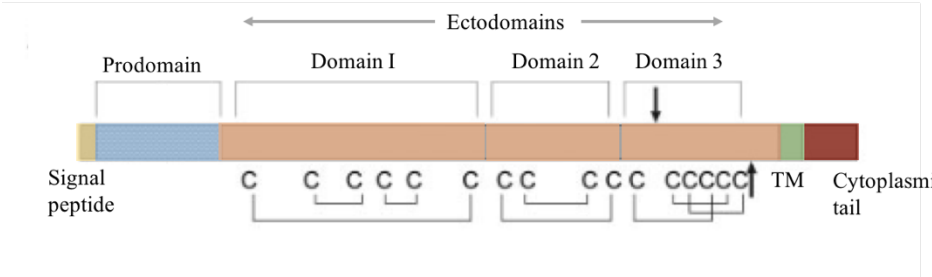


Figure 3.29. A schematic showing the primary structure and *Pf*SUB2 proteolytic cleavage sites of *Pf*AMA-1.
There are 16 conserved cysteine residues within the ectodomain regions of *Pf*AMA-1, which form intramolecular disulphide bonds (indicated by the square brackets). The two arrows indicate the proteolytic cleavage sites for *Pf*SUB2 (Adapted from Howell *et al.,* 2003).

Co-localisation experiments in this study (Figure 3.21), however, showed, that the cysteine-rich ectodomain is not required for microneme targeting of *Pf*AMA-1.

An alignment of the *Pf*AMA-1 ectodomain (position 97 to 546) and the *Pf*EBA175 cysteine-rich domain (position 1311 to 1417), shows that only 4 of the 8 conserved *Pf*EBA cysteines are shared with *Pf*AMA-1 (Figure 3.30). There is little sequence similarity between these two proteins since they come from different families.

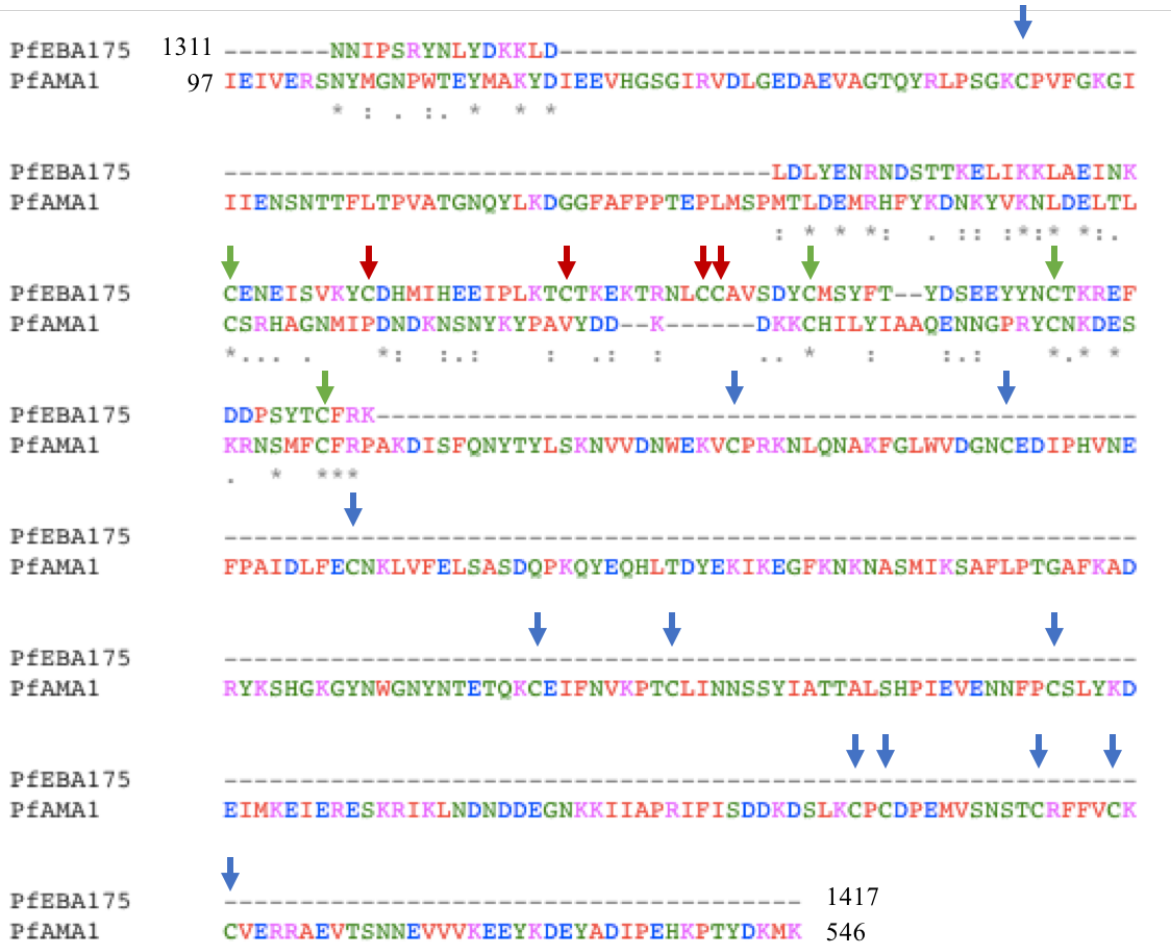


Figure 3.30. Sequence alignment of *Pf*AMA-1 ectodomain and *Pf*EBA175 C-terminal cysteine-rich domain.
There is little sequence similarity between the ectodomain of *Pf*AMA-1 (position 97 to 546) and the cysteine-rich domain of *Pf*EBA175 (position 1311 to 1417), despite the presence of a high number of cysteine residues. *Pf*AMA-1 ectodomain possesses 16 cysteine residues (indicated with blue arrows), whereas the EBA proteins all have 8 highly conserved cysteines. Of these, only four are shared with *Pf*AMA-1 (green arrows), and the remaining 4 cysteines are indicated with red arrows. The alignments were performed using Clustal Omega (EMBL-EBI, 2017).

3.4.3 The *Pf*AMA-1 Prodomain is Required for Microneme Targeting

Co-localisation experiments in this study using *Pf*AMA-1 with and without the prodomain (Figure 3.21) showed conclusively that the prodomain is required for microneme targeting. Further studies (Figure 3.28) involving sequential deletion of 18aa from the C-terminus of the prodomain showed that the C-terminal 54aa are essential for correct targeting. A loss of 18 or 36aa disrupted microneme localisation, but these truncated proteins still trafficked to the apical region. These findings imply that the whole prodomain is required for correct targeting to the micronemes.

Prodomains are usually required for proper folding of proteins. The *Pf*AMA-1 prodomain has been described as a retention mechanism for the protein to remain within the micronemes until it is required on the surface to mediate erythrocyte invasion (Healer *et al.,* 2002). The involvement of the prodomain in microneme targeting is consistent with the findings that the prodomain is cleaved off in the micronemes, before translocation onto the microneme surface (Healer *et al.,* 2002). A similar event is reported for the signal peptide, which is cleaved in the ER. Both of these domains are removed once they have served their purpose as a trafficking signal.

How the prodomain targets *Pf*AMA-1 to the micronemes is not known. It is possible that it possesses a signal sequence, or that folding of the prodomain occurs in such a way that it allows recognition and binding with an escorter protein.

In this study, the N-terminal 32aa of the prodomain were shown to be essential for localisation to the apical region, but not sufficient for microneme targeting. A 16aa C-terminal truncation of the prodomain also lead to mis-targeting of the protein, which implies that the whole prodomain is required for correct trafficking to the micronemes. These findings may suggest that instead of a signal sequence, the prodomain is implicated in targeting by folding in a way that allows recognition of *Pf*AMA-1 by a protein escorter, which is used to direct the protein to the micronemes.

3.4.4 The Role of Other Prodomains in Trafficking

P. chabaudi AMA-1 prodomain is not implicated in trafficking, however the *Pc*AMA-1 prodomain shows little homology with that of *Pf*AMA-1 (Triglia *et al.,* 2000). Other proteins, e.g. proteases that target the food vacuole (FV), possess prodomains that are

important for trafficking through the secretory pathways from the ER to the FV (Tonkin *et al.,* 2006; Deponte *et al.,* 2012). An aspartic protease, plasmepsin II, is trafficked via the cytostome by vesicular budding to the FV. At the FV, plasmepsin II binds to the membrane, and a subsequent cleavage event, which removes the transmembrane domain, triggers the entry of the processed, mature protein into the FV (Klemba *et al.,* 2004a). Another protease, DPAP1 (dipeptide aminopeptidase 1) is a soluble protein that lacks a transmembrane domain, but is also targeted to the FV utilising a different pathway (Klemba *et al.,* 2004b). This protein traffics via the ER, but accumulates in the parasitophorous vacuole, and is subsequently is transported to the FV.

Chapter 4: *P. falciparum* Subtilisin-like Protease 2

4.1 Introduction

P. falciparum subtilisin-like protease 2 (*Pf*SUB2) was first described in 1999 (Hackett *et al.,* 1999; Barale *et al.,* 1999) and is one of three subtilisin-like serine proteases of the malaria parasite (reviewed by Withers-Martinez *et al.,* 2004). It is secreted from the micronemes onto the parasite membrane during merozoite egress and is responsible for shedding of the merozoite coat proteins (*Pf*MSP1 and *Pf*AMA-1) during invasion (Howell *et al.,* 2003).

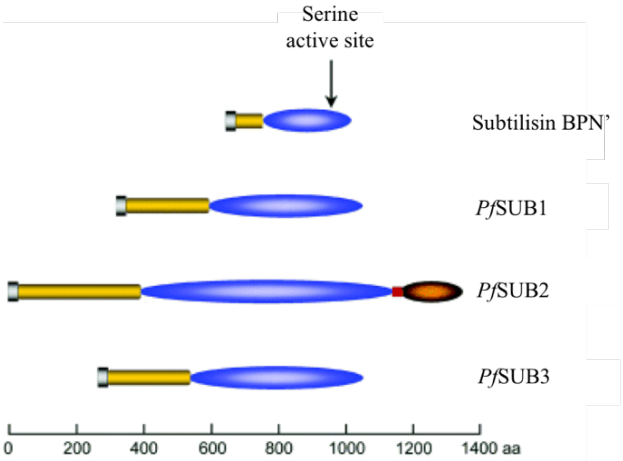


Figure 4.1. Schematic of the predicted structural features of subtilases of the malaria parasite. *Pf*SUB1, -2 and -3 are compared to the *Bacillus amyloliquefaciens* subtilisin BPN'. They all possess N-terminal secretory signal peptides (grey), putative prodomains (yellow), and catalytic domains (blue), but only *Pf*SUB2 contains a transmembrane domain (red) and cytoplasmic tail (orange). The proteins are arranged so that the predicted active-site serine residue of each subtilase aligns vertically with that of subtilisin BPN' (Ser-221). The malaria subtilases are all larger than subtilisin BPN' due to internal insertions and terminal extensions (Withers-Martinez *et al*., 2004).

4.1.1 The Importance of Proteases

Since the approval of saquinavir, a protease inhibitor, for the treatment of advanced HIV infection in 1995, antiretroviral protease inhibitor drugs have remained a mainstay of anti-HIV chemotherapy (Turk, 2006). Several other proteases have been identified and are considered good drug targets (Turk, 2006): a hepatitis C protease (Smith & Wu, 2003), as well as malaria proteases, such as the aspartic proteases (Coombs *et al.,* 2001) and cysteine proteases (Rosenthal *et al.,* 2002), which are responsible for haemoglobin digestion.

Proteases, especially ones that are unique to the malaria parasite, are considered good drug targets because they will have numerous downstream effects (Withers-Martinez *et al.,* 2004;

Blackman, 2004). The importance of proteases in the erythrocytic life stages of the malaria parasite can be seen in three areas: (1) digestion of haemoglobin during development, (2) egress of the parasite from the host cell and (3) host erythrocyte invasion (Withers-Martinez *et al.,* 2004).

The subtilases of the malaria parasite have received increased attention over the last couple of decades (Rosenthal *et al.,* 2002) since they are implicated in host cell invasion (Blackman, 2000) and are thus an attractive target for novel anti-malaria drugs.

4.1.2 Expression of *Pf*SUB2

*Pfsub*2 mRNA expression occurs at low levels throughout the asexual blood-stage life forms, with peak transcription occurring in the late schizont stage (Figure 4.2; Otto *et al.,* 2010), as indicated by microarray studies (Bozdech *et al.,* 2003; Le Roch *et al.,* 2003) and reverse transcription PCR analysis (Barale *et al.,* 1999).

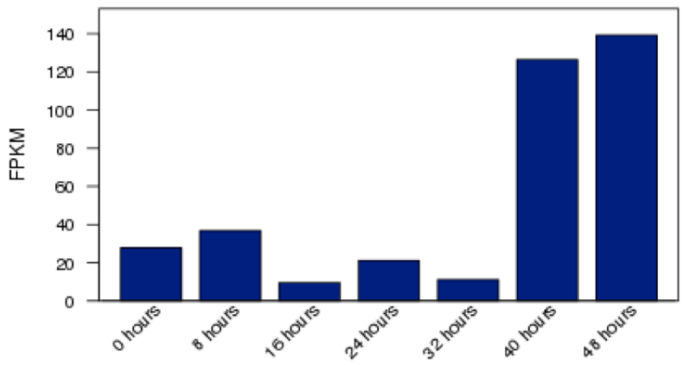


Figure 4.2. mRNA expression of *Pfsub*2 during the asexual intra-erythrocytic cycle.
RNA was extracted from synchronised 3D7 *P. falciparum* parasites at several time points post-infection (indicated on the x-axis) and the transcriptome was sequenced. Fragments per kilo-base of exon model per million mapped reads (FPKM) on the y-axis indicates the transcript levels at each of the selected time points. *Pfsub*2 expression levels peak 40 to 48 hours post-infection, during the schizont stage. (Adapted from Aurrecoechea *et al*., 2008; PlasmoDB)

Protein expression of *Pf*SUB2 is consistent with Figure 4.2, but is not limited to the intra-erythrocytic asexual life stages of malaria parasites. Studies done on *Anopheles stephensi* mosquitoes showed *Pb*SUB2 in the cytoplasm of the mosquito midgut cells after the invasion of *P. berghei* ookinetes (Han *et al.,* 2000). Additionally, a proteomics study done on the sexual stages of *P. falciparum* parasites, found *Pf*SUB2 in the gametocytes (Florens *et al.,* 2002).

4.1.3 Function of *Pf*SUB2

*Pf*SUB2 is believed to have an important role in the erythrocytic cycle of the malaria parasite, but its precise function is unknown. Detection of the protein in different parts of the life cycle may indicate that the protease performs multiple functions throughout the *Plasmodium* life stages (Withers-Martinez *et al.,* 2004).

An important feature of host cell invasion is the shedding of coat proteins from the merozoite surface. Modelling of the molecular structure of the maturase responsible for the proteolytic shedding of *Pf*MSP-1 resulted in the identification of *Pf*SUB2 (Barale *et al.,* 1999). *Pf*MSP-1 cleavage occurs at the juxtamembrane site and the protein fragment, called *Pf*MSP-1_{19}, remains bound to the parasite by a GPI anchor and is thus carried into the host cell (Barale *et al.,* 1999). Howell *et al.,* (2003) investigated the cleavage of *Pf*AMA-1, another coat protein, on the merozoite membrane and deduced that the same serine protease responsible for *Pf*MSP-1 processing was involved. Interestingly, the cleavage site of *Pf*AMA-1 shares no sequence similarity with that of *Pf*MSP-1 (Figure 4.3; Withers-Martinez *et al.,* 2004), which implies a broad substrate specificity for the protease (Howell *et al.,* 2003).

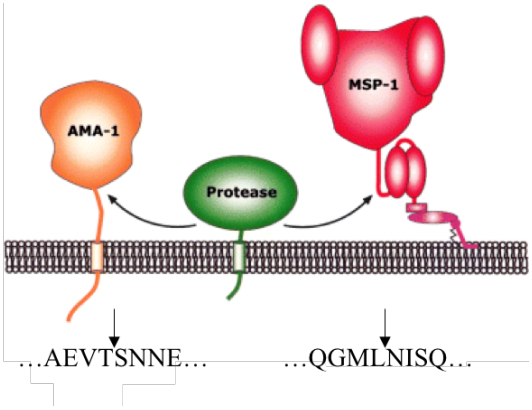


Figure 4.3. A model depicting proteolytic shedding of merozoite coat proteins.
The *Pf*SUB2 cleavage sites of *Pf*AMA-1 and *Pf*MSP-1 are indicated, which shows that there is no sequence similarity and confirms that the protease involved has a broad substrate specificity. The combination of the GPI anchor and the tandem EGF-like C-terminal domain of *Pf*MSP-1, results in the cleavage site being at a similar distance from the membrane as the cleavage site of *Pf*AMA-1. (Adapted from Blackman, 2004).

Homologous recombination strategies designed to disrupt *P. berghei sub2* were unsuccessful since no viable parasites were found after transfection (Uzureau *et al.,* 2004). The authors concluded that *Pb*SUB2 is probably essential for asexual life stage development because the

P. berghei system is known to have a high transfection efficiency. *Pfsub2* disruption has also been unsuccessful (Child *et al.,* 2013).

4.1.4 The Sequence and Structure of *Pf*SUB2

*Pf*SUB2 is a large 155 kDa type 1 integral membrane protein with a signal peptide, a large pro-region, a catalytic domain and transmembrane-spanning region (Figure 4.4; Hackett *et al*., 1999).

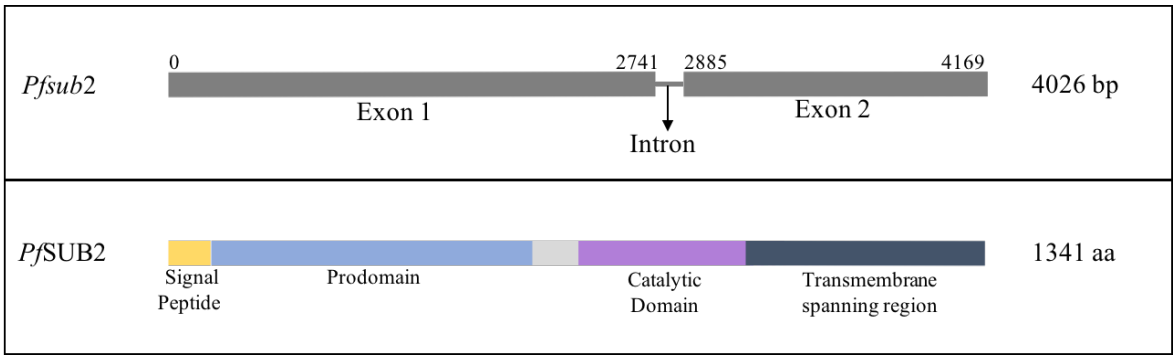


Figure 4.4. The gene and protein structure of *Pf*SUB2.
*Pfsub*2 is encoded by a gene of 4026 base pairs (bp) consisting of two exons. The position of the intron is shown by the arrow. *Pf*SUB2 is synthesized as a protein of 1341 amino acids (aa), which consists of several domains, including an N-terminal signal peptide (yellow), a prodomain (blue), a catalytic domain (purple) and a transmembrane-spanning region (dark blue).

The *Pf*SUB2 and *Pf*SUB1 prodomains are both hydrophobic, however, share no sequence similarity (Withers-Martinez *et al.,* 2004). No information for the *Pf*SUB3 prodomain is available.

Shortly after the characterisation of *Pf*SUB2, the gene encoding *Pb*SUB2 was identified. Subsequent BLAST searches of the *Plasmodium* genome sequences have shown clear orthologues in several of the *Plasmodium* species and they all share the following key traits: (1) the single intron, and (2) the overall processing pattern (Uzureau *et al.,* 2004).

4.1.5 Post-translational Modifications of *Pf*SUB2

Subtilases are synthesised as inactive enzyme precursors that require biochemical change to become active enzymes. *Pf*SUB2 is synthesised as a 155kDa protein and a primary processing event in the parasite ER results in a N-terminal truncation, which removes the signal peptide and prodomain, and reduces the protein to 75kDa (Withers-Martinez *et al.,*

2004). A second processing event results in a 72kDa product consisting of the catalytic, transmembrane and cytoplasmic domains. This second processing event is Brefeldin A sensitive, which confirms that it occurs in a post-ER compartment. The details of the two truncations are not known. The process is assumed to be autocatalytic, however, there is no evidence to support this (Harris *et al.,* 2005b; Withers-Martinez *et al.,* 2004).

4.1.6 Subcellular Localisation and Trafficking of *Pf*SUB2

Localisation studies conducted by Barale *et al.,* (1999), using polyclonal antibodies and gold-labelling immunoelectron microscopy (IEM), detected *Pf*SUB2 in the dense granules. This contrasts with subsequent studies, which reported that *Pf*SUB2 is stored in the micronemes, not dense granules, prior to translocation onto the merozoite surface (Harris *et al.,* 2005b; Child *et al.,* 2013). In these studies, monoclonal antibodies against different regions of *Pf*SUB2 were used together with several markers (surface, rhoptry and microneme; Harris *et al.,* 2005b) or a haemagglutinin tag (HA) was used to visualise *Pf*SUB2 in transgenic parasites (Child *et al.,* 2013). The difference in localisation between the experiments can be explained by the choice of polyclonal antibodies used by Barale *et al.,* (1999), which can result in cross-reactivity and thus mis-localisation of the protein (Harris *et al.,* 2005b). Given that micronemes export their proteins onto the merozoite surface prior to, and during invasion, whereas dense granules discharge their proteins following invasion (section 1.4.3; Bannister *et al.,* 2003), it seems unlikely that *Pf*SUB2 is stored in the dense granules.

4.1.7 Research Objectives

The aim of the research conducted in this chapter was to identify the molecular determinants for trafficking of *Pf*SUB2.

This was achieved by creating two transgenic parasite lines expressing fluorescently-tagged chimaeric *Pf*SUB2 peptides, and conducting co-localisation studies to determine which of the protein domains were required for the correct targeting of *Pf*SUB2 to the micronemes.

4.2 Materials and Methods

The materials and methods used to investigate *Pf*SUB2 are described in Chapter 2.

4.3 Results

4.3.1 Creation of *Pfsub*2 Mini-Genes

4.3.1.1 Bio-informatic Analysis of *Pf*SUB2

The sequence of *Pfsub*2 was obtained from the online *Plasmodium* database (PlasmoDB version 30; www.plasmodb.org; Aurrecoechea *et al*., 2008). *Pfsub*2 is encoded by PF3D7_1136900 gene, which is made up of two exons and is located on chromosome 11. *Pf*SUB2 is a protease of 1341 amino acids (aa) with a molecular weight of 155 kDa (Aurrecoechea *et al.,* 2008; Hackett *et al.,* 1999). Figure 4.5 shows the domains of this invasion protein.

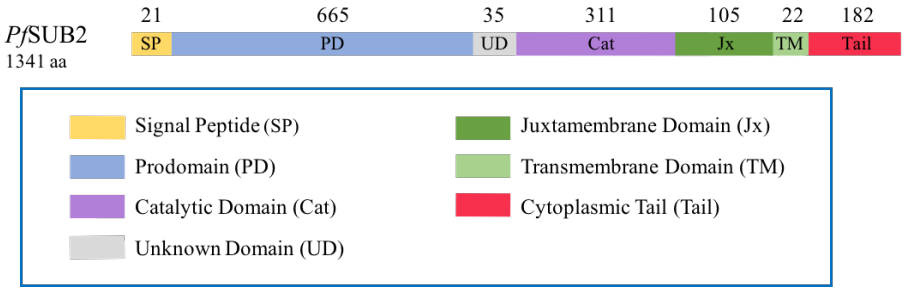


Figure 4.5. A schematic representing the domains of *Pf*SUB2, a *P. falciparum* microneme invasion protein.
The number of amino acids (aa) in each domain is indicated.

4.3.1.1 Designing *Pfsub*2 Mini-Genes for Parasite Transfections

To assess which of the various domains (Figure 4.5) were involved in targeting *Pf*SUB2 to the *P. falciparum* micronemes, two mini-genes were designed (Figure 4.6).

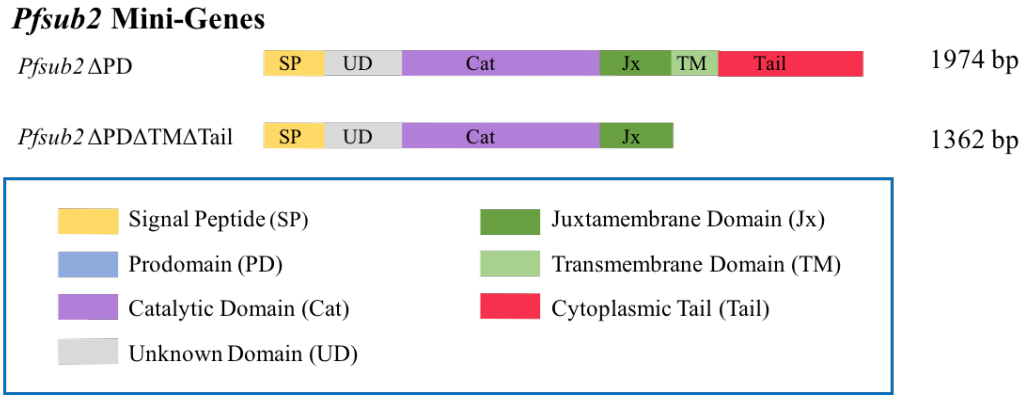


Figure 4.6. A schematic of the mini-genes designed for *P. falciparum* invasion protein, SUB2.
Base pair (bp) sizes of mini-genes are indicated on the right.

The Signal Peptide (SP) was included in both generated chimaeric proteins to ensure correct targeting via the ER. Since the prodomain is cleaved off in the ER, the mini-genes excluded the prodomain, and the second mini-gene further excluded the transmembrane domain and cytoplasmic tail.

4.3.1.2 RNA Isolation and cDNA Generation

Since *Pfsub2* contains an intron, genomic DNA was not suitable for the creation of the mini-genes. Wild-type *P. falciparum* 3D7 cultures were synchronised by two sorbitol treatments in 48 hour intervals to facilitate the isolation of schizonts. Total RNA was isolated from schizont-stage *P. falciparum* parasites approximately 24-28 hours after synchronisation. RNA samples were pure, with spectrophotometric analysis yielding A_{260}/A_{280} values of 2.0 to 2.2 and A_{260}/A_{230} values of 2.2 to 2.4 (NanoDrop® Technologies, 2007). Agarose gel electrophoresis of the samples (Figure 4.7) showed defined ribosomal RNA subunits as well as a faint mRNA smear. Isolated total RNA was used as the template for the generation of cDNA using the *Pf*SUB2 "tail" reverse primer.

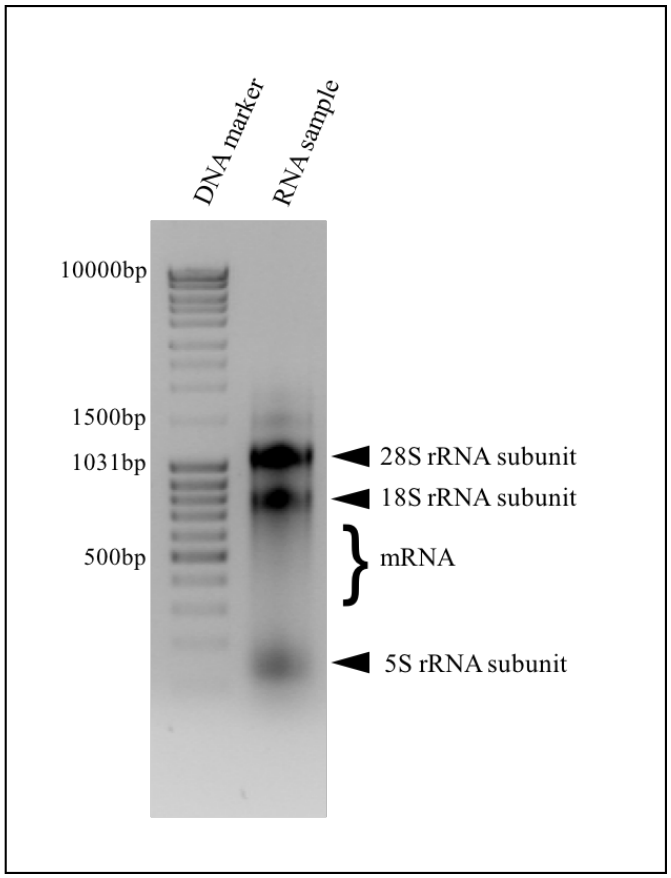


Figure 4.7. Isolated *P. falciparum* 3D7 RNA.
Assessment of isolated total RNA by agarose gel electrophoresis against a base pair standard.

4.3.1.3 PCR and Overlap Extension PCR

Pfsub2 mini-genes were generated by PCR and overlap extension PCR using cDNA and appropriate primers. In some instances, to avoid the long stretches of adenine or thymine nucleotides commonly found in *P. falciparum* or to exclude the stop codon at the end of the gene, the location of the primer binding site was selected upstream or downstream of the desired site. This resulted in the amplified regions varying from the actual domain size (Table 4.1 and Figure 4.6). The primer sequences and PCR parameters are in Appendix A.

All PCR products migrated according to their expected sizes (Table 4.1) as assessed by agarose gel electrophoresis. PCR products were slightly larger than the region to be amplified due to additions to the primers as described in Appendix A.

Table 4.1. Expected PCR product sizes of domains within *Pfsub2* mini-genes.

Gene	Mini-genes	Domains	Region to be amplified (bp)	PCR Product (bp)
Pfsub2	Product 1	SP	63	97
	ΔPD Product 2	UD-Cat-Jx-TM-Tail	1911	1921
	ΔPDΔTMΔTail Product 3	UD-Cat-Jx	1299	1309
	ΔPD Final Product	SP + UD-Cat-Jx-TM-Tail	1974	1994
	ΔPDΔTMΔTail Final Product	SP + UD-Cat-Jx	1362	1382

Both *Pfsub2* products were created by overlap extension PCR (Figure 4.8) to delete the prodomain. The signal peptide was amplified to generate a PCR product of 97bp (Product 1; Figure 4.8 A), containing a 24bp 3' overhang. Next, Products 2 and 3 were amplified (Figure 4.8 B) and due to unwanted non-specific fragments, they were purified by gel extraction of prior to the overlap extension PCRs, which joined the signal peptide to these two products (Figure 4.8 C).

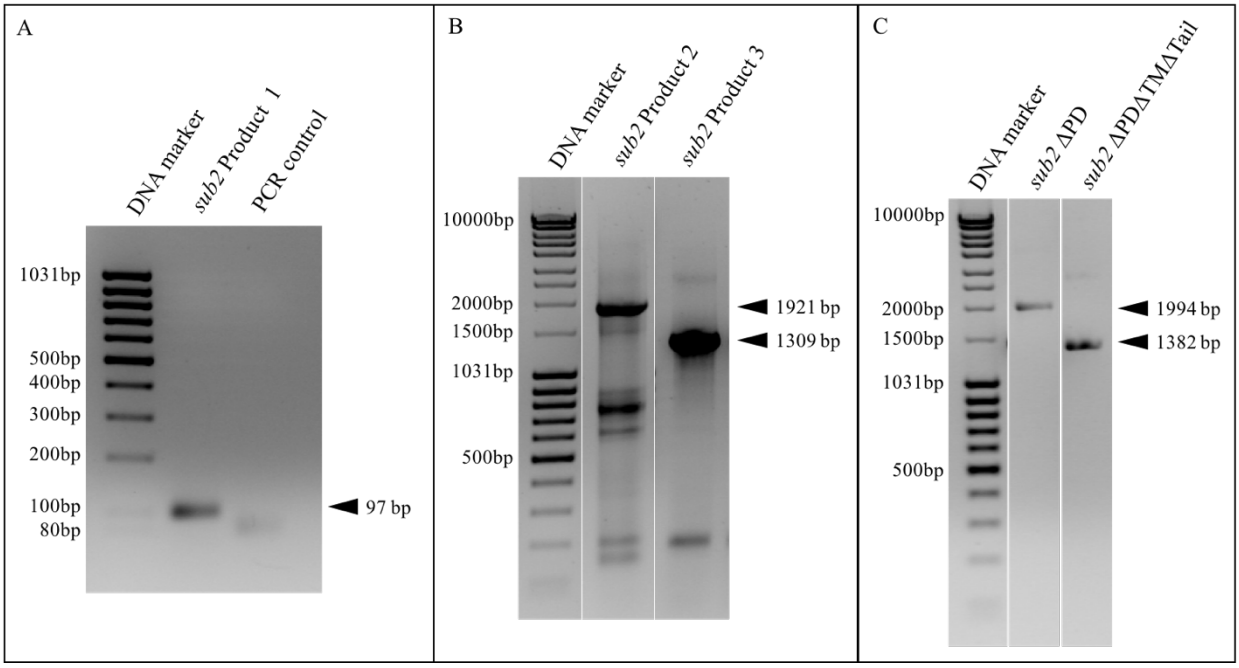


Figure 4.8. Creating *Pfsub2* mini-genes by overlap extension PCR.
Size validation of domains by agarose gel electrophoresis against a base pair standard. **A** – *Pfsub2* Product 1: signal peptide. PCR control: PCR reaction contained primers but no template DNA; shown here as an example. The band visible at ~80bp represents primer dimers. **B** – *Pfsub2* PCR products prior to gel extraction purification. *Pfsub2* Product 2: UD-Cat-Jx-TM-Tail. *Pfsub2* Product 3: UD-Cat-Jx. **C** – *Pfsub2*ΔPD was generated by overlap extension PCR using Products 1 and 2 and *Pfsub2*ΔProΔTmΔTail was generated using Products 1 and 3.

4.3.1.4 Generation & Verification of pARL-mCherry Constructs

After restriction endonuclease digestion with *Xho*I and *Avr*II, *P. falciparum* amplicons and mCherry plasmid were quantified by gel electrophoresis and ligated in a 5:1 ratio. Competent *E. coli* XL10 cells were transformed with 100ng of the ligated constructs and 10 to 500 colonies grew on the ampicillin-treated agar plates.

Colonies were picked, amplified and the plasmid isolated for verification. Restriction endonuclease digestion of the mCherry control plasmid and the two *Pfsub*2 mCherry constructs (Figure 4.9) using FastDigest® enzyme *Eco*RV, confirmed that amplicons of the correct sizes had been inserted into the mCherry plasmid. An *Eco*RV site within the inserts resulted in two fragments being visible on the agarose gel after restriction endonuclease digestion, as opposed to the single fragment in the empty mCherry control plasmid. Positive clones were sequenced by Inqaba Biotec™, which confirmed that inserts were error-free and in-frame.

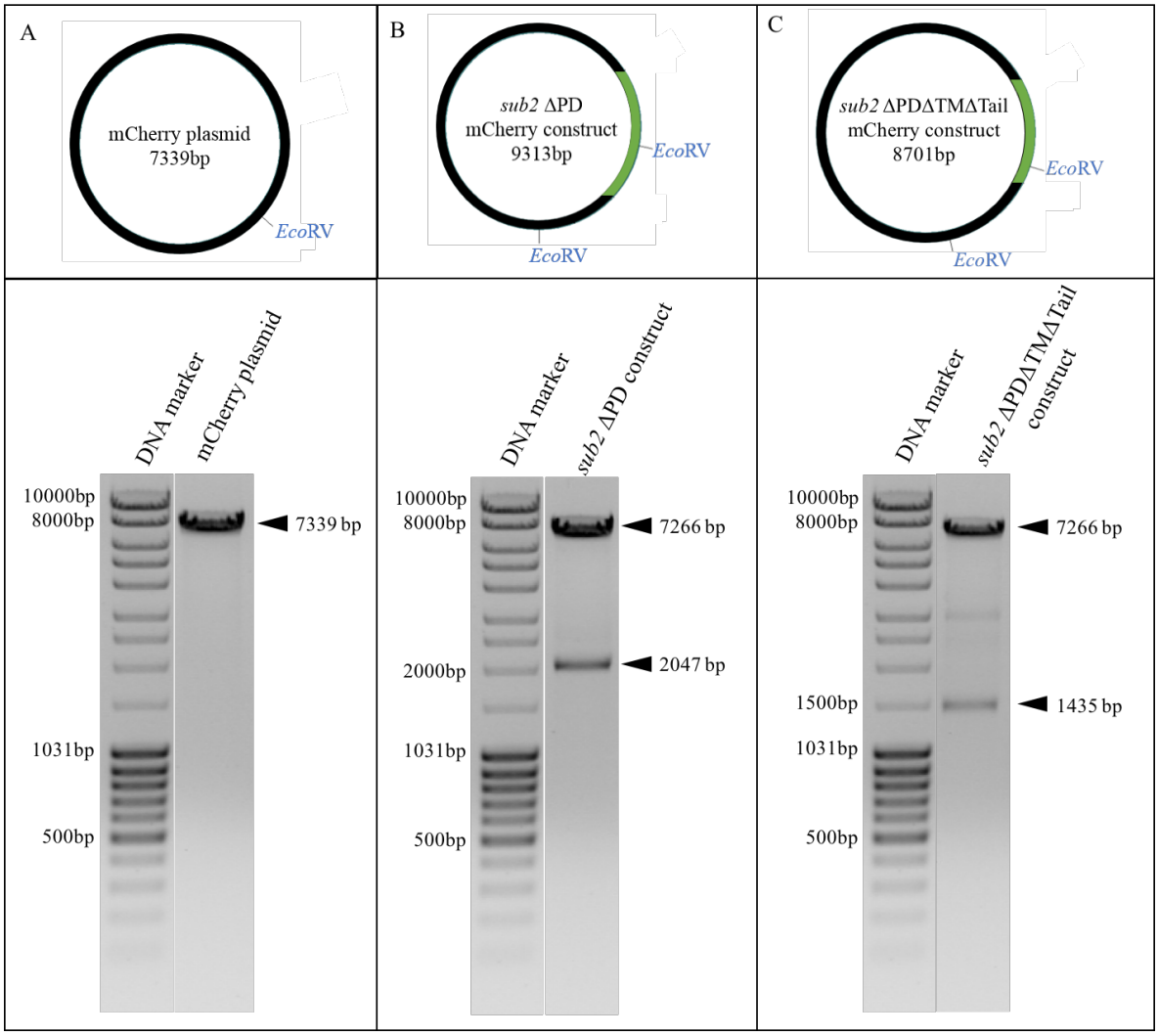


Figure 4.9. Verification of *Pfsub2* mCherry constructs.
Size validation by gel electrophoresis, against a base pair standard, of the *sub2*ΔPD and *sub2*ΔPDΔTMΔTail mCherry constructs after *Eco*RV restriction endonuclease digestion. **A –** *Eco*RV digestion of the control plasmid resulted in the linearization of mCherry, which appeared as a single 7339bp fragment on the agarose gel. **B and C –** An *Eco*RV restriction endonuclease site within the two *sub2* mini-genes resulted in an additional fragment appearing on the agarose gels.

4.3.2 *Pf*SUB2 Transgenic Parasites

3D7 *P. falciparum* parasites were electroporated with the plasmid constructs. WR99210 compound was administered to the cultures to ensure that only parasites with the plasmid survived. Live parasites were visible in the transgenic cultures approximately 40 days after transfection.

To confirm that the transgenic parasites contained the desired constructs, PCR verification was performed using mCherry backbone primers flanking the mini-gene insert site (Figure 3.18). PCR parameters and primer information can be found in Appendix A.

Assessment of the two *Pf*SUB2 transgenic lines confirmed that the resultant products migrated according to the expected sizes as determined by agarose gel electrophoresis (Figure 4.10). Due to the binding sites of the primers, all amplified products were 534bp larger (Figure 3.18) than the mini-genes: 2528bp and 1916bp for the ΔPD and ΔPDΔTMΔTail SUB2 mCherry transgenic lines, respectively. These results confirmed that both of the *Pf*SUB2 transgenic cultures carried the appropriate constructs.

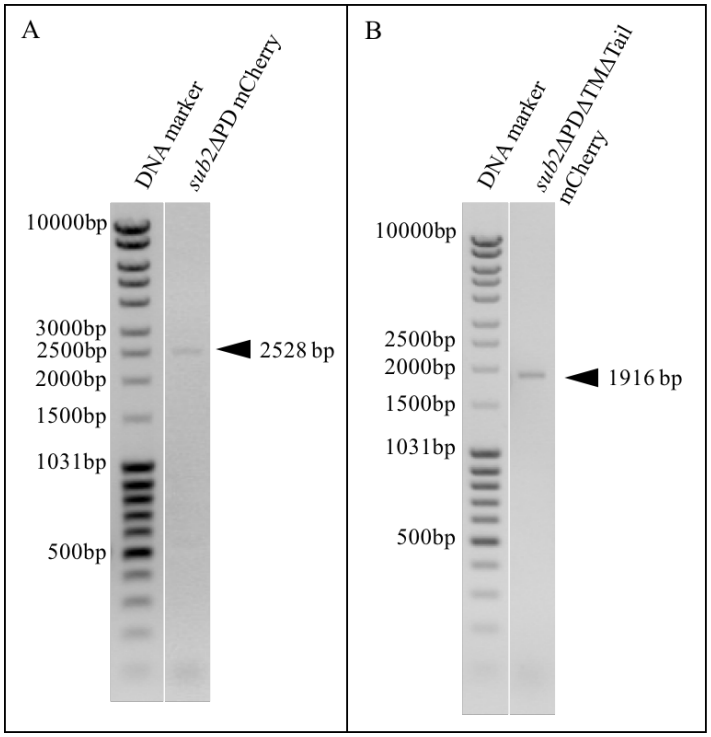


Figure 4.10. PCR verification of *Pf*SUB2 transgenic parasite lines.
Transgenic parasite DNA was amplified using mCherry backbone primers to confirm successful inclusion of plasmid constructs. Size validation was performed by gel electrophoresis against a base pair standard. **A –** The PCR product for *Pfsub*2ΔPD mCherry migrated at the expected size of 2528 base pairs. **B –** The PCR product for *Pfsub*2ΔPDΔTMΔTail mCherry migrated at the expected size of 1916 base pairs.

4.3.3 Identification of the Domain Targeting *Pf*SUB2 to the Micronemes

4.3.3.1 Live Imaging of *Pf*SUB2 Transgenic Parasites

Transgenic *P. falciparum* cultures were prepared for microscopy by DAPI treatment to stain the parasite nuclei. No auto-fluorescence or colour-bleeding was observed during microscopy (Appendix B).

*Pf*SUB2 is expressed in the schizont stages after the micronemes have developed, thus schizont-stage cultures were used for microscopy. The first transgenic line created for *Pf*SUB2 excluded the prodomain and the red fluorescence (Figure 4.11; top panel) appeared as small puncta adjacent to the nucleus of each developing parasite within the schizont. However, in parasites expressing *Pf*SUB2 with the transmembrane domain and cytoplasmic tail also deleted (Figure 4.11; bottom panel), the mCherry expression changed. The protein was no longer confined to the apical region and appeared dispersed in the cytoplasm. These findings suggest that the transmembrane domain and cytoplasmic tail are required for localisation to the apical organelles.

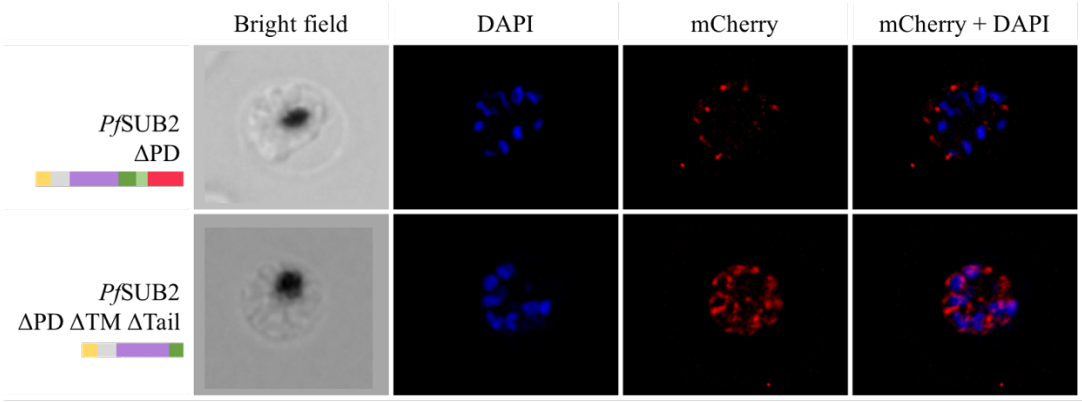


Figure 4.11. Fluorescence images of live schizont stage *P. falciparum* transgenic parasites expressing mCherry-tagged PfSUB2.
Parasites were viewed at 1000x magnification. mCherry causes red fluorescence of chimaeric *Pf*SUB2 proteins. DAPI is a blue nuclear stain. **Top Panel:** Without the prodomain, PfSUB2ΔPD, appeared punctate, and did not co-localise with the nucleus (blue). **Bottom Panel:** Further deletion of the transmembrane domain and cytoplasmic tail (ΔPDΔTMΔTail) resulted in the protein dispersing throughout the parasite cytoplasm.

4.3.3.2 Co-localisation Studies of *Pf*SUB2 Chimaeric Proteins

To determine which organelle the mCherry-tagged chimaeric proteins localised to, imaging experiments were performed using a known microneme marker, *Pf*EBA175. Transgenic parasite cultures were fixed, permeabilised and incubated with DAPI to stain the nucleus, as well as an anti-EBA175 antibody with a green fluorochrome to identify the micronemes.

*Pf*EBA175 appeared as puncta in the apical region (Figure 4.12), which is consistent with the localisation pattern of micronemes in schizont stage *P. falciparum* parasites (Treeck *et al.,* 2006). mCherry-tagged *Pf*SUB2ΔPD concentrated to punctate regions adjacent to the nuclei in the maturing schizont (Figure 4.12; top panel). When the overlay was performed

with the GFP-tagged microneme marker, yellow fluorescence was visible indicating co-localisation, however some red and green puncta were still visible. When the transmembrane domain and cytoplasmic tail were also deleted, the mCherry fluorescence appeared dispersed throughout the parasite and was no longer limited to the apical regions (Figure 4.12; bottom panel). These findings confirmed that the transmembrane domain and cytoplasmic tail of *Pf*SUB2 are required for microneme targeting. Pearson's coefficients were unfortunately not reliable for these data sets due to the extremely low levels of mCherry fluorescence detected in the microscopy experiments.

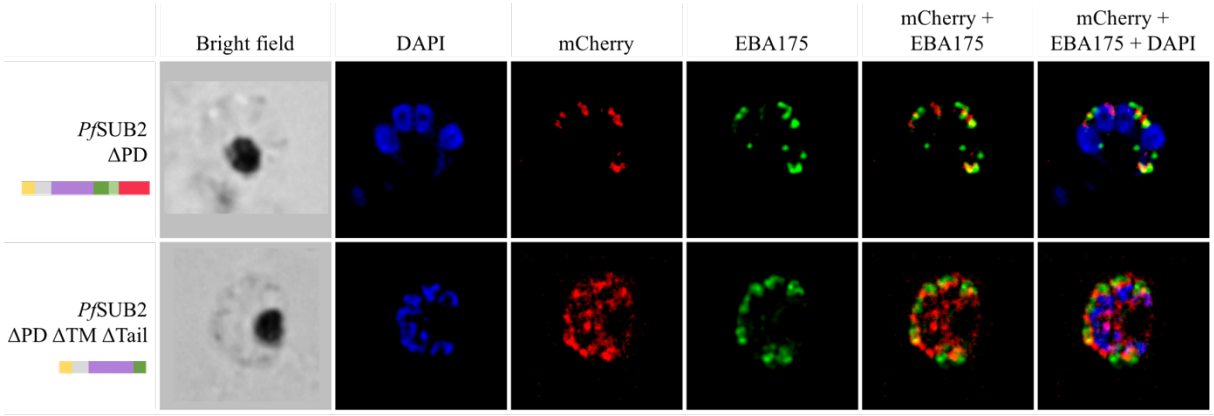


Figure 4.12. Co-localisation studies using fixed schizont stage *P. falciparum* parasites expressing mCherry-tagged *Pf*SUB2.
Parasites were viewed at 1000x magnification. mCherry causes red fluorescence of chimaeric *Pf*SUB2 proteins. DAPI is a blue nuclear stain. A microneme marker, *Pf*EBA175, with a green fluorochrome was used to determine the localisation of mCherry tagged proteins within the transgenic parasites. **Top Panel**: *Pf*SUB2ΔPD showed a punctate pattern that co-localised with the green *Pf*EBA175 signal, indicated by the yellow fluorescence observed in the overlay. **Bottom Panel**: With further removal of the transmembrane domain and cytoplasmic tail (ΔPDΔTMΔTail), the mCherry fluorescence was dispersed throughout the parasite cytoplasm and no longer co-localised with the green microneme marker.

4.4 Discussion

4.4.1 The *Pf*SUB2 Prodomain Is Not Required for Trafficking

*Pf*AMA-1 and *Pf*SUB2 are both transmembrane proteins that traffic to the micronemes via the ER and interact with each other on the merozoite surface during invasion. Given the similarity in trafficking pathways, it is possible that the two proteins may both require the same domain to target the micronemes.

Almost half of *Pf*SUB2 is made up of the prodomain, which represents 665 of the 1341 aa. The prodomains of *Pf*SUB1 and *Pf*SUB2 have been shown to act as an intra-molecular

chaperone, which is important for folding of the catalytic domain prior to secretory transport (Harris *et al.,* 2005b; Jean *et al.,* 2003; Shinde & Inouye, 1996). It was thus postulated that proper folding of *Pf*SUB2 was essential for correct localisation to the micronemes.

Results from this study, however, demonstrated that deletion of the prodomain did not affect micronemal localisation of *Pf*SUB2, implying that prodomain-assisted folding is not necessary for trafficking. Unlike *Pf*AMA-1, *Pf*SUB2 does not require the prodomain for correct targeting. Further evidence supporting this is that the prodomain of *Pf*SUB2 is cleaved off prior to arrival at the micronemes, whereas the *Pf*AMA-1 prodomain is only cleaved off in, or when leaving the micronemes.

4.4.2 The *Pf*SUB2 Transmembrane-Spanning Region is Required for Trafficking to the Micronemes

The *Pf*SUB2 mutant, which lacked the prodomain, transmembrane domain and cytoplasmic tail, was no longer confined to the apical region (Figure 4.11) and did not co-localise with the microneme marker (Figure 4.12). Since the prodomain has already been shown to be redundant for microneme targeting, these findings thus confirmed that the transmembrane domain and cytoplasmic tail are required for correct microneme trafficking.

These results were obtained during June to September 2013 and were presented at the 6th Pan-African Malaria Conference in October 2013. In July of that same year, Child *et al.,* (2013) published data that correlate with and confirm results presented in this thesis. It is encouraging to note that studies performed concurrently, in two independent laboratories, produced similar results.

In addition to showing that deletion of the transmembrane domain and cytoplasmic tail was sufficient to disrupt trafficking to the micronemes, a further deletion of the juxtamembrane domain resulted in reduced co-localisation with the micronemes (Child *et al.,* 2013). It was thus concluded that both the transmembrane and juxtamembrane domain are required for transport to the micronemes.

The change in localisation of *Pf*SUB2 from apically distinct to dispersed in the cytoplasm when the transmembrane domain and cytoplasmic tail were deleted, despite the presence of

the juxtamembrane domain (Figure 4.12), suggests that the microneme targeting signal must be located within the transmembrane domain (Figure 4.13).

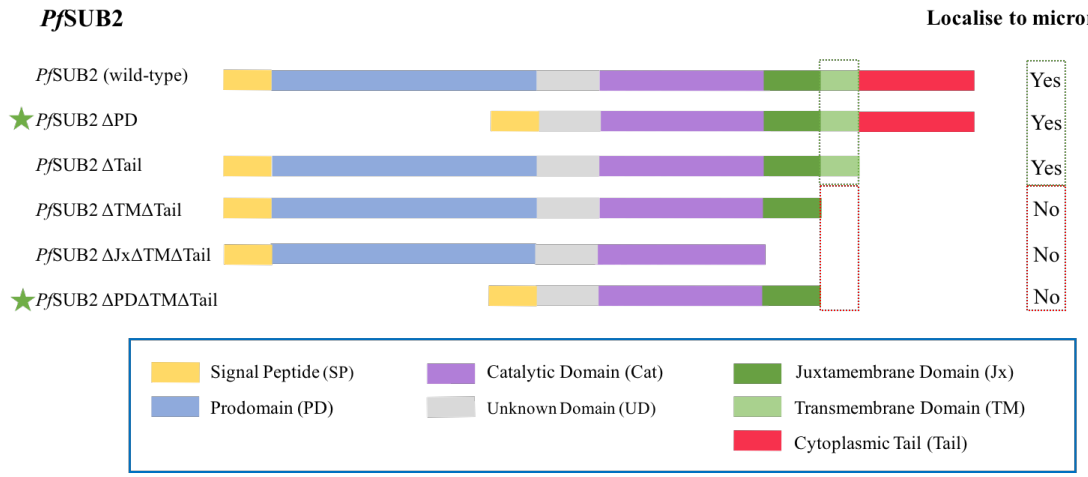


Figure 4.13. Summary of *Pf*SUB2 localisation experiments.
The data produced in this research (marked with green stars), together with the data produced by Child *et al.,* (2013), show that the transmembrane domain of *Pf*SUB2 is required to target the micronemes.

4.4.3 Does *Pf*SUB2 Require a Tyrosine Motif for Microneme Targeting?

There are multiple tyrosine motifs found within certain regions of transmembrane proteins, which are used for sorting and trafficking (Pandey, 2009; Deponte *et al.,* 2012).

One such signal motif, which is found within the cytoplasmic tails of transmembrane proteins, is the tetrapeptide sequence YXXϕ, where Y is a tyrosine residue, X is any amino acid and ϕ represents a bulky hydrophobic side chain (Trowbridge *et al.,* 1993), for example, phenylalanine (F), tryptophan (W), leucine (L) or isoleucine (I). In Apicomplexan parasites, YXXϕ has been associated with targeting proteins to the apical organelles, such as *Tg*ROP2 to the rhoptries (Hoppe *et al.,* 2000) and *Pf*TRAP (Thrombospondin-related anonymous protein) to the micronemes (Bhanot *et al.,* 2003).

Another tyrosine-based motif is the NPXY sequence, which is usually recognised by clathrin-adaptor proteins (Pandey, 2009). In *Toxoplasma*, NPXY signals have been associated with targeting of proteins from the Golgi to the micronemes (Hoppe *et al.,* 2000). *Tg*MIC proteins require tandem tyrosines, such as in the SYHYY motif (Di Cristina *et al.,* 2000), to localise to the micronemes.

*Pf*SUB2 has several tyrosine residues found within the transmembrane-spanning region (Figure 4.14), a few of which seem to concentrate at the C-terminal end of the juxtamembrane domain. There are only three tetrapeptides that could fit with the YXXϕ motif: two occur in the juxtamembrane domain (YGEI and YNLY) and one occurs in the cytoplasmic tail (YSDI). There are no tetrapeptides that could be NPXY motif (Figure 4.14).

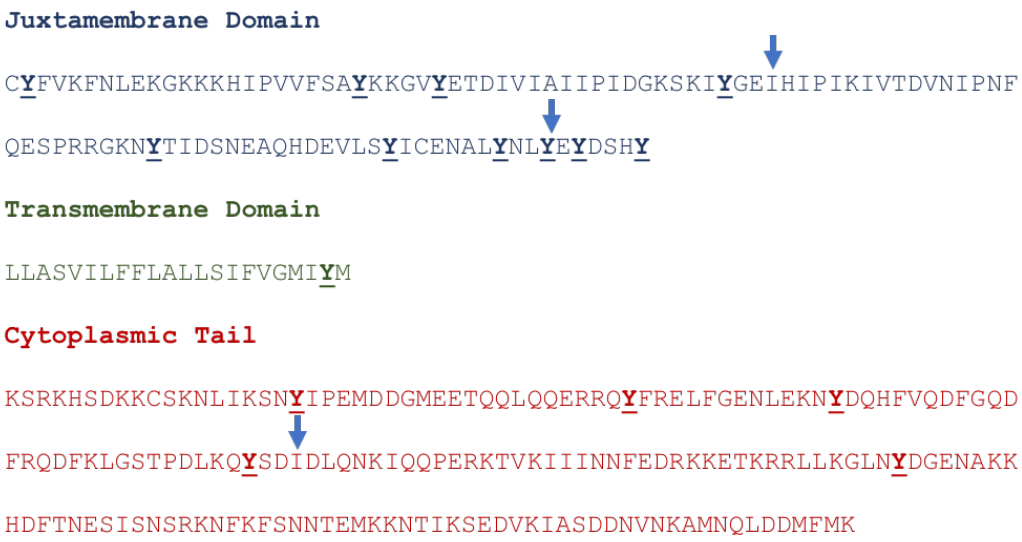


Figure 4.14. The amino acid residues in the transmembrane-spanning region of *Pf*SUB2. The sequences above are of the juxtamembrane domain (blue), transmembrane domain (green) and cytoplasmic tail (red). All tyrosine residues have been underlined, bulky hydrophobic amino acids that occur 3 residues after a tyrosine have been identified with an arrow.

Despite the presence of these potential tyrosine motifs in the juxtamembrane and cytoplasmic regions, these domains are not required for targeting to the micronemes (Figure 4.13). There is only a single tyrosine residue in the transmembrane domain (Figure 4.14), which doesn't form part of a YXXϕ or NPXY sequence. It appears that, as was shown for other microneme targeting proteins such as *Pf*AMA-1 (results from this study; Treeck *et al.,* 2009) and *Pf*EBA175 (Gilberger *et al.,* 2003b), that a tyrosine motif may not be the microneme targeting signal for *Pf*SUB2.

Chapter 5: *P. falciparum* Erythrocyte Binding Antigen 181

5.1 Introduction

P. falciparum Erythrocyte Binding Antigen 181 (*Pf*EBA181) was first identified when the genome sequence of *P. falciparum* was published in 2002 (Gardner *et al.,* 2002).

5.1.1 The Erythrocyte Binding Antigen Proteins

*Pf*EBA181, also referred to as JESEBL, is a member of the Erythrocyte binding ligand (EBL) super family (Gilberger *et al.,* 2003a), along with EBA140 (BAEBL), EBA165 (PEBL), EBA175, EBL1 and MAEBL (Adams *et al.,* 2001). The existence of multiple binding antigens enables the parasite to use different host receptors during invasion, and thus supports theories that a diverse set of ligands are available to function in alternate invasion pathways (Hadley *et al.,* 1987; Gilberger *et al.,* 2003a).

The members of this family of binding ligands have a similar exon/intron structure and are presumed to have evolved from a common gene ancestor (Adams *et al.,* 1992; Michon *et al.,* 2002). The protein structure and domain composition for these proteins are also similar (Figure 5.1; Gilberger *et al.,* 2003a). The F1/F2 Duffy binding-like domains (DBL) of *Pf*EBA181 share 25.3% and 24.6% identity with *Pf*EBA175 and *Pf*EBA140 (Gilberger *et al.,* 2003a).

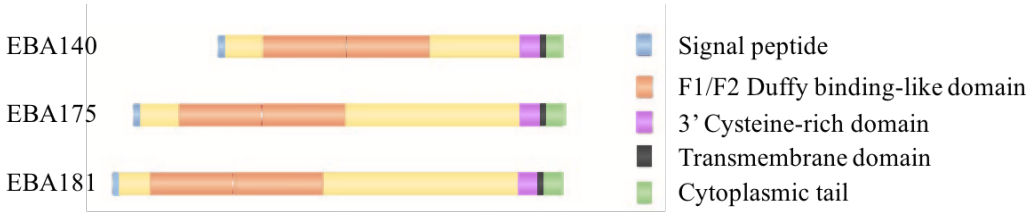


Figure 5.1. Shared structural features of members of the EBL superfamily.
A schematic showing the similarity in protein domains, shared by members of the erythrocyte binding ligand family. All members of the protein family have N-terminal tandem DBL domains (orange) for recognition by erythrocyte receptors during invasion. Yellow domains are undefined regions (Adapted from Gilberger *et al.,* 2003a).

5.1.2 The Sequence and Structure of *Pf*EBA181

*Pf*EBA181 is encoded by the *Pfeba*181 gene consisting of 4 exons and 3 introns (Figure 5.2). *Pf*EBA181 is made up of a signal peptide, two tandem DBL domains, a conserved C-

terminal cysteine-rich domain and a transmembrane-spanning region (Figure 5.2; Gilberger *et al.,* 2003a).

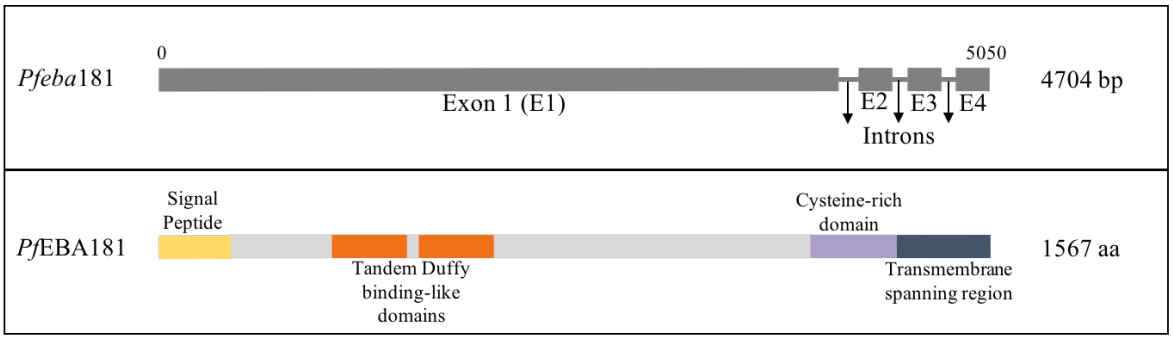


Figure 5.2. The gene and protein structure of *Pf*EBA181.
*Pf*EBA181 is encoded by a gene of 4704 bp consisting of four exons. The positions of the introns are shown using arrows. *Pf*EBA181 is synthesized as a protein of 1567 aa, which consists of several domains, including an N-terminal signal peptide (yellow), two tandem Duffy binding-like domains (orange), a cysteine-rich domain (lilac) and a transmembrane-spanning region (dark blue).

5.1.3 The Role of *Pf*EBA Proteins During Invasion

The molecular basis of merozoite invasion, particularly the use of multiple erythrocyte receptors, is not well understood. A number of erythrocyte membrane proteins are known to be utilised for invasion during the asexual cycle, including glycophorins A, B and C, as well as an unknown receptor X (Figure 5.3; Hadley *et al.,* 1987; Thompson *et al.,* 2001; Paul *et al.,* 2015).

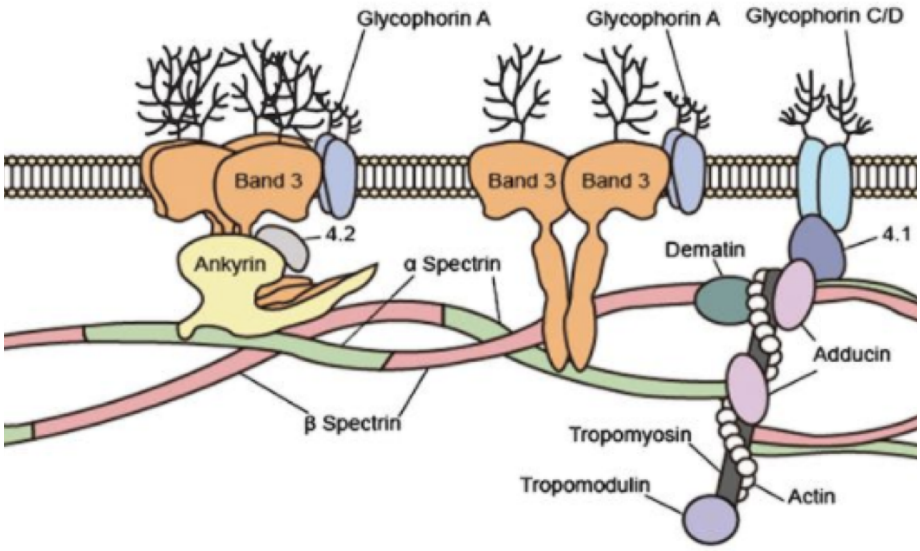


Figure 5.3. The proteins of the human erythrocyte membrane.
A schematic showing the organisation of the red blood cell membrane, with Glycophorin receptors present on the external surface. (Adapted from Kim *et al.,* 2015).

A family of EBA ligands all recognise and bind to different erythrocyte receptors (Table 5.1), in sialic acid-dependent and –independent pathways, which gives the parasite an increased chance to avoid an immune response or drug action (Gilberger *et al.,* 2003a).

*Pf*EBA175 binds to the major glycoprotein of the red cell, glycophorin A (Orlandi *et al.,* 1992), and *Pf*EBA140 binds to glycophorin C (Thompson *et al.,* 2001), and through these interactions, merozoite invasion into the red cell is mediated. The receptor-ligand interactions do not appear to be interchangeable since *Pf*EBA175 cannot bind to glycophorin B in the absence of glycophorin A (Dolan *et al.,* 1994). *Pf*EBA181 was suspected to bind to glycophorin B since both require interactions that are sialic acid-dependent (neuraminidase sensitive), trypsin resistant and chymotrypsin sensitive (Table 5.1), but studies showed that *Pf*EBA181 can still bind to erythrocytes that lack the glycophorin B receptor (Gilberger *et al.,* 2003a). A novel erythrocyte receptor, termed receptor E, is required for *Pf*EBA181 interaction (Gilberger *et al.,* 2003a). *Pf*EBL1 was later identified as the ligand that recognises and binds to glycophorin B (Mayer *et al.,* 2009).

Table 5.1. Erythrocyte receptor and *Plasmodium* ligand interactions
Five erythrocyte receptors (glycophorin A, B, C, receptor X and receptor E) interact with members of the EBL superfamily under various enzymatic conditions. Interactions are identified as resistant (R) or sensitive (S) to treatment with neuraminidase (an enzyme that removes sialic acid moieties from the cell surface), trypsin and chymotrypsin (which cleave surface proteins at specific moieties). (Data for this table are from Beeson *et al.,* 2016; Paul *et al.,* 2015; Mayer *et al.,* 2009; Gilberger *et al.,* 2003a; Dolan *et al.,* 1994; Thompson *et al.,* 2002; Orlandi *et al.,* 1992; Duraisingh *et al.,* 2003).

Enzyme Treatment	GPA	GPB	GPC	Receptor X	Receptor E
Neuraminidase	S/ R	S	S	R	S
Trypsin	S	R	S	?	R
Chymotrypsin	R	S	R	?	S
Interacting ligand	EBA175	EBL1	EBA140	?	EBA181

5.1.4 Are the *Pf*EBA Proteins Essential or Redundant?

Attempts to disrupt *Pfeba*181 in two *P. falciparum* parasite lines, W2mef and 3D7, had contrasting results. Viable parasites with no effect on invasion were obtained in the W2mef line after disruption, which is in contrast with the inability to target the gene in the 3D7 line (Gilberger *et al.,* 2003a). It was concluded that *Pf*EBA181 is redundant in *P. falciparum* W2mef parasites, but essential in 3D7 parasites (Gilberger *et al.,* 2003a).

Interestingly, similar contrasting results were observed during attempts to disrupt *Pfeba*175 and *Pfeba*140. *Pfeba*175 can be disrupted in 3D7 and W2mef, but not in D10 *P. falciparum* parasites (Reed *et al.,* 2000). *Pfeba*140 appears to have an increased importance in *P. falciparum* 3D7 parasites, as compared to W2mef parasites (Maier *et al.,* 2003). This was proposed to be due to polymorphisms that are present in the F1 DBL domain of *Pf*EBA140, which decreases the affinity of the ligand to glycophorin C (Maier *et al.,* 2003). D10 parasites lack the *Pfeba*140 gene, which suggests that not all of the parasite ligands are necessary for the sialic-acid dependent invasion pathway (Gilberger *et al.,* 2003a).

These findings seem unexpected, but the polymorphic nature of surface antigens on the host erythrocytes (Miller *et al.,* 2002) in addition to the varied immune responses by infected individuals, provides support for the theory that multiple invasion pathways exist for *Plasmodium* infection (Gilberger *et al.,* 2003a).

5.1.5 Expression of *Pf*EBA181

*Pfeba*181 mRNA expression occurs at low levels throughout the asexual blood-stage life forms, with peak transcription occurring in the late schizont stage (Figure 5.4; Aurrecoechea et al., 2008; Otto *et al.,* 2010).

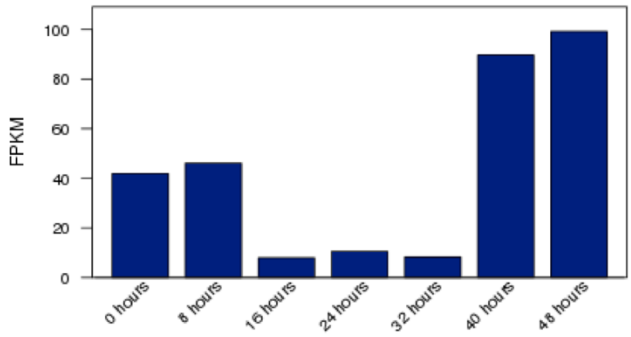


Figure 5.4. mRNA expression levels of *Pfeba*181 during the asexual intra-erythrocytic cycle. RNA was extracted from synchronised 3D7 *P. falciparum* parasites at several time points post-infection (indicated on the x-axis) and subjected to sequencing. Fragments per kilo-base of exon model per million mapped reads (FPKM) on the y-axis indicates the transcript levels at each of the selected time points. *Pfeba*181 expression levels peak 40 to 48 hours post-infection, during the schizont stage. (Adapted from Aurrecoechea *et al*., 2008; PlasmoDB)

*Pf*EBA181, is synthesised as a protein of 181kDa, and can be detected in late schizonts and in free merozoites (Aurrecoechea et al., 2008). Parasite proteins were harvested at set time-points and *Pf*EBA181 expression levels were monitored with the use of antibodies and SDS-

PAGE analysis, which showed maximal expression in the late schizont stages (Gilberger *et al.,* 2003a). *Pf*EBA181 was detected as a product of ~190kDa, as expected. A second minor product of ~170kDa, presumably a processed form of *Pf*EBA181, was detected using the same antibodies (Gilberger *et al.,* 2003a).

5.1.6 Trafficking of *Pf*EBA175

All proteins belonging to the EBL family have a conserved 3' cysteine-rich region, which has been shown to be responsible for *Pf*EBA175 localisation to the micronemes (Treeck *et al.,* 2006). The C-terminal cytoplasmic tail of *Pf*EBA175 is essential for merozoite invasion, but is not required for trafficking (Gilberger *et al.,* 2003b).

Further studies conducted on *Pf*EBA175 showed that an additional region, upstream of the cysteine-rich domain, was required for correct trafficking to the micronemes (Sakura *et al.,* 2013). By creating various transgenic parasite lines expressing recombinant *Pf*EBA175 with serial truncations in the "upstream" region, Sakura *et al.,* (2013) were able to show that the 17 amino acids from position 1250 to 1266, in addition to the cysteine-rich domain, were required for localisation to the micronemes (marked in blue in Figure 5.5).

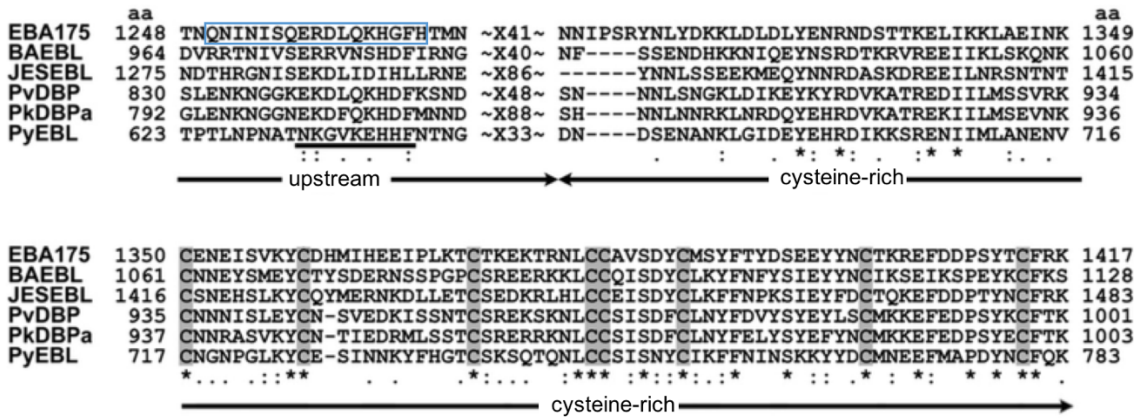


Figure 5.5. Alignment of the cysteine-rich regions of *Plasmodium* EBL proteins.
Amino acid positions (aa) of *Pf*EBA175, *Pf*EBA140 (BAEBL) and *Pf*EBA181 (JESEBL) are shown. Amino acid sequences of *Pv*DBP, *Pk*DBPα and *Py*EBL were also used. The underlined stretch of amino acids in the "upstream" region indicates a relatively conserved segment among EBL proteins. Asterisks (*), colons (:) and dots (.) are used to indicate identical, conserved and semi-conserved amino acids, respectively. Conserved cysteine residues in the cysteine-rich region are shaded in grey. The *Pf*EBA175 aa residues marked in blue are those identified as important for trafficking to the micronemes. (Adapted from Sakura *et al.,* 2013).

5.1.7 Trafficking of *Pf*EBA181

As with all other EBL proteins (except MAEBL, which is stored in the rhoptries), *Pf*EBA181 is stored in the micronemes. *Pf*EBA181 is trafficked via the ER in the early secretory pathway using the signal peptide located at the N-terminus, however the domain for trafficking to the micronemes is not known. To investigate the role of the C-terminal cysteine-rich domain in *Pf*EBA181, a colleague in the *Plasmodium* Molecular Research Unit (Wepener, 2014) designed a *Pfeba*181 mini-gene, which included only the signal peptide and cysteine-rich domain (Figure 5.6).

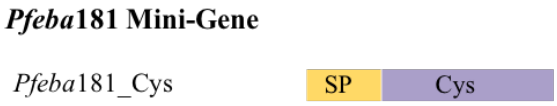


Figure 5.6. The *Pfeba*181 mini-gene.
The original mini-gene designed for *Pfeba*181, which included the signal peptide (SP) and cysteine-rich domain (Cys). (Adapted from Wepener, 2014).

The *Pfeba*181 mini-gene was cloned into the mCherry plasmid, which was used to create a transgenic parasite line expressing the mCherry-tagged *Pf*EBA181_Cys chimaeric protein (Wepener, 2014). Microscopy studies using a microneme marker, *Pf*EBA175, showed that some co-localisation occurred, but that the mCherry-tagged protein was not limited to the micronemes. It was concluded that the cysteine-rich domain of *Pf*EBA181 was necessary, but not sufficient for localisation to the micronemes (Wepener, 2014). It was thus hypothesised that *Pf*EBA181, similar to *Pf*EBA175, requires an additional region upstream of the cysteine-rich domain for correct microneme targeting.

5.1.8 Research Objectives

The aim of the research conducted in this chapter was to identify the molecular determinants for trafficking of *Pf*EBA181.

This was achieved by creating two transgenic parasite lines expressing fluorescently-tagged chimaeric *Pf*EBA181 peptides, and conducting co-localisation studies to determine which of the protein domains were required for the correct targeting of *Pf*EBA181 to the micronemes.

5.2 Materials and Methods

The materials and methods used to investigate *Pf*EBA181 are described in Chapter 2.

5.3 Results

5.3.1 Bio-informatic Analysis of *Pf*EBA181

The sequence of *Pfeba*181 was obtained from the online *Plasmodium* database (PlasmoDB version 30; www.plasmodb.org; Aurrecoechea *et al*., 2008). *Pf*EBA181 is encoded by the multi-exon PF3D7_0102500 gene, which is located on chromosome 1. *Pf*EBA181 is a protein of 1567 amino acids (aa) with a molecular weight of 181 kDa (Aurrecoechea *et al.,* 2008; Gilberger *et al.,* 2003a). Figure 5.7 shows the domains of this invasion protein.

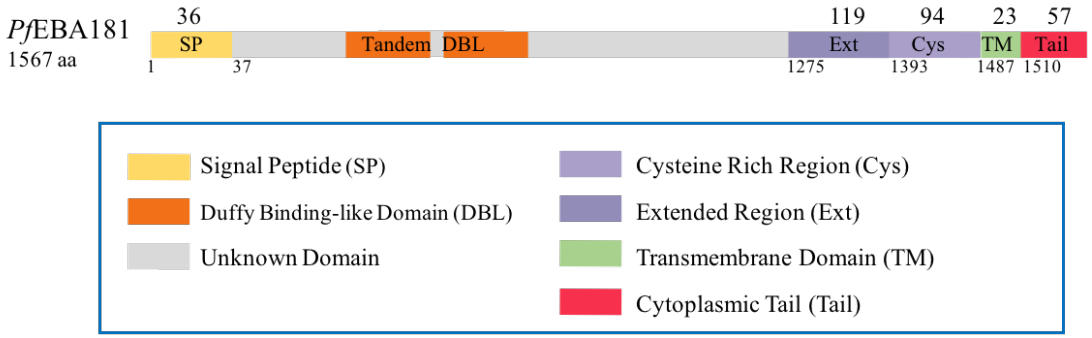


Figure 5.7. A schematic representing the domains of *Pf*EBA181, a *P. falciparum* microneme invasion protein.
The domain sizes (aa) are indicated above each domain and the positions of the first residues for each domain are indicated below.

5.3.2 Creation of *Pfeba*181 Mini-Genes

5.3.2.1 Designing *Pfeba*181 Mini-Genes for Parasite Transfections

To assess which of the various domains (Figure 5.7) are involved in targeting *Pf*EBA181 to the *P. falciparum* micronemes, two mini-genes were designed (Figure 5.8). The Signal Peptide (SP) was included in both of the chimaeric proteins to ensure correct targeting via the ER.

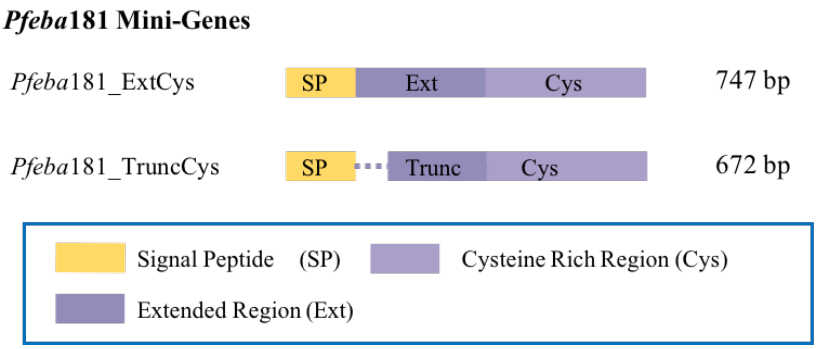


Figure 5.8. A schematic depicting the mini-genes designed for *P. falciparum* invasion protein, *Pf*EBA181.
Base pair (bp) sizes of mini-genes are indicated on the right.

The first mini-gene included the cysteine-rich domain as well as the region upstream from the cysteine-rich domain as identified by Sakura *et al.,* (2013). The second mini-gene included a truncated version of the extended cysteine-rich domain, thus lacking an N-terminal 25aa region, which overlaps with the 17aa region identified as important for *Pf*EBA175 trafficking to the micronemes (Figure 5.5; Figure 5.9).

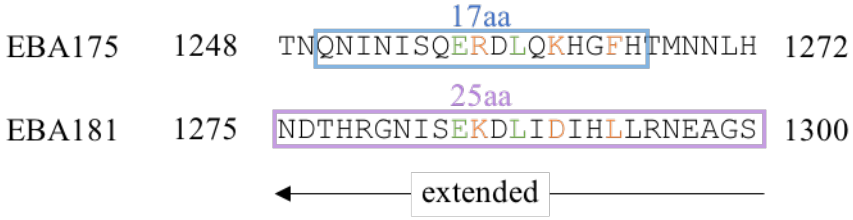


Figure 5.9. Alignment of the extended cysteine-rich regions of EBA175 and EBA181.
Amino acid positions of *Pf*EBA175 and *Pf*EBA181 are shown. Green and orange residues are those identified as conserved and semi-conserved amongst the EBL proteins: green residues are identical and orange residues differ in *Pf*EBA175 and *Pf*EBA181. The *Pf*EBA175 residues marked in blue are those identified as important for trafficking to the micronemes. The *Pf*EBA181 residues marked in purple are those which were excluded from the *Pfeba181*_TruncCys mini-gene.

5.3.2.2 RNA Isolation and cDNA Generation

Since *Pfeba181* contains several introns (Figure 5.2), genomic DNA was not suitable for the creation of the mini-genes. Total RNA (Figure 4.7) was isolated from synchronised schizont-stage *P. falciparum* 3D7 parasites and used for the generation of cDNA using the *Pf*EBA181 "C-term" reverse primer.

5.3.2.3 PCR and Overlap Extension PCR

To attach the signal peptide to the cysteine-rich regions and thus delete the interim domains, the two *Pfeba181* mini-genes were generated by PCR and overlap extension PCR using cDNA and appropriate primers. The primers and PCR parameters are in Appendix A.

All PCR products migrated according to their expected sizes (Table 5.2) as assessed by agarose gel electrophoresis. PCR products were slightly larger than the domain sizes due to additions to the primers (see Appendix A).

Table 5.2. Expected PCR product sizes of domains within *Pfeba181* mini-genes.

Gene	Mini-genes	Domains	Region to be amplified (bp)	PCR Product (bp)
Pfeba181	ExtCys Product 1	SP	108	136
	ExtCys Product 2	Ext-Cys	639	649
	ExtCys Final Product	SP + Ext-Cys	747	767
	TruncCys Product 1	SP	108	142
	TruncCys Product 2	Trunc-Cys	564	574
	TruncCys Final Product	SP + Trunc-Cys	672	692

To create the *Pfeba181* mini-genes, the signal peptide was amplified to generate a PCR product of 136bp (Product 1; Figure 5.10 A lane 2) and 142bp (Product 1; Figure 5.10 B lane 2), containing 3' overhangs of 18bp and 24bp respectively. The extended and truncated cysteine-rich regions were amplified to create products of 649bp (Product 2; Figure 5.10 A lane 3) and 574bp (Product 2; Figure 5.10 B lane 3). Subsequent overlap extension PCR amplifications were performed to fuse the respective Products 1 and 2 together and thus create the *Pfeba181*_ExtCys and *Pfeba181*_TruncCys mini-genes (Figure 5.10 C).

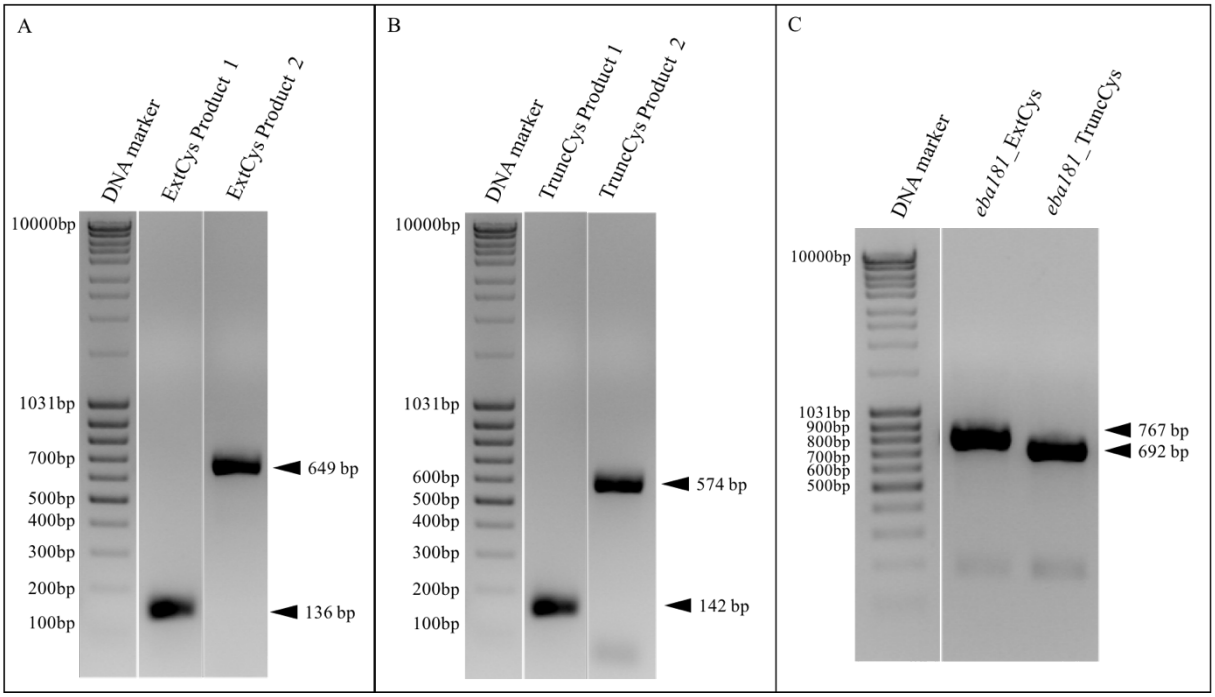


Figure 5.10. Creating *Pfeba181* mini-genes by overlap extension PCR.
Size validation of domains by gel electrophoresis against a base pair standard. **A** – *Pfeba181*_ExtCys PCR products, Product 1: signal peptide, and Product 2: ExtCys-Cys. **B** – *Pfeba181*_TruncCys PCR products, Product 1: signal peptide, and Product 2: TruncCys-Cys. **C** – Mini-genes: *Pfeba181*_ExtCys and *Pfeba181*_TruncCys generated by overlap extension PCR using Products 1 and 2.

5.3.2.4 Generation & Verification of pARL-mCherry Constructs

After restriction endonuclease digestion with *Xho*I and *Avr*II, *P. falciparum* amplicons and mCherry plasmid were quantified by gel electrophoresis and ligated in a 5:1 ratio. Competent *E. coli* XL10 cells were transformed and transferred to ampicillin-treated agar plates. Colonies were picked, amplified and the plasmid isolated for verification.

Restriction endonuclease digestion of the mCherry control plasmid and the two *Pfeba181* mCherry constructs (Figure 5.12) using FastDigest® enzymes *Xho*I and *Pst*I, confirmed that amplicons of the correct sizes had been inserted into the mCherry plasmid. Positive clones were sequenced by Inqaba Biotec™, which confirmed that inserts were error-free and in-frame.

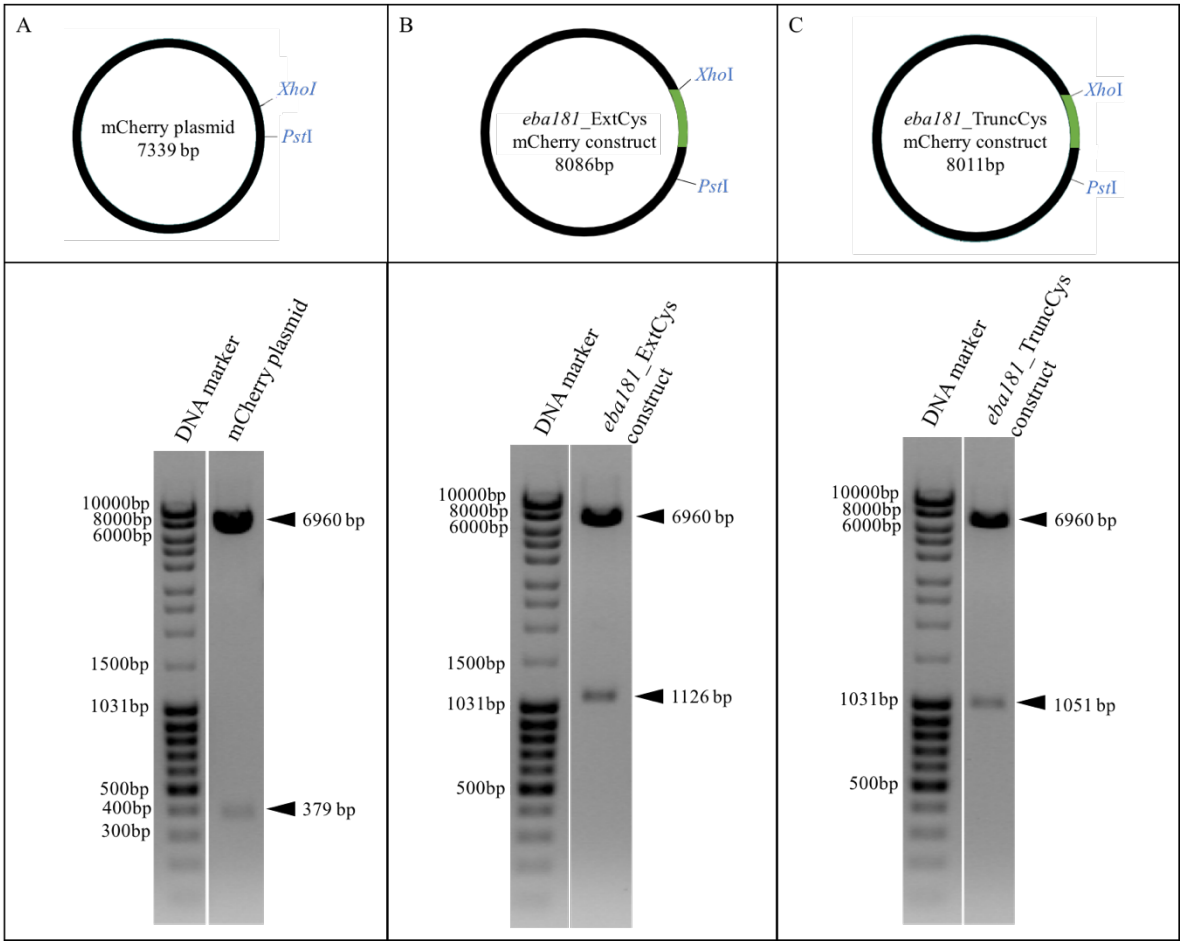


Figure 5.11. Verification of *Pfeba181* mCherry constructs.
Size validation of the *Pfeba181* mCherry constructs after *Xho*I and *Pst*I restriction endonuclease digestion by agarose gel electrophoresis against a base pair standard. **A –** Digestion of the control mCherry plasmid resulted in two fragments of 6960 and 379bp. **B –** Digestion of *Pfeba181*_ExtCys resulted in two fragments 6960 and 1126bp. **C –** Digestion of *Pfeba181*_TruncCys resulted in two fragments of 6960 and 1051bp.

5.3.3 *Pf*EBA181 Transgenic Parasites

Transgenic parasite lines were created by electroporating 3D7 *P. falciparum* parasites with the plasmid constructs. WR99210 compound was administered to the cultures to ensure that only parasites with the plasmid survived. Live parasites were visible in the transgenic cultures approximately 40 days after transfection.

To confirm that the transgenic parasites contained the desired constructs, PCR verification was performed using mCherry backbone primers flanking the mini-gene insert site (Figure 3.18). Assessment of the two *Pf*EBA181 transgenic lines confirmed that the resultant products migrated according to the expected sizes as determined by agarose gel electrophoresis (Figure 5.12). Due to the binding sites of the primers, all amplified products

were 534bp larger (Figure 3.18) than the mini-genes: 1281bp and 1206bp for the ExtCys and TruncCys EBA181 mCherry transgenic lines respectively. These results confirmed that both of *Pf*EBA181 transgenic cultures carried the appropriate constructs.

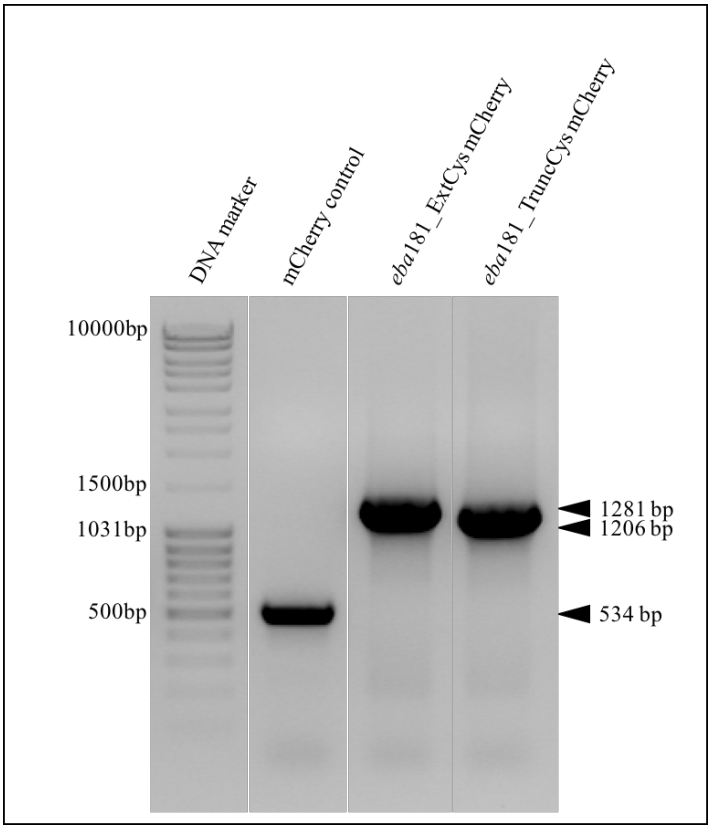


Figure 5.12. PCR verification of *Pf*EBA181 transgenic parasite lines.
Transgenic parasite DNA was amplified using mCherry backbone primers to confirm successful uptake of plasmid constructs. Size validation was performed by gel electrophoresis against a base pair standard. The PCR product of *Pfeba*181_ExtCys and *Pfeba*181_TruncCys mCherry migrated at the expected sizes of 1281bp and 1206bp, respectively.

5.3.4 Identification of the Domain Targeting *Pf*EBA181 to the Micronemes

5.3.4.1 Live Imaging of *Pf*EBA181 Transgenic Parasites

Transgenic *P. falciparum* cultures were prepared for microscopy by DAPI treatment to stain the parasite nuclei. With the addition of the extended cysteine-rich region, the mCherry fluorescence of *Pf*EBA181 appeared punctate and localised adjacent to the nuclei (Figure 5.13; top panel). When the N-terminal 25aa region was deleted to create a truncated form of the extended cysteine-rich chimaeric protein, the mCherry fluorescence changed and appeared dispersed throughout the parasite (Figure 5.13; bottom panel). These results indicate that the extra 25aa region is required for correct microneme localisation as was found for *Pf*EBA175 (Sakura *et al.,* 2013).

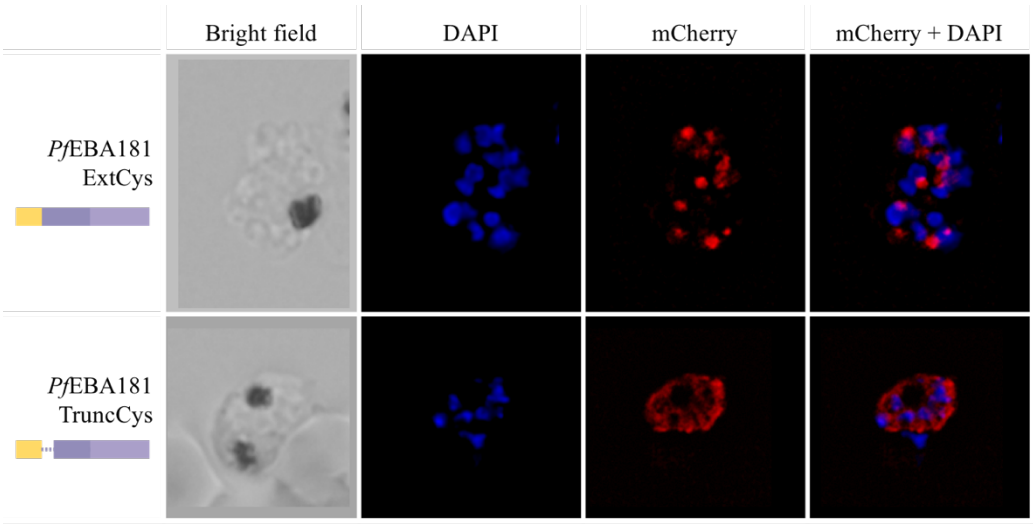


Figure 5.13. Fluorescence images of live schizont stage *P. falciparum* transgenic parasites expressing mCherry-tagged *Pf*EBA181.
Parasites were viewed at 1000x magnification. mCherry causes red fluorescence of chimaeric *Pf*EBA181 proteins. DAPI is a blue nuclear stain. **Top Panel:** *Pf*EBA181_ExtCys localised to apically distinct puncta that are adjacent to the nuclei. **Bottom Panel:** *Pf*EBA181_TruncCys had a different, dispersed pattern and occurred throughout the parasite.

5.3.4.2 Co-localisation Studies of *Pf*EBA181 Chimaeric Proteins

Microscopy experiments were performed using a known microneme marker, *Pf*EBA175, to determine the subcellular location of the mCherry-tagged chimaeric proteins. Transgenic parasite cultures were fixed, permeabilised and incubated with DAPI to stain the nucleus as well as an anti-EBA175 antibody with a green fluorochrome to identify the micronemes. The original *Pf*EBA181_Cys chimaeric protein yielded dispersed mCherry fluorescence and very little overlap with the green microneme marker (Figure 5.14), supporting findings by Wepener (2014).

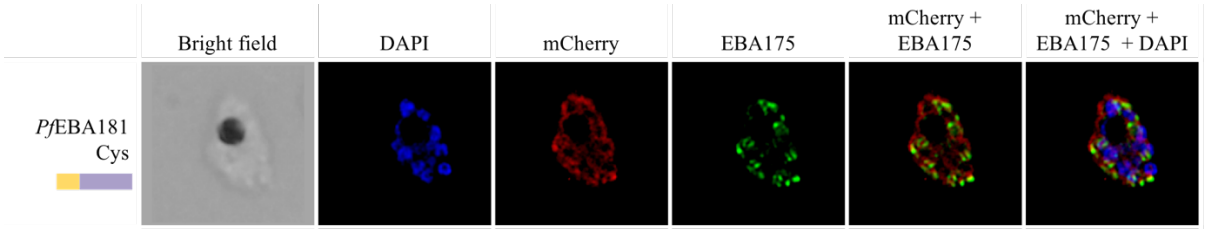


Figure 5.14. Co-localisation studies using fixed schizont stage *P. falciparum* parasites expressing the original mCherry-tagged *Pf*EBA181.
Parasites were viewed at 1000x magnification. mCherry causes red fluorescence of the chimaeric *Pf*EBA181 proteins. DAPI is a blue nuclear stain. A microneme marker, *Pf*EBA175, with a green fluorochrome was used to determine the localisation of mCherry tagged proteins within the transgenic parasites. *Pf*EBA181_Cys fluorescence appears dispersed and limited co-localisation was observed with the microneme marker.

With the addition of the extended upstream region identified by Sakura *et al.,* (2013), the mCherry fluorescence of *Pf*EBA181_ExtCys appeared as distinct puncta in the apical region and some co-localisation was observed (Figure 5.15; middle panel), which indicates that the two proteins occur in close proximity and is supported by a Pearson's coefficient of 0.66. When an N-terminal 25aa region was deleted from the extended upstream region, the mCherry fluorescence returned to being dispersed throughout the parasite and the Pearson's coefficient reduced to 0.51. These findings show that the 25aa sequence in the extended cysteine-rich region is required for microneme targeting.

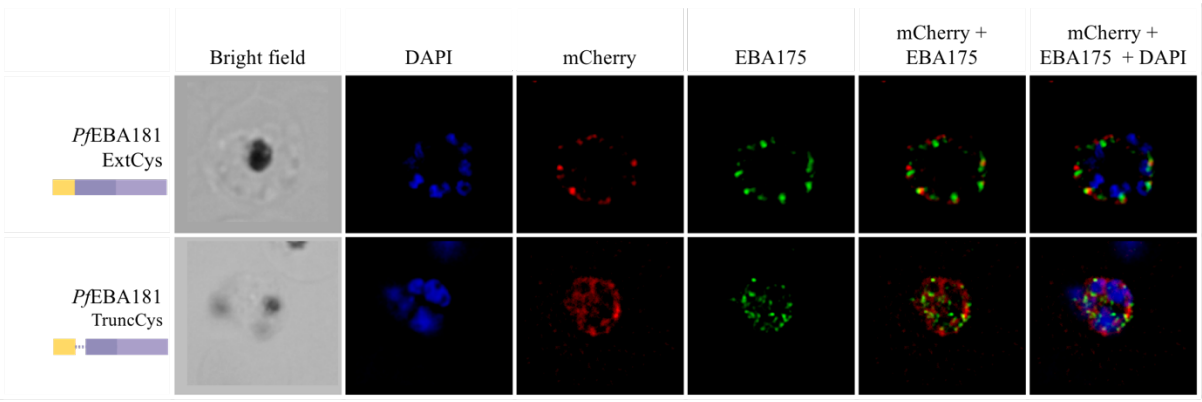


Figure 5.15. Co-localisation studies using fixed schizont stage *P. falciparum* parasites expressing mCherry-tagged *Pf*EBA181.
Parasites were viewed at 1000x magnification. mCherry causes red fluorescence of the chimaeric *Pf*EBA181 proteins. DAPI is a blue nuclear stain. A microneme marker, *Pf*EBA175, with a green fluorochrome was used to determine the localisation of mCherry tagged proteins within the transgenic parasites. Pearson's coefficients (PC) are a numerical indicator of co-localisation, with values close to 1 indicating strong co-localisation. **Top Panel:** The addition of the extended cysteine-rich domain resulted in apically distinct localisation (PC 0.66). **Bottom Panel**: The deletion of a 25aa region at the N-terminus of the extended cysteine-rich region resulted in a dispersed pattern of fluorescence and limited co-localisation with the microneme marker (PC 0.51).

5.4 Discussion

5.4.1 A Tyrosine Motif Does Not Target *Pf*EBA181 to the Micronemes

The *Pf*EBA181 transgenic line expressing the extended cysteine-rich domain, showed co-localisation of the mCherry-tagged protein with the micronemes, but this chimaera consisted of the signal peptide and extended cysteine-rich regions, and excluded the transmembrane domain or cytoplasmic tail. It is thus evident that the transmembrane-spanning region is not required for apical localisation.

Tyrosine motifs have been implicated as sorting signals, but in *Pf*EBA175 the motif YQSS at position 1446 in the cytoplasmic tail is not required for trafficking to the micronemes (Gilberger *et al.,* 2003b). This motif is not shared by *Pf*EBA181 (Figure 5.16), but another tyrosine-based sequence is present in the *Pf*EBA181 cytoplasmic tail, YNKL, which seems to conform to the YXXϕ tetrapeptide motif. Deletion of the cytoplasmic tail, however, does not prevent microneme localisation. The tyrosine motif YNKL is thus not likely to play a role in transporting *Pf*EBA181.



Figure 5.16. Sequence alignment of the transmembrane domains and cytoplasmic tails of *Pf*EBA175 and *Pf*EBA181.
The transmembrane domain (black residues) and cytoplasmic tail (coloured residues) of the two proteins have many identical conserved residues, but the tyrosine residues are not conserved. Blue arrows depict tyrosine residues found in the *Pf*EBA175 cytoplasmic tail, and green arrows depict those in *Pf*EBA181. The *Pf*EBA175 tyrosine motif, YQSS (identified by Gilberger *et al.,* 2003b; boxed in blue), is not present in *Pf*EBA181, instead a different tyrosine motif, YNKL, occurs further downstream (boxed in green). The alignments were performed using Clustal Omega (EMBL-EBI, 2017).

5.4.2 Is the *Pf*EBA181 Cysteine-Rich Domain Sufficient to Target the Micronemes?

The *Pf*EBL family proteins have two cysteine-rich regions, one at the N-terminus and another at the C-terminus. The N-terminus cysteine-rich region is the Duffy-binding like domain, which binds to the host cell receptor (Paul *et al.,* 2015).

The C-terminal cysteine-rich domain has mainly been discussed in terms of its involvement in intracellular trafficking to the micronemes. The 8 cysteines contained in this domain enables the formation of disulphide bridges (Withers-Martinez *et al.,* 2008), which have been proposed to facilitate the sorting and localisation by binding to a putative escorter protein (Gilberger *et al.,* 2003b; Treeck *et al.,* 2006). This hypothesis is supported by crystallisation of the C-terminal cysteine-rich domain of *Pf*EBA175, which revealed a KIX-like binding domain (Withers-Martinez *et al.,* 2008). Kinase-inducible domain interacting (KIX)

domains are involved in protein-protein interactions and are recognition domains for binding to other proteins (Thakur *et al.,* 2014).

A substitution of a cysteine residue in *P. yoelli* EBL disrupted of one of the disulphide bonds, which altered the subcellular localisation of the protein from the micronemes to the dense granules (Otsuki *et al.,* 2009). The authors proposed that this was due to a change in the recognition site of *Py*EBL, which thus prevented the interaction with a putative escorter protein.

Sequence alignments of the *Pf*EBA175 and *Pf*EBA181 cysteine-rich domains show conservation of all 8 cysteine residues (Figure 5.17), as described in the literature (Treeck *et al.,* 2006).

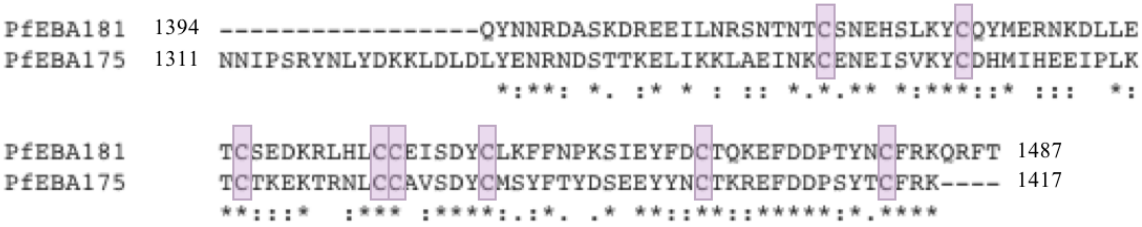


Figure 5.17. Sequence alignment of the cysteine-rich domains of *Pf*EBA181 and *Pf*EBA175. Many of the residues in the two domains are identical or conserved, with 46% identity calculated by Clustal (ebi.co.uk). The 8 cysteine residues are identical in both sequences. The alignments were performed using Clustal Omega (EMBL-EBI, 2017).

In previous studies, the C-terminal cysteine-rich domain was shown to be essential, but not sufficient for microneme localisation (Wepener, 2014). The co-localisation studies done for this thesis showed that very little fluorescence overlap occurred between the microneme marker and the mCherry-tagged *Pf*EBA181 chimaeric protein expressing only the signal peptide and cysteine-rich domain. The mCherry fluorescence was more dispersed throughout the parasite without being confined to the apex, confirming previous work by Wepener (2014). Despite the inclusion of all 8 conserved cysteine residues in the chimaeric protein, co-localisation with the micronemes was not achieved.

A recent study showed that *Pf*EBA175 requires an additional upstream region to target the protein to the micronemes, with a stretch of 17aa being absolutely necessary for correct localisation (Sakura *et al.,* 2013). Based on these findings, chimaeric proteins expressing the

upstream region (position 1275 to 1392) of the C-terminal cysteine-rich domain were used in co-localisation studies, which showed improved localisation to the apex. A deletion of the 25aa region (positon 1275 to 1300), which correlates to the 17aa region identified by Sakura *et al.,* (2013) lead to mis-targeting of the protein. These findings confirmed that the extended cysteine-rich region of *Pf*EBA181 was required for correct transport to the micronemes.

Chapter 6: Identifying Binding Partners

6.1 Introduction

6.1.1 Protein-Protein Interactions

Protein-protein interactions are required for most cellular processes and mediate a large number of regulatory pathways. These interactions are of great importance to disease control and are often exploited as targets for drug development (Mullard, 2012).

The use of small molecules (often peptides) to inhibit protein-protein interactions (Figure 6.1) is a useful tool for drug development and has received a lot of attention over the last few years.

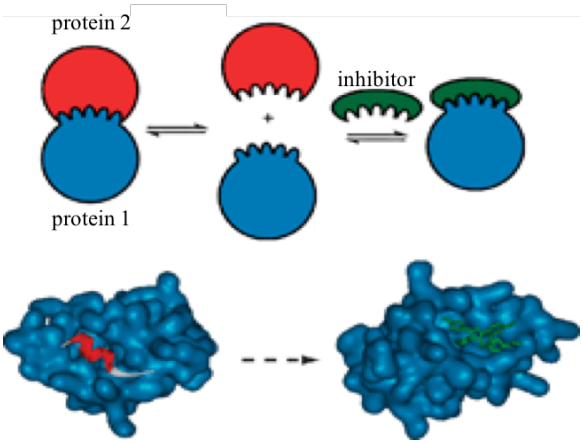


Figure 6.1. A schematic depicting the inhibition of a protein-protein interaction.
A useful tool in drug development is the design of small molecules, which compete with one of the proteins in a complex and interacts at the target binding site. The protein-protein interaction is thus prevented and can influence downstream pathways. (Adapted from Wilson, 2009).

An example is the inhibition of the *Pf*RON2 and *Pf*AMA-1 interaction by the R1 peptide (Harris *et al.,* 2005a). R1 was identified through the use of a phage-display library, and shares sequence similarity with *Pf*RON2 (Tyler & Boothroyd, 2011). R1 binds within or adjacent to the hydrophobic cleft of *Pf*AMA-1, blocks the interaction with *Pf*RON2 and prevents invasion (Harris *et al.,* 2005a). Many other molecules have been identified that can act as competitors for the binding of *Pf*AMA-1, which also prevent the interaction with *Pf*RON2 and block invasion (Pihan *et al.,* 2015).

By exploring new protein-protein interactions, it is possible to identify key new features which may help to understand and selectively inhibit cellular signaling pathways in parasitic organisms such as *P. falciparum.*

6.1.2 Identifying Protein-Protein Interactions

The isolation of protein binding partners is commonly performed *in vivo* by co-immunoprecipitation studies, which utilise a specific antibody against the protein of interest, to pull-down and identify protein complexes. The target protein can either be native or expressed episomally with a tag that is detected by the antibody. A major challenge with this technique, is the relatively low levels of expressed *P. falciparum* proteins.

Several *in vitro* techniques exist for the identification of protein binding partners. These often include the use of a large pool of proteins or peptides, which is exposed to a tagged protein and in this way, any interacting partners can be isolated and identified by sequencing. The yeast two-hybrid (Y2H) system, which exposes a bait peptide or protein to a library of prey peptides, is a popular tool for the identification of *P. falciparum* protein-protein interactions. Interaction maps and protein partner data from Y2H studies have been made publically available on PlasmoDB (Aurrecoechea et al., 2008). Affinity chromatography is another technique that can be used to identify protein-protein interaction. This technique utilises parasite-derived proteins against an immobilised peptide or protein, and the resultant binding partners can be assessed by mass spectrometry.

6.1.3 Using Phage Display Libraries to Identify Novel Binding Partners

A newer tool for the identification of protein-protein interactions in *P. falciparum* is the use of phage display libraries (Lauterbach *et al.,* 2003; Lanzillotti & Coetzer, 2008). This technique has been utilised in other organisms for more than two decades (Smith, 1985), but has only been described for use in *P. falciparum* during the last 14 years (Lauterbach *et al.,* 2003).

Early studies with phage display technology (Smith, 1985) used filamentous phage and involved the insertion of foreign DNA into a minor coat protein, which resulted in the expression of the foreign peptide on the coat of the phage. A specific antibody was exposed to this library of peptides, which was able to detect epitopes.

The *P. falciparum* phage display libraries employed in this thesis were designed by members of the *Plasmodium* Molecular Research Unit (PMRU, University of the Witwatersrand; Lauterbach *et al.,* 2003; Lanzillotti & Coetzer, 2008). These libraries utilised the T7 bacteriophage, which has several advantages over filamentous phage (highlighted in the T7Select® System Manual, Novagen). Peptides displayed on T7 bacteriophage capsids were inserted into the gene encoding the 10B coat protein, and are not secreted through the cell membrane, which is necessary for filamentous phage assembly. Other advantages include the rapid replication rates, improved stability and robustness of the phage, as well as the availability of the T7 sequence, which makes DNA sequencing a simpler process.

6.1.4 Research Objectives

To assess the possible involvement of an escorter protein to target invasion proteins to the micronemes, biopanning experiments were performed against *P. falciparum* phage display libraries, which would allow for the identification of novel binding partners for these micronemal invasion proteins.

6.2 Materials and Methods

The materials and methods used to investigate binding partners for *P. falciparum* invasion proteins are described in Chapter 2.

6.3 Results

The three *P. falciparum* invasion proteins, *Pf*AMA-1, *Pf*SUB2 and *Pf*EBA181 were considered for the biopanning assays and the domains implicated in microneme targeting were selected for cloning into pET-15b and recombinant protein expression with an N-terminal Histidine tag.

6.3.1 Preparation of the pET-15b Constructs

Genomic DNA isolated from *P. falciparum* 3D7 parasites (Figure 3.12), was used to amplify the regions identified as the microneme targeting domains of *Pf*AMA-1, *Pf*SUB2 and *Pf*EBA181 (Figure 6.2).

Primers flanking the regions of interest (depicted with coloured arrows in Figure 6.2) were used to create one *Pfama-1* amplicon, three *Pfsub2* amplicons consisting of variations of the

juxtamembrane domain, transmembrane domain and the cytoplasmic tail, as well as two amplicons of *Pfeba181*, consisting of either just the cysteine-rich domain or the extended cysteine-rich domain. PCR products of the expected sizes (as calculated in Table 6.1) were detected by agarose gel electrophoresis against a base pair standard (Figure 6.3 B to D).

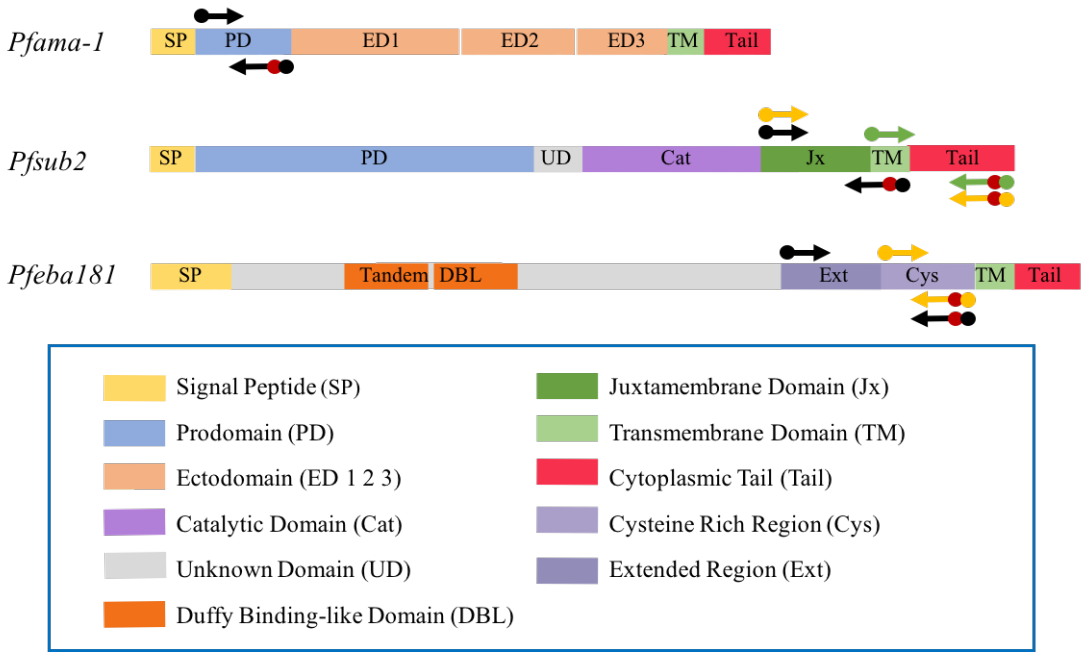


Figure 6.2. The primer binding sites for the creation of the pET-15b inserts.
The *Pfama-1* prodomain, variations of the *Pfsub2* juxtamembrane domain, transmembrane domain and cytoplasmic tail, and the *Pfeba181* cysteine and extended cysteine-rich regions were amplified using site-specific primers. Primers are indicated using coloured arrows, restriction enzyme sites are indicated with solid circles that match the primer colour; and stop codons are indicated with red solid circles.

Table 6.1. Expected PCR product and pET-15b construct sizes.
Various regions of the *Pfama-1, Pfsub2* and *Pfeba181* genes were amplified by PCR. Expected PCR product sizes represent the region size as well as the addition of random bases, restriction enzyme (RE) sites and stop codons included in the primers (listed in Appendix E). Construct sizes represent the size of the pET-15b plasmid and PCR amplicon after ligation.

Gene	Domain/s	Region (bp)	PCR product (bp)	Construct size (bp)
Pfama-1	Prodomain	216	241	5922
Pfsub2	JxTail	933	958	6635
Pfsub2	JxTM	387	412	6314
Pfsub2	TMTail	612	667	6089
Pfeba181	ExtCys	639	664	6341
Pfeba181	Cys	282	307	5988

The resultant amplicons were and the 5708bp pET-15b plasmid were prepared for ligation by endonuclease restriction digestion using *Bam*HI and *Nde*I, as well as treatment with alkaline phosphatase to dephosphorylate the plasmid. The digested plasmid was detected as a product of the expected size of 5703bp by gel electrophoresis (Figure 6.3 A).

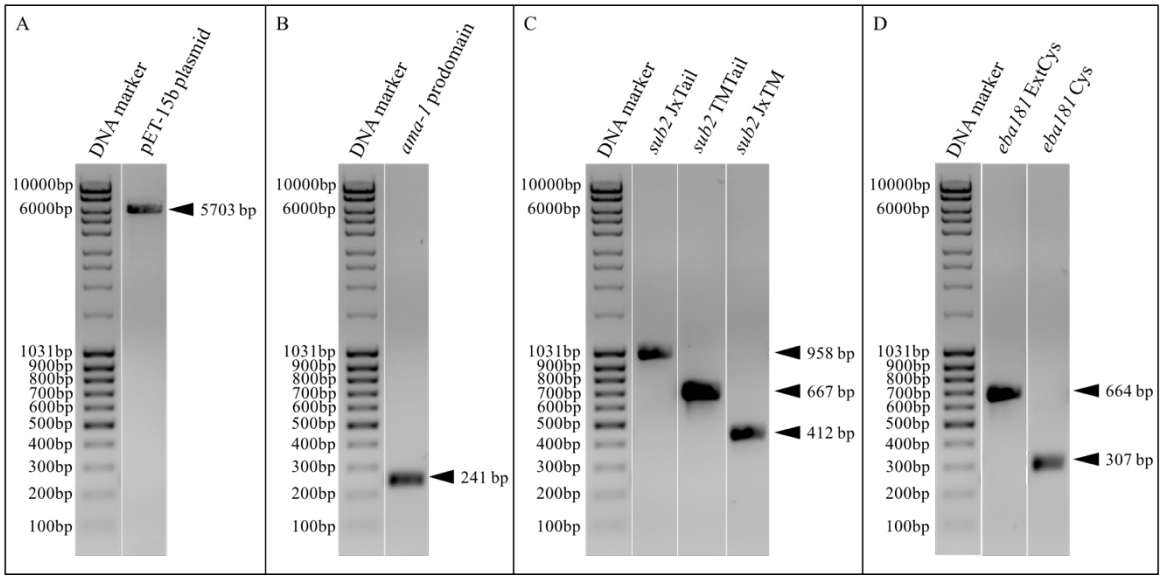


Figure 6.3. Visualisation of pET-15b plasmid and PCR amplicons for cloning.
Analysis of isolated plasmid and PCR products of *Pfama-1*, *Pfsub2* and *Pfeba181* by gel electrophoresis against a base pair standard. **A –** pET-15b plasmid was linearised by restriction endonuclease digestion using *Bam*HI and *Nde*I and migrated at the correct size of 5703bp. **B to D –** All six PCR products migrated according to their expected sizes.

6.3.2 Verification of the pET-15b Constructs

P. falciparum amplicons and pET-15b plasmid were quantified by gel electrophoresis and ligated in a 3:1 ratio. Competent *E. coli* XL10 cells were transformed and transferred to ampicillin-treated agar plates. Colonies were picked, amplified and the plasmid isolated for verification.

Restriction endonuclease digestion of the pET-15b control plasmid and the six constructs using FastDigest® enzymes *Xba*I and *Hind*III (Figure 6.4), confirmed that amplicons of the correct sizes had been inserted into the plasmid (Figure 6.5). Positive clones were sequenced by Inqaba Biotec™, which confirmed that inserts were error-free and in-frame.

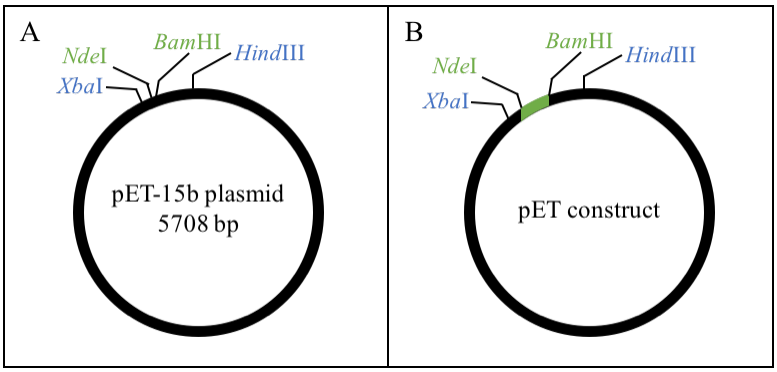


Figure 6.4. Restriction enzyme sites of pET-15b plasmid and constructs.
A – Empty pET-15b plasmid. **B –** pET construct created by directional insertion of an amplicon shown in green. Verification of clones was performed by restriction endonuclease digestion using FastDigest® enzymes *Hind*III and *Xba*I.

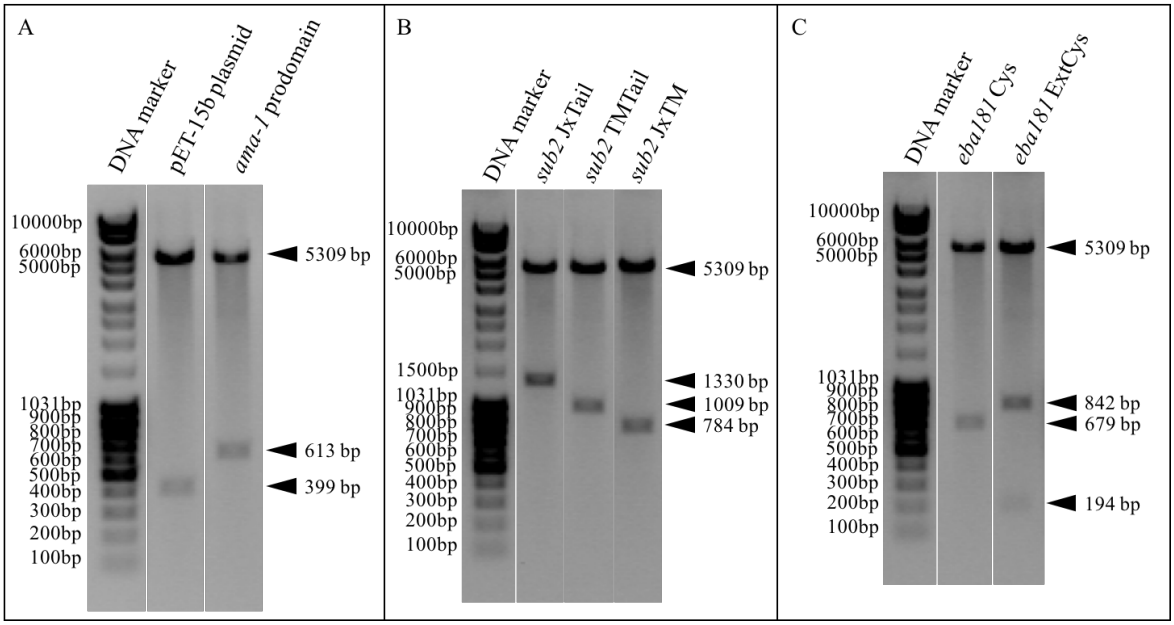


Figure 6.5. Verification of the pET-15b constructs.
Size validation of the pET-15b constructs after *Xba*I and *Hind*III restriction endonuclease digestion by gel electrophoresis against a base pair standard. All digests resulted in a plasmid backbone fragment of 5309bp, in addition to a smaller fragment that changed according to the size of the insert. **A –** Digestion of the empty plasmid yielded a fragment of 399bp. Successful insertion of the *Pfama-1* prodomain yielded a fragment of 613bp. **B –** Digestion of the *Pfsub2* constructs resulted in fragments of 1330, 1009 and 784bp respectively. **C –** Digestion of the *Pfeba181*_Cys construct yielded a fragment of 679bp. An additional *Xba*I site within the extended cysteine-rich region of *Pfeba181* resulted in 842 and 194bp fragments.

6.3.3 Recombinant Expression of the Histidine-tagged Proteins

Expression of the recombinant protein was analysed by SDS-Polyacrylamide gel electrophoresis and immunoblot detection. Due to the inclusion of the hydrophobic

transmembrane domain in the *Pf*SUB2 recombinant proteins, relatively low solubility was expected, thus three variations of the transmembrane-spanning regions were created for expression as recombinant proteins. Similarly, due the inclusion of the hydrophobic, cysteine-containing region of *Pf*EBA181 that forms disulphide bonds, low solubility was expected, thus two recombinant proteins were used. Once soluble recombinant protein was obtained, it was isolated using a MagneHis™ purification system, which utilises Nickel-coated magnetic particles.

6.3.3.1 His-tagged *Pf*EBA181

Total, soluble and insoluble fractions from 20ml Overnight Express ™ cultures expressing His-tagged *Pf*EBA181 were analysed. His-tagged *Pf*EBA181_Cys was detected as a recombinant protein at the expected size of 13.8kDa by SDS-PAGE and immunoblotting, however, very little soluble protein was detected (Figure 6.6). Attempts to improve the solubility included incubation of the cultures at lower temperatures and increasing the culture volumes. Unfortunately, low yields were still obtained, so no further studies were performed with this construct.

Recombinant His-tagged *Pf*EBA181_ExtCys was detected at ~36kDa in the total, soluble and insoluble fractions by immunoblot analysis, slightly larger than the expected size of 27.5kDa (Figure 6.6). A second, faint band at ~30kDa was also visible, which may represent a truncated form of the protein, a phenomenon that is common in recombinant expression of *P. falciparum* proteins (Mehlin *et al.,* 2006).

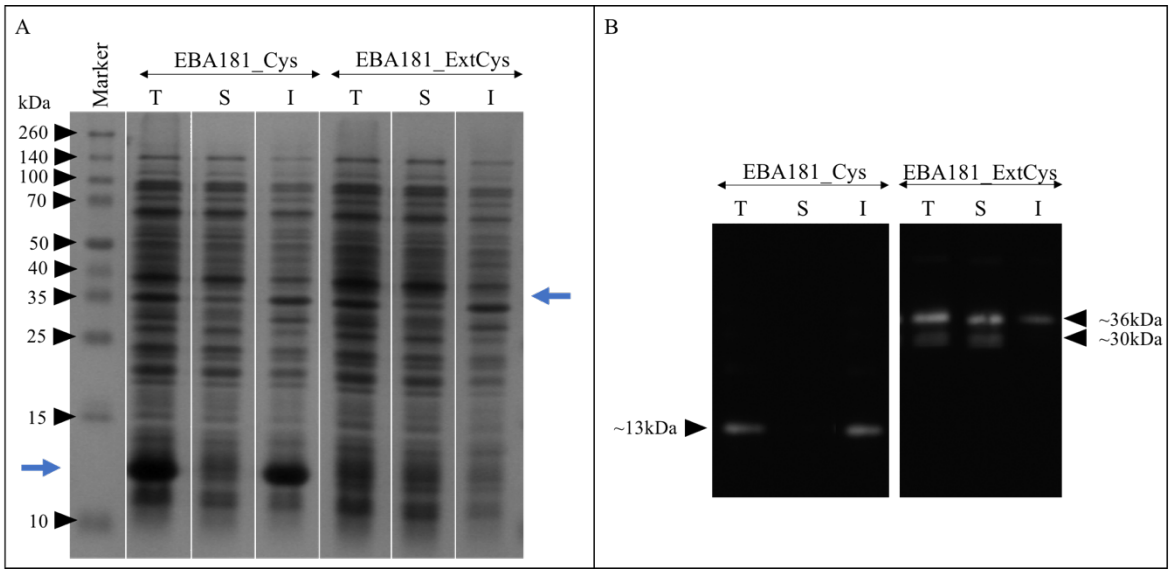


Figure 6.6. Expression and immunoblot detection of *Pf*EBA181 proteins.
A – Samples were analysed against a SpectraBR protein marker using an SDS-polyacrylamide gel, which was stained with Coomassie blue. Samples represent: 5µl of 2ml total, soluble and insoluble fractions of *Pf*EBA181_Cys and *Pf*EBA181_ExtCys. Blue arrows indicate the position of the protein on the gel. **B –** Immunoblot analysis using an anti-His antibody detected the His-tagged *Pf*EBA181_Cys protein at the expected size of 13.8kDa. Two bands were detected for *Pf*EBA181_ExtCys, a faint one at ~30kDa and another at ~36kDa, both larger than its theoretical molecular mass of 27.5kDa.

MagneHis™ particles were used to purify recombinant *Pf*EBA181_ExtCys from an 80ml Overnight Express™ culture. The purified recombinant protein was detected in low yield at ~36kDa as before and seemed pure (Figure 6.7), however, only a tenth of the eluted sample was loaded on the SDS-polacrylamide gel, so faint contaminants would not be visible. Some of the protein remained on the particles and was not recovered in the second elution.

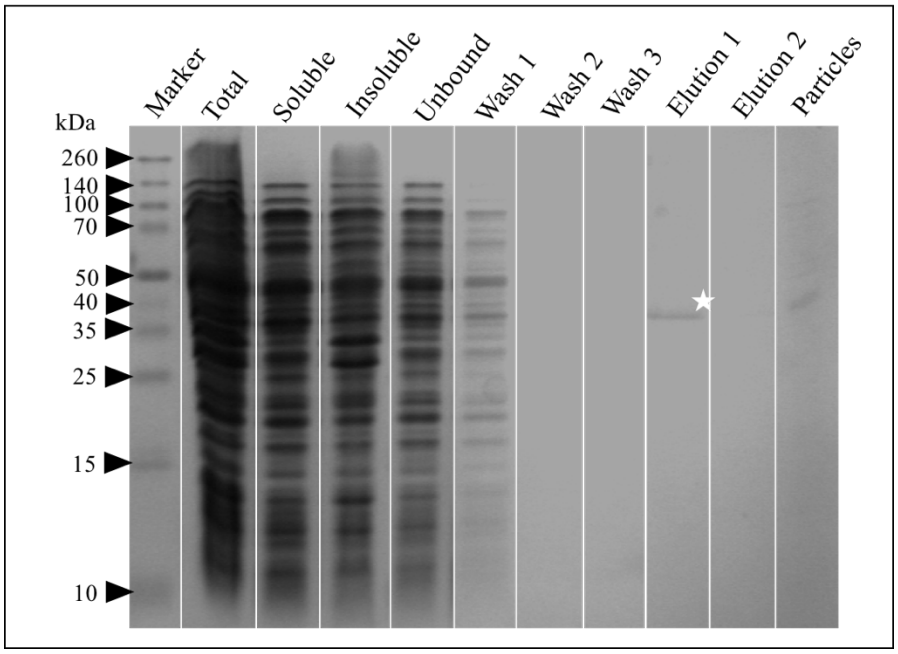


Figure 6.7. Expression and purification of His-tagged *Pf*EBA181_ExtCys.
Samples were analysed using an SDS-polyacrylamide gel, which was stained with Coomassie blue. Samples represent: 5µl of a SpectraBR protein ladder; 7µl of 8ml total, soluble, insoluble and unbound fractions; 15µl of 500µl 35mM imidazole washes; 10µl of 100µl 500mM imidazole elutions 1 and 2; 10µl of 100µl particles after elutions. The purified *Pf*EBA181 protein (indicated with a star) migrated at ~36kDa compared to its theoretical molecular weight of 27.5kDa.

6.3.3.2 His-tagged *Pf*SUB2

Overnight Express™ cultures of 20ml were used for the isolation of *Pf*SUB2 protein. Despite the inclusion of the very hydrophobic transmembrane domain in all three constructs, some soluble recombinant protein was detected for all the *Pf*SUB2 constructs. Recombinant protein was detected in the total, soluble and insoluble fractions, but at a slightly lower molecular weight (3 to 6kDa) than was expected (Figure 6.8). The JxTail and JxTM proteins had very good expression (largely insoluble), which resulted in ghost bands on the immunoblot, due to the depletion of the chemiluminescent substrate. (Figure 6.8 B).

The detection of multiple bands in the *Pf*SUB2_JxTail insoluble fraction (Figure 6.8 B) could be due to degradation of the protein samples, since no bands larger than the ~33kDa protein were detected. This was unexpected since protease inhibitors were added to the samples, which ought to have protected against degradation.

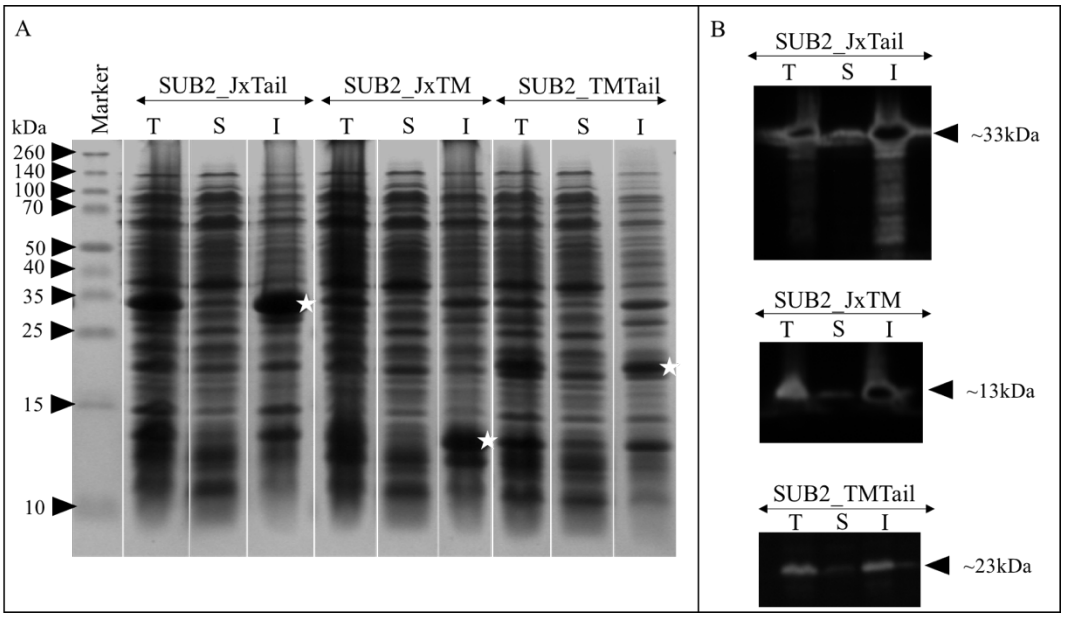


Figure 6.8. Expression and immunoblot detection of *Pf*SUB2 proteins.
A – Samples were analysed against a SpectraBR protein marker using an SDS-polyacrylamide gel, which was stained with Coomassie blue. Samples represent: 10µl of 2ml total, soluble and insoluble fractions of the three *Pf*SUB2 proteins. White stars were used to indicate the position of the proteins on the gel. **B –** Immunoblot analysis using an anti-His antibody detected the His-tagged *Pf*SUB2 proteins at ~3 to 6kDa smaller than the theoretical molecular masses: *Pf*SUB2_JxTail was ~33kDa (expected 39kDa); *Pf*SUB2_JxTM was ~13kDa (expected 17.1kDa); *Pf*SUB2_TMTail was ~23kDa (expected 26.4kDa).

The *Pf*SUB2_JxTail was selected for downstream experiments since it included the entire transmembrane-spanning domain and it produced the highest yield of soluble protein (Figure 6.8 B). Overnight Express™ cultures of 80ml expressing *Pf*SUB2_JxTail were used for the isolation of recombinant soluble protein using MagneHis™ magnetic particles. Very low yields were obtained, but the majority of the protein was retained on the beads (Figure 6.9), with a high background of other proteins. Since downstream biopanning experiments did not require the protein to be eluted from the particles, attempts were made to improve the purity. The imidazole concentration in the wash steps was increased from 20mM to 35mM, and the number of washes was increased from the recommended three to five. The highest concentration of imidazole in the wash buffer was 35mM, since it is likely that a higher imidazole concentration would have caused increased loss of the protein of interest.

The protein retention on the particles could be explained by the possibility that the recombinant protein, and not only the His-tag, bound to the metal, which could be overcome by using high concentrations of imidazole in the elution, or by using a slightly acidic buffer

(Promega, 2009). Unfortunately, the elution efficiency was not improved by using 1M imidazole, and an acidic elution buffer was not explored.

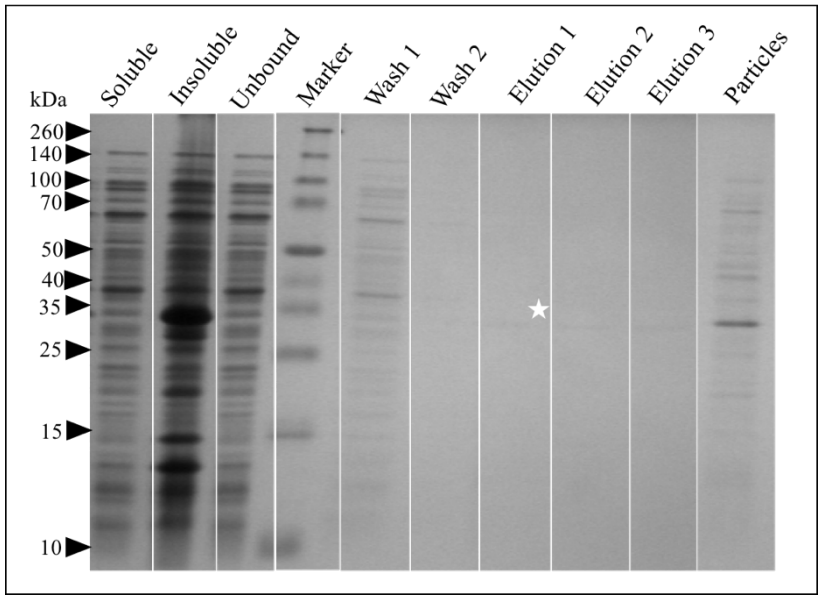


Figure 6.9. Expression and purification of His-tagged *Pf*SUB2_JxTail.
Samples were analysed against a SpectraBR protein ladder using an SDS-polyacrylamide gel, which was stained with Coomassie blue. Samples represent: 5µl of 8ml soluble, insoluble and unbound fractions; 5µl of a SpectraBR protein ladder; 20µl of the 35mM imidazole washes (5 washes were performed: 1ml wash 1, 0.5ml washes 2 to 5; only wash 1 and 2 are shown here); 10µl of each of the 3 elutions (elution 1 was 100µl 500mM imidazole; elution 2 was 50µl 500mM imidazole, and elution 3 was 100µl 1M imidazole); 10µl of 100µl particles after elutions. The purified *Pf*SUB2_JxTail protein (indicated with a star) migrated at ~33kDa compared to its theoretical molecular weight of 39kDa.

6.3.3.3 His-tagged *Pf*AMA-1

Total, soluble and insoluble fractions from 20ml Overnight Express ™ cultures expressing His-tagged *Pf*AMA-1 prodomain (from now on referred to simply as *Pf*AMA-1) were analysed. Large amounts of protein was detected at ~16kDa by SDS-PAGE (Figure 6.10), which is slightly larger than the expected theoretical molecular weight of 11kDa.

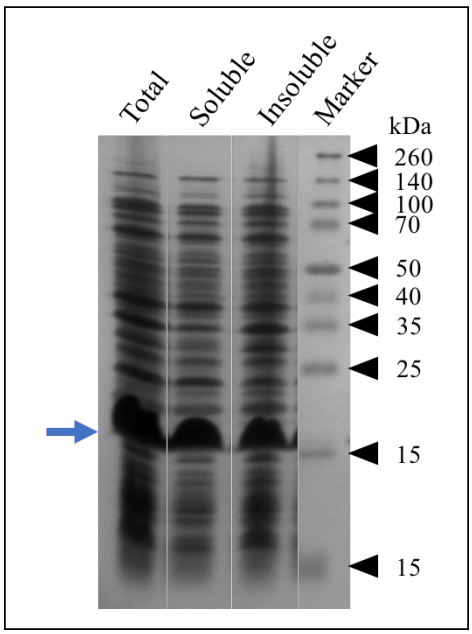


Figure 6.10. Expression of recombinant *Pf*AMA-1 protein.
Samples were analysed against a SpectraBR protein marker using an SDS-polyacrylamide gel, which was stained with Coomassie blue. Samples represent: 5µl of 8ml total, soluble and insoluble fractions. The blue arrow indicates the position of the protein on the gel. *Pf*AMA-1 was detected in all fractions at ~16kDa, which larger than its theoretical molecular mass of 11kDa.

To isolate the soluble *Pf*AMA-1, 40ml Overnight Express ™ cultures were prepared, and the protein was isolated by purification with nickel-coated magnetic beads. Optimisation experiments were performed to obtain the best yield and purity after purification. At a high wash stringency (35mM imidazole), a large amount of the protein was lost in the wash steps and the yield of the isolated protein was markedly reduced. Attempts to improve the retention included reducing the imidazole concentration in the wash buffer to as low as 10mM, and reducing the number of washes from five to two (Figure 6.11). At 10mM however, the washes were not stringent enough, and the purified fraction contained non-specific bands.

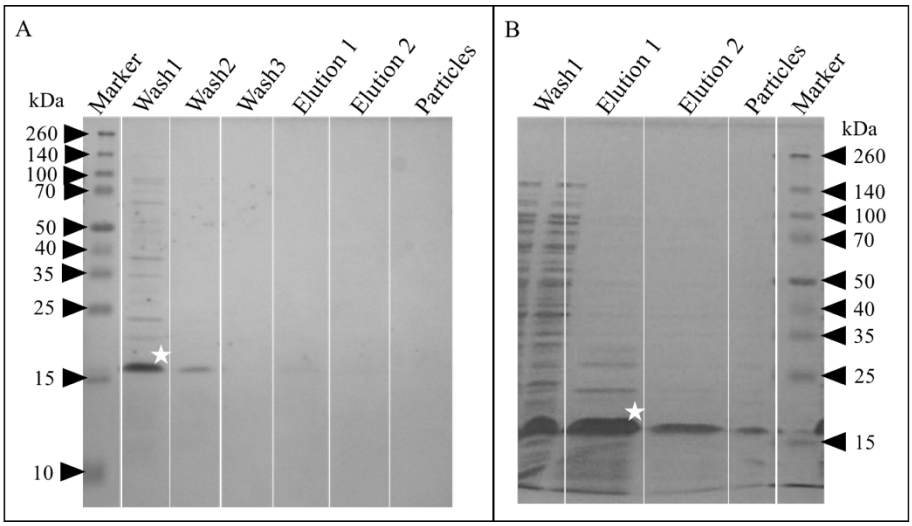


Figure 6.11. Optimisation of *Pf*AMA-1 purification.
Samples were analysed using an SDS-polyacrylamide gel, which was stained with Coomassie blue. *Pf*AMA-1 is indicated with a star. **A –** Five washes using 1ml 35mM imidazole wash buffer were performed. Samples represent: 5µl SpectraBR protein ladder; 20µl of 1ml washes (3 of 5 washes are shown); 20µl of 100µl 500mM imidazole elutions; 20µl of 100 particles after elution. **B –** Two washes using 200µl 10mM wash buffer were performed. Samples represent: 20µl of 200µl washes (1 of 2 washes is shown); 20µl of 50µl 500mM imidazole elutions 1 and 2; 20µl of 50µl particles after elution; 5µl SpectraBR protein ladder.

Three washes at 20mM (Figure 6.12 and Figure 6.13) allowed for the retention of a sufficient amount of protein, while washing away most of the non-specific bands. The band at ~22kDa on the gel, was detected using the anti-His antibody, and since it is twice the theoretical molecular weight, may represent a dimer of the *Pf*AMA-1 protein.

A substantial amount of protein was detected in the unbound fraction (Figure 6.12), which could have been re-applied to nickel-coated magnetic beads to improve the yield. This was not necessary, however, since *Pf*AMA-1 had very good expression, which resulted in an adequate yield.

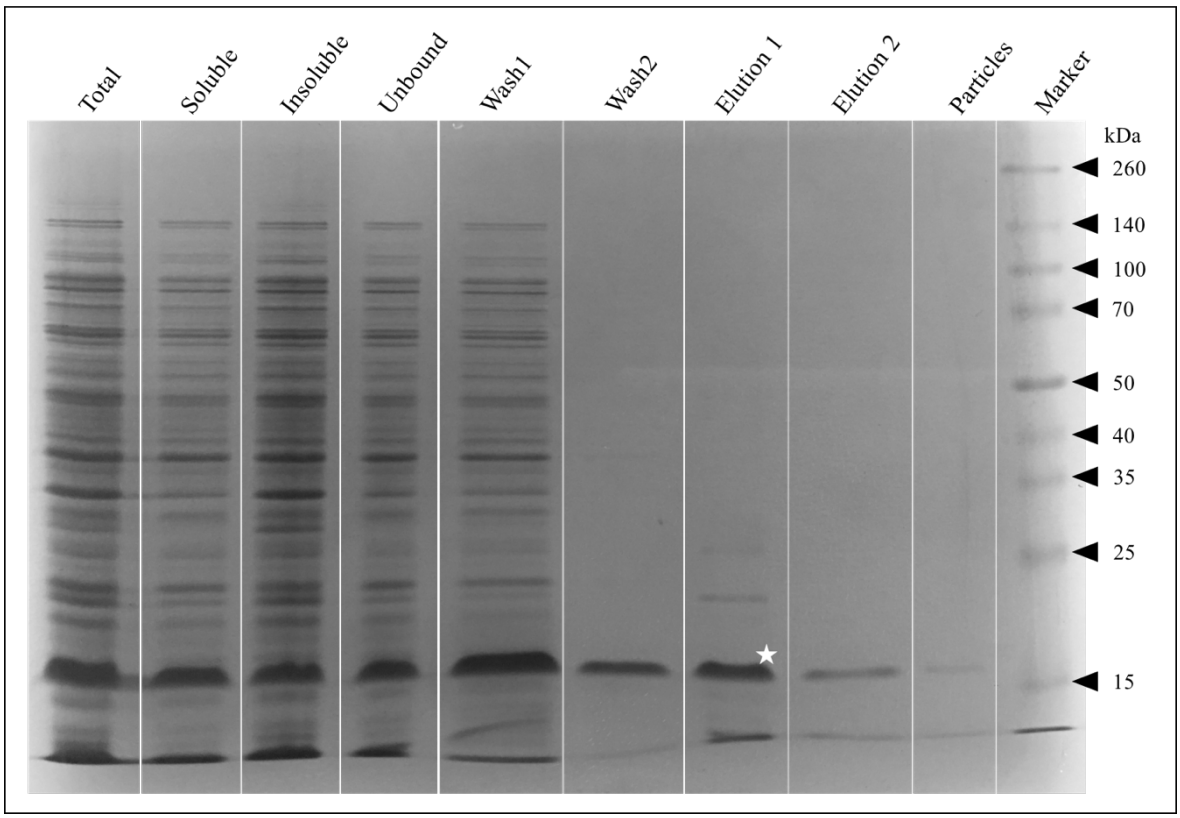


Figure 6.12. Expression and purification of His-tagged *Pf*AMA-1.
Samples were analysed using an SDS-polyacrylamide gel, which was stained with Coomassie blue. Samples represent: 1.5µl of 4ml total, soluble, insoluble and unbound fractions; 20µl of 200µl 20mM imidazole washes (only the first two washes of a total of 3 washes are shown); 5µl of 50µl 500mM imidazole elutions 1 and 2; 5µl of 50µl particles after elutions; 5µl of a SpectraBR protein ladder. The purified *Pf*AMA-1 protein (indicated with a star) migrated at ~16kDa compared to its theoretical molecular weight of 11kDa.

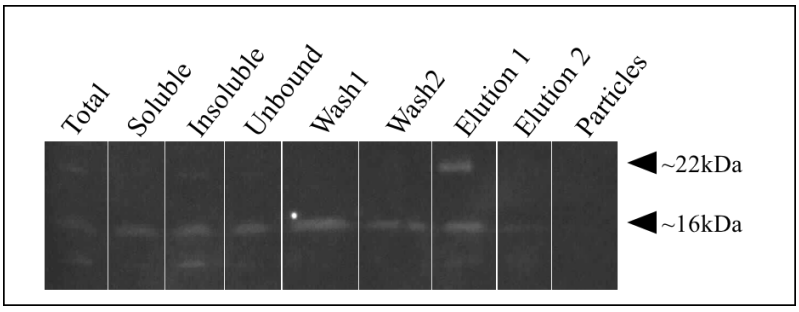


Figure 6.13. Immunoblot detection of purified His-tagged *Pf*AMA-1.
Immunoblot analysis of His-tagged *Pf*AMA-1 using an anti-His antibody, detected a band at ~16kDa in all the fractions. A second fragment was detected at ~22kDa.

6.3.4 Biopanning *Pf*AMA-1 Against Phage Display Libraries

Given the relatively high yield and good purity of His-tagged *Pf*AMA-1 compared to *Pf*EBA181 and *Pf*SUB2, *Pf*AMA-1 was selected for biopanning experiments.

Recombinant *Pf*AMA-1 was isolated and purified from 2 x 125ml Overnight Express™ cultures using MagneHis™ particles. The purified protein was subjected to biopanning against mixed stage *P. falciparum* phage display libraries as outlined in Figure 6.14 (Lauterbach *et al.,* 2003). To enrich for specific interactions, the biopanning was repeated for 4 consecutive rounds.

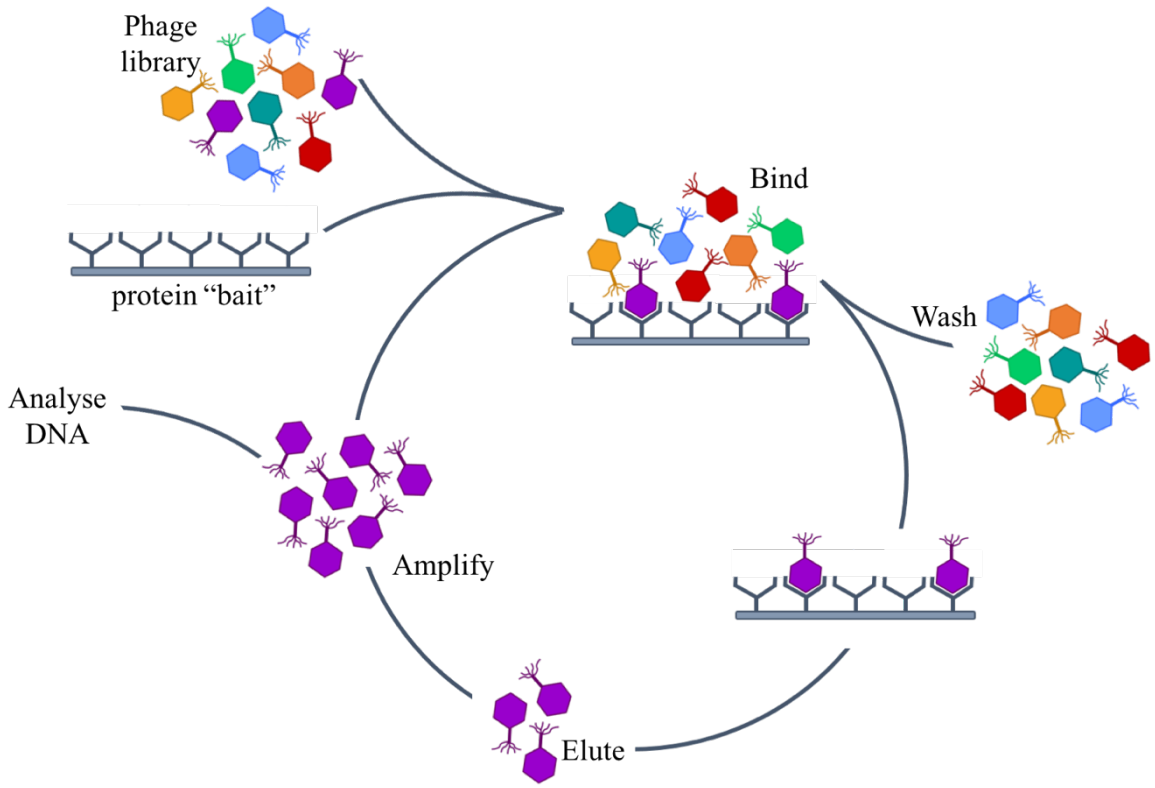


Figure 6.14. A schematic depicting biopanning of *Pf*AMA-1 against a *P. falciparum* phage display library.
The bait protein represents His-tagged *Pf*AMA-1 prodomain, which was immobilised on magnetic nickel-coated beads. The bait protein was exposed to a bacteriophage library, which expressed short fragments of various malaria parasite proteins. Protein interactions occurred, the unbound phage washed off, and the bound phage (purple) were isolated, amplified and re-applied to the immobilised ligand. Extracted phage were used for DNA analysis.

After the fourth round, 45 plaques were selected for PCR amplification and assessment by agarose gel electrophoresis (Figure 6.15).

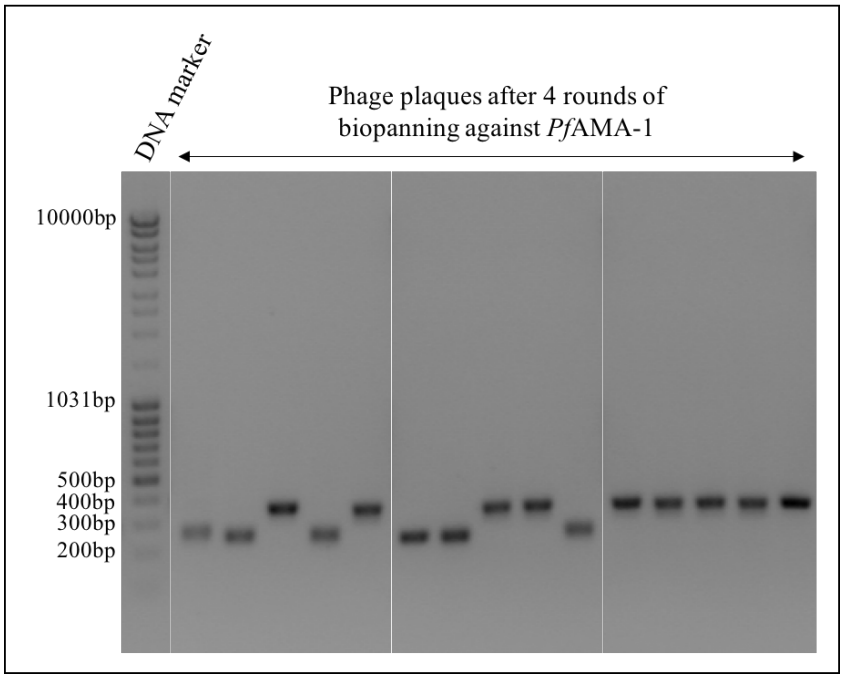


Figure 6.15. PCR amplification of phage after four rounds of biopanning against *Pf*AMA-1. Agarose gel electrophoresis of amplified phage against a base pair standard. Forty-five phage plaques were assessed, 15 are shown here as an example. The majority (29) were detected as products of ~400bp, the remainder (16) varied in size between 250 and 300bp.

PCR amplicons of 250 to ~400bp were detected, which represented relatively short cDNA inserts in the phage. The empty T7 cassette is 216bp, which indicates that the peptides isolated during the biopanning are no larger than ~60aa. The isolation of phage with short inserts was expected for this library (Lauterbach *et al.,* 2003; Vieira, 2015). Many of the PCR amplicons appeared to be the same size, indicating specific phage enrichment. Four of the phage inserts (two at 250-300bp and two of ~400bp) were selected for sequencing by Inqaba Biotec (South Africa).

6.3.5 Analysis of *Pf*AMA-1 Binding Partners

The two smaller phage inserts (that generated PCR amplicons of 250-300bp) did not result in the identification of specific binding partners. One sequence consisted of a string of lysine residues and the other sequence had very short reading frames with multiple stop codons.

The DNA sequences generated for the two larger phage inserts were translated to amino acids and searched against the PlasmoDB database and the results are summarised in Table 6.2. Two novel binding partners were identified for *Pf*AMA-1.

Table 6.2. Binding partners identified for His-*Pf*AMA-1.

Protein Name	Formin 2 (putative)	Chaperone Binding Protein (putative)
Gene ID:	PF3D7_1025000	PF3D7_1334200
Exon/Intron	7 exons; 6 introns	Single exon; no introns
Gene size	2943bp	1575bp
Protein size	980aa	526aa
Binding region (aa positions)	418 to 455	25 to 75
Sequence of binding region	KKKKMKKNKKSYTNIELNHKYK DKDKYKDKYKDKGKDK	KEFDEKVKNMSFDDKVRKILDLK LEGNNDYKNKNYEKAINKYNEG MKYMKK
Predicted function	Protein binding Calcium ion binding	Protein folding Protein binding Chaperone binding
Y2H partners identified	2 partners: SERA5 (PF3D7_0207600) Phistb (PF3D7_0702100)	1 partner: NAPS – nucleosome assembly protein (PF3D7_0919000)

6.3.6 Verification of *Pf*AMA-1 Binding Partners

Due to the possibility that non-specific binding occurred during biopanning (Lanzillotti & Coetzer, 2008; Lauterbach *et al.,* 2003), protein partners were verified. Both the *Pf*AMA-1 binding partners, *Pf*Formin2 and *Pf*CBP (chaperone binding protein), were expressed as GST-tagged recombinant proteins for use in *in vitro* binding assays.

6.3.7 Preparation of the pGEX-4T-2 Constructs

Extended regions correlating to the binding domains identified in Table 6.2 were amplified by PCR using genomic DNA and primers flanking the regions of interest (Figure 6.16).

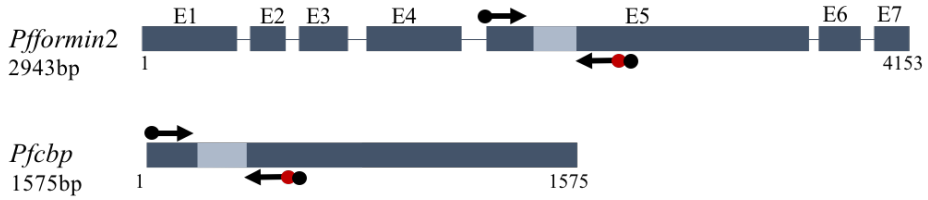


Figure 6.16. The primer binding sites for PCR amplification of the *Pf*AMA-1 binding partners. The gene structures of *Pfformin2* and *Pfcbp* are shown, with the exons labeled (E1 etc.). The binding region is shaded in a lighter colour. Primer binding sites are indicated with arrows, restriction endonuclease sites with solid circles and stop codons are indicated in red.

The amplicons were prepared for cloning by endonuclease digestion with FastDigest® *Xho*I and *Bam*HI. The PCR products for *Pfformin*2 and *Pfcbp* migrated at the expected sizes of 789 and 288bp, respectively (Table 6.3; Figure 6.17 B).

Table 6.3. Expected PCR product and pGEX-4T-2 construct sizes.
The binding regions of the *Pf*AMA-1 binding partners were amplified by PCR. Expected PCR product sizes represent the region size as well as the addition of random bases, restriction enzyme (RE) sites and stop codons included in the primers (listed in Appendix E). Construct sizes represent the size of the pGEX plasmid and PCR amplicon after ligation.

Gene	Region (bp)	PCR product (bp)	Construct size (bp)
Pfformin2	768	789	5719
Pfcbp	267	288	5218

The 4970bp pGEX-4T-2 plasmid was prepared by restriction endonuclease digestion with FastDigest® *Xho*I and *Bam*HI, as well as alkaline phosphatase treatment. The digested plasmid migrated at the expected size of 4945bp (Figure 6.17 A).

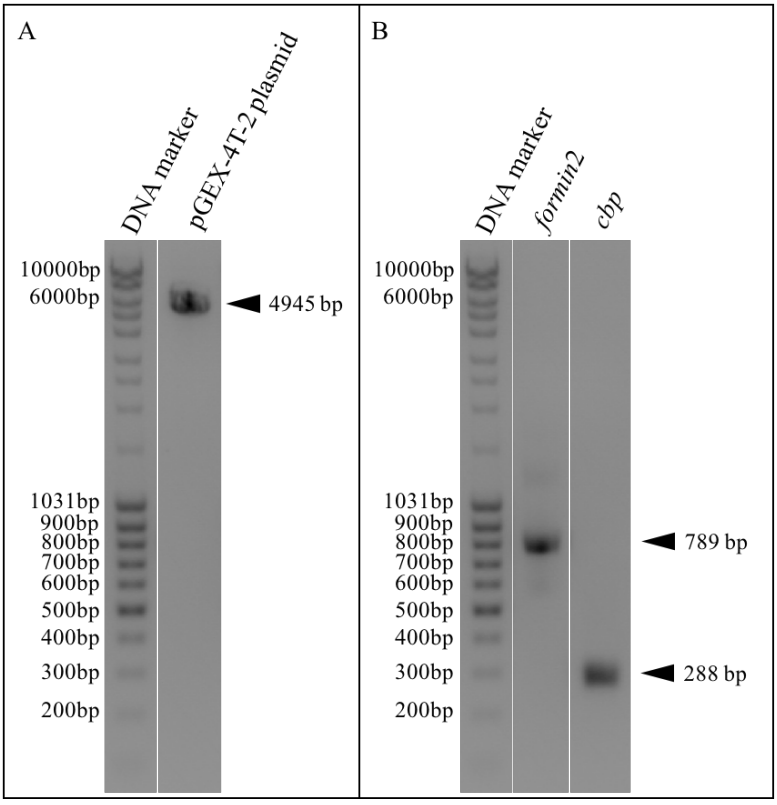


Figure 6.17. Visualisation of pGEX-4T-2 plasmid and PCR amplicons for cloning.
Analysis of isolated plasmid and PCR products of *Pfformin2* and *Pfcbp* by gel electrophoresis against a base pair standard. **A –** pGEX-4T-2 plasmid was linearised by restriction endonuclease digestion using *Bam*HI and *Xho*I and migrated at the correct size of 4945bp. **B –** Both PCR products migrated according to their expected sizes.

6.3.8 Verification of the pGEX-4T-2 Constructs

P. falciparum amplicons and pGEX-4T-2 plasmid were quantified by gel electrophoresis and ligated in a 3:1 ratio. Competent *E. coli* XL10 cells were transformed and transferred to ampicillin-treated agar plates. Colonies were picked, amplified and the plasmid isolated for verification.

Restriction endonuclease digestion of the pET-15b control plasmid and the six constructs using various FastDigest® enzymes (Figure 6.18), confirmed that amplicons of the correct sizes had been inserted into the plasmid (Figure 6.19). Positive clones were sequenced by Inqaba Biotec™, which confirmed that inserts were error-free and in-frame.

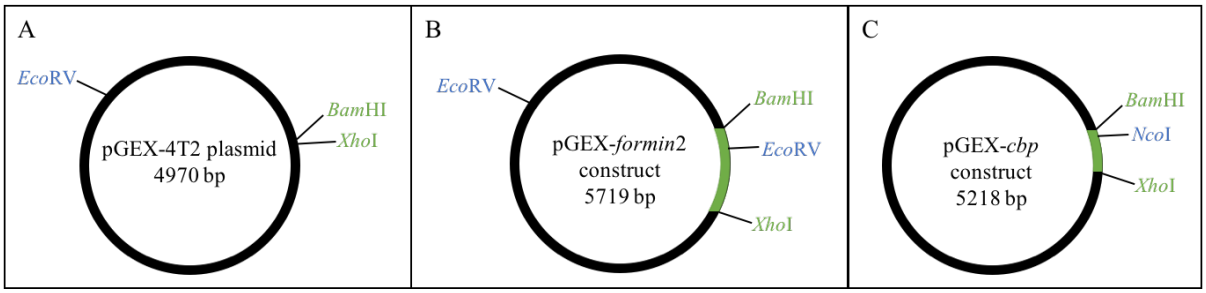


Figure 6.18. Restriction enzyme sites of pGEX-4T-2 plasmid and constructs.
A – Empty pGEX-4T-2 plasmid. **B and C –** pGEX-4T-2 constructs created by directional insertion of *Pfformin2* and *Pfcbp* amplicons shown in green. Verification of clones was performed by restriction endonuclease digestion using FastDigest® enzymes *Bam*HI and *Xho*I; *Eco*RV; or *Nco*I.

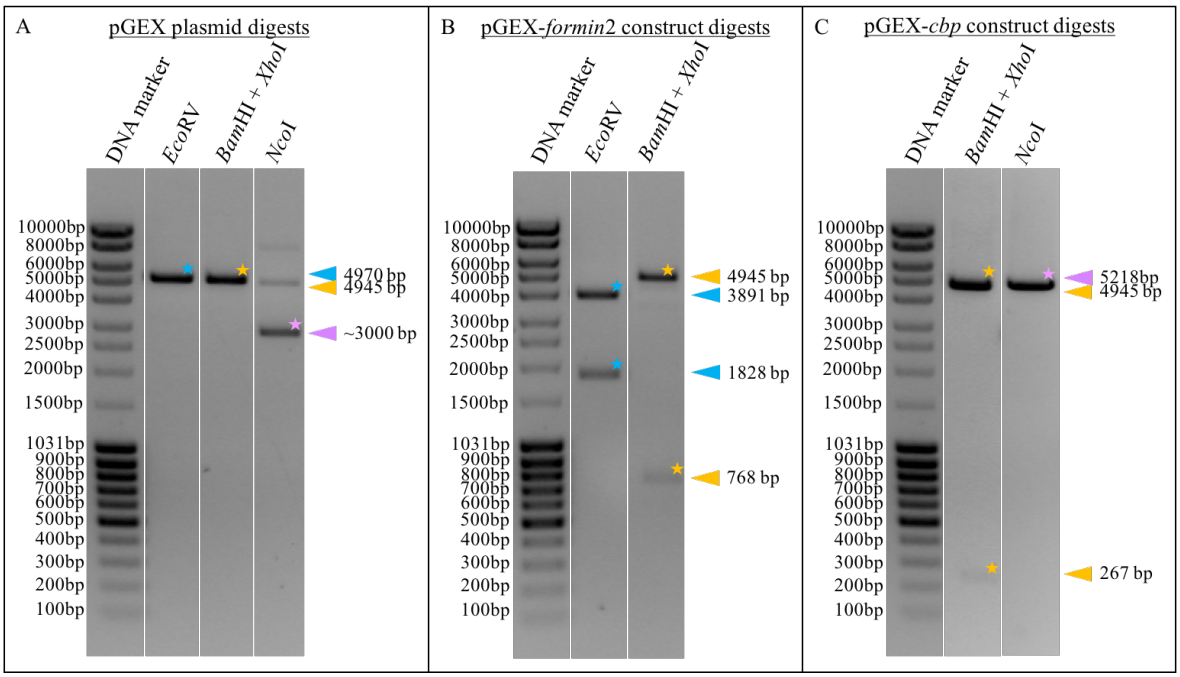


Figure 6.19. Verification of the pGEX-4T-2 constructs.
Size validation of the pGEX-4T-2 constructs after restriction endonuclease digestion by gel electrophoresis against a base pair standard. **A –** Digestion of the empty plasmid resulted in fragments that were distinct from the positive constructs: *Eco*RV = 4970; *Bam*HI+*Xho*I = 4945bp; *Nco*I = no site; plasmid remains intact and migrates at ~3000bp. **B –** pGEX-*formin*2 constructs were verified by: *Bam*HI+*Xho*I = 4945 and 768bp; *Eco*RV = 3891 and 1828bp. **C –** pGEX-*cbp* constructs were verified by: *Bam*HI+*Xho*I = 4945 and 267bp; *Nco*I = 5218bp.

6.3.9 Recombinant Expression of the GST-tagged Proteins

The two GST-tagged binding partners, *Pf*Formin2 and *Pf*CBP, were analysed by SDS-polyacrylamide gel electrophoresis and immunoblot detection. Soluble recombinant protein was isolated and purified using a MagneGST™ purification system, which utilises glutathione-coated beads.

6.3.9.1 GST-tagged *Pf*Formin2

Very low concentrations of soluble recombinant GST-tagged *Pf*Formin2 were isolated using the MagneGST™ purification system. The volume of Overnight Express™ cultures was increased from 1x20ml culture to 5x20ml cultures to attempt to recover larger amounts of protein, but this did not produce a 5-fold increase in the amount of purified protein obtained (Figure 6.20 shows the purified protein from 100ml of culture). Further attempts to increase the yield included performing a two-step binding incubation, which required a 1-hour incubation of the magnetic particles and the soluble fraction of GST-tagged *Pf*Formin2, followed by 2 washes with 140mM NaCl buffer, and then another 1-hour incubation. This

binding strategy would limit the amount of non-specific binding and increase the yield of recombinant protein.

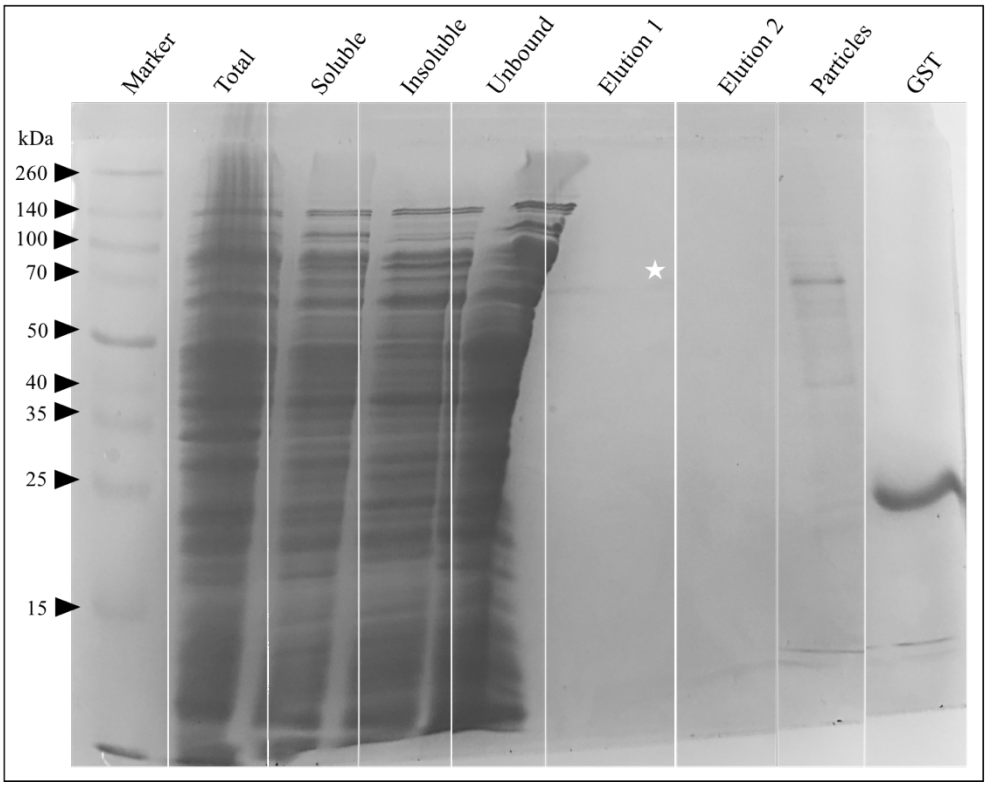


Figure 6.20. Expression and purification of GST-tagged *Pf*Formin2.
Samples were analysed using an SDS-polyacrylamide gel, which was stained with Coomassie blue. Samples represent: 5µl of a SpectraBR protein ladder; 6µl of 10ml total, soluble and insoluble fractions; 20µl of 1.5ml unbound fraction; 30µl of 100µl 500mM glutathione elutions 1 and 2; 30µl of 100µl particles after elutions; 10µl purified GST as a control. Five washes were performed using 500mM NaCl wash buffer, but are not shown here. The purified *Pf*Formin2 protein (indicated with a star) migrated at ~60kDa, slightly larger than its theoretical molecular weight of 57.3kDa.

Most of the protein was retained on the particles after two elutions with 500mM glutathione, and despite the use of a higher NaCl concentration in the wash buffer (500mM as opposed to 140mM) as recommended by the troubleshooting manual (Promega, 2014), some contaminating bands were also visible on the particles. The presence of high salt concentrations in the elution fractions often resulted in the protein bands spreading out horizontally (e.g. Figure 6.20; Hycult Biotec, 2010).

Recombinant GST-tagged *Pf*Formin2 migrated at ~60kDa, as determined by SDS-PAGE, which is slightly larger than its theoretical molecular weight of 57.3kDa, but could not be verified by immunoblot analysis due to the low amount of protein present.

6.3.9.2 GST-tagged *Pf*CBP

Recombinant GST-tagged *Pf*CBP expressed as a soluble protein of ~32kDa, compared to its theoretical molecular weight of 37.7kDa, as verified by SDS-PAGE (Figure 6.21) and immunoblot detection using anti-GST antibodies (Figure 6.22).

Due to contaminating bands in the eluate, optimisation of GST-*Pf*CBP expression was performed. When a lower NaCl (140mM) wash buffer was used, a slightly higher yield of *Pf*CBP protein was recovered, but the eluate contained many contaminating proteins. Washes with the higher NaCl (500mM) buffer improved the purity of the protein, but resulted in a slight reduction in yield. Despite performing the washes using the high NaCl concentration, a faint second band was detected at ~25kDa in the elution fraction, which may represent a truncated version of the protein, but it was not detected in the immunoblot (Figure 6.22).

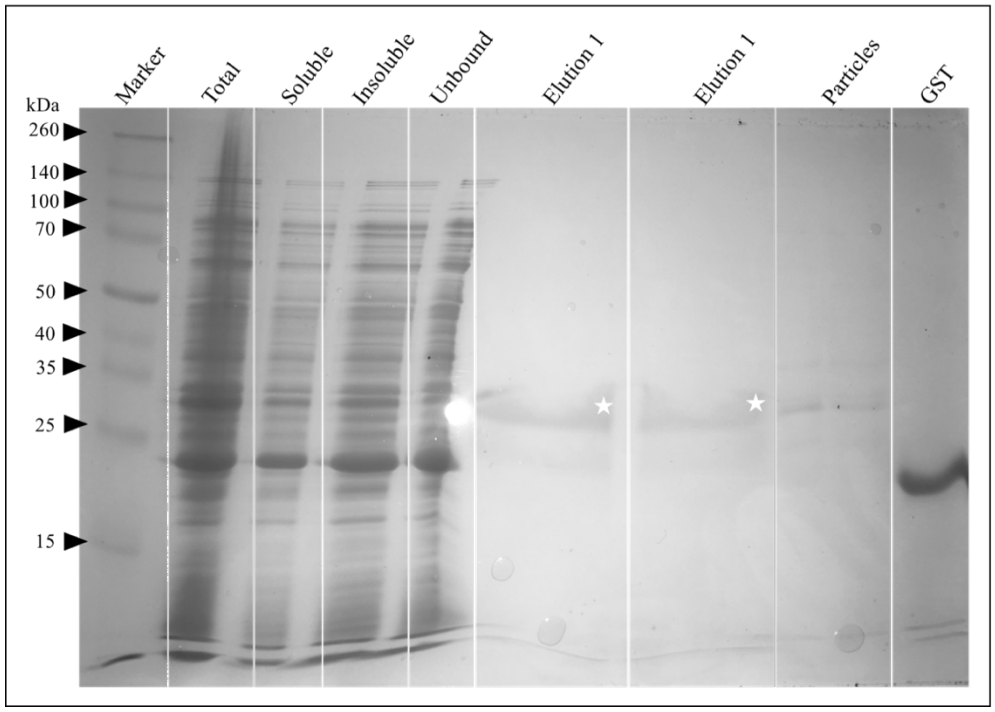


Figure 6.21. Expression and purification of GST-tagged *Pf*CBP.
Samples were analysed using an SDS-polyacrylamide gel, which was stained with Coomassie blue. Samples represent: 5µl of a SpectraBR protein ladder; 6µl of 1.5ml total, soluble and insoluble fractions; 20µl of 1.5ml unbound fraction; 30µl of 100µl 500mM glutathione elution 1 (loaded twice); 30µl of 100µl particles after elutions; 10µl purified GST as a control. Five washes were performed using 500mM NaCl wash buffer, but are not shown here. The purified *Pf*CBP protein (indicated with stars) migrated at ~32kDa, slightly lower than its theoretical molecular weight of 37.7kDa. A second, faint, band was visible at ~25kDa.

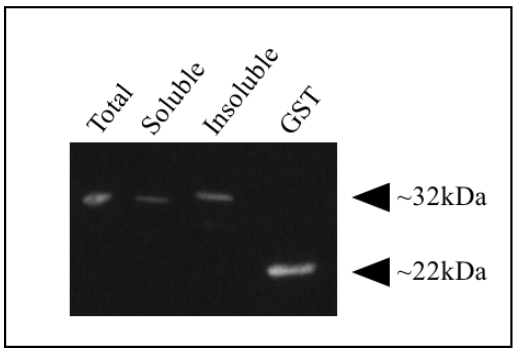


Figure 6.22. Immunoblot detection of GST-tagged *Pf*CBP.
Immunoblot analysis using an anti-GST antibody detected the GST-tagged *Pf*CBP protein in total, soluble and insoluble fractions, at ~32kDa, which is slightly lower than the expected size of 37.7kDa. The purified GST control was also detected at a slightly lower molecular weight of ~22kDa instead of ~26kDa.

6.3.9.3 *In Vitro* Binding Assays

To verify the interactions identified by biopanning against *P. falciparum* phage display libraries using *Pf*AMA-1, *in vitro* binding assays were performed. Due to the low yield of purified *Pf*Formin2, binding assays were limited to *Pf*CBP.

Overnight Express™ cultures of 40ml for the GST control, 200ml for GST-*Pf*CBP and 80ml for His-*Pf*AMA-1 were used to isolate purified recombinant protein using MagneGST™ or MagneHis™ particles. The eluates were dialysed using Mini-dialysis units and the recovered samples were quantitated by SDS-Polyacrylamide gel electrophoresis (Figure 6.23).

The first attempt to isolate purified GST-*Pf*CBP for the binding assay used 200µl of 500mM glutathione elution buffer, which resulted in a protein sample that was not detectable by SDS-PAGE. In a subsequent attempt, only half of the elution buffer was used, which still resulted in a very low yield and produced a mere 14ng/µl (Table 6.4), with 10 and 20-fold higher concentrations obtained for GST and His-*Pf*AMA-1.

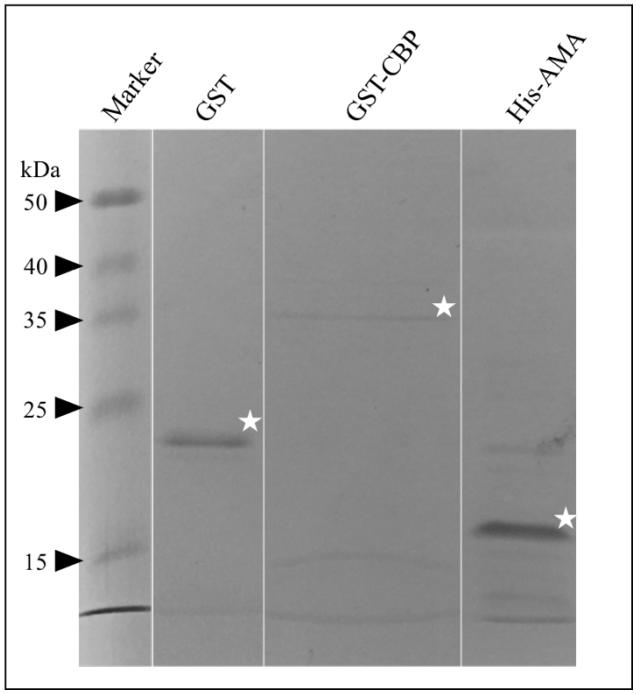


Figure 6.23. SDS-PAGE quantitation of proteins for *in vitro* binding assays.
Purified and dialysed samples were analysed using an SDS-polyacrylamide gel, which was stained with Coomassie blue. Samples represent: 5µl SpectraBR protein ladder; 5µl of 200µl GST control; 10µl of 100µl GST-*Pf*CBP; 5µl of 200µl His-*Pf*AMA-1. Stars identify each protein.

Table 6.4. Quantities of GST- and His-tagged proteins for *in vitro* binding assays.
Quantitation of samples after purification and dialysis was performed by densitometry relative to BSA protein standards of known concentrations using SynGene® software.

Protein	Concentration (ng/µl)	Total volume (µl)	Total yield (µg)
GST control	157	200	31.4
GST-*Pf*CBP	14	100	1.4
His-*Pf*AMA-1	321	200	64.2

Binding assays are performed by attaching a constant concentration of His-*Pf*AMA-1 (0.5µg) to magnetic particles, and incubating with increasing concentrations of GST-*Pf*CBP. After washing away low affinity or non-specific partners, the quantities of each protein that remained is determined by SDS-PAGE analysis and densitometry. To perform a satisfactory binding assay that will provide evidence of an interaction, at least three different concentrations (e.g. 0.1µg, 0.5µg and 1.0µg) should be used for GST-*Pf*CBP. Several control reactions include adding heat-denatured GST-*Pf*CBP to native His-*Pf*AMA-1, as well as loading the two proteins individually on the gel. As such, a minimum of ~3.5µg of the protein in solution, i.e. GST-*Pf*CBP, is required.

Unfortunately, despite the substantial increase in the volume of Overnight Express™ cultures and a decreased volume of the elution buffer, the *Pf*CBP yield and concentration remained low. At 14ng/µl and only 90µl of sample remaining (10µl was used for quantitation), only ~1.2µg protein was available. A binding assay was attempted using 2 concentrations of 400ng and 800ng of GST-*Pf*CBP, incubated with 500ng of immobilised His-*Pf*AMA-1, but the results of this experiment were inconclusive and further extensive optimisation will be required.

6.4 Discussion

The use of escorters in rhoptry targeting has been described for Apicomplexan parasites *T. gondii* and *P. falciparum* (Sloves *et al.,* 2012; Robinson & Bonifacino, 2001; Topolska *et al.,* 2004; Baldi *et al.,* 2000). Several studies have alluded to escorter-based trafficking to the micronemes (Treeck *et al.,* 2006; Di Cristina *et al.,* 2000; Sakura *et al.,* 2013), but to the best knowledge of the author, no actual microneme targeting escorter has been identified for *P. falciparum.* In this study, potential escorters interacting with *Pf*AMA-1 were identified using phage display technology.

6.4.1 Utility of Phage Display Libraries

The use of phage display libraries for the identification of interacting proteins in *P. falciparum* is an invaluable tool that has led to the discovery of many novel protein complexes, and may provide insight that can be exploited in the search for drug targets.

To investigate the possibility of an escorter for *Pf*AMA-1, the prodomain (identified as the trafficking domain in Chapter 3), was expressed as a recombinant His-tagged protein and used in biopanning experiments against a *P. falciparum* phage display library. Two novel binding partners were identified: a putative Formin2 (*Pf*Formin2), which is encoded by PF3D7_1025000; and a putative Chaperone Binding Protein (*Pf*CBP), which is encoded by PF3D7_133400.

Despite the useful nature of this system, there are intricacies that may pose problems (reviewed by Lanzillotti & Coetzer, 2008). One of the complexities of the mixed asexual stage *P. falciparum* library, is that the cDNA fragments inserted into the phage coat gene are not representative of the entire transcriptome of the parasite. Certain mRNA sequences may

be under-represented, while others may be disproportionally present, due to the continuous variation in the transcriptome over the 48-hour asexual developmental stage. The implication is that two partners may have a high affinity for one another in the *in vitro* biopanning experiment, but never co-exist *in vivo*.

The isolation of phage presenting unusual cDNA inserts is a common complication (Lanzillotti & Coetzer, 2008). The *P. falciparum* genome consists of ~80% AT nucleotides (Gardner *et al.,* 2002), and, coupled with the absence of translational control during packaging of the sequences, not all inserts will be in frame, which will lead to the phage expressing unnatural or very short. In this study, two such examples were identified: one phage contained a sequence of only lysine residues (encoded by AAA), and another presented a sequence with a number of stop codons in all reading frames.

Since biopanning experiments may identify false-positive partners, several control steps were included to minimise non-specific binding: (1) pre-screening using MagneHis™ particles was performed to remove any phage that had an affinity to the Nickel, (2) high stringency washes were used to disrupt low affinity interactions, which would minimise false-positive results, (3) four rounds of biopanning were performed to select for high affinity interactions. Well-isolated plaques from different plates were screened by PCR and several amplicons were the same size, which indicated enrichment of specific partners.

To verify the biopanning interactions, a second independent method of in solution binding was attempted. The binding partners were expressed as recombinant GST-tagged proteins, which were exposed to His-tagged *Pf*AMA-1 and the interaction was evaluated by SDS-PAGE analysis. Unfortunately, due to particularly poor expression of soluble recombinant protein for both binding partners, verification of the interaction was not possible.

6.4.2 Challenges in Recombinant Expression of *P. falciparum* Proteins

6.4.2.1 Expression of Eukaryotic Proteins in Prokaryotic Hosts

Protein expression is a complex process that is tightly regulated (reviewed by Berg *et al.,* 2002). Briefly, transcription of DNA into RNA occurs, followed by the processing of nascent pre-mRNA into mRNA, and finally translation of the proteins. Most proteins undergo

extensive processing prior to achieving the final product. In eukaryotes, transcription and translation are separate events, but in prokaryotes, the two processes occur simultaneously.

Expression of eukaryotic *P. falciparum* proteins in a prokaryotic *E. coli* host, is challenging, but it is a commonly used tool. The advantages are the rapid growth of the bacteria and the ease of transforming *E. coli* with various expression vectors. Unfortunately, there are several disadvantages associated with the expression system, which resulted in poor and/or insoluble expression of the recombinant proteins created for this study (summarised in Table 6.5). An alternative expression system utilises insect cells, which, coupled with codon optimisation, may assist in improved expression of these malaria proteins *in vitro* (Birkholtz *et al.,* 2008).

Several solubility prediction algorithms are available online (e.g. www.biotech.ou.edu; Diaz *et al.,* 2009), which will consider the amino acid composition, molecular weight and iso-electric point (pI) of the protein, when predicting what percentage of the expressed protein will be soluble. Unfortunately, these algorithms can give false predictions as illustrated in this study. *Pf*AMA-1 was predicted to have 0% chance of solubility when overexpressed in *E. coli*, *Pf*Formin2 had a 35% chance and *Pf*CBP was given a 100% chance of solubility (Diaz *et al.,* 2009), which contradicted the actual yield of soluble proteins.

Table 6.5. Summary of Recombinant Proteins.
The expected molecular weight (MW) and pI for each tagged recombinant protein was calculated using expasy.org. Domains or features that may contribute to low or insoluble expression are listed.

Protein Name	Tag	Expected MW	Observed MW	pI	Domains/ Features
*Pf*AMA-1	6xHis	11kDa	~16kDa	5.45	none
*Pf*Formin	GST	57.3kDa	~60kDa	5.19	Low complexity regions
*Pf*CBP	GST	37.7kDa	~32kDa	8.49	Low complexity regions

6.4.2.2 Insoluble Proteins and Low Expression Levels

The formation of inclusion bodies as a result of overexpression of proteins in *E. coli* is relatively common (Birkholtz *et al.,* 2008), which leads to expression of insoluble recombinant protein. Large recombinant proteins (>40kDa) are more likely to mis-fold and aggregate into inclusion bodies than smaller proteins (Mehlin *et al.,* 2006), which may explain the very low yield of soluble protein for *Pf*Formin, compared to *Pf*AMA-1 or *Pf*CBP.

Most of the fusion tags that are used in these expression systems are highly soluble, such as GST, and to a lesser extent, 6xHis. Despite the soluble nature of the GST tag, *Pf*Formin2 and *Pf*CBP were mainly insoluble.

The pI of a protein may provide insight into the solubility: a pI below 6 or above 8 has been described to reduce protein expression (Mehlin *et al.,* 2006). The pI of *Pf*Formin2 is 5.19 and *Pf*CBP is 8.49 (calculated using expasy.org), which may also explain the low yield of soluble protein. The pI of *Pf*AMA-1 was also low (5.45), but the protein was small, and it contained a hydrophilic domain with no low complexity regions (Figure 6.24), which would contribute to the overall good soluble yield.

Several other features of the recombinant proteins may also affect the yield and likelihood of soluble expression. *Pf*EBA181, for example, has disulphide bonds, which makes it difficult to express and may require oxidative refolding so that correctly-folded proteins can be obtained (de Marco, 2009). The expression of peptides with low complexity regions can also contribute to low expression, as was noted for *Pf*Formin2 & *Pf*CBP (Figure 6.24).

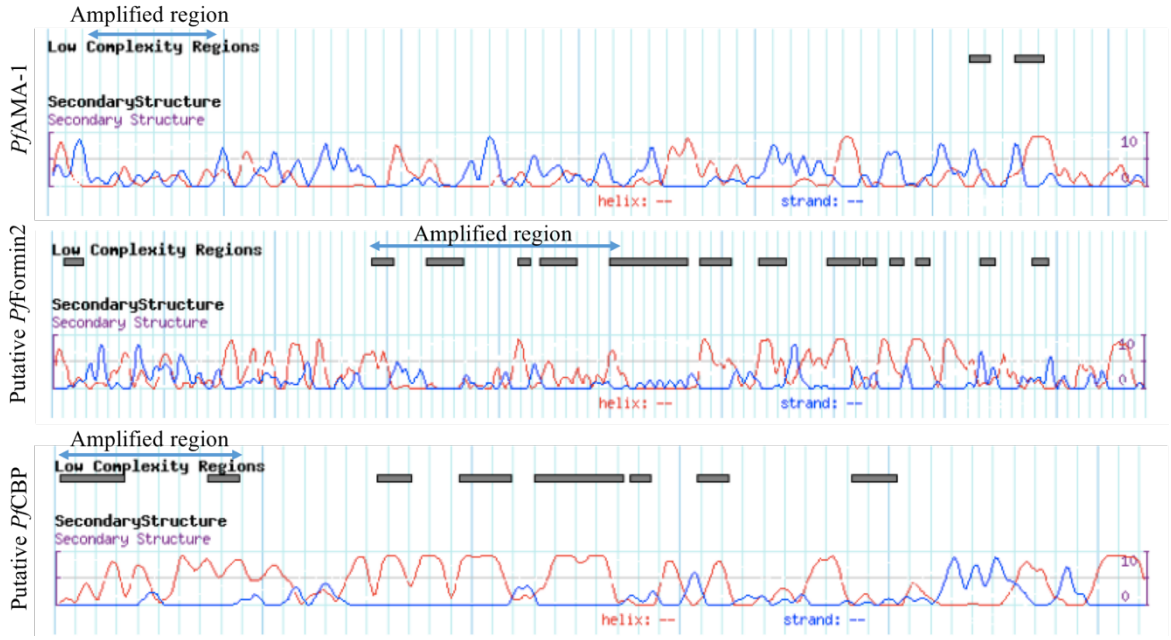


Figure 6.24. Secondary structure predictions of *Pf*AMA-1, putative *Pf*Formin2 and putative *Pf*CBP.
The occurrence of helices and strands are indicated with red or blue peaks, respectively. Low complexity regions are indicated with grey bars above stretches that lack helices. The regions amplified for expression as tagged proteins are identified using blue arrows. (Adapted from PlasmoDB; Aurrecoechea *et al.,* 2008).

Several procedures exist to enhance the expression of soluble protein (reviewed in Sorensen & Mortensen, 2005). Expression at lower temperatures allow the expression machinery in the host *E. coli* more time to properly fold the newly synthesised protein, which may improve the yield of soluble protein, and as such, the Overnight Express™ cultures were incubated at 20ºC. Certain strains of *E. coli* have also been created to facilitate the expression of foreign DNA, such as Rosetta2(DE3) cells that provide rare codons for the translation of *P. falciparum* sequences, and were thus used for these studies.

For future experiments, several other options for improving the expression and solubility of *Pf*Formin and *Pf*CBP are available (Birkholtz *et al.,* 2008; Mehlin *et al.,* 2006): (1) other tags, for example maltose binding protein (MBP), may be used, (2) the constructs can be codon optimised for *E. coli,* or, (3) expression in eukaryotic insect cells may also prove beneficial.

6.4.2.3 Abnormal Migration of Recombinant Proteins on Polyacrylamide Gels

Slight differences were noted in terms of the calculated molecular weights of the recombinant proteins, versus the molecular weights determined by SDS-polyacrylamide gel electrophoresis (Table 6.5). Migration of proteins at unexpected sizes is not uncommon for *P. falciparum* proteins. Proteins are denatured in the presence of sodium dodecyl sulphate (SDS), which will bind to the proteins and facilitate their migration according to molecular weight. Several factors can influence this binding, which can result in a shift in migration. The presence of numerous lysine residues in *Pf*Formin2 (and to some extent *Pf*CBP), is likely to cause more SDS to bind to the protein and hence it will migrate faster and appear to have a lower molecular weight (Tompa, 2002; Table 6.5). Low complexity regions (e.g. *Pf*Formin2 and *Pf*CBP) or hydrophobic regions (e.g. *Pf*SUB2 or *Pf*EBA181) may result in less SDS binding, which will cause the protein to migrate slower and thus appear to have a larger molecular weight (Mehlin *et al.,* 2006).

6.4.3 *P. falciparum* Formin2 is Unlikely to be a Microneme Protein Escorter

P. falciparum Formin 2 identified in this study, is described as a putative protein encoded by the PF3D7_1025000 multi-exon gene on chromosome 10 (PlasmoDB; Aurrecoechea *et al*., 2008). Peak mRNA expression occurs during the schizont and ookinete stages (Figure

6.25), with protein detected in all the life stages (Lopez-Barragan *et al.,* 2011), which may suggest that the protein is multifunctional.

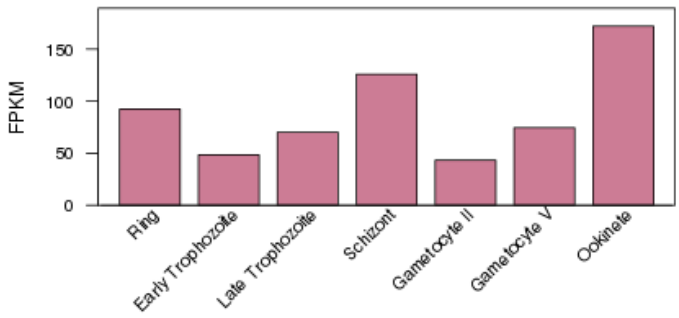


Figure 6.25. mRNA expression levels of *Pf*Formin2.
RNA was extracted from synchronised 3D7 *P. falciparum* parasites at several time points post-infection (indicated on the x-axis) and subjected to sequencing. Fragments per kilo-base of exon model per million mapped reads (FPKM) on the y-axis indicates the transcript levels at each of the selected time points. *Pfformin*2 expression levels peak during the intra-erythrocytic schizont stage and ookinete stage in the mosquito host. (Adapted from Aurrecoechea *et al*., 2008; PlasmoDB)

There are two formins – *Pf*Formin1 and *Pf*Formin2 – that have been identified in *P. falciparum* (Ignatev *et al.,* 2012): *Pf*Formin1 is encoded by the PF3D7_0530900 gene found on chromosome 5; and *Pf*Formin2 is encoded by the PF3D7_1219000 gene found on chromosome 12.

The host erythrocyte invasion mechanism requires actin filament nucleation and polymerisation. Formins are characterised by the presence of two domains: the filamentous-actin-binding formin homology (FH) 2 domain, and the proline-rich FH1 domain (Ignatev *et al.,* 2012). These proteins are both involved in the regulation of actin polymerisation during invasion (Baum *et al.,* 2008), as well as microtubule dynamics (Kovar, 2006; Paul & Pollard, 2009). *Pf*Formin2 localises to the moving junction during invasion (Baum *et al.,* 2008) and has been detected in the barbed ends of filaments during nucleation (Baum *et al.,* 2008; Ignatev *et al.,* 2012).

It is unclear why the protein encoded by PF3D7_1025000 is labeled as a putative Formin2 on PlasmoDB (Aurrecoechea *et al*., 2008**)**. Functional predictions include calcium ion binding and protein binding, with no direct mention of actin binding or actin polymerisation as is the case for *Pf*Formin1 and 2. The putative Formin2 is also not predicted to have any FH domains, but rather has EH domains (Eps15 domain, a protein-protein interaction motif),

EF-hand domains (helix-loop-helix structures associated with calcium-binding proteins), and cytoskeletal regulatory domains.

There is no localisation prediction available for the putative *Pf*Formin2 (PF3D7_1025000; identified in this study), but based on similarity to *Pf*Formin2 (PF3D7_1219000) and the predicted involvement in calcium-binding, it may be expressed at the moving junction to interact with the cytoskeleton. It is thus likely that it may interact with *Pf*AMA-1 during invasion, but its involvement as an escorter protein in the trafficking pathway of *P. falciparum* seems unlikely.

6.4.4 Could *Pf*CBP be an Invasion Protein Escorter?

As with the putative *Pf*Formin2, very little information is available for the second binding partner, *Pf*CBP. This putative protein is encoded by the single exon PF3D7_1334200 gene which is located on chromosome 13. Peak mRNA expression occurs during the early intra-erythrocytic ring and trophozoite stages (Figure 6.26; Lopez-Barragan *et al.,* 2011), with protein detected in ring, trophozoite, schizont and mature gametocyte stages (PlasmoDB, Aurrecoechea *et al*., 2008).

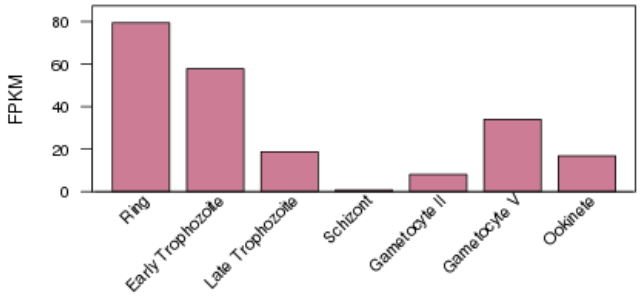


Figure 6.26. mRNA expression levels of *Pf*CBP.
RNA was extracted from synchronised 3D7 *P. falciparum* parasites at several time points post-infection (indicated on the x-axis) and subjected to sequencing. Fragments per kilo-base of exon model per million mapped reads (FPKM) on the y-axis indicates the transcript levels at each of the selected time points. *Pfcbp* expression levels peak during the early intra-erythrocytic stages. (Adapted from Aurrecoechea *et al*., 2008; PlasmoDB)

Localisation predictions include the nucleus and the cytoplasm, and functional predictions for *Pf*CBP include protein folding and chaperone binding (Aurrecoechea *et al*., 2008; PlasmoDB), which seems promising as an escorter protein. The *Pf*CBP protein is predicted to have TPR (tetratrico peptide repeat) domains, which are known to mediate protein-protein interactions and to assemble multi-protein complexes. The identification of the nucleosome

assembly protein (PF3D7_0919000) as a partner of PfCBP by Y2H experiments, further supports the hypothesis that PfCBP may be involved in the formation of protein complexes.

The expression profile of *Pf*CBP does not correlate with that of *Pf*AMA-1 (and other invasion proteins), where peak expression occurs in the schizont stage (Figure 6.27; Lopez-Barragan *et al.,* 2011). There is, however, overlap in expression during the late trophozoite stages, which may still allow *Pf*CBP to serve as an escorter for late-stage invasion proteins, especially since trafficking to the apical organelles occurs soon after synthesis.

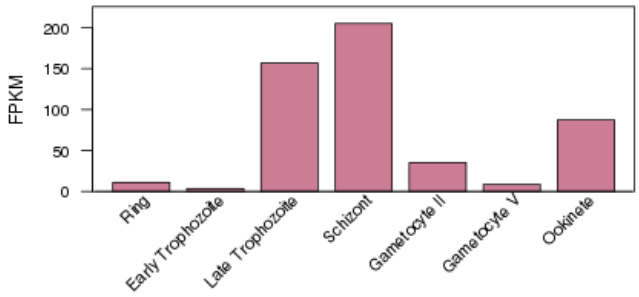


Figure 6.27. mRNA expression levels of *Pf*AMA-1.
RNA was extracted from synchronised 3D7 *P. falciparum* parasites at several time points post-infection (indicated on the x-axis) and subjected to sequencing. Fragments per kilo-base of exon model per million mapped reads (FPKM) on the y-axis indicates the transcript levels at each of the selected time points. *Pfama-1* expression levels peak during the late intra-erythrocytic stages. (Adapted from Aurrecoechea *et al*., 2008; PlasmoDB)

Molecular chaperones in *P. falciparum* are often heat shock proteins (HSPs) that are involved in folding of newly synthesised proteins, protein trafficking, signal transduction and development (reviewed by Acharya *et al.,* 2007). In addition to protein folding and chaperone binding, another predicted function of *Pf*CBP is that it is an activator of HSP90 ATPase (Aurrecoechea *et al*., 2008; PlasmoDB).

HSP90 and HSP70 are the most studied of these heat shock molecular chaperones, and are responsible for facilitating proper folding of other proteins (Gitau *et al.,* 2012). Five co-chaperones have been described for *Pf*HSP90, which regulate its functions (Chua *et al.,* 2014).

HSP40 is a co-chaperone for the interaction of HSP70 with so-called "client" proteins by performing a number of functions (Pavithra *et al.,* 2007): (1) HSP40 activates ATPase

activity of HSP70, (2) HSP40 binds to, and delivers specific client proteins to HSP70, and (3) HSP40 serves by recruiting HSP70 to specific sub-cellular locations.

The functional predictions of *Pf*CBP, coupled with the possession of TPR domains, which have been described for other HSP proteins (Odunuga *et al.,* 2003), seem to suggest that *Pf*CBP may be a HSP-like protein, or function as a co-chaperone for HSP proteins. The involvement of *Pf*CBP as a molecular chaperone for invasion proteins in the trafficking pathway remains unknown.

Chapter 7: Discussion

Protein trafficking to the apical organelles is an important, yet inadequately understood, aspect of the *P. falciparum* parasite biology. Microneme targeting, in particular, remains poorly characterised and at the commencement of this study, no microneme targeting signals had been identified for *Pf*AMA-1, *Pf*SUB2 and *Pf*EBA181. Through the evaluation of parasites expressing fluorescently-tagged chimaeric proteins, the molecular microneme targeting determinants of these proteins were identified. The findings from this study are novel, and contribute to an improved understanding of protein trafficking to the micronemes, which may provide an alternative route for therapeutic interventions.

*Pf*AMA-1 is a key component of the erythrocyte invasion machinery, and thus a promising vaccine candidate for malaria. In a novel discovery, the N-terminal prodomain was identified as essential for localisation to the micronemes. *Pf*SUB2 is a surface antigen sheddase, which is crucial for the proteolytic shedding required by parasite surface antigens in order to invade the host erythrocyte. Findings from this study, which were confirmed by an independent study by Child *et al.,* (2013), showed that the transmembrane domain is required for trafficking to the micronemes. *Pf*EBA181 is a member of the large family of erythrocyte binding ligands. This family of proteins all contain a conserved C-terminal cysteine-rich domain, which, in addition to an upstream region, is responsible for microneme localisation.

Interestingly, these three invasion proteins, which are stored in the micronemes prior to invasion, all require different protein domains to get there. These findings led to the hypothesis that a promiscuous microneme targeting escorter may be required for microneme localisation. This was explored by exposing the prodomain of *Pf*AMA-1 to a library of bacteriophage displaying short *P. falciparum* peptides. In these experiments, two novel binding partners were identified. One is a putative chaperone binding protein, *Pf*CBP, which is predicted to be involved in protein binding and chaperone binding, and thus may play a role in a microneme trafficking pathway.

7.1 Stage-Specific Expression of Invasion Proteins

Invasion proteins adhere to a ‘just-in-time’ mechanism of expression to avoid detection by the host immune system, and as such these proteins are mostly expressed during the late

schizont stage of intra-erythrocytic development (Kats *et al.,* 2008). For this reason, a stage-specific promoter system is preferable for episomal expression systems (Treeck *et al.,* 2006) and all mini-genes designed for this study were inserted into a modified pARL-mCherry plasmid, which contained a *Pfama-1* promoter instead of the original *Pfcrt* promoter. The *Pfama-1* promoter ensured that the chimaeric proteins were expressed in the schizont stage only, as opposed to the *Pfcrt* promoter that ensures ubiquitous expression. The schizont stage is eight hours long, and no distinction was made between early and late schizonts in this study.

The similarity in the expression profiles of *Pf*AMA-1, *Pf*SUB2 and *Pf*EBA181 (Figure 7.1), prompted the choice of a single promoter, rather than three different gene-specific promoters. The use of a *Pfama-1* promoter for the expression of other late-stage invasion proteins, such as *Pf*EBA175, is described in the literature (Treeck *et al.,* 2006) and was thus the promoter of choice in this study.

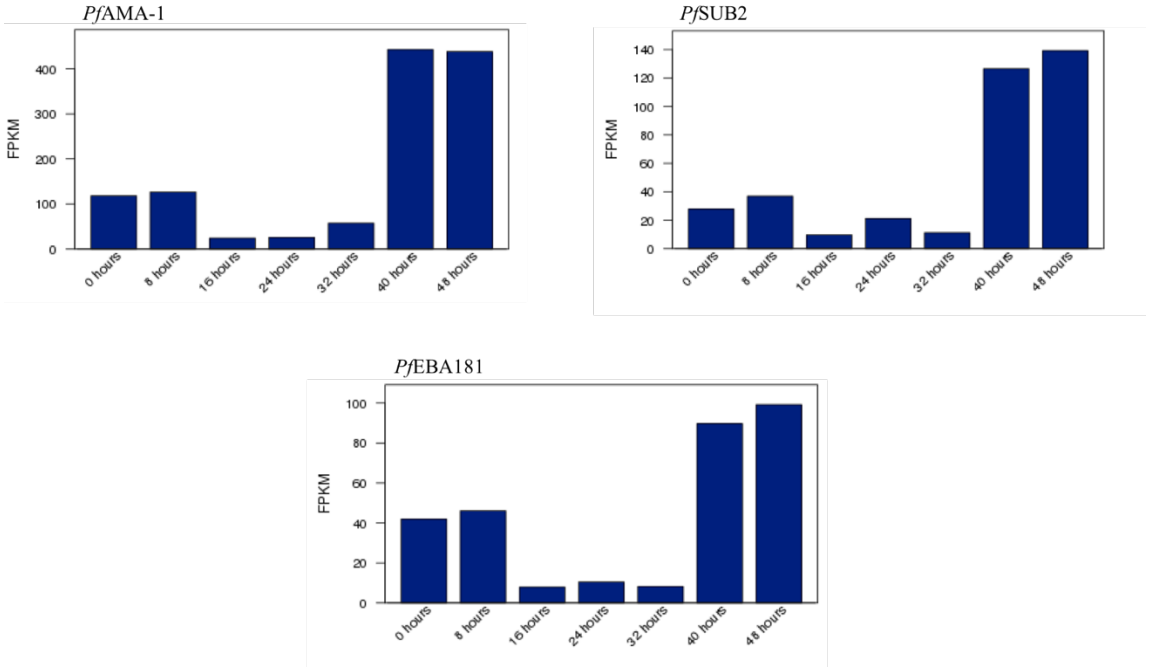


Figure 7.1. Comparison of the transcription levels of *P. falciparum* invasion proteins.
RNA was extracted from synchronised 3D7 *P. falciparum* parasites at several time points post-infection (indicated on the x-axis) and subjected to sequencing. Fragments per kilo-base of exon model per million mapped reads (FPKM) on the y-axis indicates the transcript levels at each of the selected time points for four proteins: *Pf*AMA-1, *Pf*SUB2 and *Pf*EBA181. All have similar expression profiles, with maximal expression during the schizont stages. (Adapted from Aurrecoechea *et al*., 2008; PlasmoDB; Otto *et al.,* 2010).

A recent study on *Pf*SUB2 localisation compared episomal expression using the *Pfama-1* promoter, as well as a protein specific promoter, i.e. *Pfsub2* (Child *et al.,* 2013). The findings showed that in some instances only partial co-localisation was observed when using the *Pfama-1* promoter (Pearson's coefficient of 0.63), and that the *Pfsub2* promoter yielded better co-localisation (Pearson's coefficient 0.93). The authors thus suggest that the use of a protein-specific promoter is ideal for the purpose of co-localisation studies. This may explain why in some of the co-localisation experiments in this study, distinct green and red puncta were still visible, despite similar patterns of localisation.

7.2 Limitations of the pARL-mCherry Expression System

The episomal expression of fluorescently-tagged chimaeric proteins has been a useful tool for the detection of proteins within a live parasite culture. The system allows for the localisation of chimaeric proteins, where parts of the protein have been deleted or substituted, relative to markers of subcellular organelles of the parasite (Treeck *et al.,* 2006; Przyborski *et al*., 2005).

Unfortunately, the mCherry tag associated with the pARL-mCherry plasmid gives a very weak signal, as is evident by the 800+ milliseconds light exposure required to capture the images. Furthermore, rapid photo-bleaching was experienced: once the samples were exposed to the light, signals faded rapidly and were no longer visible. Similar findings have been reported in the literature (Richard *et al.,* 2009).

Not every parasite viewed yielded visible red fluorescence, and in some of the transgenic lines, relatively few red fluorescent parasites were seen. Western blots were attempted to verify expression of the fusion proteins, but were unsuccessful due to the weak expression. This lack of mCherry expression could be due to a number of reasons: (1) expression was limited to late schizonts only, (2) mCherry yields a weak signal, which may have bleached before the photo was captured, or (3) the least likely reason could be that the parasites had lost the plasmid, since WR99210 was added to the transgenic cultures to keep them under constant selective pressure. An option would have been to subject the cultures to "on-off" selection cycles, which would ensure that the parasites didn't develop resistance to the compound. This did not seem necessary since the cultures were only maintained long enough

for DNA isolation and microscopy experiments, before being frozen in liquid nitrogen. Cultures were thawed again for any further experiments.

The pARL2-GFP plasmid was also available, which encodes a green fluorescent tag and requires only approximately 400 milliseconds of exposure to capture a photo. The pARL2-GFP plasmid also contains a *Pfcrt* promoter, which was replaced with the late stage *Pfama-1* promoter. Attempts were made to clone the *Pf*AMA-1 mini-genes into the pARL2-GFP plasmid, but unfortunately no positive clones were obtained.

Despite the challenges with the system, red fluorescence was visible in all the transgenic lines created for this study. Clear changes in the localisation patterns were obtained when certain domains were deleted, which was supported by Pearson's coefficients in the *Pf*AMA-1 and *Pf*EBA181 experiments, and thus provided sufficient evidence to conclude that certain deletion had resulted in mis-targeting of the protein.

7.3 Visualisation of Apically-Located Chimaeric Proteins

When the merozoites ready themselves for erythrocyte rupture, the apical ends of the individual daughter parasites point outward, and the posterior nucleus-containing ends will face the centrally located haemozoin (Figure 7.2 A). This careful positioning will give the new merozoites a greater chance of encountering and quickly invading a new host erythrocyte.

What does this look like under the microscope? The blue nucleus will be located near the centre of the cell. The red puncta depicting the mCherry-tagged protein, which has been correctly targeted to the micronemes, will be closer to the erythrocyte membrane, but will be distinct from the blue nucleus (Figure 7.2 B).

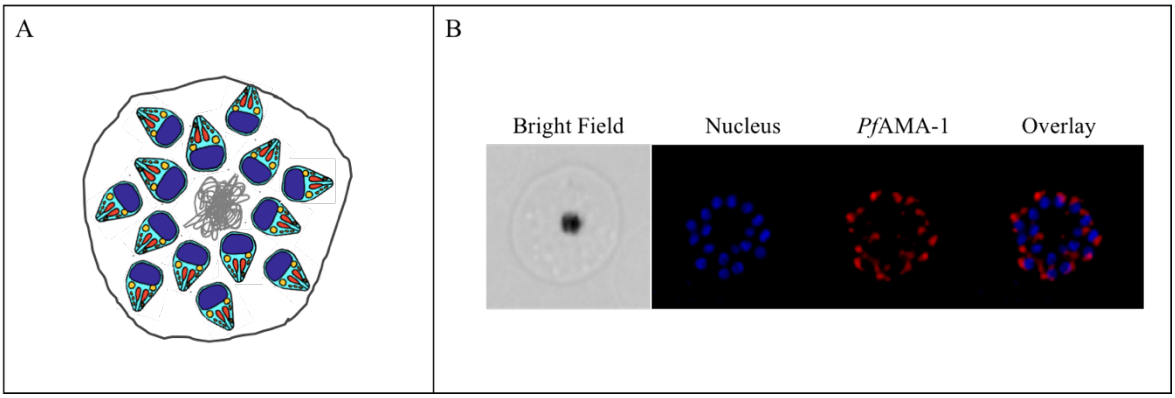


Figure 7.2. Visual representation of apical localisation.
A – A diagrammatic representation of a mature schizont, with the haemozoin located at the centre and the newly formed daughter merozoites positioned with the apical ends pointing towards the host cell membrane. **B –** Fluorescence images of a schizont stage parasite expressing mCherry-tagged *Pf*AMA-1, which localises to the apically located micronemes (red) and the nuclei stained with DAPI (blue).

7.4 Visualisation of Microneme Localisation

Given the close proximity of the micronemes and the rhoptries within the apex of the merozoite, it would have been preferable to have performed co-localisation with a rhoptry marker in addition to the microneme marker (*Pf*EBA175), which was used for these studies. Unfortunately, a rhoptry marker was not available.

Full length *Pf*AMA-1, which served as a control for these studies, showed a punctate pattern characteristic of the apical localisation of merozoites. The microneme marker, *Pf*EBA175, showed the same apically distinct pattern, and overlays of the images suggested that the proteins were co-localised in the same subcellular compartment. Similarly, certain *Pf*AMA-1, *Pf*SUB2 and *Pf*EBA181 chimaeric proteins also co-localised with the microneme marker. Although the merged images resulted in yellow fluorescence, indicative of co-localisation, there were still some areas that had distinct green or red signals and Pearson's coefficients ranged between 0.66 and 0.8. There are numerous possible reasons for this finding: (1) the microscope required manual changing of the colour cubes, which could result in movement of the stage, (2) the amount of the mCherry protein relative to the amount of *Pf*EBA175 present, varied, thus not producing a perfect yellow signal (also discussed in Healer *et al.,* 2002), (3) the *Pfama-1* promoter was not optimal for *Pf*SUB2 and *Pf*EBA181 localisation studies.

Despite the distinct green and red puncta that were sometimes visible in the overlay images, it is likely that localisation was still limited to the micronemes, since all three of the proteins used in these experiments are known microneme proteins (Healer *et al.,* 2002; Harris *et al.,* 2005b; Treeck *et al.,* 2006; Sakura *et al.,* 2013). In the studies presented in this thesis, the localisation patterns were either: (1) punctate and confined to the apex, similar to that of the *Pf*EBA175 microneme marker, or, (2) the red fluorescence changed from apically distinct puncta, to clearly dispersed throughout the parasite, representing a prominent change in localisation. The altered pattern, coupled with noticeable decreases in the Pearson's coefficients, was sufficient indication that the protein no longer localised to the micronemes, and that the domain required for microneme targeting had been deleted.

7.5 What Does Disrupted Trafficking Look Like?

The fluorescence patterns observed in the studies for this thesis is consistent with most other studies that employed similar techniques, for example: *Pf*EBA175 (Treeck *et al.,* 2006; Gilberger *et al.,* 2003b), *Pf*AMA-1 (Treeck *et al.,* 2009) and *Pf*SUB2 (Child *et al.,* 2013), all reported a change of localisation from distinct puncta in the apical region, to fluorescence that was dispersed.

In some instances, however, disrupted targeting has been presented in other ways. In *P. yoelii*, for example, a single amino acid substitution in *Py*EBL resulted in a change of localisation from the micronemes to the dense granules (Otsuki *et al.,* 2009). In this instance, determining the altered location of the protein required the use of an electron microscope, or a large panel of organelle markers coupled with a high-resolution fluorescence or confocal microscope. In *T. gondii,* a substitution of a tyrosine residue in the *Tg*MIC2 signal sequence SYHYY resulted in disrupted targeting. Instead of localising to the micronemes, the protein was erroneously targeted to the parasitophorous vacuole "outside the parasite body" (Di Cristina *et al.,* 2000).

In a different study, a deletion of the rhoptry targeting domain of *Pf*RAP1 altered the localisation from the rhoptries to the parasitophorous vacuole (Richard *et al.,* 2009). In both these instances, the pattern changed from apically distinct puncta to circular fluorescence that appeared to surround the schizont (Figure 7.3).

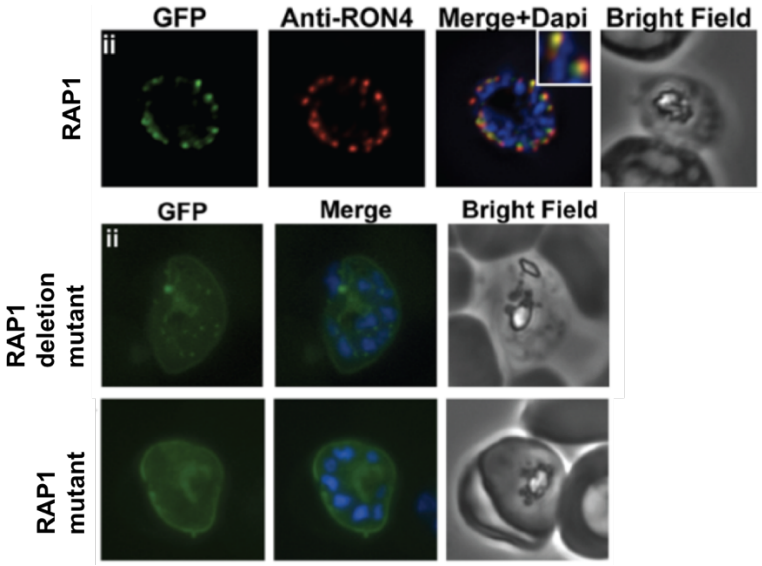


Figure 7.3. Deletion of the trafficking domain results in a localisation change from the rhoptries to the parasitophorous vacuole (adapted from Richard *et al.*, 2009).
Top panel: *Pf*RAP1 localises to the rhoptry neck as determined by co-localisation studies using *Pf*RON4 antibodies. **Middle panel:** The deletion of a 30aa segment determined to be the rhoptry targeting signal for *Pf*RAP1, resulted in a change in localisation of the GFP-tagged protein, to the parasitophorous vacuole. **Bottom panel:** Similarly, changing certain amino acids also resulted in erroneous localisation to the parasitophorous vacuole. (adapted from Richard *et al.,* 2009).

The exact localisation of the mis-targeted proteins in the experiments presented in this thesis was not evaluated. Further studies with a range of markers for different subcellular locations will have to be performed to determine the localisation of these mis-targeted mCherry chimaeras.

7.6 How Are the Micronemes Targeted?

Protein trafficking to the apical organelles remains poorly understood (Deponte *et al.,* 2012) and no specific signal motif or trafficking mechanism has been identified for targeting the micronemes. Since humans don't have micronemes, these trafficking mechanisms are unique to *P. falciparum* (and other Apicomplexan parasites) and can be explored as novel treatment strategies. By identifying the domain responsible for microneme targeting, we are one step closer to identifying the exact trafficking mechanisms of transport to the micronemes.

In the work presented for this thesis, various parasite lines were created to episomally express chimaeras of three *P. falciparum* invasion proteins (Figure 7.4), in order to assess the molecular determinants for trafficking. A microneme marker, *Pf*EBA175, was used to

determine the localisation of each mutant protein and in so doing, determine which domain was required for microneme targeting.

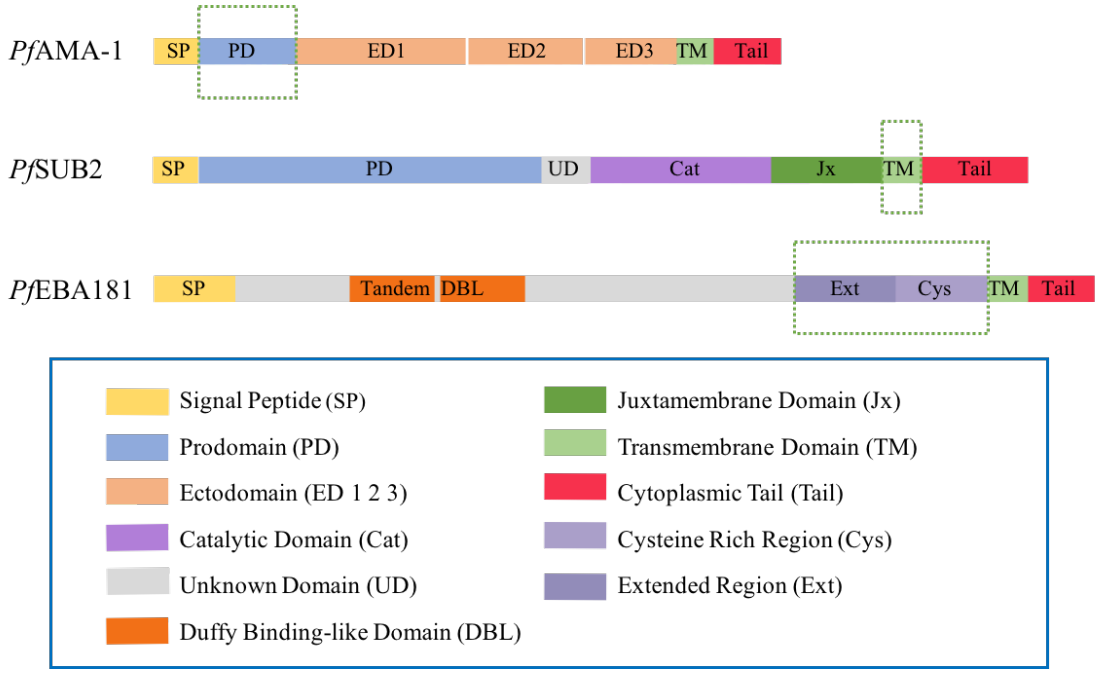


Figure 7.4. Domains of three *P. falciparum* invasion proteins: *Pf*AMA-1, *Pf*SUB2 and *Pf*EBA181.
The domains that make up each of the three proteins are shown, with the microneme targeting domains boxed in green.

The findings in this thesis indicate that all three proteins require different domains to target the micronemes: *Pf*AMA-1 requires the N-terminal prodomain, *Pf*SUB2 requires the transmembrane domain, and *Pf*EBA181, like *Pf*EBA175, requires the conserved C-terminal cysteine-rich domain, as well as an upstream region (Figure 7.4).

These data suggest that there is no common microneme targeting signal, but that an escorter for transporting microneme proteins may be involved.

7.7 Are Escorters Involved in Targeting Apical Organelles?

Escorters in rhoptry targeting have been described in Apicomplexan organisms *T. gondii* and *P. falciparum*. An example is the targeting of *Pf*RAP2 to the rhoptries through an interaction with *Pf*RAP1 (Baldi *et al.,* 2000), which in turn is bound to RAMA (Richard *et al.,* 2009), a GPI-anchored protein that is stored in the rhoptries (Figure 7.5; Topolska *et al.,* 2004).

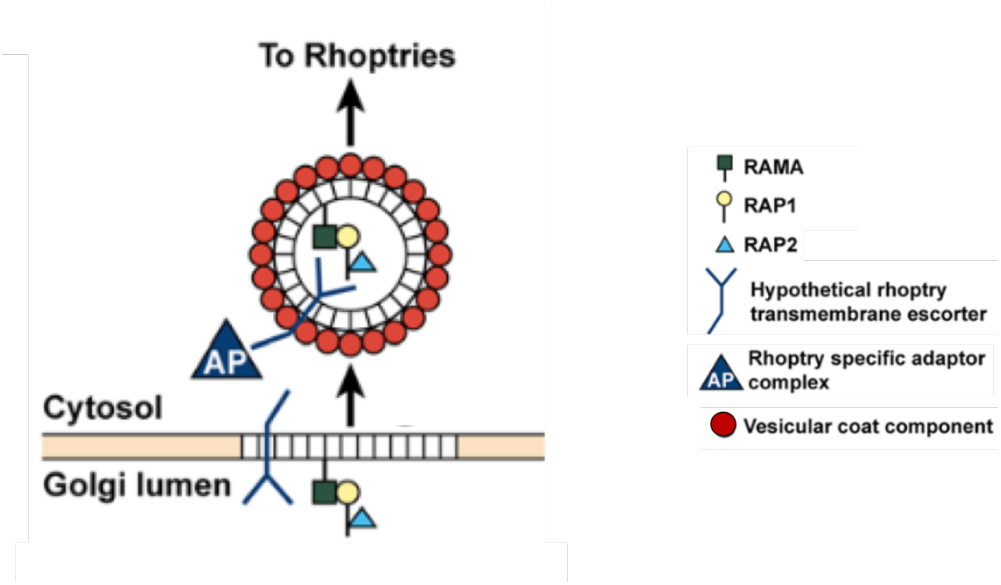


Figure 7.5. A hypothetical rhoptry targeting model.
Proteins destined for the rhoptries are co-translationally inserted into the ER and are trafficked to the Golgi. Within the Golgi, specific escorters that are exposed on the cytoplasmic face of the Golgi recruit adaptor and vesicle coat proteins. The vesicles bud off and are directed to the rhoptries by specific interactions with the vesicular trafficking machinery. The example depicted in this model is that of *Pf*RAP2 targeting to the rhoptry by formation of a protein complex with *Pf*RAP1 and *Pf*RAMA. (Adapted from Richard *et al.,* 2009).

Another escorter protein, *Tg*SORTLR, has been identified recently and is implicated in the transport of transmembrane proteins, *Tg*ROP (rhoptry protein) and *Tg*MIC (microneme protein) to the apical organelles (Sloves *et al.,* 2012). The *Tg*SORTLR cytoplasmic tail interacts with other proteins involved in trafficking, such as adaptor complexes and clathrin to facilitate vesicle sorting. A putative SORTLR homologue has been identified in *P. falciparum* (PF3D7_1451800; Krai *et al.,* 2014). Expression of *Pf*SORTLR in the Golgi in late trophozoite and schizont stages suggests a role in targeting proteins to the apical organelles (Krai *et al.,* 2014).

Biopanning experiments against a *P. falciparum* phage display library, presented in this thesis, identified two novel binding partners. The most likely candidate for involvement in the microneme trafficking pathway is a putative *P. falciparum* Chaperone Binding Protein (PF3D7_1334200). Functional predictions suggest that it may be involved in protein folding, protein binding and chaperone binding activities (PlasmoDB, Aurrecoechea *et al*., 2008).

7.8 A Hypothetical Microneme Targeting Model

To date there is no proven and accepted model for microneme targeting. It has been assumed that it might look similar to a rhoptry targeting model, but most proteins destined for the rhoptries are directed via the Golgi. However, none of the proteins studied in this thesis have been shown to localise to the Golgi. Trafficking from the Golgi to the apical organelles involves packaging the cargo protein into a vesicle, which is guided to the target destination by specific adaptors and a rhoptry escorter.

Based on the information obtained in these studies, together with knowledge from the literature (e.g. Richard *et al.,* 2009), a microneme trafficking model is proposed. In this model, invasion proteins are directed by an N-terminal signal peptide to the ER after synthesis, where they will undergo post-translational modification by cleavage of the signal peptide. This modification is likely to alter protein folding in a way that exposes new binding areas (e.g. the prodomain of *Pf*AMA-1) for the recognition by escorter protein complexes (e.g. *Pf*SORTLR). As with rhoptry targeting, the formation of a vesicle is triggered and vesicle budding will ensue. The protein-escorter complex, coupled with a microneme specific chaperone protein (e.g. *Pf*CBP) will be directed to the micronemes.

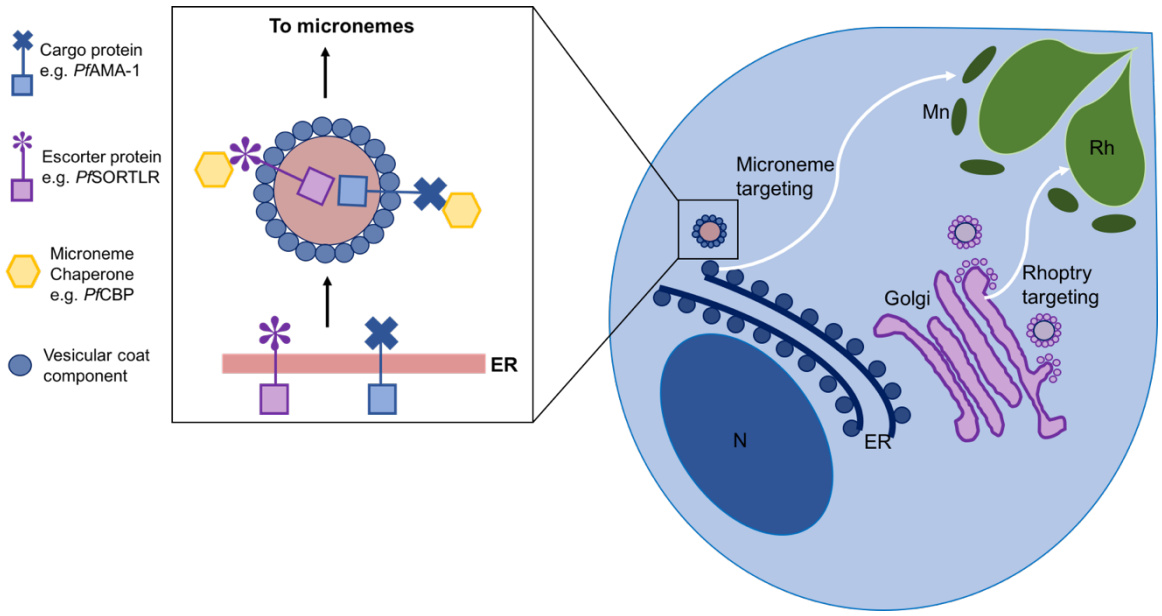


Figure 7.6. Hypothetical intracellular trafficking pathway to the micronemes.
The microneme trafficking pathway is proposed to occur directly between the ER and the micronemes, as opposed to the Golgi to rhoptry pathway. A hypothetical transmembrane escorter will recognise and form a protein complex with a cargo protein on the surface of the ER. Vesicle budding occurs and a chaperone protein will facilitate transport of the complex to the micronemes.

7.9 Future Work

These studies have provided a foundation for further investigation of how invasion proteins are transported to the micronemes. *In vitro* binding assays with *Pf*CBP can be performed with all three invasion proteins, to confirm the *Pf*AMA-1 interaction, and to determine if the same protein is perhaps involved in the transport of *Pf*SUB2 and *Pf*EBA181.

To further elucidate the involvement of escorter proteins in the microneme targeting pathways, it will be interesting to perform either binding assays, or phage display biopanning experiments with other potential escorters, such as *Pf*SORTLR or *Pf*AP1.

Gene knock-outs, by double homologous cross-over or by using the CRISPR-Cas9 technology, can be performed to determine if *Pfcbp* is essential for parasite survival, and thus perhaps a good drug target. Performing binding assays with an invasion protein (e.g. *Pf*AMA-1) and *Pf*CBP, in combination with a drug which can prevent the binding, may provide more evidence about the suitability of *Pf*CBP as a drug target.

Appendix A – mCherry cloning

mCherry Mini-Genes: PCR Conditions

Enzyme used: PhusionFlash or Q5 (www.neb.com)

Initial denaturation: 98°C for 10 seconds

Denaturation: 98°C for 1 second

Primer annealing: T_{a1} for 5 seconds

Elongation: 72°C for 15-30 seconds (depending on size of amplicon)

Repeat for 5 cycles

Denaturation: 98°C for 1 second

Primer annealing: T_{a2} for 5 seconds

Elongation: 72°C for 30-60 seconds (depending on size of amplicon)

Repeat for 30 cycles

Final extension: 72°C for 1 minute

Note: The T_a was determined empirically, but was always lower than the T_m of the primer.

Table 8.1. Primer information for generating *Pfama-1* mini-genes for mCherry constructs. Random bases are indicated in green, restriction sites are indicated in blue, and purple regions indicate complementary overhangs. Annealing temperatures for primer sets are indicated in ºC.

Region	Primer Direction	Primer Sequence (5' to 3')	T_{a1} (ºC)	T_{a2} (ºC)
Full length	Forward	gataCTCGAGATGAGAAAATTATACTGCGTATT	50	55
	Reverse	gataCCTAGGATAGTATGGTTTTTCCATCAGAAC		
ΔTMΔTail	Forward	gataCTCGAGATGAGAAAATTATACTGCGTATT	50	55
	Reverse	gataCCTAGGAATTTTCATTTTATCATAAGTTGG		
ΔEDΔTM ΔTail	Forward	gataCTCGAGATGAGAAAATTATACTGCGTATT	45	50
	Reverse	atgcCCTAGGATTACCCATATAATTACTTCT		
SP for ΔPD	Forward	gataCTCGAGATGAGAAAATTATACTGCGTATT	60	60
	Reverse	ACTTCTTTCTACTATTTCAATTCCTCTTCCAAA GTTTATCAT		
ED-TM-Tail for ΔPD	Forward	ATTGAAATAGTAGAAAGAAGT	47	47
	Reverse	gataCCTAGGATAGTATGGTTTTTCCATCAGAAC		
Overlap for ΔPD	Forward	gataCTCGAGATGAGAAAATTATACTGCGTATT	60	60
	Reverse	gataCCTAGGATAGTATGGTTTTTCCATCAGAAC		
PDΔ54	Forward	gataCTCGAGATGAGAAAATTATACTGCGTATT	45	60
	Reverse	gctaCCTAGGTGGATATGCGTGTTGTAATGT		
PDΔ108	Forward	gataCTCGAGATGAGAAAATTATACTGCGTATT	45	60
	Reverse	gctaCCTAGGTGTATGTTCCTGGTGTAATGG		
PDΔ162	Forward	gataCTCGAGATGAGAAAATTATACTGCGTATT	45	60
	Reverse	gctaCCTAGGTGTATGTTCCTGGTGTAATGG		

Table 8.2. Primer information for generating *Pfsub2* mini-genes for mCherry constructs.
Random bases are indicated in green, restriction sites are indicated in blue, and purple regions indicate complementary overhangs. Annealing temperatures for primer sets are indicated in ºC.

Region	Primer Direction	Primer Sequence (5' to 3')	T_{a1} (ºC)	T_{a2} (ºC)
SP for ΔPD	Forward	gataCTCGAGATGCTGAATATTATTTATGTGG	42	52
	Reverse	TTCTTTCTCAATATTTGAACgTTTACATTCCTTATAAAAGATAAA		
CD-TM-Tail for ΔPD	Forward	AAACGTTCAAATATTGAGAAAGAA	40	50
	Reverse	gataCCTAGGTTTCATAAACATATCATCAAGTTG		
Overlap for ΔPD	Forward	gataCTCGAGATGCTGAATATTATTTATGTGG	40	53
	Reverse	gataCCTAGGTTTCATAAACATATCATCAAGTTG		
SP for ΔPDΔTM ΔTail	Forward	gataCTCGAGATGCTGAATATTATTTATGTGG	42	52
	Reverse	TTCTTTCTCAATATTTGAACGTTTACATTCCTTATAAAAGATAAA		
CD-UD for ΔPDΔTM ΔTail	Forward	AAACGTTCAAATATTGAGAAAGAA	50	55
	Reverse	cataCCTAGGATAATGACTATCATATTCATACAA		
Overlap for ΔPDΔTM ΔTail	Forward	gataCTCGAGATGCTGAATATTATTTATGTGG	42	53
	Reverse	cataCCTAGGATAATGACTATCATATTCATACAA		

Table 8.3. Primer information for generating *Pfeba181* mini-genes for mCherry constructs.
Random bases are indicated in green, restriction sites are indicated in blue, and purple regions indicate complementary overhangs. Annealing temperatures for primer sets are indicated in ºC.

Region	Primer Direction	Primer Sequence (5' to 3')	T_{a1} (ºC)	T_{a2} (ºC)
SP for ExtCys	Forward	cgcgCTCGAGATgAAAGGGAAAATGAATATGTGT	38	50
	Reverse	TCCTCTgTgTgTATCATTGGGCCTTTCCTTCAAATACTCTTC		
ExtCys	Forward	AATGATACACACAGAGGA	50	65
	Reverse	cgcgCCTAGGTGTAAATCTTTGTTTTCT		
Overlap for ExtCys	Forward	cgcgCTCGAGATGAAAGGGAAAATGAATATGTGT	38	61
	Reverse	cgcgCCTAGGTGTAAATCTTTGTTTTCT		
SP for TruncCys	Forward	cgcgCTCGAGATGAAAGGGAAAATGAATATGTGT	38	50
	Reverse	TCTTCTAGAATCATCTAATATTGTGGGCCTTTCCTTCAAATACTCTTC		
TruncCys	Forward	ACAATATTAGATGATTCTAGAAGA	50	65
	Reverse	cgcgCCTAGGTGTAAATCTTTGTTTTCT		
Overlap for TruncCys	Forward	cgcgCTCGAGATGAAAGGGAAAATGAATATGTGT	38	61
	Reverse	CgcgCCTAGGTGTAAATCTTTGTTTTCT		

Table 8.4. Primer information for verification of mCherry-expressing transgenic parasites.

Vector	Primer Name	Primer Direction	Primer Sequence (5' to 3')	T_m (ºC)
mCherry	Fwd-within-amapro	Forward	ACACAAACGTTATACGTACACAGGTT	61.4
	pARL mCherry Rev	Reverse	CCTTGAAGCGCATGAACTCCTTGA	64.6

mCherry Transgenic PCR Conditions

Enzyme used: GoTaq or DreamTaq (Promega)

Initial denaturation: 94°C for 2 minutes

Denaturation: 94°C for 60 seconds

Primer annealing: 55°C for 60 seconds

Elongation: 64°C for 210 seconds

Repeat steps 2 to 4 for 30 cycles

Final extension: 64°C for 6 minutes

Note: extension temperatures are set to 64ºC due to the AT-rich promoter.

Appendix B – Microscopy Controls

Live Imaging

For visualisation of live transgenic parasites, cultures were treated with DAPI for blue staining of the nucleus. Two colour filters were fitted to the Olympus BX-41 fluorescence microscope for the acquisition of fluorescence images of the parasites: a "blue filter", U-MWU2, to view the nuclei and a "red filter", Chroma 49306, to view the mCherry-tagged proteins.

Control experiments were conducted to ensure that no auto-fluorescence or colour-bleeding occurred. Wild-type 3D7 *P. falciparum* parasites were prepared for microscopy in the presence and absence of DAPI before visualisation using both the red and blue filters.

Wild-type parasites without DAPI:

No red or blue fluorescence was observed for the parasites prepared in the absence of DAPI.

Wild-type parasites with DAPI only:

In the presence of DAPI, blue nuclei were observed consistent with the life stage of the parasite: an example can be seen in Figure 9.1, where several blue nuclei were observed in the schizont stage parasite depicted.

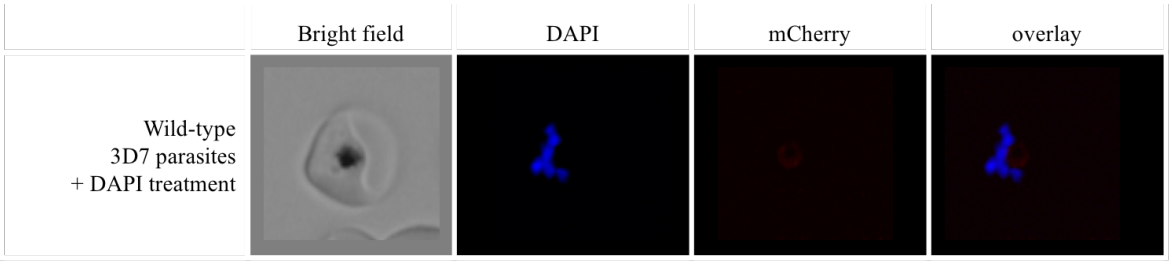


Figure 9.1. Fluorescence images of control experiment using wild-type *P. falciparum* parasites. Wild-type 3D7 *P. falciparum* parasites were treated with DAPI and visualised using a fluorescence microscope fitted with a "blue" U-MWU2 filter for DAPI fluorescence and a "red" Chroma 49306 filter for mCherry fluorescence. As expected, several blue nuclei were visible using the blue filter. Very faint red fluorescence was visible in a few parasites when using the red filter (mCherry panel).

In the majority of the parasites viewed, no red fluorescence was visible. In a select few parasites, especially at very high exposure times (>800 milliseconds), faint red fluorescence was visible around the haemozoin (Figure 9.1; mCherry panel). This phenomenon also

occurred in a few of the transgenic parasites, but could clearly be distinguished from the highly specific fluorescence patterns observed for microneme localisation (ie. Punctate localisation).

Microscopy controls confirmed that any blue or red fluorescence obtained in live imaging of transgenic parasites was a direct result of either DAPI treatment or mCherry-tagged proteins.

Co-localisation Studies

For visualisation of fixed transgenic parasites using the co-localisation protocol, an Olympus BX-41 fluorescence microscope was fitted with several colour filters: U-MWU2 for DAPI visualisation (excitation between 330 and 385nm; emission above 410mn), U-MWB2 for GFP visualisation (excitation between 460 and 490nm; emission above 510nm), Chroma 49306 Filter for mCherry visualisation (excitation between 467 and 596nm; emission above 609nm).

To confirm that the fixation protocol did not result in auto-fluorescence, transgenic cultures expressing the mCherry construct were treated with DAPI, in the presence and absence of EBA175 antibodies and fluorochromes.

Wild-type parasites without DAPI and antibodies

Normal 3D7 parasites, with no fluorochromes, DAPI or antibodies, did not show any colour when any of the filters were used, regardless of the order in which they were applied. This confirmed that no auto-fluorescence was observed as a result of the fixation or co-localisation protocol.

Wild-type parasites with EBA antibody and green fluorochrome

In this control experiment, normal 3D7 parasites were treated with DAPI and an anti-EBA175 antibody coupled with a green fluorophore (AlexaFluor® 488).

When the green filter was used, the micronemes were detected as green puncta adjacent to the nuclei (Figure 9.2; top panel) and when the red filter was used, no fluorescence was observed (not shown).

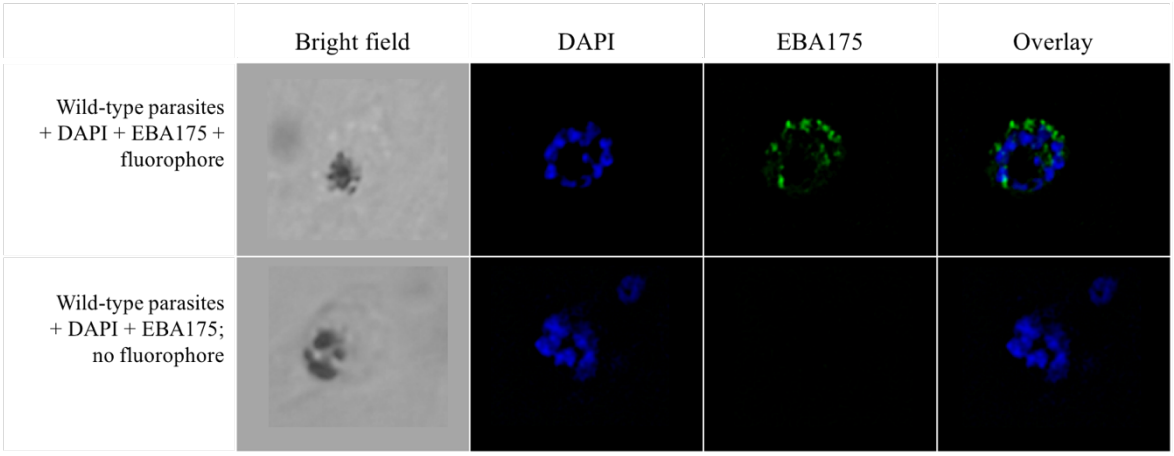


Figure 9.2. Co-localisation controls: EBA antibody with and without a fluorophore.
Top panel: Wild-type 3D7 parasites were treated with DAPI, an anti-EBA175 antibody and an AlexaFluor® 488 fluorophore. Green micronemes were visible as puncta adjacent to the nuclei. **Bottom panel:** Wild-type 3D7 parasites were treated with DAPI and an anti-EBA175 antibody without the addition of a fluorophore. The nuclei were stained blue, but no green fluorescence was detected.

Wild-type parasites with EBA antibody and no fluorochrome

In this control experiment, normal 3D7 parasites were treated with DAPI and an anti-EBA175 antibody without the addition of a fluorophore (Figure 9.2 bottom panel). The parasite nuclei stained blue, but no microneme fluorescence was observed.

Microscopy controls confirmed that any blue or green fluorescence obtained in fixed parasites was a direct result of either DAPI treatment or fluorophores attached to the anti-EBA175 antibody.

Appendix C – Enlarged Images

An enlargement of Figure 3.21:

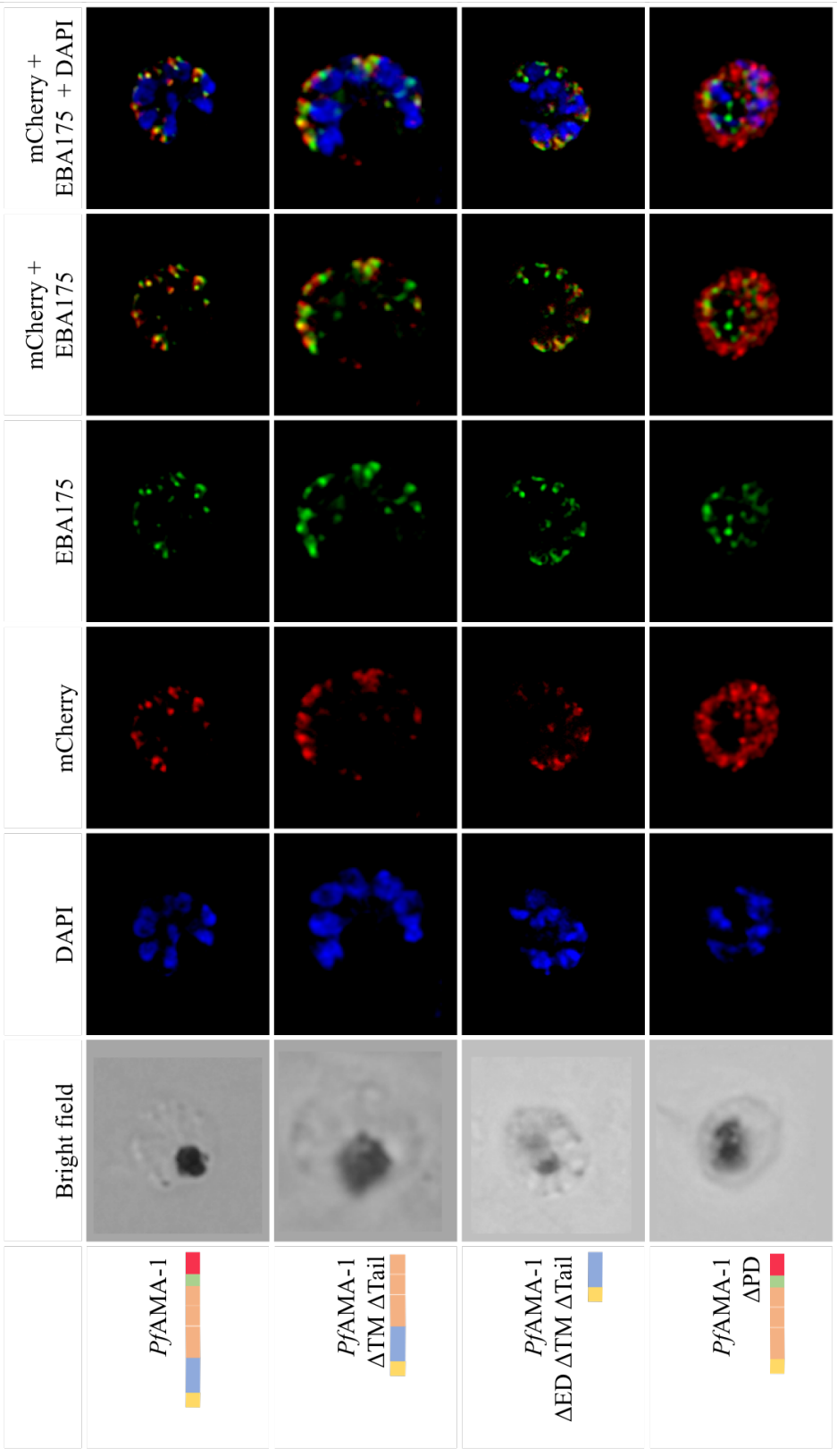


Figure 10.1. Co-localisation studies using fixed schizont stage *P. falciparum* parasites expressing mCherry-tagged *Pf*AMA-1. Parasites were viewed at 1000x magnification. mCherry causes red fluorescence of chimaeric *Pf*AMA-1 proteins. DAPI is a blue nuclear stain. A microneme marker, *Pf*EBA175, with a green fluorochrome was used to determine the localisation of mCherry tagged proteins within the transgenic parasites. Should the red mCherry-tagged proteins co-localise with the green micronemes, a yellow signal will be obtained when an overlay between the red and green colour channels is performed. Pearson's coefficients (PC) are a numerical indicator of co-localisation, with values close to 1 indicating strong co-localisation. **Top Panel**: Full length *Pf*AMA-1 showed a punctate pattern that co-localised with the green *Pf*EBA175 microneme signal, indicated by the yellow fluorescence observed in the overlay (PC 0.70). **Middle Panels**: Removal of the transmembrane domain and cytoplasmic tail (ΔTM and ΔTail; PC 0.69) and ectodomains (ΔED; PC 0.80) gave a similar pattern. **Bottom Panel**: In the absence of only the prodomain (ΔPD), the mCherry fluorescence was dispersed and no longer co-localised with the green microneme marker (PC 0.24).

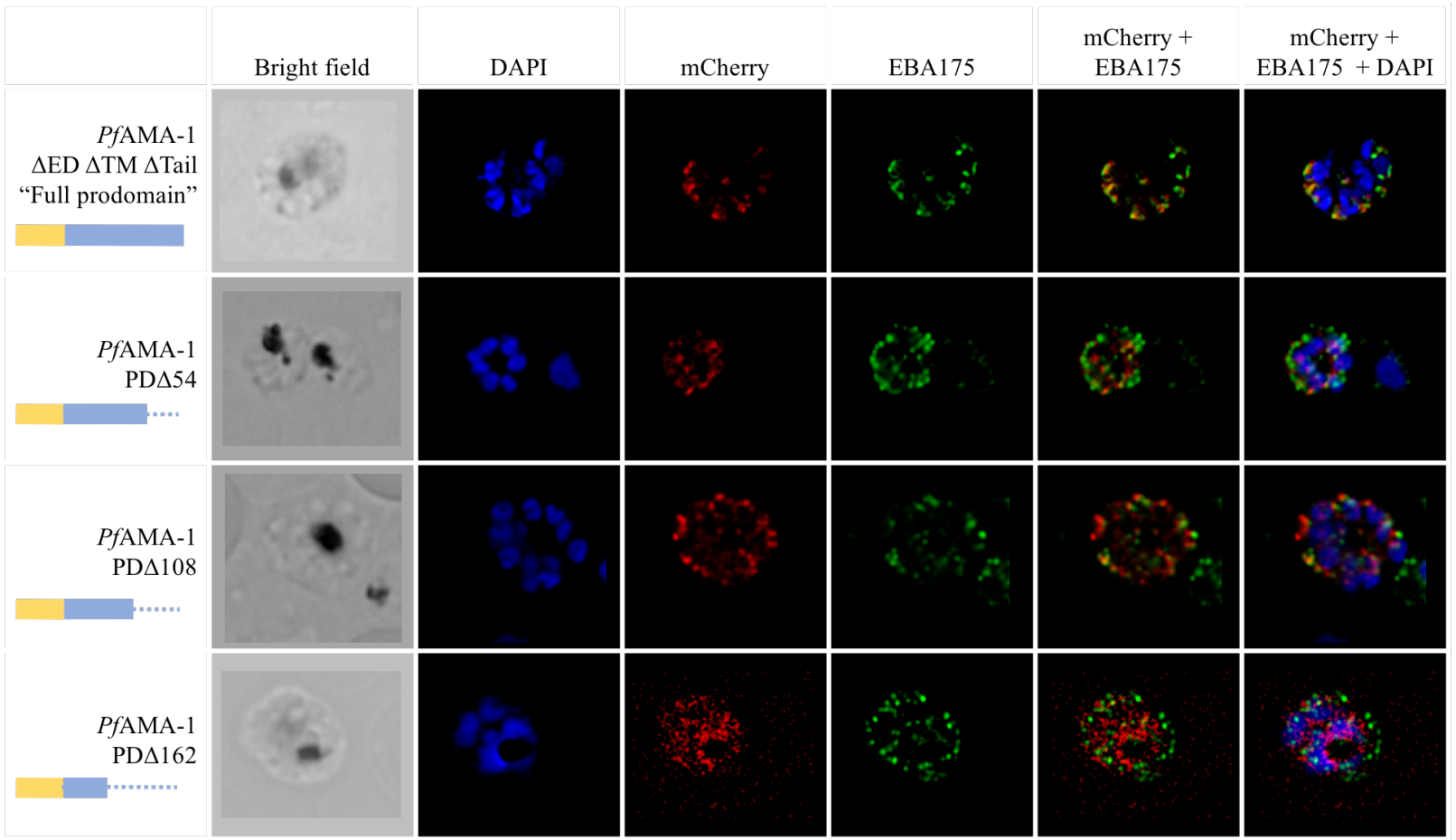


Figure 10.2. Co-localisation studies using fixed schizont stage *P. falciparum* parasites expressing mCherry-tagged *Pf*AMA-1 prodomain truncations.

Parasites were viewed at 1000x magnification. mCherry causes red fluorescence of the chimaeric *Pf*AMA-1 prodomain truncated proteins. DAPI is a blue nuclear stain. A microneme marker, *Pf*EBA175, with a green fluorochrome was used to determine the localisation of mCherry tagged proteins within the transgenic parasites. Pearson's coefficients (PC) are a numerical indicator of co-localisation, with values close to 1 indicating strong co-localisation. **Top Panel**: *Pf*AMA-1ΔEDΔTMΔTail, which consisted only of the signal peptide and the prodomain, were present in the apex and co-localised with the microneme marker (PC 0.80). **Second and Third Panels:** *Pf*AMA-1 PDΔ54 and PDΔ108 yielded partial apical localisation, with minimal overlap with the microneme marker (PC 0.56 and 0.46 respectively). **Bottom Panel**: *Pf*AMA-1 PDΔ162 was dispersed throughout the parasite (PC 0.26).

Appendix D – Plasmid Maps

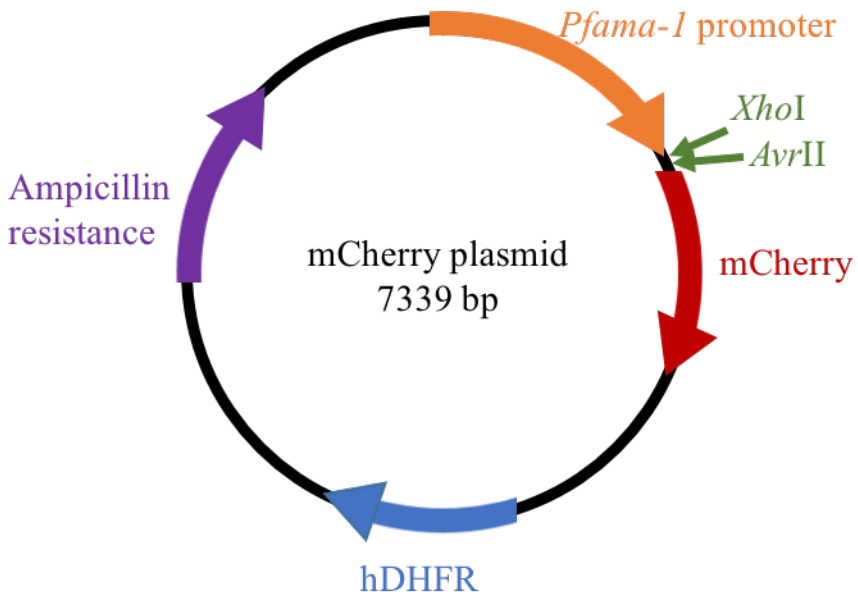


Figure 11.1. The mCherry plasmid.
A schematic depicting the pARL-mCherry plasmid, modified from the pARL2-GFP vector (Przyborski *et al.,* 2005). The *Pfama-1* promoter ensures that expression of the chimaeric proteins occurs only during the late stages of the parasite life cycle (Wepener, 2014). The plasmid encodes an ampicillin resistance gene for positive selection after bacterial transformation and a human dihydrofolate reductase (hDHFR) gene which confers resistance against WR99210 compound as a positive selection strategy after parasite transfection (Fidock & Wellems, 1997). *Xho*I and *Avr*II restriction endonuclease sites were used for directional insertion of the mini-genes into the mCherry backbone.

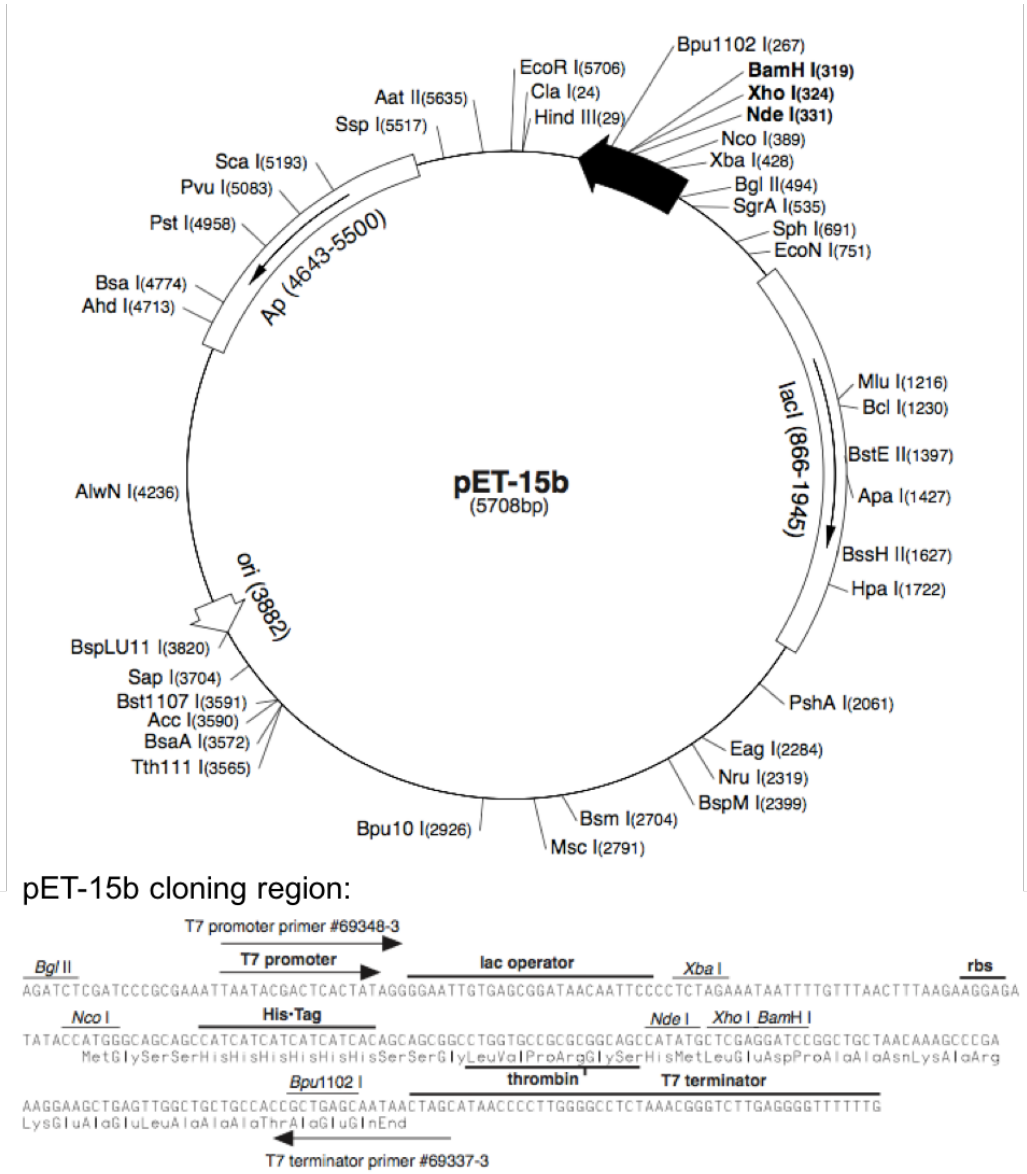


Figure 11.2. The pET-15b plasmid.
pET-15b is a low copy number plasmid and is used for the expression of His-tagged proteins. The sequence encodes: the ampicillin resistance gene ß-lactamase (for positive selection); the pBR322 origin of replication; and the *lac*I repressor. *Nde*I and *Bam*HI restriction endonuclease sites were used for directional insertion of the amplicons into the pET backbone, which fused an N-terminal 6xHis tag onto the proteins. (Adapted from Novagen, 2011).

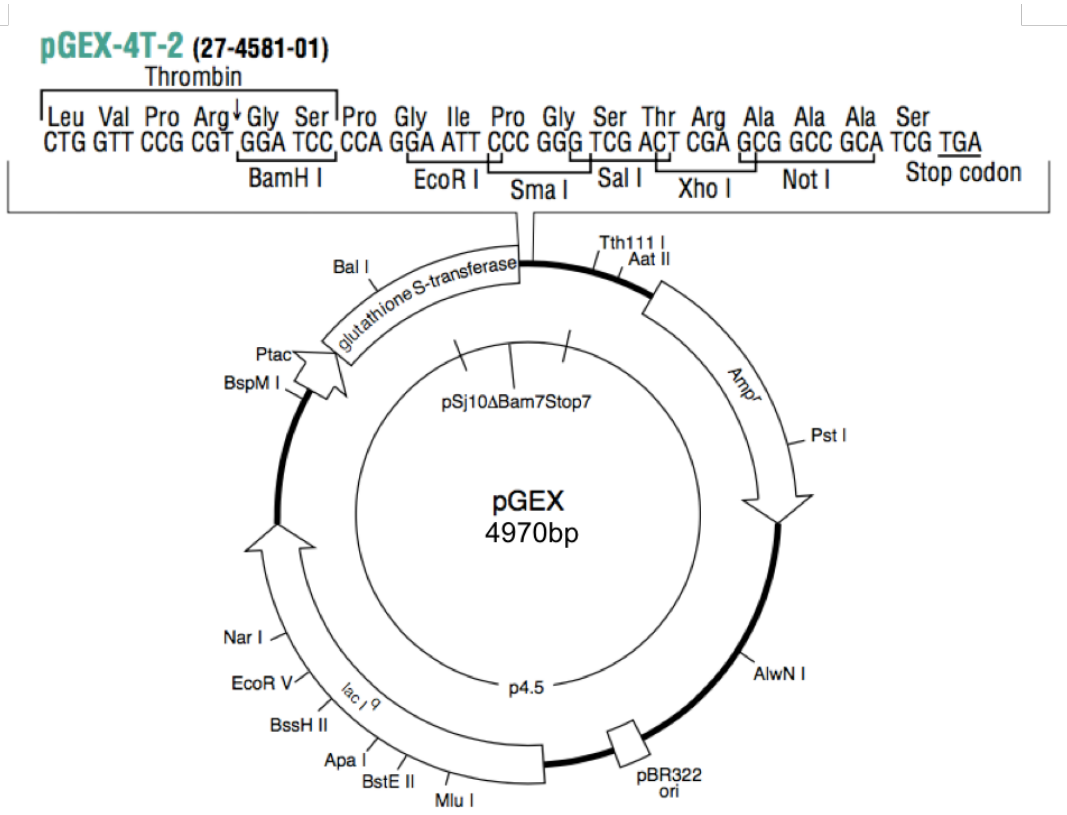


Figure 11.3. The pGEX-4T-2 plasmid.
pGEX-4T-2 is a low copy number plasmid used for the expression of GST-tagged proteins. The sequence encodes: the ampicillin resistance gene ß-lactamase (for positive selection); the pBR322 origin of replication; and the hybrid *tac* promoter (a fusion of *E. coli trp* and *lac* promoters). *Bam*HI and *Xho*I restriction endonuclease sites were used for directional insertion of the amplicons into the pGEX backbone, which fused an N-terminal glutathione S-transferase (GST) tag onto the protein. (Adapted from Healthcare, 2009).

Appendix E – Biopanning

pET-15b Amplicon PCR Conditions

Enzyme used: PhusionFlash or Q5 (www.neb.com)

Initial denaturation: 98°C for 10 seconds

Denaturation:	98°C for 1 second
Primer annealing:	T_{a1} for 5 seconds
Elongation:	72°C for 30 seconds

Repeat for 5 cycles

Denaturation:	98°C for 1 second
Primer annealing:	T_{a2} for 5 seconds
Elongation:	72°C for 30 seconds

Repeat for 30 cycles

Final extension: 72°C for 1 minute

Note: The T_a was determined empirically, but was always lower than the T_m of the primer.

Table 12.1. Primer information for generating amplicons for pET-15b constructs.
Random bases are indicated in green, restriction sites are indicated in blue, stop codons are in red.

Gene of interest	Region	Primer Direction	Primer Sequence (5' to 3')	T_{a1} (°C)	T_{a2} (°C)
Pfama-1	prodomain	Forward	gctctaCATATGCAGAATTATTGGGAACATC	37	54
		Reverse	gctcGGATCCTTAGCTTGAAAATAAATTTTG		
Pfeba181	cysteine rich domain	Forward	gctctaCATATGCAATATAATAATAGAGATGCTTCT	37	54
		Reverse	gctcGGATCCTTATGTAAATCTTTGTTTTCT		
	extended cysteine rich domain	Forward	gctctaCATATGAATGATACACACAGAGGA	37	54
		Reverse	gctcGGATCCTTATGTAAATCTTTGTTTTCT		
Pfsub2	JxTail	Forward	gctctaCATATGATGGATTGTTATTTTGTT	40	52
		Reverse	gctcGGATCCTTATTTCATAAACATATCATCAAG		
	JxTM	Forward	gctctaCATATGATGGATTGTTATTTTGTT	36	52
		Reverse	gctcGGATCCTTACATATATATCATTCCAAC		
	TMTail	Forward	gctctaCATATGTTGTTGGCTTCTGTC	36	52
		Reverse	gctcGGATCCTTATTTCATAAACATATCAAG		

Table 12.2. Primer information for sequencing of T7 bacteriophage.

Vector	Primer Name	Primer Direction	Primer Sequence (5' to 3')	Predicted T_m (ºC)
T7 phage	T7Select-UP-2	Forward	GCT AAC TTC CAA GCG GAC CA	62.5
	T7Select-DOWN	Reverse	GCT AGT TAT TGC TCA GCG GT	60.4

T7 PCR Conditions

Enzyme used: GoTaq or DreamTaq

Initial denaturation: 94°C for 2 minutes

Denaturation: 94°C for 50 seconds

Primer annealing: 50°C for 60 seconds

Elongation: 72°C for 60 seconds

Repeat steps 2 to 4 for 35 cycles

Final extension: 72°C for 6 minutes

pGEX-4T-2 Amplicon PCR Conditions

Enzyme used: PhusionFlash (www.neb.com)

Initial denaturation: 98°C for 10 seconds

Denaturation: 98°C for 1 second

Primer annealing: T_{a1} for 5 seconds

Elongation: 72°C for 15 seconds

Repeat for 5 cycles

Denaturation: 98°C for 1 second

Primer annealing: T_{a2} for 5 seconds

Elongation: 72°C for 15 seconds

Repeat for 30 cycles

Final extension: 72°C for 1 minute

Table 12.3. Primer information for generating amplicons for pGEX-4T-2 constructs.
Random bases are indicated in green, restriction sites are indicated in blue, stop codons are in red.

Gene of interest	Primer Direction	Primer Sequence (5' to 3')	T_{a1} (°C)	T_{a2} (°C)
Pfformin2	Forward	gagGGATCCGAAAGCATAAAATTG	32	51
	Reverse	gccCTCGAGTTATGTATTATTATTATCATC		
Pfcbp	Forward	gagGGATCCATGGTCGACGATAAG	34	56
	Reverse	gccCTCGAGTCAAGCTATTTCTAACTC		

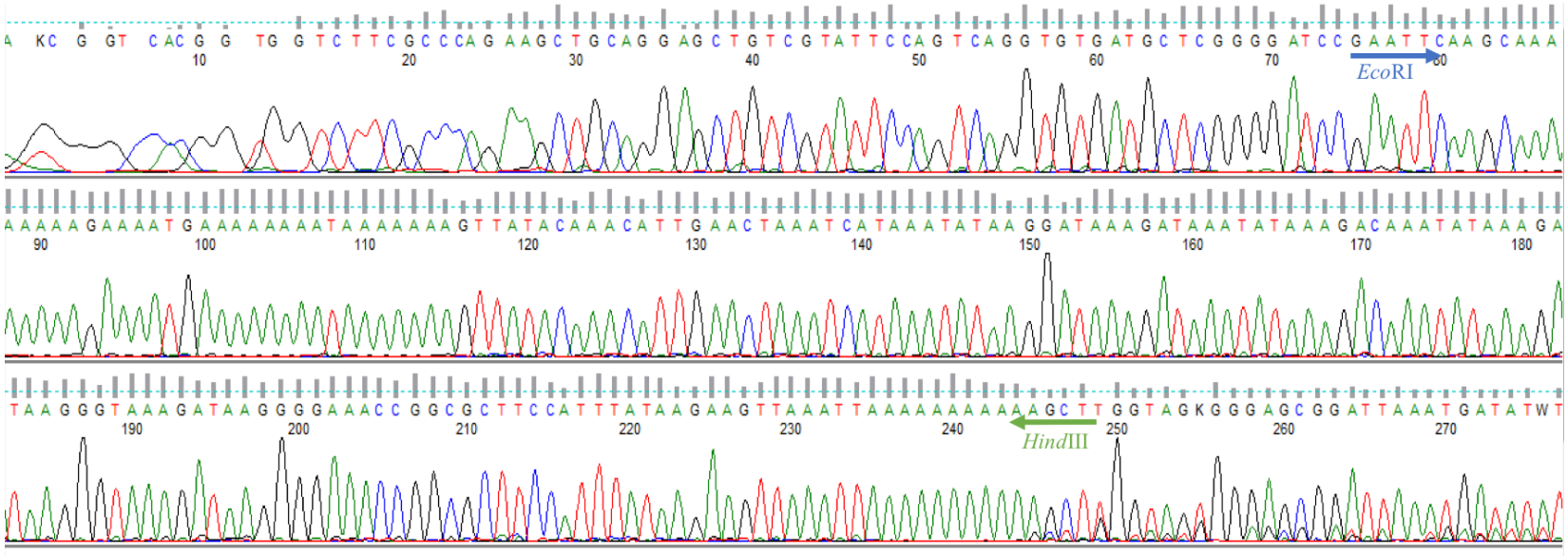


Figure 12.1. Identification of putative *P. falciparum* Formin2 as a binding partner of *Pf*AMA-1.
Chromatogram showing the sequencing results which identified putative *Pf*Formin2 in the T7 phage expression cassette. The blue and green arrows indicate the positions of *Eco*RI and *Hind*III in the phage backbone, flanking the cDNA malaria sequence

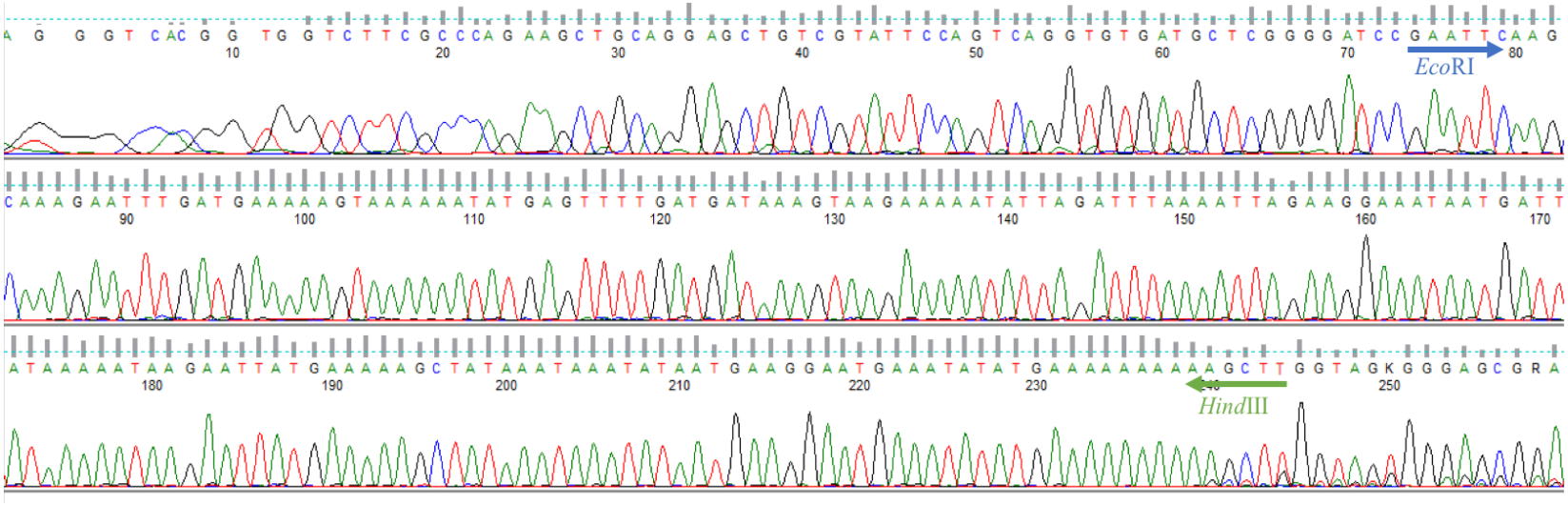


Figure 12.2. Identification of putative *P. falciparum* Chaperone Binding Protein as a binding partner of *Pf*AMA-1.
Chromatogram showing the sequencing results which identified putative *Pf*CBP in the T7 phage expression cassette. The blue and green arrows indicate the positions of *Eco*RI and *Hind*III in the phage backbone, flanking the cDNA malaria sequence.

Appendix F – List of Suppliers

Antibodies

Alexa Fluor® 594 Goat Anti-Mouse Antibody	Life Technologies Corporation, USA
Anti-GFP Rabbit Antibody Alexa Fluor® 488 Conjugate	Life Technologies Corporation, USA
Anti-GST HRP Conjugated Primary Antibody	Amersham Biosciences, UK
Anti-His HRP Conjugate Primary Antibody	Qiagen, Germany

Chemicals

Acrylamide	Promega, USA
Agarose	Sigma-Aldrich Corporation, USA
Albumax II	Life Technologies Corporation, USA
Ammonium Chloride	Saarchem (Pty) Ltd., RSA
Ammonium Persulfate	Promega, USA
Ammonium Sulphate	Saarchem (Pty) Ltd., RSA
Ampicillin	Roche, Germany
Agar	Merck, Germany
Bis-Acrylamide	Sigma-Aldrich Corporation, USA
Boric Acid	Sigma-Aldrich Corporation, USA
Bovine Serum Albumen (BSA)	Pierce, USA
Bromophenol Blue	Merck, Germany
Calcium Chloride	Merck, Germany
Chloramphenicol	Roche, Germany
Chloroform	Merck, Germany
Coomassie Brilliant Blue R-250	BDH, UK
DAPI	Sigma-Aldrich Corporation, USA
Disodium Phosphate	Saarchem (Pty) Ltd., RSA
Dithiothreitol (DTT)	Boehringer Mannhein, Germany
DMSO	BDH, UK
DNaseI	Fermentas International Inc., USA
D-Sorbitol	Sigma, USA
EDTA	Merck, Germany
EGTA	BDH, UK
Ethanol	Merck, Germany
Ethidium Bromide	Sigma-Aldrich Corporation, USA
Formaldehyde	
Gentamycin	Sigma, USA

Glacial Acetic Acid	Merck, Germany
Glucose	Merck, Germany
Glutathione, Reduced	Sigma, USA
Glycerol	Merck, Germany
HEPES	Merck, Germany
Hoechst 33258 Pentahydrate	Invitrogen, USA
Hypoxanthine	Sigma, USA
Imidazole	Sigma, USA
Isopropanol	Merck, Germany
Magnesium Chloride	Merck, Germany
Magnesium Sulphate	Merck, Germany
Maleic Acid	Merck, Germany
Monopotassium Phosphate	Merck, Germany
Monosodium Phosphate	Merck, Germany
Nuclease Free Water	Fermentas International Inc., USA
Overnight Express™ Instant TB Medium	Novagen, Inc., USA
Paraformaldehyde	
Phenol	Merck, Germany
Ponceau S	Sigma-Aldrich Corporation, St. Louis, USA
Potassium Acetate	Merck, Germany
Potassium Chloride	Merck, Germany
Protease Inhibitor Cocktail Set III	Calbiochem®, USA
RNase A	Thermo Fisher Scientific Inc., USA
RPMI Culture Medium	GibcoBRL, USA
Saponin	USB, USA
Sodium Dodecyl Sulfate (SDS)	Merck, Germany
Silver Nitrate	Merck, Germany
Sodium Acetate	Merck, Germany
Sodium Bicarbonate	PAL Chemicals, UK
Sodium Chloride	Merck, Germany
Sodium Citrate	Holpro Fine Chemicals, RSA
Sodium Hydroxide	Merck, Germany
Sodium Thiosulfate	Merck, Germany
Sorbitol	Sigma-Aldrich Corporation, USA
Sucrose	Merck, Germany
TEMED	Promega, USA
The SuperSignal® West Pico Chemiluminescent Substrate	Thermo Fisher Scientific Inc., USA
Tris	Sigma-Aldrich Corporation, USA



Triton-X	BDH, UK
Tryptone [Pancreatic Digest of Casein]	Merck, Germany
Tween-20	Calbiochem®, USA
Yeast Extract	Oxoid, UK
β-Mercaptoethanol	Merck, Germany

Competent Cells

DH5α Competent Cells	Invitrogen, USA
Rosetta™ 2 (DE3) Competent Cells	Novagen, Inc., USA
XL10-Gold® Ultracompetent Cells	Stratagene, USA

Consumables

0.22µm Filters	Millipore, USA
Acid Citrate Dextrose (ACD) Tubes	BD Vacutainer, UK
Cryotubes	Nunc, Denmark
Culture Flasks	Thermo Fisher Scientific Inc., USA
Eppendorf Tubes	Eppendorf, Germany
Falcon™ Round Bottom Tubes	Becton Dickinson, USA
FastAP™ Thermosensitive Alkaline Phosphatase	Thermo Fisher Scientific Inc., USA
FastDigest® Restriction Endonucleases	Thermo Fisher Scientific Inc., USA
Filter Tips	QSP, USA
Gas Mixture	Afrox, RSA
Hybond™-C Extra Supported Nitrocellulose Membrane	Amersham Biosciences, UK
MassRuler DNA Ladders	Thermo Fisher Scientific Inc., USA
Microscope Slides	Thermo Fisher Scientific Inc., USA
Nunc Tubes	Nunc, Germany
Petri Dishes	Costar, USA
Phusion® Flash High-Fidelity PCR Master Mix	Thermo Fisher Scientific Inc., USA
Slide-A-Lyzer Mini Dialysis Unit	Pierce, USA
SpectraBR Protein Ladder	Pierce, USA
Sterile Culture Flasks	Nunc, Germany
Vacucap® 90 PF 0.8/0.2µm Filter Unit	Pall Life Sciences, USA

Equipment

49306 Filter	Chroma Technologies, USA

Avanti® J-E Centrifuge	Beckman Coulter, USA
Axiostar Plus Transmitted Light Microscope	Zeiss, Germany
Biomate 5 Spectrophotometer	Thermo Fisher Scientific Inc., USA
BX41 Olympus Microscope	Olympus, Japan
Cellsense Dimensions 1.7 Software	Olympus, Japan
Centrifuge 5415R	Eppendorf, Germany
Centrifuge 5702R	Eppendorf, Germany
CPE 50 Circulator	Labcon, RSA
DP72 Camera	Olympus, Japan
Gene Pulser® Cuvette	Bio-Rad Laboratories, USA
GeneGenius Gel Doc System	Syngene, UK
Incubator	Heraeus Instruments, Germany
Intelli-Mixer	ELMI Ltd., Latvia
Laminar Flow Hood	Labotec, RSA
Mastercycler Gradient Thermocycler	Eppendorf, Germany
Mighty Small Mighty Small II SE250 Gel Cassette	Hoefer Scientific Instruments, USA
MWB2 Filter	Olympus, Tokyo, Japan
Nanodrop® 1000	Thermo Fisher Scientific Inc., USA
Orbital Shaker	Labotec, RSA
pH Meter	Beckman Coulter, USA
PR250 Orbital Bench Top Shaker	Hoefer Scientific Instruments, USA
Sonopuls HD3100 Ultrasonic Homogenizer with Microtip MS73	Bandelin Electronic, Germany
U-25ND25 Olympus Neutral Density Filter	Olympus, Japan
U-MWB2 Filter	Olympus, Japan
U-MWU2 Filter	Olympus, Japan
Vacuum Pump	Millipore, USA
Water Bath	Lauda, Germany

Kits

GenElute™ Plasmid Miniprep Kit	Sigma-Aldrich, USA
MagneGST™ Protein Purification System	Promega, USA
MagneHis™ Protein Purification System	Promega, USA
Nucleobond® Xtra Maxi Plus Plasmid DNA Purification Kit	Macherey-Nagel, Germany
Nucleospin® Gel And PCR Clean Up Kit	Macherey-Nagel, Germany
Nucleospin® Plasmid Extraction Kit	Macherey-Nagel, Germany

Penta·His HRP Conjugate Kit	Qiagen, Germany
QIAquick PCR Purification Kit	Qiagen, Germany
Rapid DNA Ligation Kit	Roche Diagnostics, Germany
Rapi-Diff Staining Kit	Diagnostic Media Products, RSA

Appendix G – Ethics Clearance

R14/49 Ms Alisje Churchyard

HUMAN RESEARCH ETHICS COMMITTEE (MEDICAL)

CLEARANCE CERTIFICATE NO. M1702106

NAME: (Principal Investigator)	Ms Alisje Churchyard
DEPARTMENT:	Molecular Medicine and Haematology University of the Witwatersrand
PROJECT TITLE:	Trafficking of P. Falciparum Invasion Proteins to the Parasite Micronemes
DATE CONSIDERED:	Adhoc
DECISION:	Approved unconditionally
CONDITIONS:	Sub-Study (M130569)
SUPERVISOR:	Prof TL Coetzer
APPROVED BY:	Professor A. Woodiwiss, Co-Chairperson, HREC (Medical)
DATE OF APPROVAL:	04/04/2017

This clearance certificate is valid for 5 years from date of approval. Extension may be applied for.

DECLARATION OF INVESTIGATORS

To be completed in duplicate and **ONE COPY** returned to the Research Office Secretary in Room 10004,10th floor, Senate House/2nd floor, Phillip Tobias Building, Parktown, University of the Witwatersrand. I/We fully understand the the conditions under which I am/we are authorised to carry out the above-mentioned research and I/we undertake to ensure compliance with these conditions. Should any departure be contemplated, from the research protocol as approved, I/we undertake to resubmit to the Committee. **I agree to submit a yearly progress report**. The date for annual re-certification will be one year after the date of convened meeting where the study was initially reviewed. in this case, the study was initially review in February and will therefore be due in the month of February each year. Unreported changes to the application may invalidate the clearance given by the HREC (Medical).

Principal Investigator Signature

Date 4 April 2017

Appendix H – Plagiarism Report

AChurchyardThesiswithoutimagesforturnitin.pdf

ORIGINALITY REPORT

13%	7%	7%	7%
SIMILARITY INDEX	INTERNET SOURCES	PUBLICATIONS	STUDENT PAPERS
A. Churchyard	Churchyard	Prof. T.L. Coetzer	8/4/17

PRIMARY SOURCES

1	Submitted to University of Witwatersrand Student Paper	3%
2	ash.confex.com Internet Source	1%
3	lra.le.ac.uk Internet Source	<1%
4	Luc Reininger. "An essential Aurora-related kinase transiently associates with spindle pole bodies during Plasmodium falciparum erythrocytic schizogony : P. falciparum Aurora-related protein kinases", Molecular Microbiology, 01/2011 Publication	<1%
5	www.sajei.co.za Internet Source	<1%
6	edoc.ub.uni-muenchen.de Internet Source	<1%
7	Submitted to University of Melbourne Student Paper	<1%
8	Heat Shock Proteins of Malaria, 2014. Publication	<1%

References

Acharya P, Kumar R & Tatu U (2007). Chaperoning a cellular upheaval in malaria: Heat shock proteins in *Plasmodium falciparum*. *Molecular and Biochemical Parasitology, 153(2): 85-94.*

Adams JH, Blair PL, Kaneko O & Peterson DS (2001). An expanding *ebl* family of *Plasmodium falciparum*. *Trends in Parasitology,* 17: 297-299.

Adams JH, Hudson DE, Tori M, Ward GE, Wellems TE, Aikawa M & Miller LH (1990). The Duffy receptor family of *Plasmodium knowlesi* is located within the micronemes of invasive malaria merozoites. *Cell,* 63: 141-153.

Adams JH, Sim BK, Dolan SA, Fang X, Kaslow DC & Miller LH (1992). A family of erythrocyte binding proteins of malaria parasites. *Proceedings of Natural Academy of Sciences USA,* 89: 7085-7089.

Ahouidi AD, Amambua-Ngwa A, Awandare GA, Bei AK, Conway DJ, Diakite M, Duraisingh MT, Rayner JC & Zenonos ZA (2016). Malaria vaccine development: Focusing field erythrocyte invasion studies on phenotypic diversity. *Trends in Parasitology*, 32(4): 274-283.

Aikawa M, Miller LH, Johnson J & Rabbege J (1978). Erythrocyte entry by malarial parasites: A moving junction between erythrocyte and parasite. *Journal of Cell Biology*, 77(1):72-82.

Aurrecoechea C, Brestelli J, Brunk BP, Dommer J, Fischer S, Gajria B, Gao X, Gingle A, Grant G, Harb OS, Heiges M, Innamorato F, Iodice J, Kissinger JC, Kraemer E, Li W, Miller jA, Nayak V, Pennington C, Pinney DF, Roos DS, Ross C, Stoeckert CJ, Treatman C, Wang H (2009). PlasmoDB: a functional genomic database for malaria parasites. *Nucleic Acids Research*, 37: D539-D543.

Bai T, Becker M, Gupta A, Strike P, Murphy VJ, Anders RF & Batchelor AH (2005). Structure of AMA1 from *Plasmodium falciparum* reveals a clustering of polymorphisms that surround a conserved hydrophobic pocket. *Proceedings of Natural Academy of Sciences USA*, 102: 12736-12741.

Baldi DL, Andrews KT, Waller RF, Roos DS, Howard RF, Crabb BS & Cowman AF (2000). RAP1 controls rhoptry targeting of RAP2 in the malaria parasite *Plasmodium falciparum*. *The European Molecular Biology Organization Journal*, 19: 2435-2443.

Bannister LH & Dluzewski AR (1990). The ultrastructure of red cell invasion in malaria infections: a review. *Blood Cells*, 16: 257-292.

Bannister LH, Hopkins JM, Dluzewski AR, Margos G, Williams IT, Blackman MJ, Hocken CH, Thomas AW & Mitchell GH (2003). *Plasmodium falciparum* apical membrane antigen 1 (*Pf*AMA-1) is translocated within micronemes along subpellicular microtubules during merozoite development. *Journal of Cell Science,* 116: 3825-3834.

Bannister LH, Hopkins JM, Fowler RE, Krishna S & Mitchell GH (2000). Ultrastructure of rhoptry development in *Plasmodium falciparum* erythrocytic schizonts. *Parasitology*, 121(3): 273-287.

Barale JC, Blisnick T, Fujioka H, Alzari PM, Aikawa M, Braun-Breton C & Langsley G (1999). *Plasmodium falciparum* subtilisin-like protease 2, a merozoite candidate for the merozoite surface protein 1–42 maturase. *Proceedings of Natural Academy of Sciences USA,* 96: 6445-6450.

Baum J, Papenfuss AT, Baum B, Speed TP & Cowman AF (2006). Regulation of apicomplexan actin-based motility. *Nature Reviews Microbiology*, 4: 621-628.

Baum J, Tonkin CJ, Paul AS, Rug M, Smith BJ, Gould SB, Richard D, Pollard TD & Cowman AF (2008). A malaria parasite formin regulates actin polymerization and localizes to the parasite-erythrocyte moving junction during invasion. *Cell Host & Microbe*, 3(3): 188-198.

Beck JR, Muralidharan V, Oksman A & Goldberg DE (2014). PTEX component HSP101 mediates export of diverse malaria effectors into host erythrocytes. *Nature,* 511(7511): 592-595.

Berg JM, Tymoczko JL & Stryer L (2002). Eukaryotic transcription and translation are separated in space and time. WH Freeman and Co: *Biochemistry 5th Edition,* New York.

Beeson JG, Drew DR, Boyle MJ, Geng G, Fowkes FJI & Richards JS (2016). Merozoite surface proteins in red blood cell invasion, immunity and vaccines against malaria. *Federation of European Microbiological Societies Microbiology Reviews*, 40: 343-372.

Besterio S, Michelin A, Poncet J, Dubremetz J-F & Lebrun M (2009). Export of a *Toxoplasma gondii* rhoptry neck protein complex at the host cell membrane to form the moving junction during invasion. *Public Library of Science Pathogens*, 5(2): e1000309.

Bhanot P, Frevert U, Nussenzweig V & Persson C (2003). Defective sorting of the thrombospondin-related anonymous protein (TRAP) inhibits *Plasmodium* infectivity. *Molecular and Biochemical Parasitology,*126: 263-273.

Birkholtz LM, Blatch G, Coetzer TL, Hoppe H, Human E, Morris EJ, Ngcete Z, Oldfield L, Roth R, Shonhai A, Stephens L & Louw AI (2008). Heterologous expression of plasmodial proteins for structural studies and functional annotation. *Malaria Journal,* 7: 197.

Birnboim HC & Doly J (1979) A rapid alkaline extraction method for the isolation of plasmid DNA. *Nucleic Acids Research,* 7: 1513-1523.

Blackman MJ (2000). Proteases involved in erythrocyte invasion by the malaria parasite: function and potential as chemotherapeutic targets. *Current Drug Targets,* 1: 59-83.

Blackman MJ (2004). Proteases in host cell invasion by the malaria parasite. *Cellular Microbiology*, 6: 893-903.

Blackman MJ & Bannister LH (2001). Apical organelles of Apicomplexa: biology and isolation by subcellular fractionation. *Molecular and Biochemical Parasitology*, 117: 11-25.

Blomqvist K (2008). Thawing of glycerolyte-frozen parasites with NaCl. *Methods in Malaria Research*, Fifth Edition. Moll K, Ljungström I, Perlmann H, Scherf A & Wahlgren M (Editors).

Boyle MJ, Wilson DW & Beeson JG (2013). New approaches to studying *Plasmodium falciparum* merozoite invasion and insights into invasion biology. *International Journal of Parasitology*, 43: 1-10.

Bozdech Z, Llinas M, Pulliam BL, Wong ED, Zhu J & DeRisi JL (2003). The transcriptome of the intraerythrocytic developmental cycle of *Plasmodium falciparum*. *Public Library of Science Biology,* 1: E5.

Bullen HE, Charnaud SC, Kalanon M, Riglar DT, Dekiwadia C, Kangwanrangsan N, Torii M, Tsuboi T, Baum J, Ralph SA, Cowman AF, de-Koning-Ward TF, Crabb BS & Gilson PR (2012). Biosynthesis, localization, and macromolecular arrangement of the *Plasmodium falciparum* translocon of exported proteins (PTEX). *Journal of Biological Chemistry*, 287: 7871-7884.

Carruthers VB (1999). Armed and dangerous: *Toxoplasma gondii* uses an arsenal of secretory proteins to infect host cells. *Parasitology International*, 48: 1-10.

Carruthers VB & Sibley LD (1997). Sequential protein secretion from three distinct organelles of *Toxoplasma gondii* accompanies invasion of human fibroblasts. *European Journal of Cell Biology*, 73: 114-123.

Carruthers VB, Giddings OK & Sibley LD (1999). Secretion of micronemal proteins is associated with *Toxoplasma* invasion of host cells. *Cellular Microbiology*, 1:225-235.

Child MA, Harris PK, Collins CR, Withers-Martinez C, Yeoh S & Blackman MJ (2013). Molecular determinants for subcellular trafficking of the malarial sheddase *Pf*SUB2. *Traffic,* 14: 1053-1064.

Chua C-S, Low H & Sim T-S (2014). Co-chaperones of Hsp90 in *Plasmodium falciparum* and their concerted roles in cellular regulation. *Parasitology,* 141(9): 1177-1191.

Collins CR, Withers-Martinez C, Hackett F & Blacman MJ (2009). An inhibitory antibody blocks interactions between components of the malarial invasion machinery. *Public Library of Science Pathogens*, 5: e1000273.

Cooke BM, Buckingham DW, Glenister FK, Fernandez KM, Bannister LH, Marti M, Mohandas N & Coppel RL (2006). A Maurer's cleft-associated protein is essential for expression of the major malaria virulence antigen on the surface of infected red blood cells. *The Journal of Cell Biology*, 172:899-908.

Coombs GH, Goldberg DE, Klemba M, Berry C, Kay J & Mottram JC (2001). Aspartic proteases of Plasmodium falciparum and other parasitic protozoa as drug targets. Trends in Parasitology, 11: 532-537.

Cowman AF & Crabb BS (2006). Invasion of red blood cells by malaria parasites. *Cell*, 124: 755-766.

Cowman AF, Berry D & Baum J (2012). The cellular and molecular basis for malaria parasite invasions of the human red blood cell. *The Journal of Cell Biology*, 198(6): 961-971.

Cowman AF, Crabb BS, Maier AG, Tonkin CJ, Healer J, Gibson P & De Koning-Ward T (2008). Preparation of *P. falciparum* genomic DNA. *Methods in Malaria Research*, Fifth Edition. Moll K, Ljungström I, Perlmann H, Scherf A & Wahlgren M (Editors).

Crosnier C, Bustamante LY, Bartholdson SJ, Bei AK, Theron M, Uchikawa M, Mboup S, Ndir O, Kwiatkowski DP, Duraisingh MT, Rayner JC & Wright GJ (2011). Basigin is a receptor essential for erythrocyte invasion by *Plasmodium falciparum*. *Nature,* 480: 534-537.

De Koning-Ward TF, Gilson PR, Boddey JA, Rug M, Smith BJ, Papenfuss AT, Sanders PR, Lundie RJ, Maier AG, Cowman AF & Crabb BS (2009). A newly discovered protein export machine in malaria parasites. *Nature*, 459: 945-950.

de Marco A (2009). Strategies for successful expression of disulfide bond-dependent proteins in *Escherichia coli*. *Microbial Cell Factories,* 8: 26-43.

Deans JA, Alderson T, Thomas AW, Mitchell GH & Lennox ES (1982). Rat monoclonal antibodies which inhibit the in vitro multiplication of *Plasmodium knowlesi*. *Clinical and Experimental Immunology,* 49: 297-309.

Dell'Angelica EC, Mullins C, Caplan S & Bonifacino JS (2000). Lysosome-related organelles. *The Federation of American Societies for Experimental Biology Journal*, 14: 1265-1278.

Deponte M, Hoppe HC, Lee M, Maier AG, Richard D, Rug M, Spielmann T & Przyborski JM (2012). Wherever I may roam: Protein and membrane trafficking in *P. falciparum*-infected red blood cells. *Molecular and Biochemical Parasitology*, 186(2): 95-116.

Di Cristina M, Spaccapelo R, Soldati D, Bistoni F & Crisanti A (2000). Two conserved amino acid motifs mediate protein targeting to the micronemes of the apicomplexan parasite *Toxoplasma gondii*. *Molecular and Cellular Biology,* 20: 7332-7341.

Diaz A, Tomba E, Lennarson R, Richard R, Bagajewicz M & Harrison RG (2009). Prediction of protein solubility in *Escherichia coli* using logistic regression. *Biotechnology and Bioengineering,* 105(2): 374-383.

Dolan SA, Proctor JL, Alling DW, Okubo Y, Wellems TE & Miller LH (1994). Glycophorin B as an EBA-175 independent *Plasmodium falciparum* receptor of human erythrocytes. *Molecular and Biochemical Parasitology,* 64: 55-63.

Duraisingh MT, Maier AG, Triglia T & Cowman AF (2003). Erythrocyte binding antigen 175 mediates invasion in *Plasmodium falciparum* utilizing sialic acid-dependent and -independent pathways. *Proceedings of Natural Academy of Sciences USA*, 100: 4796-4801.

Eisele TP, Thwing J & Keating J (2011). Claims about the Misuse of Insecticide-Treated Mosquito Nets: Are These Evidence-Based? *Public Library of Science Medicine*, 8(4): e1001019.

Elsworth B, Crabb BS & Gilson PR (2014a). Protein export in malaria parasites: an update. *Cellular Microbiology*, 16(3): 355-363.

Elsworth B, Matthews K, Nie CQ, Kalanon M, Charnaud SC, Sanders PR, Chisholm SA, Counihan NA, Shaw PJ, Pino P, Chan JA, Azevedo MF, Rogerson SJ, Beeson JG, Crabb BS, Gilson PR & de

Koning-Ward TF (2014b). PTEX is an essential nexus for protein export in malaria parasites. *Nature,* 511(7511): 587-591.

Fidock D & Wellems T (1997). Transformation with human dihydrofolate reductase renders malaria parasites insensitive to WR99210 but does not affect the intrinsic activity of proguanil. *Proceedings of the National Academy of Sciences USA,* 64: 10931-10936.

Florens L, Washburn MP, Raine JD, Anthony RM, Grainger M, Haynes JD, Moch JK, Muster N, Sacci JB, Tabb DL, Witney AA, Wolters D, Wu Y, Gardner MJ, Holder AA, Sinden RE, Yates JR & Carucci DJ (2002). A proteomic view of the *Plasmodium falciparum* life cycle. *Nature*, 419: 520-526.

Gallagher SR (2006). Unit 10.2A.1-10.2A.37: SDS-PAGE. Published in: Ausuble FM, Brent R, Kingston RE, Moore DD, Seidman JG, Smith JA & Struhl K (editors). *Current protocols in molecular biology*, John Wiley & Son, Inc.

Gallagher SR, Winston SE, Fuller SA & Hurrell JGR (2004). Unit 10.8.1-10.8.24: Protein Blotting with Tank Transfer Systems. Published in: Ausuble FM, Brent R, Kingston RE, Moore DD, Seidman JG, Smith JA & Struhl K (editors). *Current protocols in molecular biology*, John Wiley & Son, Inc.

Gardner MJ, Hall N, Fung E, White O, Berriman M, Hyman RW, Carlton JM, Pain A, Nelson KE, Bowman S, Paulsen IT, James K, Eisen JA, Rutherford K, Salzberg SL, Craig A, Kyes S, Chan MS, Nene V, Shallom SJ, Suh B, Peterson J, Angiuoli S, Pertea M, Allen J, Selegut J, Haft D, Mather MW, Vadiya AB, Martin DM, Fairlamb AH, Fraunholz MJ, Roos DS, Ralph SA, McFadden GI, Cummings LM, Subramanian GM, Mungall C, Venter JC, Carucci DJ, Hoffman SL, Newbold C, Davis RW, Fraser CM & Barrell B (2002). Genome sequence of the human malaria parasite *Plasmodium falciparum*. *Nature*, 419: 498-511.

Gaur D, Mayer DC & Miller LH (2004). Parasite ligand-host receptor interactions during invasion of erythrocytes by *Plasmodium* merozoites. *International Journal of Parasitology*; 34: 1413-1429.

Gilberger TW, Thompson JK, Triglia T, Good RT, Duraisingh MT & Cowman AF (2003a). A novel Erythrocyte Binding Antigen-175 paralogue from *Plasmodium falciparum* defines a new trypsin-resistant receptor on human erythrocytes. *The Journal of Biological Chemistry,* 278(26): 14480-14486.

Gilberger TW, Thompson JK, Reed MB, Good RT & Cowman AF (2003b). The cytoplasmic domain of the *Plasmodium falciparum* ligand EBA-175 is essential for invasion but not protein trafficking. *The Journal of Cell Biology,* 162: 317-327.

Gitau GW, Mandal P, Blatch GL, Przyborski J & Shonhai A (2012). Characterisation of the *Plasmodium falciparum* Hsp70-Hsp90 organising protein (*Pf*Hop). *Cell Stress and Chaperones,* 17: 191-202.

Hackett F, Sajid M, Withers-Martinez, Grainger M & Blackman MJ (1999). *Pf*SUB2: a second subtilisin-like protein in *Plasmodium falciparum* merozoites. *Molecular and Biochemical Parasitology*, 103: 183-195.

Hadley TJ, Klotz FW, Pasvol G, Haynes JD, McGinniss MH, Okubo Y & Miller LH (1987). *Falciparum* malaria parasites invade erythrocytes that lack glycophorin A and B (MkMk). Strain

differences indicate receptor heterogeneity and two pathways for invasion. *Journal of Clinical Investigation,* 80: 1190-1193.

Hafalla JC, Silvie O & Matuschewski K (2011). Cell biology and immunology of malaria. *Immunological Reviews*, 240: 297-316.

Han YS, Thompson J, Kafatos FC & Barillas-Mury C (2000). Molecular interactions between *Anopheles stephensi* midgut cells and *Plasmodium berghei*: the time bomb theory of ookinete invasion of mosquitoes. *European Molecular Biology Organization Journal,* 19: 6030-6040.

Harris KS, Casey JL, Coley AM, Masciantonio R, Sabo JK, Keizer DW, Lee EF, McMahon A, Norton RS, Anders RF & Foley M (2005 a). Binding hot spot for invasion inhibitory molecules on *Plasmodium falciparum* apical membrane antigen 1. *Infection and Immunity*, 73: 6981-6989.

Harris PK, Yeoh S, Dluzewski AR, O'Donnell RA, Withers-Martinez C, Hackett F, Bannister LH, Mitchell GH & Blackman MJ (2005 b). Molecular identification of a malaria merozoite surface sheddase. *Public Library of Science Pathology,* 1: 241-251.

Healer J, Crawford S, Ralph S, McFadden G & Cowman AF (2002). Independent translocation of two micronemal proteins in developing *Plasmodium falciparum* merozoites. *Infection and Immunity*, 70(10): 5751-5758.

Hiller NL, Bhattacharjee S, van Ooij C, Liolios K, Harrison T, Lopez-Estraño C & Haldar K (2004). A host-targeting signal in virulence proteins reveals a secretome in malarial infection. *Science,* 306(5703): 1934-1937.

Hirst J & Robinson MS (1998). Clathrin and adaptors. *Biochimica et Biophysica Acta*,1404: 173-193.

Ho SH, Hunt HD, Horton RM, Pullen JK & Pease LR (1989). Site-directed mutagenesis by overlap extension using the polymerase chain reaction. *Gene*, 77: 51-59.

Hodder AN, Crewther PE, Matthew ML, Reid GE, Moritz RL, Simpson RJ & Anders RF (1996). The disulfide bond structure of *Plasmodium* apical membrane antigen-1. *Journal of Biological Chemistry,* 271: 29446-29452.

Hoppe HC, Ngo HM, Yang M & Joiner KA (2000). Targeting to rhoptry organelles of *Toxoplasma gondii* involves evolutionarily conserved mechanisms. *Nature Cell Biology*, 2: 449-456.

Howard RF & Schmidt CM (1995). The secretory pathway of *Plasmodium falciparum* regulates transport of p82/RAP1 to the rhoptries. *Molecular and Biochemical Parasitology*, 74: 43-54.

Howell SA, Well I, Fleck SL, Kettleborough C, Collins CR & Blackman MJ (2003). A single malaria merozoite serine protease mediates shedding of multiple surface proteins by juxtamembrane cleavage. *Journal of Biological Chemistry,* 278(26): 23890-23898.

Howell SA, Withers-Martinez C, Kocken CHM, Thomas AW & Blackman MJ (2001). Proteolytic processing and primary structure of *Plasmodium falciparum* apical membrane antigen-1. *Journal of Biological Chemistry*, 276(33): 31311-31320.

Huang S (2011). And now there are five: A new player in intracellular trafficking pathways. *Public Library of Science Biology*, 9: e1001173.

Hycult Biotec (2010). Troubleshooting Sodium Dodecyl Sulfate-polyacrylamide gel electrophoresis (SDS-PAGE). Version 04-2010 (www.hycultbiotech.com).

Ignatev A, Bhargav SP, Vohokoski J, Kursula P & Kursula I (2012). The Lasso Segment Is Required for Functional Dimerization of the *Plasmodium* Formin 1 FH2 Domain. *Public Library of Science One*, 7(3): e33586.

Jean L, Hackett F, Martin SR & Blackman MJ (2003). Functional characterization of the propeptide of *Plasmodium falciparum* Subtilisin-like protease-1. *Journal of Biological Chemistry,* 278: 28572-28579.

Josling GA & Llinas M (2015). Sexual development in *Plasmodium falciparum* parasites: knowing when it's time to commit. *Nature Reviews Microbiology,* 13: 573-587.

Kats LM, Black CG, Proellocks NI & Coppel RL (2006). *Plasmodium* rhoptries: how things went pear-shaped. *Trends in Parasitology*, 22: 269-276.

Kats LM, Cooke BM, Coppel RL & Black CG (2008). Protein trafficking to apical organelles of malaria parasites – building an invasion machine. *Traffic*, 9: 176-186.

Keeley A & Soldati D (2004). The glideosome: a molecular machine powering motility and host-cell invasion by Apicomplexa. *Trends in Cell Biology*, 14: 528-532.

Kim J, Lee H & Shin S (2015). Advances in the measurement of red blood cell deformability: A brief review. *Journal of Cellular Biotechnology*, 1(1): 63-79.

Klausner RD, Donaldson JG & Lippincott-Schwartz J (1992). Brefeldin A: Insights into the control of membrane traffic and organelle structure. *The Journal of Cell Biology*, 116(5): 1071-1080.

Klemba M, Beatty W, Gluzman I & Goldberg DE (2004a). Trafficking of plasmepsin II to the food vacuole of the malaria parasite *Plasmodium falciparum. The Journal of Cell Biology,* 164(1): 47-56.

Klemba M, Gluzman I & Goldberg DE (2004b). A *Plasmodium falciparum* dipeptidyl aminopeptidase I participates in vacuolar hemoglobin degradation. *Journal of Biological Chemistry,* 279(41): 43000-43007.

Kocken CH, Narum DL, Massougbodji A, Ayiyi B, Dubbeld MA, van der Wel A, Conway DJ Sanni A & Thomas AW (2000). Molecular characterisation of *Plasmodium rechenowi* apical membrane antigen-1 (AMA-1), comparison with *P. falciparum* AMA-1, and antibody-mediated inhibition of red cell invasion. *Molecular and Biochemical Parasitology,* 109: 147-156.

Koella JC, Sorensen FL & Anderson RA (1998). The malaria parasite, *Plasmodium falciparum*, increases the frequency of multiple feeding of its mosquito vector, *Anopheles gambiae*. *Proceedings of the Royal Society London B*, 265: 763-768.

Kovar DR (2006). Molecular details of formin-mediated actin assembly. *Current Opinion in Cell Biology,* 18:11-17.

Krai P, Dalal S & Klemba M (2014). Evidence for a Golgi-to-Endosome Protein Sorting Pathway in *Plasmodium falciparum*. *Public Library of Science One*, 9(2): e89771.

Laemmli UK (1970). Cleavage of structural proteins during the assembly of the head of bacteriophage T4. *Nature,* 227(5259): 680-685.

Lamarque M, Besteiro S, Papoin J, Roques M, Vulliez-Le Normand B, Morlon-Guyot J, Dubremetz J-F, Fauquenoy S, Tomavo S, Faber BW, Kocken CH, Thomas AW, Boulanger MJ, Bentley GA & Lebrun M (2011). The RON2-AMA1 interaction is a critical step in moving junction-dependent invasion by Apicomplexan parasites. *Public Library of Science Pathogens*, 7: e1001276.

Lambros C & Vanderberg JP (1979). Synchronization of *Plasmodium falciparum* erythrocytic stages in culture. *Journal of Parasitology*, 65(3): 418-420.

Lanzillotti R & Coetzer TL (2008). Phage display: a useful tool for malaria research? *Trends in Parasitology,* 24: 18-23.

Lauterbach SB, Lanzillotti R & Coetzer TL (2003). Construction and use of *Plasmodium falciparum* phage display libraries to identify host parasite interactions. *Malaria Journal,* 2(1): 47.

Le Roch KG, Zhou Y, Blair PL, Grainger M, Moch JK, Haynes JD De La Vega P, Holder AA, Batalov S, Carucci DJ & Winzeler EA (2003). Discovery of gene function by expression profiling of the malaria parasite life cycle. *Science,* 301: 1503-1508.

Leykauf K, Treeck M, Gilson PR, Nebl T, Braulke T, Cowman AF, Gilberger TW & Crabb BS (2010). Protein kinase A dependent phosphorylation of apical membrane antigen 1 plays an important role in erythrocyte invasion by the malaria parasite. *Public Library of Science Pathology*, 6(6): e1000941.

Li X, Chen H, Oo TH, Daly TM, Bergman LW, Liu SC, Chishti AH, Oh SS (2004). A co-ligand complex anchors *Plasmodium falciparum* merozoites to the erythrocyte invasion receptor band 3. *Journal of Biological Chemistry*, 279: 5765-5771.

Lobo CA, Rodriguez M, Hou G, Perkins M, Oskov Y & Lustigman S (2003). Characterization of *Pf*Rhop148, a novel rhoptry protein of *Plasmodium falciparum*. *Molecular and Biochemical Parasitology*, 128: 59-65.

Lopez-Barragan MJ, Lemieux J, Quinones M, Williamson KC, Molina-Cruz A, Cui K, Barillas-Mury C, Zhao K & Su X-Z (2011). Directional gene expression and antisense transcripts in sexual and asexual stages of *Plasmodium falciparum. BioMed Central Genomics,* 12: 587.

Maier AG, Duraisingh MD, Reeder JC, Patel SS, Kazura JW, Zimmerman PW & Cowman AF (2003). *Plasmodium falciparum* erythrocyte invasion through glycophorin C and selection for Gerbich negativity in human populations. *Nature Medicine,* 9: 87-92.

Margos G, Bannister LH, Dluzewski AR, Hopkins J, Williams IT & Mitchell GH (2004). Correlation of structural development and differential expression of invasion-related molecules in schizonts of *Plasmodium falciparum*. *Parasitology*, 129: 273-287.

Marti M, Good RT, Rug M, Knuepfer E & Cowman AF (2004). Targeting malaria virulence and remodeling proteins to the host erythrocyte. *Science*, 306: 1930-1933.

Mayer DCG, Cofie J, Jiang L, Hartl DL, Tracy E, Kabat J, Mendoza LH & Miller LH (2009). Glycophorin B is the erythrocyte receptor of *Plasmodium falciparum* erythrocyte-binding ligand, EBL-1. *Proceedings of Natural Academy of Sciences USA,* 106(13): 5348-5352.

McLean KA, Byanaku A, Kubikonse A, Tshowe V, Katensi S & Lehman AG (2014). Fishing with bed nets on Lake Tanganyika: a randomized survey. *Malaria Journal*, 13: 395.

Mehlin C, Boni E, Buckner FS, Engel L, Feist T, Gelb MH, Haji L, Kim D, Liu C, Mueller N, Myler PJ, Reddy JT, Sampson JN, Subramanian E, Van Voorhis WC, Worthey E, Zucker F & Hol WGJ (2006). Heterologous expression of proteins from *Plasmodium falciparum:* Results from 1000 genes. *Molecular and Biochemical Parasitology,* 148: 144-160.

Menard R (2001). Gliding motility and cell invasion by Ampicomplexa: insights from the *Plasmodium* sporozoite. *Cellular Microbiology,* 3: 63-73.

Menard, R (2005). Medicine: Knockout malaria vaccine? *Nature,* 433: 113-114.

Michon P, Stevens JR, Kaneko O & Adams JH (2002). Evolutionary relationships of conserved cysteine-rich motifs in adhesive molecules of malaria parasites. *Molecular Biology and Evolution,* 19: 1128-1142.

Miller LH, Baruch DI, Marsh K & Doumbo OK (2002). The pathogenic basis of malaria. *Nature,* 415: 673-679.

Minakawa N, Dida GO, Sonye GO, Futami K & Kaneko S (2008). Unforeseen misuses of bed nets in fishing villages along Lake Victoria. *Malaria Journal*, 7: 165.

Mishra N, Prajapati SK, Kaitholia K, Bharti RS, Srivastava B, Phookan S & Valecha N (2015). Surveillance of Artemisinin Resistance in *Plasmodium falciparum* in India Using the kelch13 Molecular Marker. *Antimicrobial Agents and Chemotherapy*, 59(5): 2548-2553.

Mital J, Meissner M, Soldati D & Ward GE (2005) Conditional expression of *Toxoplasma gondii* apical membrane antigen-1 (*Tg*AMA1) demonstrates that *Tg*AMA1 plays a critical role in host cell invasion. *Molecular Biology of the Cell,* 16: 4341-4349.

Mitchell GH, Thomas AW, Margos G, Dluzewski AR & Bannister LH (2004). Apical membrane antigen 1, a major malaria vaccine candidate, mediates the close attachment of invasive merozoites to host red blood cells. *Infection and Immunity*, 72: 154-158.

Mullard A (2012). Protein-protein interaction inhibitors get into the groove. *Nature Reviews Drug Discovery* ,11(3): 173-175.

NanoDrop Technologies, Inc (2007). ND-1000 spectrophotometer V3.3 user's manual.

Ngô, H.M., Yang, M., Paprotka, Pypaert M, Hoppe H & Joiner KA (2003). AP-1 in *Toxoplasma gondii* mediates biogenesis of the rhoptry secretory organelle from a post-golgi compartment. *The Journal of Biological Chemistry*, 278: 5343-5352.

Normark J (2008). Freezing of patient isolates and strains with glycerolyte. *Methods in Malaria Research*, Fifth Edition. Moll K, Ljungström I, Perlmann H, Scherf A & Wahlgren M (Editors).

Novagen (2011). *Competent Cells,* Germany, EMD Biosciences, Inc.

Novagen (2011). T7Select® System Manual. Darmstadt.

O'Donnell RA, Saul A, Cowman AF & Crabb BS (2000). Functional conservation of the malaria vaccine antigen MSP-1$_{19}$ across distantly related *Plasmodium* species. *Nature Medicine*, 6: 91-95.

Odunuga OO, Hornby JA, Bies C, Zimmermann R, Pugh DJ & Blatch GL (2003). Tetratricopeptide Repeat Motif-mediated Hsc70-mSTI1 interaction. *JBC,* 278: 6896-6904.

Orlandi PA, Klotz FW & Haynes JD (1992). A malaria invasion receptor, the 175-kilodalton erythrocyte binding antigen of *Plasmodium falciparum* recognizes the terminal Neu5Ac(alpha 2-3)Gal- sequences of glycophorin A. *The Journal of Cell Biology,* 116: 901-909.

Otsuki H, Kaneko O, Thongkukiatkul A, Tachibana M, Iriko H, Takeo S, Tsuboi T & Torii M (2009). Single amino acid substitution in *Plasmodium yoelii* erythrocyte ligand determines its localization and controls parasite virulence. *Proceedings of the National Academy of Sciences USA*, 106: 7167-7172.

Otto TD, Wilinski D, Assefa S, Keane TM, Sarry LR, Böhme U, Lemieux J, Barrell B, Pain A, Berriman M, Newbold C & Llinás M (2010). New insightws into the blood-stage transcriptome of *Plasmodium falciparum* using RNA-Seq. *Molecular Microbiology,* 76(1): 12-24.

Pandey KN (2009) Functional roles of short sequence motifs in the endocytosis of membrane receptors. *Frontiers in Bioscience Landmark*, 14: 5339–5360.

Paul AS & Pollard TD (2009). Review of the mechanism of processive actin filament elongation by formins. *Cell Motility and the Cytoskeleton*, 66: 606-617.

Paul AS, Egan ES & Duraisingh MT (2015). Host-parasite interactions that guide red blood cell invasion by malarial parasites. *Current Opinion in Haematology*; 22(3): 220-226.

Pavithra SR, Kumar R & Tatu U (2007). Systems analysis of chaperone networks in the malarial parasite *Plasmodium falciparum. Public Library of Sciences Computational Biology,* 3(9): e168.

Pearse BMF (1976). Clathrin: a unique protein associated with intracellular transfer of membrane by coated vesicles. *Proceedings of the National Academy of Sciences USA*, 73: 1255-1259.

Peterson MG, Marshall VM, Smythe JA, Crewther PE, Lew A, Silva A, Anders RF & Kemp DJ (1989). Integral membrane protein located in the apical complex of *Plasmodium falciparum*. *Molecular and Cellular Biology*, 9(7): 3151-3154.

Pihan E, Delgadillo RF, Tonkin ML, Pugnie're M, Lebrun M, Boulanger MJ & Douguet D (2015). Computational and biophysical approaches to protein–protein interaction inhibition of *Plasmodium falciparum* AMA1/RON2 complex. *Journal of Computer-Aided Molecular Design,* 29(6): 525-539.

Pizarro JC, Vulliez-Le Normand B, Chesne-Seck ML, Collins CR, Withers-Martinez C, Hackett F, Blackman MJ, Faber BW, Remarque EJ, Kocken CH, Thomas AW & Bentley GA (2005). Crystal structure of the malaria vaccine candidate apical membrane antigen 1. *Science* 308(5720): 408-411.

Promega (2009). Technical Manual: MagneHis™ Protein Purification System. Madison: Promega Corporation.

Promega (2014). Technical Manual: MagneGST™ Protein Purification System. Madison: Promega Corporation.

Przyborski JM, Miller SK, Pfahler JM, Henrich PP, Rohrbach P, Crabb BS & Lanzer M (2005). Trafficking of STEVOR to the Maurer's clefts in *Plasmodium falciparum*-infected erythrocytes. *The European Molecular Biology Organization Journal,* 24, 2306-17.

Pulford J, Hetzel MW, Bryant M, Siba PM & Mueller I (2011). Reported reasons for not using a mosquito net when one is available: a review of the published literature. *Malaria Journal,* 10: 83.

Reed MB, Caruana SR, Batchelor AH, Thompson JK, Crabb BS & Cowman AF (2000). Targeted disruption of an erythrocyte binding antigen in *Plasmodium falciparum* is associated with a switch toward a sialic acid-independent pathway of invasion. *Proceedings of the Natural Academy of Sciences USA,* 97, 7509-7514.

Reiff SB & Striepen B (2009). The gatekeeper revealed. *Nature,* 459: 918-919.

Reiss M, Viebig N, Brecht S, Fourmaux MN, Soete M, Di Cristina M, Dubremetz JF & Soldati D (2001). Identification and characterization of an escorter for two secretory adhesins in *Toxoplasma gondii. Journal of Cell Biology*, 152: 563-578.

Remarque EJ, Faber BW, Kocken CH & Thomas AW (2008). Apical membrane antigen 1: a malaria vaccine candidate in review. *Trends in Parasitology*, 24(2): 74-84.

Richard D, Kats LM, Langer C, Black CG, Mitri K, Boddey JA, Cowman AF & Coppel RL (2009). Identification of rhoptry trafficking determinants and evidence for a novel sorting mechanism in the malaria parasite *Plasmodium falciparum. Public Library of Sciences Pathology,* 5: e1000328.

Robinson MS (2004). Adaptable adaptors for coated vesicles. *Trends in Cell Biology*,14: 167-174.

Robinson MS & Bonifacino JS (2001). Adaptor-related proteins. *Current Opinion in Cell Biology*, 13(4): 444-453.

Rodriquez LE, Urquiza M, Ocampo M, Suarez J, Curtidor H, Guzman F, Vargas LE, Triviños M, Rosas M & Patarroyo ME (2000). *Plasmodium falciparum* EBA-175 kDa protein peptides which bind to human red blood cells. *Parasitology*, 120(3): 225-235.

Rosenthal PJ, Sijwali PS, Singh A & Shenai BR. (2002). Cysteine proteases of malaria parasites: targets for chemotherapy. Current Pharmaceutical Design, 8(18): 1659-1672.

Sakura T, Yahata K & Kaneko O (2013). The upstream sequence segment of the C-terminal cysteine-rich domain is required for microneme trafficking of *Plasmodium falciparum* erythrocyte binding antigen 175. *Parasitology International,* 62:157-164.

Sasse J & Gallagher SR (2003). Unit 10.6.1-10.6.25: Coomassie Blue Staining. Published in: Ausuble FM, Brent R, Kingston RE, Moore DD, Seidman JG, Smith JA & Struhl K (editors). *Current protocols in molecular biology*, John Wiley & Son, Inc.

Scherf A, Lopez-Rubio JJ & Riviere L (2008). Antigenic variation in *Plasmodium falciparum*. *Annual Review of Microbiology*, 62: 445-470.

Schlichtherle M & Wahlgren M (2008). *Methods in Malaria Research*, Fifth Edition. Moll K, Ljungström I, Perlmann H, Scherf A & Wahlgren M (Editors): 199-200.

Sebastian R, Diaz E, Ayla G, Diaz ME, Zoncu R & Toomre D (2006). Studying endocytosis in space and time by means of temporal Boolean models. *Pattern Recognition*, 39: 2175-2185.

Seidman CE, Struhl K, Sheen J & Jessen T (1997). Unit 1.8.1-1.8.10: Competent Cells. Published in: Ausuble FM, Brent R, Kingston RE, Moore DD, Seidman JG, Smith JA & Struhl K (editors). *Current protocols in molecular biology*, John Wiley & Son, Inc.

Shinde U & Inouye M (1996). Propeptide-mediated folding in subtilisin: the intramolecular chaperone concept. *Advances in Experimental Medicine and Biology,* 379: 147-154.

Silvie O, Franetich JF, Charrin S, Mueller MS, Siau A, Bodescot M, Rubinstein E, Hannoun L, Charoenvit Y, Kocken CH, Thomas AW, Van Gemert GJ, Sauerwein RW, Blackman MJ, Anders RF, Pluschke G & Mazier D (2004). A role for apical membrane antigen 1 during invasion of hepatocytes by *Plasmodium falciparum* sporozoites. *The Journal of Biological Chemistry*, 279: 9490-9496.

Sloves PJ, Delhaye S, Mouveaux T, Werkmeister E, Slomianny C, Hovasse A, Dilezitoko Alayi T, Callebaut I, Gaji RY, Schaeffer-Reiss C, Van Dorsselear A, Carruthers VB & Tomavo S (2012). *Toxoplasma* sortilin-like receptor regulates protein transport and is essential for apical secretory organelle biogenesis and host infection. *Cell Host and Microbe*, 11(5): 515-527.

Smith GP (1985). Filamentous fusion phage: novel expression vectors that display cloned antigens on the virion surface. *Science*, 228: 1315-1317.

Smith RM, Wu GY. (2003). Structure-based design of hepatitis C virus inhibitors. Journal of Viral Hepatitis, 10(6): 405-412.

Sokhna C, Ndiath MO & Rogier C (2013). The changes in mosquito vector behaviour and the emerging resistance to insecticides will challenge the decline of malaria. *Clinical Microbiology and Infection*, 19(10): 902-907.

Sorensen HP & Mortensen KK (2005). Soluble expression of recombinant proteins in the cytoplasm of *Escherichia coli*. *Microbial Cell Factories*, 4: 1-8.

Stubbs J, Simpson KM, Triglia T, Plouffe D, Tonkin CJ, Duraisingh MT, Maier AG, Winzeler EA & Cowman AF (2005) Molecular mechanism for switching of *P. falciparum* invasion pathways into human erythrocytes. *Science,* 309: 1384-1387.

Thakur JK, Yadav A & Yadav G (2014). Molecular recognition by the KIX domain and its role in gene regulation. *Nucleic Acids Research*, 42(4): 2112-2125.

Thomas AW, Deans JA, Mitchell GH, Alderson T & Cohen S (1984). The Fab fragments of monoclonal IgG to a merozoite surface antigen inhibit *Plasmodium* knowlesi invasion of erythrocytes. *Molecular and Biochemical Parasitology*, 13: 187-199.

Thompson JK, Triglia T, Reed MB & Cowman AF (2001). A novel ligand from *Plasmodium falciparum* that binds to a sialic acid-containing receptor on the surface of human erythrocytes. *Molecular Microbiology,* 41: 47-58.

Tirados I, Constantini C, Gibson G & Torr SJ (2006). Blood-feeding behaviour of the malarial mosquito *Anopheles arabiensis*: implications for vector control. *Medical and Veterinary Entomology,* 20: 425-437.

Tirasophon W, Ponglikitmongkol M, Wilairat P, Boonsaeng V & Panyim S (1991). A novel detection of a single *Plasmodium falciparum* in infected blood. *Biochemical and Biophysical Research Communications,* 175: 179-184.

Tompa P (2002). Intrinsically unstructured proteins. *Trends in Biochemical Sciences,* 27: 527-33.

Tonkin CJ, Pearce JA, McFadden GI & Cowman AF (2006). Protein targeting to destinations of the secretory pathway in the malaria parasite *Plasmodium falciparum*. *Current Opinion in Microbiology*, 9: 1-7.

Tonkin CJ, Van Dooren GG, Spurck TP, Struck NS, Good RT, Handman E, Cowman AF & McFadden GI (2004). Localization of organellar proteins in *Plasmodium falciparum* using a novel set of transfection vectors and a new immunofluorescence fixation method. *Molecular & Biochemical Parasitology,* 137: 13-21.

Topolska AE, Lidgett A, Truman D, Fujioka H & Coppel RL (2004). Characterization of a membrane-associated rhoptry protein of *Plasmodium falciparum*. *The Journal of Biological Chemistry*, 279: 4648-4656.

Trager W & Jensen JB (1976). Human malaria parasites in continuous culture. *Science*, 193:673-675.

Treeck M, Struck NS, Haase S, Langer C, Herrmann S, Healer J, Cowman AF & Gilberger TW (2006). A conserved region in the EBL proteins is implicated in microneme targeting of the malaria parasite *Plasmodium falciparum*. *The Journal of Biological Chemistry,* 281: 31995-32003.

Treeck M, Zacherl S, Herrmann S, Cabera A, Kono M, Struck NS, Engelberg K, Haase S, Frischknecht F, Miura K, Spielmann T & Gilberger TW (2009). Functional analysis of the leading malaria vaccine candidate AMA-1 reveals an essential role for the cytoplasmic domain in the invasion process. *Public Library of Science Pathogens*, 5(3): e1000322.

Triglia T, Duraisingh MT, Good RT & Cowman AF (2005). Reticulocyte-binding protein homologue 1 is required for sialic acid-dependent invasion into human erythrocytes by *Plasmodium falciparum*. *Molecular Microbiology,* 55: 162-174.

Triglia T, Healer J, Caruana SR, Hodder AN, Anders RF, Crabb BS & Cowman AF (2000). Apical membrane antigen 1 plays a central role in erythrocyte invasion by *Plasmodium* species. *Molecular Microbiology*, 38(4): 706-718.

Trowbridge IS, Collawn JF & Hopkins CR (1993). Signal-dependent membrane protein trafficking in the endocytic pathway. *Annual Review of Cell and Developmental Biology*, 9:129-161.

Turk B (2006). Targeting proteases: successes, failures and future prospects. *Nature Reviews Drug Discovery*, 5(9): 785-99.

Tyler JS & Boothroyd JC (2011). The C-terminus of *Toxoplasma* RON2 provides the crucial link between AMA1 and the host-associated invasion complex. Public Library of Science Pathogens, 7: e1001282.

Tyler JS, Treeck M & Boothroyd JC (2011). Focus on the ringleader: the role of AMA1 in apicomplexan invasion and replication. *Trends in Parasitology*, 27(9): 410-420.

Uzureau P, Barale JC, Janse CJ, Waters AP & Breton CB (2004). Gene targeting demonstrates that the *Plasmodium berghei* subtilisin *Pb*SUB2 is essential for red cell invasion and reveals spontaneous genetic recombination events. *Cellular Microbiology,* 6: 65-78.

Vieira WA (2015). Investigating the molecular participants of programmed cell death in *Plasmodium falciparum.* PhD Thesis: University of the Witwatersrand, South Africa.

Wepener M (2014). Identification of trafficking determinants needed for targeting of apical organelle proteins in *P. falciparum*. M.Sc. Dissertation: University of the Witwatersrand, South Africa.

Vu TT, Tran VB, Phan NT, Le TT, Luong VH, O'Brien E & Morris GE (1995). Screening donor blood for malaria by polymerase chain reaction. *Transactions of the Royal Society of Tropical Medicine and Hygiene,* 89: 44-47.

Waller RF, Reed MB, Cowman AF & McFadden GI (2000). Protein trafficking to the plastid of *Plasmodium falciparum* is via the secretory pathway. *European Molecular Biology Organization Journal*, 19: 1794-1802.

Waters AP, Thomas AW, Van Dijk MR & Janse CJ (1997). Transfection of malaria parasites. *Methods,* 13, 134-47.

Weiss GE, Gilson PR, Taechalertpaisarn T, Tham W-H, de Jong NWM, Harvey KL, Fowkes FJI, Barlow PN, Rayner JC, Wright GJ, Cowman AF & Crabb BS (2015). Revealing the sequence and resulting cellular morphology of receptor-ligand interactions during *Plasmodium falciparum* invasion of erythrocytes. *Public Library of Science Pathogens*, 11: e1004670.

Wepener M (2014). Identification of trafficking determinants needed for targeting of apical organelle proteins in *P. falciparum*. M.Sc. Dissertation: University of the Witwatersrand, South Africa.

Wilfinger WW, Mackey K & Chomczynski P (1997). Effect of pH and ionic strength on the spectrophotometric assessment of nucleic acid purify. *BioTechniques,* 22: 474-481.

Wilson AJ (2009) Inhibition of protein–protein interactions using designed molecules. *Chemical Society Reviews*, 38(12): 3289-3300.

Wilson AJ (2009). Inhibition of protein–protein interactions using designed molecules. *Chemical Society Reviews*, 38: 3289-3300.

Withers-Martinez C, Haire LF, Hackett F, Walker PA, Howell SA, Smerdon SJ, Dodson GG & Blackman MJ (2008). Malarial EBA-175 region VI crystallographic structure reveals a KIX-like binding interface. *Journal of Molecular Biology*, 375: 773-781.

Withers-Martinez C, Jean L & Blackman MJ (2004). Subtilisin-like proteases of the malaria parasite. *Molecular Microbiology*, 53(1): 55-63.

Woehlbier U, Epp C, Hackett F, Blackman MJ & Bujard H (2010). Antibodies against multiple merozoite surface antigens of the human malaria parasite *Plasmodium falciparum* inhibit parasite maturation and red blood cell invasion. *Malaria Journal*, 9:77.

World Health Organization (2016). World Malaria Report 2016.